APPLICATION OF CHEMICAL TRANSPORT MODELS TO STUDY GLOBAL AND REGIONAL AIR QUALITY AND HUMAN HEALTH

Yuqiang Zhang

A dissertation submitted to the faculty at the University of North Carolina at Chapel Hill in partial fulfillment of the requirements for the degree of Doctor of Philosophy in the Department of Environmental Sciences and Engineering in the Gillings School of Global Public Health.

Chapel Hill
2016

Approved by:

J. Jason West

Will Vizuete

Jason Surratt

Jared Bowden

Chip Konrad

ABSTRACT

Yuqiang Zhang: Application of Chemical Transport Models to Study Global and Regional Air Quality and Human Health
(Under the direction of J. Jason West)

Climate change and air quality are interrelated issues. Policies to mitigate greenhouse gas (GHG) emissions will not only slow climate change, but can also bring co-benefits of improved air quality and avoided mortality.

Here I examine the co-benefits of global and regional GHG mitigation on US air quality and human health in 2050 at fine resolution by dynamically downscaling a previous global study on the co-benefits of global GHG mitigation. The US average total co-benefits of global GHG mitigation in RCP4.5 are 0.47 μg m^{-3} for annual average $PM_{2.5}$ and 3.55 ppb for ozone-season maximum daily 8-hour average O_3, avoiding 24500 (90% confidence interval, 17800-31100) all-cause deaths related to $PM_{2.5}$, and 12200 (5400-18900) respiratory deaths for O_3. Reductions in co-emitted air pollutants dominate the total co-benefits, much higher than those via slowing climate change. GHG mitigation from foreign countries avoids 3700 (2700-4700) $PM_{2.5}$-related deaths (15% of the total), and contributes more to the US O_3 reduction than domestic GHG mitigation, avoiding 7600 O_3-related deaths (3400-11900, 62%), highlighting the importance of global methane reductions and intercontinental air pollutant transport. GHG mitigation in the US residential sector brings the largest co-benefits for $PM_{2.5}$-related deaths (21% of the total domestic co-benefits), and industry for O_3 (17%). The US gains significantly greater co-benefits

by coordinating GHG reductions with foreign countries. Previous studies estimating co-benefits locally or regionally may greatly underestimate the full co-benefits of coordinated global actions.

I also investigated the causes of changes in the global tropospheric ozone burden (B_{O3}) from 1980 to 2010 using a global atmospheric model, isolating the effect of the emissions shifting southwards from emission increases in developing countries and decreases in developed countries. The global emission spatial distribution change accounts for more than half of the total B_{O3} change (28.12 Tg), even larger than the combined effects of the global emission magnitude change and global methane change. This highlights the dominant role of emissions from the tropics, especially over South and Southeast Asia, for the tropospheric O_3 burden, and suggests that B_{O3} might continue to increase as emissions shift south, even if global emissions remain unchanged or even decrease.

ACKNOWLEDGEMENTS

I am sincerely grateful to my advisor, Dr. J Jason West, for his continual support throughout my doctoral program, for his patience, guidance and extensive knowledge. His mentorship helped me throughout my research and dissertation. His kindness and patience makes the Ph.D. process more sufferable. I am thankful for the pleasant research environment he provided for me.

Besides my advisor, I would also thank all my committee members, Dr. Will Vizuete, Dr. Jason Surratt, Dr. Jared Bowden and Dr. Chip Konrad for their insightful comments and suggestions toward improving this work, also for their hard questions which incented me to deepen my research and broaden my perspective. I especially thank Jared Bowden, who guided me on the WRF downscaling process, and was always a good mentor and friend to me.

I also thank my fellow labmates for accompanying me on the sleepless nights we worked on environmental physics which I will never forget, for the stimulating discussions on research questions and their tremendous help on model runs. Also to all my friends in US and China, who always trusts me, believe in me and encourages me on my journey.

Last but not least, I would like to thank my parents for their continued support and faith in me. Also extremely thankful for my wonderful and lovely wife, Xiaoni, who sacrificed a lot for me by moving to US with me in 2011, and who always looks after at me, encourages me, and stands by me especially in my times of frustration. The whole journey would have been completely different without her companionship.

TABLE OF CONTENTS

LIST OF TABLES

LIST OF FIGURES

LIST OF ABBREVIATIONS

ACCMIP	Atmospheric Chemistry and Climate Model Intercomparison Project
ACS	American Cancer Society
AE6	Aerosol 6 Module
AF	Attributable Fraction
AM3	NOAA GFDL Atmospheric Model Component of CM3
AMWG	Atmosphere Model Working Group
AQS	Air Quality System
BC	Black Carbon
BCs	Boundary Conditions
BenMAP-CE	Benefits Mapping and Analysis Program-Community Edition
BEIS	Biogenic Emission Inventory System
ΔB_{O3}	Change in tropospheric ozone burden
B_{O3}	Tropospheric ozone burden
BVOC	Biogenic Volatile Organic Compound
CA	California
CAM-Chem	Community Atmosphere Model with Chemistry
CASTNET	Clean Air Status and Trends Network
CB05	Chemical Bond 2005
CESM	Community Earth System Model
CH_4	Methane

CI	Confidence Interval
Cl^-	Chloride
CMAQ	Community Multi-scale Air Quality
CO	Carbon Monoxide
CO_2	Carbon dioxide
CONUS	CONtiguous United States
CPD	Cardiopulmonary disease
CRF	Concentration Response Function
CSN	Chemical Speciation Network
CTMs	Chemical Transport Models
CV	Coefficient of Variation
DU	Dobson Unit
EC	Elemental Carbon
ENE	Energy
EPA	Environmental Protection Agency
GCAM	Global Change Assessment Model
GCMs	General Circulation Models
GDP	Gross Domestic Product
GEOS-5	The Goddard Earth Observing System Model, Version 5
GFDL	Geophysical Fluid Dynamics Laboratory
GHG	Greenhouse gas
GMAO	Global Modeling and Assimilation Office
GMD	Global Monitoring Division

HIF	Health Impact Function
hPa	hectopascal
IC	Initial Condition
IMPROVE	Interagency Monitoring of PROtected Visual Environments
IND	Industry
IPCC	Intergovernmental Panel on Climate Change
$ISOPNO_3$	peroxy radical from NO_3+ isoprene
Km	Kilometer
LC	Lung cancer
L_{O3}	ozone chemical loss rate
MEGAN	Model of Emissions of Gases and Aerosols from Nature
MCIP	Meteorology-Chemistry Interface Processor
MDA8	Maximum Daily 8-hour Average
MdnB	Median Bias
MdnE	Median Error
MOZART-4	Model for OZone And Related chemical Tracers, version 4
MPAN	methacryloyl peroxynitrate
$\mu g\ m^{-3}$	Micrograms per cubic meter
°N	Degrees North
Na^+	Sodium
NAAQS	National Ambient Air Quality Standards
NASA	National Aeronautics and Space Administration
NCOM	Non-Carbon Organic Matter

NEI	National Emission Inventory
NH_4^+	Ammonium
NH	North Hemisphere
NMdnB	Normalized Median Bias
NMdnE	Normalized Median Error
NMVOCs	Non-Methane Volatile Organic Compounds
NOAA	National Oceanic and Atmospheric Administration
NO	nitrogen monoxide
NO_2	nitrogen dioxide
NO_3^-	Nitrate
NO_x	Nitrogen oxides
NO_y	total reactive nitrogen
N_2O_5	Dinitrogen pentoxide
NY	New York state
O_3	Ozone
OA	Organic Aerosol
OC	Organic Carbon
OM	Organic Matter
OMI	Ozone Monitoring Instrument
OPE	Ozone Production Efficiency
PAN	Peroxyacyl nitrates
PI	Posterior interval
PM	Particulate Matter

PMC	Particulate Matter Coarse
$PM_{2.5}$	Particles with aerodynamic diameters of 2.5 µm or less
P_{O3}	ozone chemical production rate
Pop	Exposed population
ppbv	Parts per billion by volume
RCMs	Regional Climate Models
RCP	Representative Concentration Pathway
RCP4.5	Representative Concentration Pathway 4.5
RCP8.5	Representative Concentration Pathway 8.5
REF	REFerence
Res	Respiratory disease
RES	Residential
RETRO	Reanalysis of the Tropospheric Chemical Composition over the past 40 years
RF	Radiative Forcing
RR	Relative Risk
°S	Degrees South
SCC	Source Clarification Codes
SH	South Hemisphere
SMOKE	Sparse Matrix Operator Kernel Emissions
SIP	State Implementation Plans
SOA	Secondary organic aerosol
SO_4^{2-}	Sulfate
STE	Stratosphere-troposphere-exchange

Tg	Teragram
TX	Texas
US	United States of America
UTC	Coordinated Universal Time
VOCs	Volatile organic compounds
WACCM	Whole Atmosphere Community Climate Model
WEST2013	West et al., 2013
WHO	World Health Organization
$W\ m^{-2}$	Watts per square meter
WRF	Weather Research and Forecasting
ΔX	Change in concentration of air pollutants
y_0	baseline mortality rates

CHAPTER 1. INTRODUCTION

The 20th century was a rapid changing period, featured with increasing of global population from 1.7 billion to 6.1 billion (United Nations, 2001), global gross domestic product (GDP) by 19 times (International Monetary Fund, 2000), and fossil fuel consumption by 15 times (Smil, 2003). Air pollution is among one of the top issues raised by this unprecedented change. Clean air is a basic requirement for human health, crop yield and ecosystems (Royal Society, 2008). A recent study attributed the global deaths and disability-adjusted life years in 2010 to 67 risk factors using global scale modeling (Lim et al., 2013), and found that three risk factors in the category of "Air Pollution" have important health impacts: ambient particulate matter pollution (attributing 3.2±0.4 million deaths in 2010), household air pollution from solid fuels (3.5 million deaths, ranging from 2.7 to 4.4 million) and ambient ozone pollution (0.2 million deaths, ranging from 0.1 to 0.3 million). Fine particulate matter ($PM_{2.5}$, particles with aerodynamic diameter of 2.5 μm or less) and ozone (O_3) therefore directly link air quality and human health impacts.

Pollutants that are directly emitted into the atmosphere are referred to as primary pollutants, such as nitrogen oxide (NO_x) and carbon monoxide (CO). Those produced chemically in the atmosphere are called secondary pollutants. $PM_{2.5}$ is a very complex air pollutant, composed of extremely small particles and liquid droplets and including both primary and secondary sources. For example, the major components for $PM_{2.5}$ are nitrate (NO_3^-), sulfate (SO_4^{2-}), ammonium (NH_4^+), which are mostly from direct emissions, and secondary organic aerosols (SOA), which are produced though gas-phase and liquid-phase reactions in the

atmosphere. For O_3 in the troposphere, it is secondary air pollutant, mainly produced by photochemical reactions of CO, non-methane volatile organic compounds (NMVOCs), and methane (CH_4) in the presence of NO_x and sunlight. Tropospheric O_3 can also be transported from stratosphere through the stratosphere-troposphere-exchange (STE), but this is less important than chemical production (Young et al., 2013).

1.1 Air pollution as a global issue

Despite a relatively short lifetime in the atmosphere (days to weeks), $PM_{2.5}$ and its precursors can be transported long-distance from source region to another reception region (Ewing et al., 2010; Hadley et al., 2007; Han et al., 2008; Heald et al., 2006; Kondo et al., 2011; Liu et al., 2009a, b; Nam et al., 2010; TF HTAP, 2010; Wuebbles et al., 2007; Yu et al., 2012; Yumimoto et al., 2010). For example, Liu et al. (2009a) found that the influence from intercontinental transport of air pollutants contributed to 36-97% of background surface aerosol concentrations, depending on the receptor locations. Compared with $PM_{2.5}$, the intercontinental transport of O_3 is more interesting to scientists and policy makers since it has a much longer lifetime in the troposphere (weeks to months) (Akimoto et al., 2003; Anenberg et al., 2009; Auvray and Bey, 2005; Cooper et al., 2010; Derwent et al., 2004; Doherty et al., 2013; Lin et al., 2008; Lin et a., 2012; Liu et al., 2003; Liang et al., 2004, 2007; Trickl, 2003; Wild and Akimoto, 2001; West et al., 2009a; Yoshitomi et al., 2011; Zhang et al., 2008, 2010). Recent studies have attributed the degradation of air quality in the western US, especially in spring, to the influence from rising anthropogenic emissions in East Asia (Cooper et al., 2010, 2015; Jacob et al., 1999; Lin et al., 2012; Verstraeten et al., 2015), making it more challenging to reach the US ozone standard, which decreased from 75 ppb to 70 ppb recently (US EPA, 2015). However, $PM_{2.5}$ has a greater effect on human mortality (Bell et al., 2004; Jerrett et al., 2009; Krewski et al., 2009),

dominating the premature mortality from outdoor pollution, compared with O_3 (Anenberg et al., 2010; Lim et al., 2013; Silva et al., 2013). So both $PM_{2.5}$ and O_3 are increasingly recognized as a global issue instead of regional one, demanding more international collaborations (Holloway et al., 2003; Keating et al., 2004; TF HTAP, 2010).

To control outdoor air pollution on national scale, strict standards should be made to reduce the air pollutants emissions from domestic emissions sectors, such as power plants, cement industry and ground transportation (e.g., the State Implementation Plans, a.k.a., SIP in US; Wang et al., 2012, 2014). On international scale, close collaborations should be established to keep the air pollutants global background levels from increasing, and to help reach individual goal of the air quality standards for concerned countries. The air pollutants in the North Hemisphere (NH) can be transported from East Asia to North America, from North America across the North Atlantic Ocean to Europe, and from Europe into the Arctic and East Asia. Studies have shown that the global O_3 burdens are more sensitive to the air pollutants changes in the tropical regionals and the South Hemisphere (SH) (Berntsen et al., 2005; Derwent et al., 2008; Fuglestvedt et al., 1999, 2010; Fry et al., 2012, 2014; Naik et al., 2005; West et al., 2009a). So to control $PM_{2.5}$ and O_3 as both a global and regional issue, not only the magnitude of emissions of the air pollutants and its precursors should be considered, but also where these emissions should be reduced.

The concentrations and the distributions of the air pollutants in the atmosphere are determined by their emissions (including anthropogenic, biogenic and other natural sources such as volcanos and soil), chemistry, transport and deposition. To study processes in the atmosphere, atmospheric scientists made reasonable assumptions and simplifications to convert the real, complex atmosphere into model systems leading to analytical or numerical solutions.

Atmospheric chemical transport models (CTMs) are great tools to study the large-scale or continental-scale air pollutants distributions and transport. The CTMs are designed to calculate and predict the chemical reactions, physical processes and the transport of the air pollutants within the atmosphere. Since monitor sites, including ground surface observations, balloons and satellites, cannot provide complete spatial and temporal coverage for the interest of domain, under these circumstances, CTMs are widely used in global and regional studies for regulatory or policy assessment, understanding chemical and physical processes, source attribution, and health impact assessments. More recently, the CTMs are used heavily to predict future air quality changes under future climate change of different projections.

1.2 Air pollution and premature mortality

A larger number of epidemiological studies have quantified the relationship between adverse health effects with $PM_{2.5}$ (Dockery et al., 1993; Laden et al., 2006; Krewski et al., 2009; Roman et al., 2008) and O_3 (Bell et al., 2004, 2005; Jerrett et al., 2009; Levy et al., 2005). An early study was the 1993 Harvard Six Cities study, which found associations between expose to $PM_{2.5}$ and lung cancer and cardiopulmonary mortality (Dockery et al., 1993). An extended follow-up study was performed later with 8 more years' data to study the reduced mortality from the reduced $PM_{2.5}$ pollution (Laden et al., 2006). Reduced mortality risks were associated with reduced ambient $PM_{2.5}$ concentrations, reaffirming the associations between the $PM_{2.5}$ and the mortality. In this latest cohort study, the relative risks (RR) for total all-cause mortality, lung cancer and the cardiovascular deaths were 1.16 (with a 95% confidence interval, CI of 1.07-1.26), 1.27 (95% CI, 0.96-1.69), and 1.28 (95% CI, 1.13-1.44), with each 10 $\mu g/m^3$ increases in ambient $PM_{2.5}$ concentration (Krewski et al., 2009).

An extended follow-up and spatial analysis of the American Cancer Society (ACS) study was also conducted to examine the association between the long-term exposure of ambient $PM_{2.5}$ pollution and mortality in major large US cities (Krewski et al., 2009). This is the largest cohort study so far, involving approximately 1.2 million participants across many US large cities, and also applying state-of-art statistical approaches. This study confirmed strong associations between the ambient $PM_{2.5}$ and mortality as shown in previous studies, and also established new relationships for the RRs of the total all-cause, cardiopulmonary disease and lung cancer mortality, with 1.06 (95% CI, 1.04-1.08), 1.13 (95% CI, 1.10-1.16), and 1.14 (95% CI, 1.06-1.23) individually (Krewski et al., 2009). The RRs from the ACS study are lower than the estimates from the Harvard Six City studies.

Studies have shown that different components of $PM_{2.5}$ may have different associations with mortality, for example, the ambient black carbon (BC) may have stronger association with mortality than other components and PM as a whole (Adar et al., 2007; Bell et al., 2009; Janssen et al., 2011, 2012; Ostro et al., 2007; Peng et al., 2009; Power et al., 2011; Qiao et al., 2014; Suh et al., 2010; WHO, 2012; Wilker et al., 2013). However, a recent review by the US EPA (2010) revealed that the differences in the mortality risks associated with long-term exposure to $PM_{2.5}$ components were not discernable. Studies that assess premature mortality associated with $PM_{2.5}$ overwhelmingly use $PM_{2.5}$ as an indicator, rather than different species.

Surface O_3 in the ambient environment has also been associated with mortality (e.g., Bell et al., 2005; Ito et al., 2005; Levy et al., 2005; Jerrett et al., 2009). A study which used mortality data in 95 US communities from 1987-2000 has found that with 10-ppb increase of ozone, the RRs in daily mortality would increase by 0.52% (95% posterior interval, PI, 0.27%-0.77%), and the RRs in cardiovascular and respiratory mortality would increase by 0.64% (95% PI, 0.31%-

0.98%) (Bell et al., 2004). Moreover, surface ozone exposure is also associated with the chronic mortality. A recent long-term large-scale study cohort of the American Cancer Society Cancer Prevention Study is the first to establish the association between the long-term ozone exposure and mortality (Jerrett et al., 2009). Using the two-pollutant model, the authors found strong associations with the risk from respiratory causes, and the estimated RR was 1.40 (95% CI, 1.010-1.040) with a 10-ppb increases for the ozone season of 1-hour daily maximum O_3 concentrations.

1.3 Interactions between climate change and air quality

Climate change and air quality are interrelated issues, suggesting that these two should be considered together under the mitigation strategies (Ramanathan and Feng, 2009). First, air pollutants can cause climate forcing. For example, O_3 in the troposphere can warm the earth, while aerosols, such as NO_3^- and SO_4^{2-}, two very important components of $PM_{2.5}$, can cool the atmosphere by reflecting the sunlight back into the space.

Second, changing climate can also affect the formation, destruction and transport of both $PM_{2.5}$ and O_3 (Weaver et al., 2009; Jacob and Winner, 2009; Fiore et al., 2012, 2015). This is a long-term effect, which could be made evident in several ways. Changing climate can affect the photochemical reaction and destruction rates in the atmosphere (Hogrefe et al., 2004; Jacob and Winner, 2009; Leung and Gustason, 2005), and also impact air quality through modification of global circulation dynamics (Fiore et al., 2012, 2015). Modeling work by Mickley et al. (2004) implied that future summertime pollution episodes over the Midwest and Northeast U.S. would increase as a result of a decline in the numbers of mid-latitude cyclones tracking across southern Canada. Horton et al. (2014) forecasted that more frequent and longer duration atmospheric stagnation events would occur by the late twenty-first century, which was predictive of poorer air

quality and greater human health risk exposure in the future. Variations of temperature, water vapor and concentration of CO_2 from climate change could also affect the natural biogenic emissions, which are shown to be very important in the formation of $PM_{2.5}$ and O_3 in rural sites (Fiore et al., 2011; Koo et al., 2010; Lam et al., 2011; Pun et al., 2002; Wiedinmyer et al., 2006).

Previous studies have used both global and regional CTMs to study the single or combined changes in future climate and emissions on global and regional air quality (Weaver et al., 2009; Jacob and Winner, 2009; Fiore et al., 2012). Climate change is likely to decrease background O_3 over remote places due to the elevated humidity, and increase O_3 over urban and polluted areas, in part because of higher temperature (Jacob and Winner, 2009). However, the role of climate change on $PM_{2.5}$ is less clear as different components of $PM_{2.5}$ may respond differently to changes in climate variables (Jacob and Winner, 2009; Tai et al., 2010; Fiore et al., 2012, 2015).

Third, the sources of emissions of greenhouse gases (GHGs) and air pollutants are usually shared (Haines et al., 2009; Nemet et al., 2010; Ramanathan and Feng, 2009; Reynolds and Kandlikar, 2008; West et al., 2004). In particular, the combustion of fossil fuels is the major source for both GHGs and air pollutants. Actions to control one can also influence the other. So the climate policies to reduce the GHGs will not only get the benefits of slowing climate change, but can also have the co-benefits of improved air quality and then human health (Bell et al., 2008; Cifuentes et al., 2001; Driscoll et al., 2015; Garcia-Menendez et al., 2015; Jacobson, 2001; Markandya et al., 2009; Schucht et a., 2015; Thompson et al., 2014; Trail et al., 2015). Policies targeted at improving future air quality could also influence future climate, but the influences have large uncertainties as different air pollutants have different effects on the radiative forcing (RF) (Andreae et al., 2005; Arneth et al., 2009; Kloster et al., 2010; Levy et al., 2008; Parrish and Zhu, 2009; Shindell et al., 2008).

1.4 Dynamical downscaling

To study the future air quality changes under the changing climate at regional scale at fine resolution, dynamical downscaling is usually adopted to provide high quality input data for the regional CTMs. Dynamical meteorological downscaling refers to the process of taking global climate change responses from global General Circulation Models (GCMs) and translating them to a finer temporal and spatial scale which are more meaningful in the context of local and regional impacts by using the Regional Climate Models (RCMs) with the lateral boundary conditions provided from the GCMs. GCMs are used to study Earth's climate system and simulate the future climate change. RCMs are used to simulate the climate change for a limited area at much higher spatial resolutions. The advantages of the dynamical meteorological downscaling are that a regional model can simulate local fine-scale feedback processes better than the GCMs. The disadvantages are that it requires more computational resources and the performances of the regional climate depend strictly on the input data and physical configurations of the RCMs. The meteorological downscaling has been broadly used in previous research to study the future regional climate change under different emission projections (Bowden et al., 2012, 2013; Liu et al., 2012; Nolte et al., 2014; Trail et al., 2013), and to project the effects of global and regional climate change on global and regional air quality (Dawson et al., 2008, 2009; Fann et al., 2015; Nolte et al., 2008; Wu et al., 2008a). When using coarse-scale data from GCMs as lateral boundary conditions for the RCMs without further constraint, the interior meteorological fields simulated by the RCMs may deviate significantly from the driving fields. "Nudging" techniques provide one way to constrain the RCMs and keep them from diverging too far from the coarse-scale fields. If the RCMs are constrained too strongly to the GCM fields, however, there is the possibility that the benefits of using the higher-resolution

RCMs will not be realized. A delicate balance is needed between the amount of constraint given to the RCM and the freedom of the RCM to simulate its own mesoscale features (Otte et al., 2012).

Chemical downscaling refers to the process that simulating global perturbations in global CTMs to provide initial and boundary conditions (BCs) for regional CTMs at greater resolution in a region of interest. The proper chemical BCs are also crucial for the regional CTMs as the effects of intercontinental transport of air pollutants (Lam et al., 2009; Lin et al., 2008) and enhancement of background pollutant concentrations emerged (Fiore et al., 2003). Numerous studies implied that providing dynamical chemical BCs for the regional CTMs instead of the profiles would best capturing the temporal and spatial variations distributions of air pollutants in the regions (Byun et al., 2004; Fu et al., 2008; Tang et al., 2007). Song et al. (2008) compared the performances of CMAQ simulating vertical ozone profile by using profile BCs and dynamical BCs, and found that dynamical BCs performed better than the scenarios with profile BCs. By providing dynamical BCs for the regional CTMs, we have the ability to consider global changes in air pollutants in the global CTMs, while simulating the effects on a finer scale at a region of interest. It will also allow us to consider the intercontinental transport of air pollutants as well as the global climate change on the influence of regional air quality.

1.5 Motivations and objectives

Many studies have also been carried out to estimate the co-benefits of regional or local GHG on air quality and human health through reductions in co-emitted air pollutants. Nemet et al. (2010) summarized previous literature and found that, when monetized, the co-benefits from the GHG mitigation ranges from \$2-196 /tCO_2, comparable to the costs of GHG reductions.

Recent studies also estimated the future regional GHG mitigation scenarios on the co-benefits of air quality and human health (Thompson et al., 2014; Trail et al., 2015).

However, these studies may underestimate the true co-benefits as they do not consider GHG mitigation from the whole world: GHG mitigation as a whole may slow global climate change significantly, which then could decrease the air pollutants. GHG mitigation could bring air quality improvement for those countries who participate, and can also affect air quality in the adjacent countries due to long-range air pollutant transport, especially for O_3, even though those countries will not or delay participating in the mitigation policies. Under this circumstance, a recent study led by Dr. J. Jason West from UNC, which I was also involved, used a global CTM to study the global GHG mitigation on future air quality and human health (West et al., 2013). This is the first study to consider the global air quality and human health benefits by assuming all countries participate in the mitigation strategies. By using the global CTM, this study is also the first to consider the influence of global air pollution transport and long-term influences via global CH_4. This study concluded that global GHG mitigation could bring significant air quality improvement for both $PM_{2.5}$ and O_3, and avoid 2.2±0.8 million premature deaths globally by 2100 due to the improved air quality; it also found that when monetized, the global average marginal co-benefits of avoided mortality were \$50–380/tCO_2, higher than the previous estimates (Nemet et al., 2010).

This global co-benefits study also has limitation by using a coarse resolution in the CTM ($2^o \times 2.5^o$ horizontally), making it hard to understand co-benefits in small domains. So the major goal for my dissertation aims at quantifying the co-benefits of global GHG mitigation at regional scale at much finer resolution. I will focus on the temporal and spatial distributions of the co-benefits on air quality and human health at state or regional level in US, which are missing from

the global co-benefits study. By embedding this fine-resolution regional co-benefits study into a consistent global context, I can also quantify the co-benefits from domestic GHG mitigation versus the contributions from foreign countries reductions, which has never done before. In Chapter 2, I discuss the co-benefits of global and regional greenhouse gas mitigation on U.S. air quality in 2050 (Zhang et al., 2016a). In Chapter 3, I quantify the co-benefits of global, domestic, and sectoral greenhouse gas mitigation on US air pollution and human health in 2050 (Zhang et al., 2016b).

A second motivation for my Ph.D. work is to study the global emission redistribution on the influence of global ozone burden. Since 1980, anthropogenic emissions of ozone precursors have decreased in developed regions such as North America and Europe, but increased in developing regions, particularly East and South Asia, redistributing the emissions southwards (Granier et al, 2011; Lamarque et al., 2010; Ohara et al., 2007; Richter et al., 2005; van der A et al., 2008). Modeling studies have shown that the tropospheric ozone burden and resulting radiative forcing are much more sensitive to emission changes in the tropics and Southern Hemisphere than other regions (Naik et al., 2005; West et al., 2009a; Fry et al., 2012, 2014). However, the effect of the spatial redistribution of emissions has not been isolated. In Chapter 4, I investigate the influence of the change in global emissions shifting southwards on the global tropospheric O_3 burden and surface air quality from 1980 to 2010, and then compare this influence with those from the changes in global emissions magnitude and global CH_4 concentration. In Chapter 5, I summarize the key findings from my dissertation, uncertainties associated with each study, future research directions and policy implications.

CHAPTER 2. CO-BENEFITS OF GLOBAL AND REGIONAL GREENHOUSE GAS MITIGATION ON U.S. AIR QUALITY IN 2050

(Yuqiang Zhang, Jared H. Bowden, Zachariah Adelman, Vaishali Naik, Larry W. Horowitz, Steven J. Smith, J. Jason West. Submitted to ***Atmospheric Chemistry and Physics***)

2.1 Introduction

Climate change and air quality are interrelated problems. First, climate change can affect the formation, destruction and transport of major air pollutants, through changes in meteorological variables of temperature, precipitation, air stagnation events, etc. (Weaver et al., 2009; Jacob and Winner, 2009; Fiore et al., 2012, 2015). It can also affect natural emissions (biogenic, dust, fire and lighting) that influence air quality. Second, air pollutants such as particulate matter (PM) and ozone (O_3) can change the climate by altering the solar and terrestrial radiation balance through direct and indirect effects (Myhre et al., 2013). Third, the sources of emissions of greenhouse gases (GHGs) and air pollutants are usually shared, particularly through the combustion of fossil fuels, so actions to control one can also influence emissions of the other. Policies to control GHG emissions will therefore not only slow climate change in the future, but will also provide co-benefits of improvements to air quality and consequently to human health (Bell et al., 2008; Nemet et al., 2010).

Recent studies that model future air quality have focused on single or combined changes in future climate and emissions on global and regional air quality, using both global and regional Chemical Transport Models (CTMs) (Weaver et al., 2009; Jacob and Winner, 2009; Fiore et al., 2012). Climate change is likely to decrease background O_3 over remote places due to the

elevated humidity, and increase O_3 over urban and polluted areas, in part because of higher temperature. Jacob and Winner (2009) concluded that future climate change could increase summertime O_3 by 1-10 ppb over polluted regions in the U.S. in scenarios from the Special Report on Emission Scenarios (SRES; Nakicenovic and Swart, 2000). In one study, climate change in 2050 under the SRES A1B scenario is projected to increase summertime O_3 by 2-5 ppb over large areas in the U.S., comparable to the effect of reduced anthropogenic emissions which reduces O_3 by 2-15 ppb, especially in the east (Wu et al., 2008). The overall effect of climate change on PM is less clear, as different components of PM may respond differently to changes in climate variables (Jacob and Winner, 2009; Tai et al., 2010; Fiore et al., 2012, 2015).

Many studies have also estimated the co-benefits of regional or local GHG mitigation on air quality and human health through reductions in co-emitted air pollutants. Cifuentes et al. (2001) found that GHG mitigation through reduced fossil fuel combustion could bring significant local air pollution-related health benefits to some megacities. These health benefits have been estimated in many studies (Bell et al., 2008), and give co-benefits ranging from \$2-196 /tCO_2 when monetized, comparable to the costs of GHG reductions (Nemet et al., 2010). A few studies also analyze the co-benefits on future air quality and human health from future regional GHG mitigation scenarios (Thompson et al., 2014; Trail et al., 2015). Thompson et al. (2014) studied the co-benefits of different U.S. climate policies on 2030 domestic air quality, and found that when monetized, the human health benefits due to the improved air quality can offset 26-1050% of the cost of the carbon polices, depending on the policy.

These co-benefits studies may underestimate the total co-benefits as they only consider local or regional climate policies, neglecting benefits outside of the region considered, and benefits within those regions from global GHG mitigation. The total co-benefits of global

mitigation are relevant as meaningful GHG mitigation requires participation from at least several of the most highly-emitting nations. We examined the co-benefits of global GHG reductions on both global and regional air quality and human health, using a global atmospheric model (Model for OZone And Related chemical Tracers, version 4, MOZART-4, hereafter referred to as MZ4) and self-consistent future scenarios (West et al., 2013, referenced hereafter as WEST2013). In addition to evaluating co-benefits through reductions in co-emitted air pollutants, WEST2013 was the first study to quantify co-benefits through a second mechanism: slowing climate change and its effects on air quality. There are several other innovations of WEST2013: we account for global air pollution transport and long-term influences of methane using the global CTM; we consider realistic scenarios in which air pollutant emissions, demographics, and economic valuation are modeled consistently; and we evaluate chronic mortality influences of fine PM ($PM_{2.5}$, PM with diameter smaller than 2.5 μm) as well as O_3. WEST2013 concluded that global GHG mitigation could bring significant air quality improvement for both $PM_{2.5}$ and O_3, and avoid 2.2±0.8 million premature deaths globally by 2100 due to the improved air quality. When monetized, the global average marginal co-benefits of avoided mortality were \$50–380/tCO_2, higher than the previous estimates (Nemet et al., 2010). The co-benefits from the first mechanism of reduced co-emitted air pollutants were shown to be much greater than the co-benefits from the second mechanism via slowing climate change.

The WEST2013 study is limited by the coarse resolution of the CTM used (2º×2.5º horizontally). Here we investigate the co-benefits of global GHG mitigation on U.S. air quality at much finer resolution (36km×36km), building on the scenarios in the global study. WEST2013 simulated co-benefits in 2030, 2050, and 2100, and we choose here to downscale the results in 2050, as climate change influences air quality by 2050 and it is within the timeframe of current

decision-making for both climate change and air quality. We use a comprehensive modeling framework in the downscaling process, including a regional climate model to dynamically downscale the global climate to the contiguous United States (CONUS), an emissions processing program to directly process the global anthropogenic emissions to the regional scale, and we create dynamical boundary conditions (BCs) from the global co-benefits outputs for the regional CTM. We quantify the total co-benefits of global GHG mitigation on U.S. air quality for both $PM_{2.5}$ and O_3, and then separate the co-benefits from the two mechanisms analyzed by WEST2013. We also quantify the co-benefits from domestic GHG mitigation versus the co-benefits from those of foreign countries' reductions. We then present the co-benefits from global and domestic GHG mitigation on nine U.S. regions.

With regard to previous studies on the effect of climate change on future air quality (e.g. Jacob and Winner, 2009), our work differs in our reframing of this impact as a co-benefit of slowing climate change from GHG mitigation, and by analyzing that co-benefit through realistic future scenarios, following WEST2013. With regard to previous co-benefits studies that have been conducted on a regional scale (e.g., Thompson et al., 2014), this research differs by embedding the regional co-benefits study in consistent global context, accounting for the effects of changes in global air pollutant emissions and climate change on U.S. air quality.

2.2 Methodology

Future air quality changes under global and regional GHG mitigation scenarios are simulated using a regional CTM. The scenarios modeled here are built on those of WEST2013, who compared the Representative Concentration Pathway 4.5 (RCP4.5) scenario with its associated reference scenario (REF). Air pollutant emissions in REF are state of the art long-term emissions projections created by using the Global Change Assessment Model (GCAM)

(Thomson et al., 2011). RCP4.5 was developed based on REF by applying a global carbon price to all world regions and all sectors including carbon in terrestrial systems. As discussed by van Vuuren et al. (2011), the air pollutant emissions for the four RCP scenarios were prepared by different groups using different models and assumptions, so they are inconsistent with one another. But by comparing REF with RCP4.5, we use a self-consistent pair of scenarios, where the difference is uniquely attributed to a climate policy. WEST2013 used both emissions and meteorology from RCP4.5 to simulate future air quality under the RCP4.5 climate policy, and used emissions from REF and meteorology from RCP8.5 to simulate future air quality assuming no climate policy. Since no General Circulation Model (GCM) conducted future climate simulations for the REF scenario, RCP8.5 is used as a proxy for the future climate under REF. The differences between these two scenarios give the total co-benefits for future air quality under climate policy from RCP4.5. Through one extra simulation with emissions from RCP4.5 together with RCP8.5 meteorology (e45m85 in Table 2.1), and by comparing with REF and RCP4.5, WEST2013 separated the total co-benefits into the two mechanisms: the co-benefits from reductions in co-emitted air pollutants, and co-benefits from slowing climate change and its influence on air quality.

Here we conduct downscaling processes to provide fine-resolution inputs for the regional CTM. We use the Weather Research and Forecasting model version 3.4.1 (WRF, Skamarock and Klemp, 2008) to downscale the future global climate from the GCM to the regional scale at a horizontal resolution of 36×36 km for the CONUS. We directly process global anthropogenic emissions to regional scale using the Sparse Matrix Operator Kernel Emissions (SMOKE, v3.5, https://www.cmascenter.org/smoke/) program. The outputs from the global MZ4 simulations of WEST2013 (Table 2.1) are downscaled to provide initial condition (IC) and dynamic hourly BCs

for the regional CTM. The latest version of the Community Multi-scale Air Quality model (CMAQ, v5.0.1, Byun and Schere, 2006) is used as the regional CTM to simulate air quality changes over the CONUS domain. WEST2013 simulated five consecutive years for each scenario, and used the last four years' average for the data analysis with the first year as a spin-up. Due to the limitations of computational resources, we run CMAQ for 40 months consecutively for each scenario, with the first 4 months as spin-up, and analyze the results as three-year averages.

2.2.1 Regional meteorology

WEST2013 used NOAA Geophysical Fluid Dynamics Laboratory (GFDL) atmospheric model AM3 (Donner et al., 2011; Naik et al., 2013) simulations to provide global meteorology for MZ4. Here we dynamically downscale GFDL AM3, which has a horizontal resolution of 2°×2.5°, to 36 km over the CONUS using the WRF model. GFDL AM3 meteorology for the two RCP scenarios (RCP8.5 and RCP4.5) in 2050 used by WEST2013 are downscaled using a one-way nesting configuration for five consecutive years. WRF is initialized at 0000 Coordinated Universal Time (UTC) 1 January 2048 and run for a 12-month spin-up, then run continuously through 0000 UTC 1 January 2053. A historical period from GFDL AM3 is also downscaled with WRF initialized at 0000UTC 1 January 1999 and run for a 12-month spin-up, then run continuously through 0000 UTC 1 January 2004. The WRF physics options include the Rapid Radiative Transfer Model for global climate models (Iacono et al., 2008) for longwave and shortwave radiation, WRF single-moment 6-class microphysics scheme (Hong and Lim, 2006), the Grell ensemble convective parameterization scheme (Grell and Devenyi, 2002), the Yonsei University planetary boundary layer scheme (Hong et al., 2006), and the Noah land surface model (Chen and Dudhia, 2001). The WRF configuration also applies spectral nudging. Otte et

al. (2012) and Bowden et al. (2012, 2013) demonstrated that using nudging in WRF improves the overall accuracy of the simulated climate over the CONUS at 36-km and does not squelch extremes in temperature and precipitation. In particular, spectral nudging affects the model solution through a nonphysical term in the prognostic equations based on the difference between the spectral decomposition of the model solution and the reference analysis. Spectral nudging is used to constrain WRF toward synoptic-scale wavelengths resolved by GFDL AM3 exceeding 1200 km. Nudging is applied equally to potential temperature, wind, and geopotential with a nudging coefficient of 1.0×10^{-4}, which is equivalent to a time scale of 2.8 hours. The downscaled meteorology from WRF is used to provide meteorological inputs to CMAQ. Hourly WRF outputs are processed using Meteorology-Chemistry Interface Processor (MCIP v4.1; Otte and Pleim, 2010) to provide meteorological inputs for CMAQ.

Comparing the downscaling results between WRF with the GFDL AM3 simulation for three-year averages of the 2-m temperature (we present three-year averages instead of four to be consistent with CMAQ outputs below), we see that the large-scale spatial patterns for temperature are similar (Fig. A.1). However, the downscaling clearly improves the resolved features related to topography and provides a different realization of average regional climate throughout the CONUS. Comparing WRF future projected change centered on 2050 with 2000, we see that the three-year average of 2-m temperature generally increases over the entire U.S. for both RCP8.5 and RCP4.5 (Fig. A.2-A.3). Temperature increases are largest for extreme northeastern latitudes, the Southeast and Southwest U.S. in both scenarios, with U.S. average warming of 3.05°C and 2.59°C for RCP8.5 and RCP4.5, respectively. Additionally, precipitation is projected to increase over most of the U.S. in both scenarios with U.S. average increases of 0.20 and 0.15 mm day^{-1} in RCP8.5 and RCP4.5. Comparing the changes between scenarios

(RCP8.5 minus RCP4.5), Fig. 2.1 illustrates that temperature increases are smaller in RCP4.5 throughout the CONUS, except in the Northwest. The precipitation difference between scenarios has a larger spatial variability than the 2-m temperature. However, the only region where the regional climate is warmer and drier in RCP4.5 is in the Northwest U.S. Ignoring other influences of climate change, increases in precipitation would be expected to increase PM wet scavenging, and decrease PM concentration.

2.2.2 Regional emissions

Similar studies in the past have typically chosen to run SMOKE with the present-day U.S. National Emission Inventory (NEI), and then scale the SMOKE outputs into future years, using the mass ratio of projected future to present-day emissions from global inventories (e.g., Hogrefe et al., 2004; Nolte et al., 2008; Avise et al., 2009; Chen et al., 2009; Gao et al., 2013). Instead, we use SMOKE to directly process the global emissions in 2000 and in 2050 from REF and RCP4.5 to provide temporally- and spatially-resolved CMAQ emission input files. We first regrid the global emissions datasets at 0.5º×0.5º into finer resolution (36km×36km), and then take advantage of the temporal and speciation profiles inside SMOKE to assign temporal variations and re-speciate the PM and VOCs species. By doing this, we account better for the spatial distribution changes of future emissions projected in the RCPs (Fig. S4-S10), whereas the traditional method only considers changes in the magnitude of air pollutants in the future, assuming a constant spatial and sectoral distribution.

In addition, the RCP datasets report only elemental carbon (EC) and organic carbon (OC), but ignore emissions of other primary PM species. Here we back-calculate the total $PM_{2.5}$ and PM coarse (PMC) primary emissions for all sectors from the reported EC and OC. We first

derive the emission fractions of EC and OC in each sector by cross-comparing the definitions of the sectors in IPCC, the Source Clarification Codes (SCC) in the speciation cross-reference file (http://www.airqualitymodeling.org/cmaqwiki/index.php?title=CMAQv5.0_GSREF_example, accessed 5 September 2013), and the EPA PM speciation profile file built into SMOKE (http://www.airqualitymodeling.org/cmaqwiki/index.php?title=CMAQv5.0_GSPRO_Example, accessed 5 September 2013) (Table A.1). If multiple sources are included in one IPCC sector (e.g., energy and industries in Table A.1), we use the mass ratio from the source that contributes the largest fraction by referring to previous studies (Reff et al., 2009; Xing et al., 2013). Then we calculate the total $PM_{2.5}$ and PMC in each grid cell by dividing the reported EC and OC by their emission fractions individually, and average these two. By doing this, we increase the total $PM_{2.5}$ emissions of the RCPs by incorporating the inorganic components of primary PM, such as sulfate and nitrate. We check these results by comparing the total 2000 $PM_{2.5}$ emissions of 4.14 Tg yr^{-1} in this study (Table 2.2) with other studies, finding that it is comparable to the total of 4.69 Tg yr^{-1} in 2001 from the U.S. NEI (http://www.epa.gov/ttnchie1/trends/, accessed 5 October 2013). Our calculated $PM_{2.5}$ emission is also lower than the estimated 5.53 Tg yr^{-1} in 2000 by Xing et al. (2013), which used an activity data based approach to develop consistent temporally-resolved emissions from 1999 to 2010.

In Table 2.2, we list the U.S. anthropogenic emissions for major air pollutants in 2000 and 2050 from REF and RCP4.5. Significant decreases are seen for most pollutants from 2000 to 2050 for both REF and RCP4.5, except for NH_3 which is projected to increase due to agricultural activity (van Vuuren et al., 2011). Comparing RCP4.5 and REF, emissions of $PM_{2.5}$ and O_3 precursors also decrease, including EC (7.59%) and OC (6.17%), with NO_x and NMVOC decreasing by more than 10%. SO_2 has the largest relative decreases between RCP4.5 and REF

in 2050 (28.78%). Large spatial variations in emissions reductions are also seen over the U.S., with the largest reductions seen on the east and west urban areas of U.S. for most air pollutants and smaller reductions in the Great Plains (Fig. A.4-A.10).

Biogenic emissions are estimated using the Biogenic Emission Inventory System (BEIS v3.14), which responds to the changing climate for different scenarios. It is configured to run on-line in CMAQ, and calculates the emissions of 35 chemical species including 14 monoterpenes and 1 sesquiterpene. We assume that land use and land cover will stay constant in the future for the purpose of estimating biogenic emissions. The on-line option of lightning is also turned on to calculate the NO_x emissions by estimating the number of lightning flashes based on the modeled convective precipitation, which also changes with climate. We prepare the ocean/land mask for the domain to calculate sea salt emissions which can be significant in coastal environments (Kelly et al., 2010). We also use the BEIS on-line calculation for natural soil NO_x emissions.

2.2.3 Regional air quality model and dynamical chemical BCs

The latest CMAQ model (https://www.cmascenter.org/cmaq/index.cfm, accessed 15 June 2012) is used to perform the regional air quality simulations with the CB05 chemical mechanism and updated toluene reactions. The model incorporates the newest aerosol module (AE6), including features of new PM speciation (Reff et al., 2009), oxidative aging of primary organic carbon (Simon and Bhave, 2012), and an updated treatment and tracking of crustal species (e.g., Ca^{2}+, K^{+}, Mg^{2+}) and trace metals (e.g., Fe, Mn) (Fountoukis and Nenes, 2007). Several other enhancements in v5.0 of CMAQ were discussed by Appel et al. (2013) and Nolte et al. (2015), and there are no significant changes for the aerosol module between v5.0 and v5.0.1 (http://www.airqualitymodeling.org/cmaqwiki/index.php?title=CMAQ_version_5.0.1_%28July_2012_release%29_Technical_Documentation, accessed 15 August 2012). The model is

configured with 34 vertical layers, with the lowest level being 34 m high, to the highest level at 50 hPa. The horizontal resolution is 36 km by 36 km for the CONUS domain. $PM_{2.5}$ is calculated from the CMAQ output as the sum of the species EC, OC, secondary organic aerosol (SOA), non-carbon organic matter (NCOM), nitrate (NO_3^-), sulfate (SO_4^{2-}), ammonium (NH_4^+), sodium (Na^+), chloride (Cl^-), eight crustal and trace metal species, and other unspeciated fine PM (OTHER).

The dynamical BCs for this study are provided by the global MZ4 simulations of WEST2013. The hourly boundary values from MZ4 are horizontally interpolated from coarser resolution to the regional finer resolution, and also vertically interpolated as MZ4 and CMAQ have different vertical layers. Chemical species are mapped between MZ4 and CMAQ v5.0.1, due to the different chemical mechanisms used by these two models, following the descriptions of Emmons et al. (2010) and ENVIRON (http://www.camx.com/download/support-software.aspx, accessed 19 September 2013). For the chemical species in CMAQ that do not exist in MZ4, values are set to defaults as suggested by the CMAQ website.

2.2.4 Scenarios

We simulate scenarios in CMAQ comparable to WEST2013, except that we carry out one extra scenario to quantify the co-benefits from domestic versus foreign GHG mitigation (Table 2.1). S_2000 is conducted to evaluate CMAQ model performance and to compare with future scenarios. For this study, we run four scenarios in 2050. The differences between S_RCP45 and S_REF are the total co-benefits on U.S. air quality from global GHG mitigation. The emission benefit from the first mechanism is calculated as the difference between S_Emis and S_REF, and the meteorology benefit is calculated as S_RCP45 minus S_Emis. By comparing S_Dom (applying GHG mitigation from RCP4.5 scenario in the U.S. only) with S_REF, and S_RCP45

with S_Dom, we quantify the co-benefits from domestic and foreign GHG mitigation. In estimating the co-benefits of domestic reductions, we account for the influences of global climate change as a foreign influence (as most GHG emissions are global), assuming that U.S. air pollutant emissions have small effects on global or regional climate, such as through aerosol forcing. In each scenario, we fix global methane at concentrations given by the RCPs (Table 2.1), and account for methane changes as a foreign influence, neglecting the fraction of global methane emissions that are from the U.S. All scenarios are set up as continuous runs, with S_2000 running from September, 2000 to December, 2003, with the first four months in 2000 as spin-up. The future scenarios are run from September, 2049 to December, 2052 with the months in 2049 as spin-up. Results are presented as the average of three years.

2.3 Results

2.3.1 CMAQ model evaluation

The CMAQ model has been broadly used to study regional future air quality (Hogrefe et al., 2004; Tagaris et al., 2007; Nolte et al., 2008; Lam et al., 2011; Gao et al., 2013) and has been evaluated in many applications (Appel et al., 2010, 2011, 2013; Nolte et al., 2015). Here we evaluate the CMAQ v5.0.1 performance by comparing the model outputs from S_2000 with observations in 2000 from the Interagency Monitoring of PROtected Visual Environments (IMPROVE; http://vista.cira.colostate.edu/improve/, accessed 9 May 2014), the Chemical Speciation Network (CSN; previously known as STN, http://www.epa.gov/ttn/amtic/speciepg.html, accessed 9 May 2014), and the Clean Air Status and Trends Network (CASTNET; http://epa.gov/castnet/javaweb/index.html, accessed 9 May 2014) for total $PM_{2.5}$ and its components, and the EPA Air Quality System (AQS; http://www.epa.gov/ttn/airs/airsaqs/detaildata/downloadaqsdata.htm, accessed 9 May 2014) for

O_3. We pair the model outputs with observations in space and time, and calculate four groups of statistics to evaluate model performance: Median Bias (MdnB, μg m^{-3} for $PM_{2.5}$ and ppb for O_3), Normalized Median Bias (NMdnB, %), Median Error (MdnE, μg m^{-3} and ppb) and Normalized Median Error (NMdnE, %) (Appendix A). Median metrics are used here instead of the mean, as for data with non-normal distributions (i.e., PM species) the median gives a better representation of the central tendency of the data (USEPA 2007). For O_3 evaluation, we use both the maximum daily 1-hour (1hr_O_3) and Maximum Daily 8-hour Average (MDA8), and also calculate these metrics with a cutoff value of 40 ppb for the observed O_3 to evaluate the model's reliability in predicting ozone values relevant for the NAAQS (USEPA, 2007). Model performance is not expected to be perfect as meteorology does not correspond with actual year 2000 meteorology, and emissions are derived from global datasets rather than specific emissions for the U.S.

For total $PM_{2.5,}$ overall model performance is good and the NMdnE for IMPROVE and CSN are less than 50%, with slight differences in performance (Table 2.3). CMAQ underestimates $PM_{2.5}$ in these two networks and also its components in all three networks (Table A.2), except that it overestimates SO_4^{2-} compared with IMPROVE, and NH_3^+ with CSN. Compared with other components, OC and EC are not well predicted, with higher NMdnB, -63.55% and -37.00% in IMPROVE (OC and EC are not measured in the other two networks). In simulating $PM_{2.5}$ and its species, model performance is better in winter than in summer (not shown here). The model overestimates surface O_3 as indicated by the positive MdnB (ppb) and NMdnB (%). The NMdnE for the 1hr-O_3 (MDA8-O_3) declines from 27.60% (33.35%) to 17.36% (16.95%) after we apply the cutoff value of 40 ppb. The overprediction is slightly higher for 1hr-O_3 than for MDA8-O_3, however this difference becomes smaller when we consider the cutoff values.

2.3.2 Air quality changes in 2050

Here we show the seasonal and spatial patterns of future air quality changes centered in 2050 relative to 2000 from REF and RCP4.5 (Figs. A.11 to A.14). The three-year seasonal averages of $PM_{2.5}$ over the entire U.S. decrease in 2050 in both S_REF and S_RCP45 compared with S_2000, especially in the Eastern U.S. and California (CA). The seasonal decreases are largest in winter, with U.S. averages in S_REF (S_RCP45) of 4.42 (4.88) μg m^{-3}, and lowest in the summer of 1.55 (2.00) μg m^{-3}, with annual average of 2.76 (3.23) μg m^{-3}. The three-year seasonal averages of O_3 decrease significantly in summer in both the east and west coast, with U.S. average of 6.31 (9.50) ppb in S_REF (S_RCP45). O_3 increases over the Northeast and West U.S. in winter in both S_REF and S_RCP45, caused by the weakened NO_x titration as a result of the large NO_x decrease in the two scenarios (Table 2.2), as also reported in other studies (Gao et al., 2013; Fiore et al., 2015). The magnitude of the decreases between S_REF and S_2000 is lower than that between S_RCP45 and S_2000, as the REF scenario did not apply a GHG mitigation policy, and thus has less emission reductions.

We then compare these air quality changes in 2050 with the MZ4 simulations of WEST2013 for both S_REF (Fig. A.15) and S_RCP45 (Fig. 2.2), and for S_RCP45 with the ensemble model means from the Atmospheric Chemistry and Climate Model Intercomparison Project (ACCMIP, Lamarque et al., 2013) following Fiore et al. (2012), as no ACCMIP models simulated REF in 2050. For the U.S. annual average $PM_{2.5}$, the decrease in 2050 for S_RCP45 relative to 2000 in this study (3.23 μg m^{-3}) is modestly higher than both the results from MZ4 and the ACCMIP ensemble mean, but within the range of ACCMIP models when $PM_{2.5}$ is calculated as a sum of species. The future O_3 changes in our study (5.20 ppb) are clearly in the range of ACCMIP results, and nearly identical to MZ4 (5.13 ppb). Comparisons of the air quality

changes in 2050 for S_REF relative to 2000 between CMAQ and MZ4 are similar, except that the magnitudes of the changes are smaller than those for S_RCP45 (Fig. A.15).

2.3.3 Total co-benefits for U.S. air quality from global GHG mitigation

Projected three-year average $PM_{2.5}$ concentrations in 2050 in both scenarios (S_REF and S_RCP45) are higher in the Eastern U.S. and the west coast of CA, and lower in the Western U.S. (Fig. 2.3). The total co-benefits for U.S. air quality (S_RCP45 minus S_REF) show notable decreases of major air pollutants in 2050. The total co-benefits for $PM_{2.5}$ over the U.S. show a significant spatial gradient over the U.S. domain, greatest in the eastern U.S., especially urban areas, as well as CA, ranging from 0.4 to 1.0 μg m^{-3}, and least in the Rocky Mountains and Northwest with values below 0.4 μg m^{-3}. The total co-benefits for $PM_{2.5}$ averaged over the U.S. is 0.47 μg m^{-3}, with the largest contribution from organic matter (OM, including primary OC, SOA and NCOM), accounting for the 45% of the total (0.21 μg m^{-3}), followed by sulfate (0.11 μg m^{-3}) and ammonia (0.05 μg m^{-3}) (Fig. A.16). The total co-benefits are highest in fall, with U.S. domain average of 0.55 μg m^{-3}, and lowest in spring (0.41 μg m^{-3}) (Fig. 2.4). Notice that the region with greatest co-benefits shifts from Central areas in winter and spring to the East in summer and fall, with the largest component of OM also shifting from primary OC to SOA (Fig. A.17).

Future O_3 is presented here as the ozone-season average (from May to October) of MDA8. In general, 2050 O_3 concentrations in S_REF and S_RCP45 are projected to be high in the Southern U.S., especially over the coastal areas, and higher in the West than the East (Fig. 2.5). The total co-benefits for O_3 are fairly uniformly significant over the entire U.S. domain, slightly higher in the Northeast and Northwest, and range from 2-5 ppb with a domain average of 3.55

ppb, unlike $PM_{2.5}$ which is higher over urban regions. The uniformity of the total O_3 co-benefits suggests that they are strongly influenced by global O_3 reductions.

The total co-benefit for $PM_{2.5}$ from this study (0.47 μg m^{-3} over U.S.) is lower than WEST2013 (area-weighted three-year averages of 0.72 μg m^{-3} over U.S.), especially over the Northwest and Central of U.S. (Fig. A.18)**.** Analyzing the components of $PM_{2.5}$, we find that this difference is mainly caused by OM, with a U.S. annual average of 0.40 μg m^{-3} in WEST2013 and 0.21 μg m^{-3} in this study (Fig. A.19). For other components (EC, SO_4^{2-}, NO_3^- as reported in MZ4 of WEST2013), the CMAQ results are slightly lower than WEST2013 but share a similar spatial pattern (Fig. A.20-A.22). We expect that the total co-benefits of $PM_{2.5}$ in this study might be higher than WEST2013, as we account for inorganic primary PM emissions in SMOKE. A possible explanation may be that different chemical mechanisms and deposition processes are adopted for organic aerosols in MZ4 and CMAQ, which may make a shorter atmospheric lifetime for PM in CMAQ than that in MZ4. The differences of the meteorology (e.g., the precipitation and temperature) between the downscaled WRF and the GFDL could also contribute to this difference. Total co-benefit of O_3 from this study (3.55 ppb over U.S.) is comparable to WEST2013 (3.71 ppb) in both the magnitude and spatial distribution (Fig. A.23).

2.3.4 Co-benefits from the two mechanisms

We quantify the co-benefits of global GHG mitigation on $PM_{2.5}$ and O_3 through the two mechanisms: reduced co-emitted air pollutants (S_Emis—S_REF) and slowing climate change and its effect on air quality (S_RCP45—S_Emis). The reduction of co-emitted air pollutants has a much greater effect than slowing climate change for $PM_{2.5}$, accounting for 96% of the U.S. average $PM_{2.5}$ decrease. The emission benefit for $PM_{2.5}$ over the U.S. domain is 0.45 μg m^{-3}, greatest near urban areas where emissions are reduced (Fig. 2.6), with the largest contribution

from OM (0.172 μg m^{-3} over the U.S.), followed by sulfate (0.107 μg m^{-3}) and ammonia (0.048 μg m^{-3}). Slowing climate change only accounts for 4% of the U.S. average total $PM_{2.5}$ decreases (0.02 μg m^{-3}). It also has different signs of effect over the U.S., reducing $PM_{2.5}$ in the Southern U.S. but increasing in the North.

For O_3, the emission benefit is also larger than the climate benefit, accounting for 89% of the total O_3 decreases averaged over the U.S. The emission benefit for O_3 over the U.S. domain is 3.16 ppb, and much more uniform over the U.S., slightly higher over Northeast and Northwest. Slowing climate change accounts for 0.39 ppb O_3 decreases, 11% of the total and mainly in the Great Plains and the East, where temperatures are cooler under RCP4.5 compared with RCP8.5 (Fig. 2.1). The dominance of the emission co-benefit over the climate co-benefit for both $PM_{2.5}$ and O_3 is consistent with WEST2013.

2.3.5 Co-benefits from domestic and foreign GHG mitigation

We also investigate the co-benefits from domestic GHG mitigation by comparing S_Dom with S_REF, versus foreign GHG reductions by comparing S_RCP45 with S_Dom (Fig. 2.7). For $PM_{2.5}$, domestic GHG mitigation accounts for 74% (0.35 μg m^{-3}) of the total $PM_{2.5}$ decrease over the whole U.S., with the greatest effect over the East and CA, where emissions of $PM_{2.5}$ and its precursors are greatly reduced (Figs. A.3-A.9). The benefits from foreign GHG reductions on the U.S. $PM_{2.5}$ change are only obvious in the Southern U.S., influenced by emission reductions in Mexico and global climate change. We conclude that domestic GHG mitigation has a greater influence on U.S. $PM_{2.5}$ than reductions in foreign countries, but that foreign reductions also make a noticeable contribution, accounting for 26% of total $PM_{2.5}$ decreases over the U.S., and a greater fraction in the Southern U.S.

For O_3, foreign countries' GHG mitigation has a much larger influence on the U.S., accounting for 76% (2.69 ppb) of the total O_3 decrease, compared with 24% from domestic GHG mitigation (Fig. 2.7). The U.S. experiences greater O_3 decreases in the North than the South, which is likely influenced in part by the air quality improvement in Western Canada as a result of slowing deforestation due to the climate policy in RCP4.5 (West et al., 2013). This large influence of foreign reductions for O_3 highlights the importance of global methane reductions in RCP4.5 and global emission reductions, particularly in Asia and intercontinental transport.

2.3.6 Regional co-benefits and variability

We then quantify the co-benefits over nine U.S. climate regions defined by the National Oceanic and Atmospheric Administration (Fig. A.24), and their domestic and foreign components. The Central, Southeast, Northeast and South regions have the largest total co-benefits for $PM_{2.5}$ (regional annual means of 0.78, 0.75, 0.62 and 0.62 μg m^{-3}), and the Northwest has the lowest total co-benefits (0.16 μg m^{-3}) (Fig. 2.8). Domestic GHG mitigation has the largest effect over these same regions and lowest effects over Northwest and West North Central, with means of 0.13 μg m^{-3}. Foreign co-benefits are greatest over the South, Southwest, Central and Southeast, and lowest over Northwest (Table A.3). As a fraction of the total co-benefits, the domestic co-benefit is highest in the Northeast, East North Central and Central accounting for more than 80% of the total, while foreign co-benefits are highest over Southwest, South and West North Central, accounting for about 40% of the total.

For O_3, the Northeast, East North Central, and Northwest have the highest total co-benefits, (regional means of 4.61, 4.25, 4.15 ppb; Fig. 2.9 and Table A.3), although the total co-benefits for O_3 are fairly uniform over the U.S (Fig. 2.5). The Southeast has the lowest total co-benefits, with 2.67 ppb for the regional mean. Domestic co-benefits are higher over the Central, Northeast

and Southeast, with regional means of 1.25, 1.16 and 1.14 ppb, and lowest over Northwest (0.4 ppb). In general, foreign mitigation contributes more in the west than the east, most likely influenced by intercontinental transport from Asia. It is highest in the Northwest, West North Central and Northeast, with regional means of 3.75, 3.45 and 3.45 ppb. The fraction of co-benefits from foreign mitigation is larger than 60% in most regions, highest over the Northwest (90%), and lowest over the Southeast (57%).

We also evaluate the variability in co-benefits for the three years simulated (Table A.3). Over the U.S., the coefficient of variation (CV) for the total co-benefits for $PM_{2.5}$ (7%) is much lower than that of the total co-benefits for O_3 (37%), which is controlled by the intercontinental transport and global CH_4. The Southeast has the highest CV (29%) for the total co-benefits of $PM_{2.5}$, while other regions are lower than 15%, lowest in the East North Central and Northeast (3%). Southwest and South have the highest CV (70%, 69%) for the total co-benefits of O_3, and lowest in Northwest (21%). For regions with higher variability, longer simulations would be desirable to better quantify the annual average co-benefits.

2.4 Discussion

The co-benefits we present here are specific to the reference (REF) and mitigation (RCP4.5) scenarios we choose, and results would differ for other baseline and mitigation scenarios. The estimated co-benefits also depend on participation of many nations in the mitigation policies, and delaying participation will likely change the co-benefits.

The total co-benefits for O_3 when downscaled are comparable to the global study in both magnitude and spatial pattern, but the downscaled simulations capture some local features better than the global model, such the effects of topography and urban areas. For $PM_{2.5}$, significant differences are seen from the downscaling due to the fine resolution and different chemical

mechanisms between the global and the regional model. The resolution we are using for this study (36km by 36 km) is fine enough for us to analyze the co-benefits at a state level, but insufficient to fully resolve urban areas. Finer resolution simulations (such as 12 km by 12 km) with CMAQ or other CTMs can be carried out to better quantify the co-benefits over urban areas.

For this study, uncertainties and errors may exist under the assumptions and choices we make for each model. For example, the co-benefits of $PM_{2.5}$ have large contributions from OC and SOA over the Central and East U.S. (Fig. 2.4, Fig. A.16). However, our model evaluations show that CMAQ greatly underestimates the OC concentration compared with surface observations. We have not included the model evaluation for the SOA due to the limitation of the observation datasets, even though recent studies found that the CMAQ also greatly underestimated the SOA species (Baek et al., 2015; Hayes et al., 2015; Woody et al., 2015). New gas-phase and aqueous-phase oxidation pathways for SOA formation are found to play significant roles in producing organic aerosols (Lin et al., 2014; Pye and Pouliot, 2012; Pye et al., 2013), which are missing in the CMAQ version used in this study. The underestimation of the both OC and SOA in the current CMAQ model would greatly reduce the total co-benefits on both air quality and reduced premature mortality estimated from this study. We use BEIS model to estimate the biogenic VOC (BVOC) emissions, but studies have shown that the BVOCs from the Model of Emissions of Gases and Aerosols from Nature (MEGAN) are higher than those from BEIS by a factor 2 (Pouliot, 2008; Pouliot and Pierce, 2009), which highlights the uncertainty in representing these emissions and simulating both $PM_{2.5}$ and O_3 (Hogrefe et al., 2011).

We assume constant land use in the GCM, WRF and CMAQ when simulating the global and regional climate and estimating the biogenic emissions, which could introduce errors in our

results (Unger, 2014; Heald and Spracklen, 2015). When we process the global anthropogenic emissions with SMOKE, we back-calculate the total $PM_{2.5}$ and PMC from OC and BC, which introduces inorganic PM emissions and may make our results for co-benefits of $PM_{2.5}$ higher. By doing this, we account for missing emissions but also increase the total uncertainties in the emission inventory. Spectral nudging is adopted in this study to restrain WRF from drifting from the GCM, which has been shown to be better for some meteorological variables, but spectral nudging better for others (Bowden et al., 2012, 2013; Liu et al., 2012; Otte et al., 2012). Moreover, only one model is used at each step during downscaling, and ensemble model means can be used to reduce the single model's variability. Simulations are based on three-year averages, due to computational limitations, but these three years may reflect meteorological variability and not only climate change. This uncertainty may be greater for the total co-benefits of O_3, for which we see greater year-to-year variations than for $PM_{2.5}$. CMAQ simulations could be performed over more years to reduce the influence of the climate variability. In separating domestic and foreign co-benefits, we assume that global and regional climate will be controlled by foreign GHGs emissions, and not influenced by GHG mitigation in the U.S., which may also introduce errors into our results. We similarly attribute the global methane change as a foreign influence, as U.S. methane emissions are a small fraction of the global.

2.5 Conclusions

Climate polices to control GHG emissions will not only have the benefit of slowing climate change, but can also have co-benefits of improved air quality. Previous co-benefits studies focus mostly on local or regional GHG reductions. As a result, these studies omit air quality benefits outside of the domain considered, and neglect benefits from global GHG mitigation. In this study we adopt a systematic approach to quantify the co-benefits from both the

global and regional GHG mitigation on regional air quality over U.S. at fine resolution in 2050, building on the global co-benefits study from West et al. (2013). The co-benefits of global GHG mitigation on U.S. air quality are discussed through two mechanisms: reduced co-emitted air pollutants and slowing climate change and its influence on air quality. We also quantify the co-benefits from domestic GHG mitigation versus foreign countries' reduction.

We find that there are significant benefits for both $PM_{2.5}$ and O_3 over U.S. by 2050 from the global GHG mitigation in RCP4.5. The total co-benefits for $PM_{2.5}$ are higher in the east than the west, with an average of 0.47 μg m^{-3} over U.S. For O_3, the total co-benefits are fairly uniform across the U.S. at 2-5 ppb, with U.S. average of 3.55 ppb. The co-benefits from reductions of co-emitted air pollutants have a greater influence on both $PM_{2.5}$ (accounting for 96% of total decreases) and O_3 (89% of the total decreases) than the second mechanism via slowing climate change, consistent with West et al. (2013).

Foreign countries' GHG reductions have a much greater influence on the U.S. O_3 reduction (76% of the total), compared with that from domestic GHG mitigation only (24%), highlighting the importance of global methane reductions and the intercontinental transport of air pollutants. For $PM_{2.5}$, the benefits of foreign GHG control are less than domestic, but still a considerable portion of the total (26%). We conclude that the U.S. can gain significantly greater domestic air quality co-benefits by engaging with other nations for GHG control to combat climate change, especially for O_3. This also applies to other nations which can be expected to have ancillary air quality benefits from foreign countries' GHG mitigation. We also conclude that previous studies that estimate co-benefits for one nation or region (e.g., Thomson et al., 2014), may significantly underestimate the full co-benefits when many countries reduce GHGs together, particularly for O_3.

2.6 Figures and Tables

Table 2. 1. List of CMAQv5.0.1 simulations in this study. Hourly BCs are from the MOZART-4 (MZ4) simulations of WEST2013. We fix the methane (CH_4) background concentrations in CMAQ consistent with the RCP scenarios and WEST2013.

Years	Scenario	Emissions	Meteorology	BCs	CH_4
2000	S_2000	2000	2000	MZ4 2000	1766 ppbv
2050	S_REF	REF	RCP8.5	MZ4 REF	2267 ppbv
	S_RCP45	RCP4.5	RCP4.5	MZ4 RCP4.5	1833 ppbv
	S_Emis	RCP4.5	RCP8.5	MZ4 e45m85[b]	1833 ppbv
	S_Dom	RCP4.5 for U.S., REF for Can, Mex[a]	RCP8.5	MZ4 REF	2267 ppbv

[a]the part of Canada and Mexico in the domain.

[b]global simulation using RCP4.5 emissions together with RCP8.5 meteorology in 2050.

Table 2. 2. Anthropogenic emissions in the U.S. for major air pollutants in 2000 and 2050 from REF and RCP4.5 (Tg yr^{-1}), and the relative differences (Relative Diff) between RCP4.5 and REF in 2050 ((RCP4.5 - REF)/REF×100).

	2000	**2050 REF**	**2050 RCP4.5**	**Relative Diff (%)**
SO_2	14.84	2.46	1.75	-28.78
NH_3	3.34	4.56	4.30	-5.56
NO_x	19.57	4.40	3.92	-10.93
CO	92.74	11.42	11.25	-1.48
NMVOC	15.23	8.07	7.16	-11.21
EC	0.42	0.22	0.21	-7.59
OC	0.71	0.35	0.33	-6.17
$PM_{2.5}$[1]	4.14	1.87	1.57	-15.80
PMC[2]	11.02	5.50	4.63	-15.80

[1,2]$PM_{2.5}$ & PMC are the total emissions back-calculated based on the EC & OC.

Table 2. 3. Evaluation of the S_2000 simulation (average of three years modeled) with surface observations in 2000 for $PM_{2.5}$ (μg m^{-3}) and O_3 (ppb)**.**

	2000	**2050 REF**	**2050 RCP4.5**	**Relative Diff (%)**
SO_2	14.84	2.46	1.75	-28.78
NH_3	3.34	4.56	4.30	-5.56
NO_x	19.57	4.40	3.92	-10.93
CO	92.74	11.42	11.25	-1.48
NMVOC	15.23	8.07	7.16	-11.21
EC	0.42	0.22	0.21	-7.59
OC	0.71	0.35	0.33	-6.17
$PM_{2.5}$[1]	4.14	1.87	1.57	-15.80
PMC[2]	11.02	5.50	4.63	-15.80

[1,2]$PM_{2.5}$ & PMC are the total emissions back-calculated based on the EC & OC.

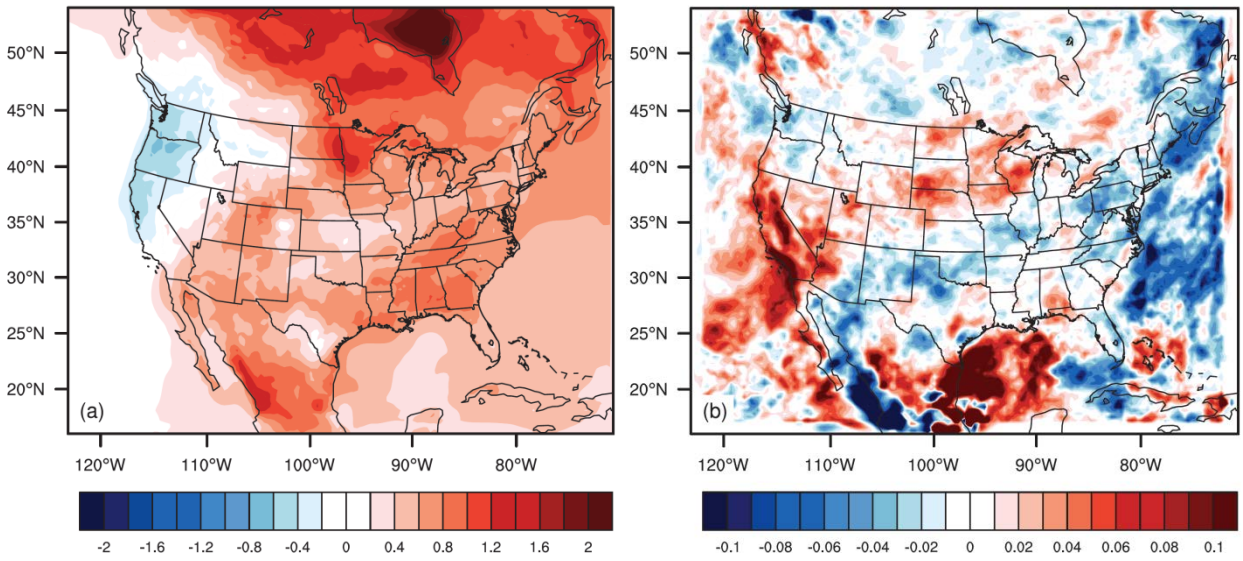

Fig. 2. 1. Changes in (a) 2-m temperature (°C) and (b) precipitation (mm day^{-1}) centered on 2050 between RCP8.5 and RCP4.5 (RCP8.5—RCP4.5).

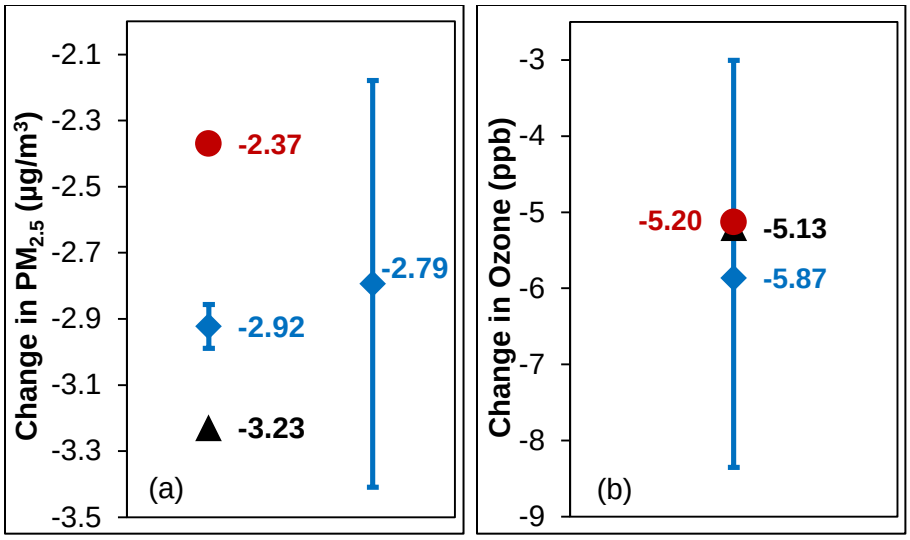

Fig. 2. 2. Comparison of annual U.S. average concentration changes for RCP4.5 in 2050 relative to 2000, for this study (black triangle), MZ4 from WEST2013 (red circle), and the ensemble mean (blue diamond) and multi-model range from ACCMIP (blue lines), for (a) $PM_{2.5}$, and (b) O_3. In panel a, the total $PM_{2.5}$ reported by the ACCMIP models is shown on the left, and the $PM_{2.5}$ estimated as a sum of species BC+OA+SOA+SO_4+NO_3+NH_4+0.25*SeaSalt+0.1*Dust following Fiore et al. (2012) and Silva et al. (2013) shown on the right. Values shown are the average of three years for CMAQ and MZ4, and 5 to 10 years for ACCMIP for three models (LMDzORINCA, GFDL-AM3 and GISS-E2-R) that report O_3 and two models (GFDL-AM3 and GISS-E2-R) that report $PM_{2.5}$.

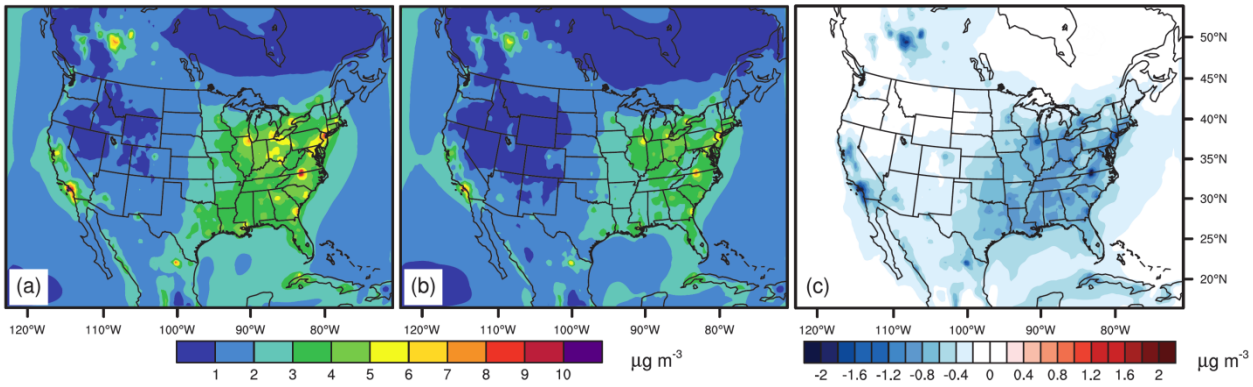

Fig. 2. 3. The three-year average $PM_{2.5}$ (μg m^{-3}) distributions in 2050 from (a) S_REF, (b) S_RCP45, and (c) the total co-benefits (shown as the difference between S_RCP45 and S_REF). Blue colors in panel (c) indicate an air quality improvement.

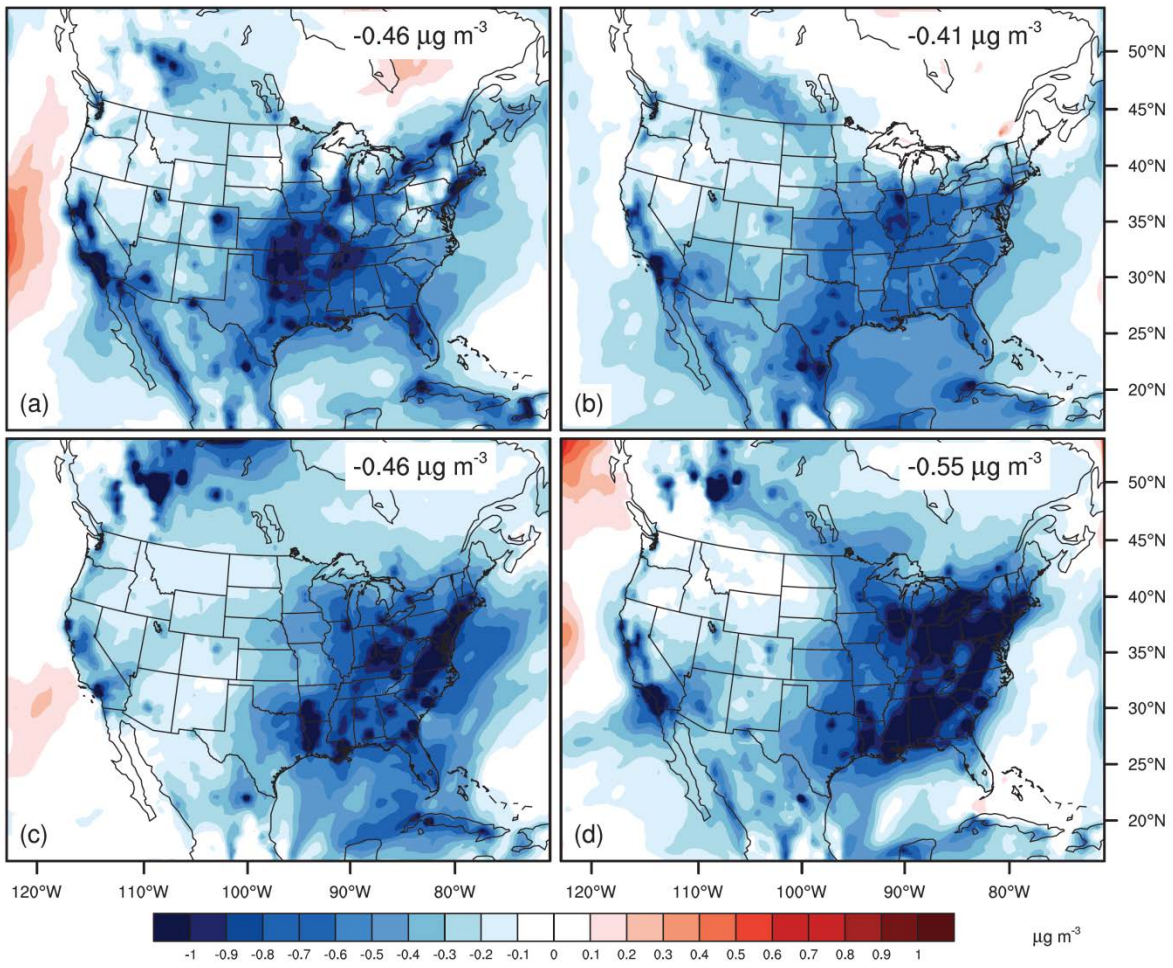

Fig. 2. 4. Seasonal distributions of total co-benefits for $PM_{2.5}$ (µg m^{-3}) for (a) winter, (b) spring, (c) summer and (d) fall.

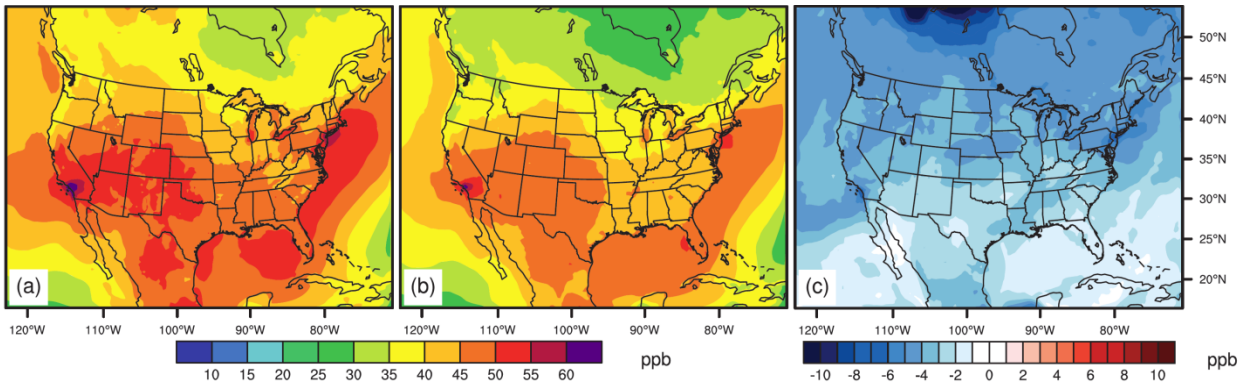

Fig. 2. 5. The three-year ozone-season average (May to October) of MDA8 O_3 (ppb) from (a) S_ REF, (b) S_ RCP45, and (c) the total co-benefits (shown as the difference between S_RCP45 and S_REF). Blue colors in panel (c) indicate an air quality improvement.

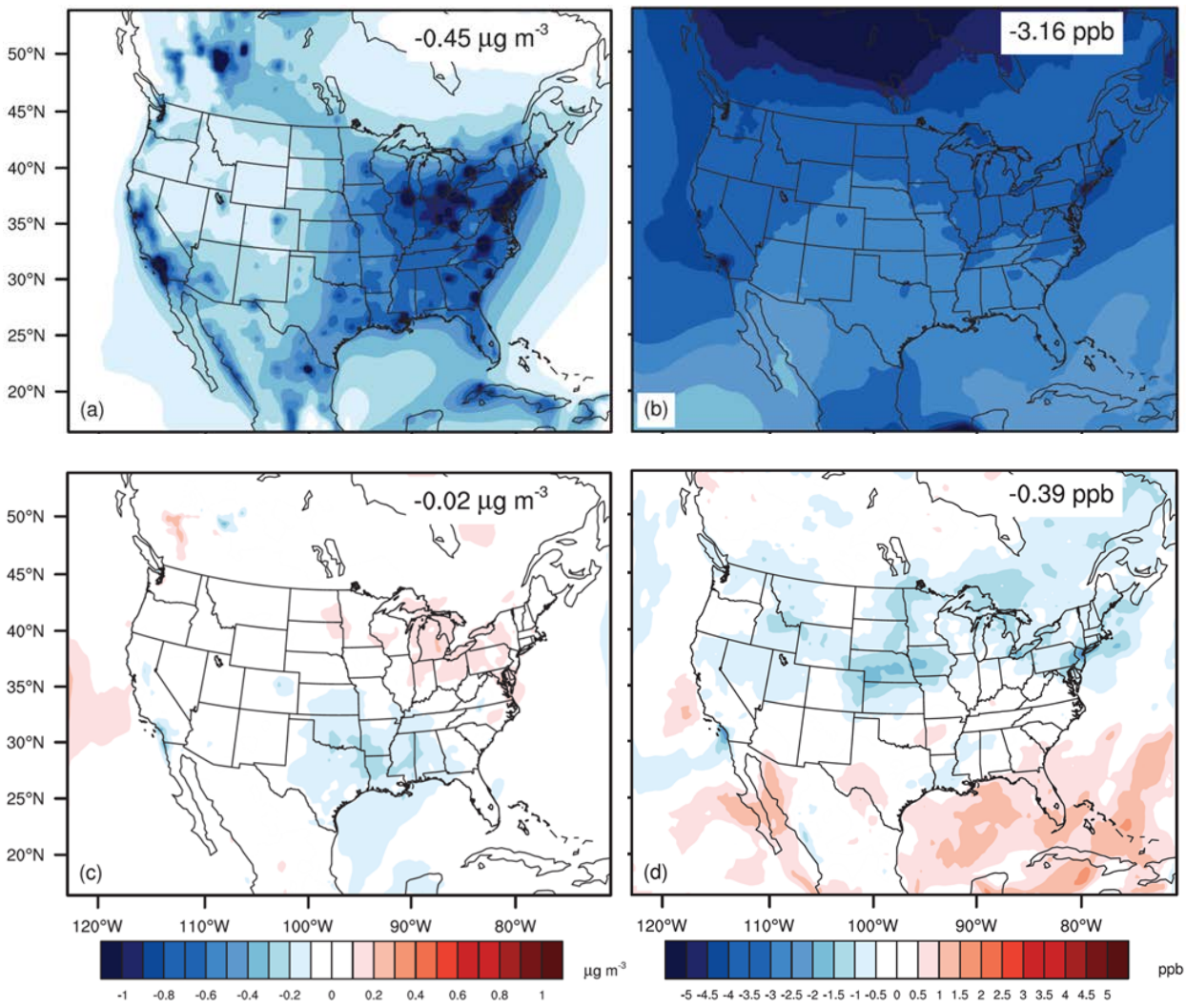

Fig. 2. 6. Benefits of reduced co-emitted air pollutants (a, b) versus slowing climate change (c, d) for $PM_{2.5}$ (a, c) and ozone season MDA8 surface O_3 (b, d). Blue colors indicate an air quality improvement. The numbers on the plots are three-year average of air quality changes over the U.S.

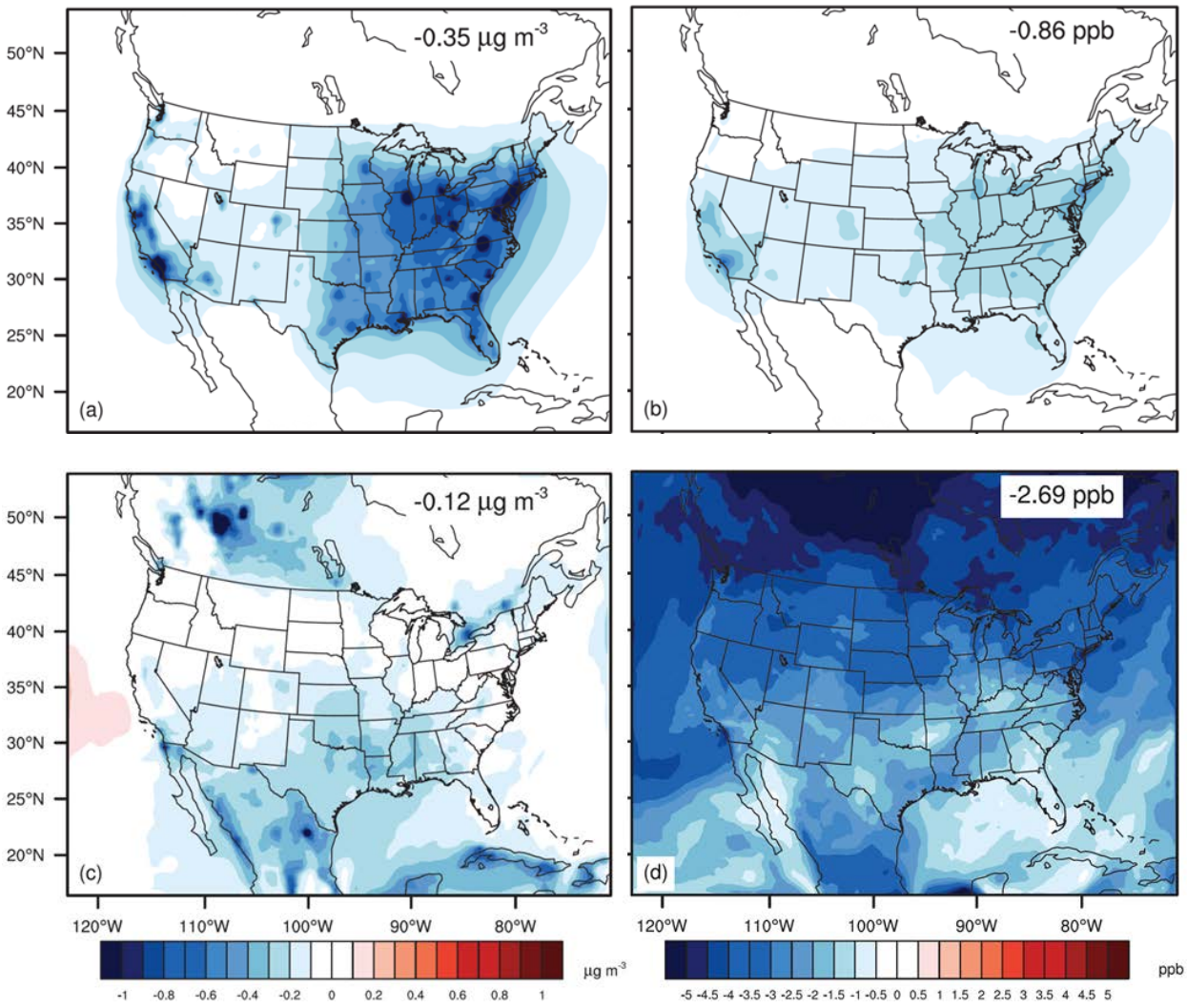

Fig. 2. 7. Benefits of domestic (a, b) versus foreign (c, d) GHG reductions for $PM_{2.5}$ (a, c) and ozone season MDA8 surface O_3 (b, d). Blue colors indicate an air quality improvement. The numbers on the plots are three-year average of air quality changes over the U.S.

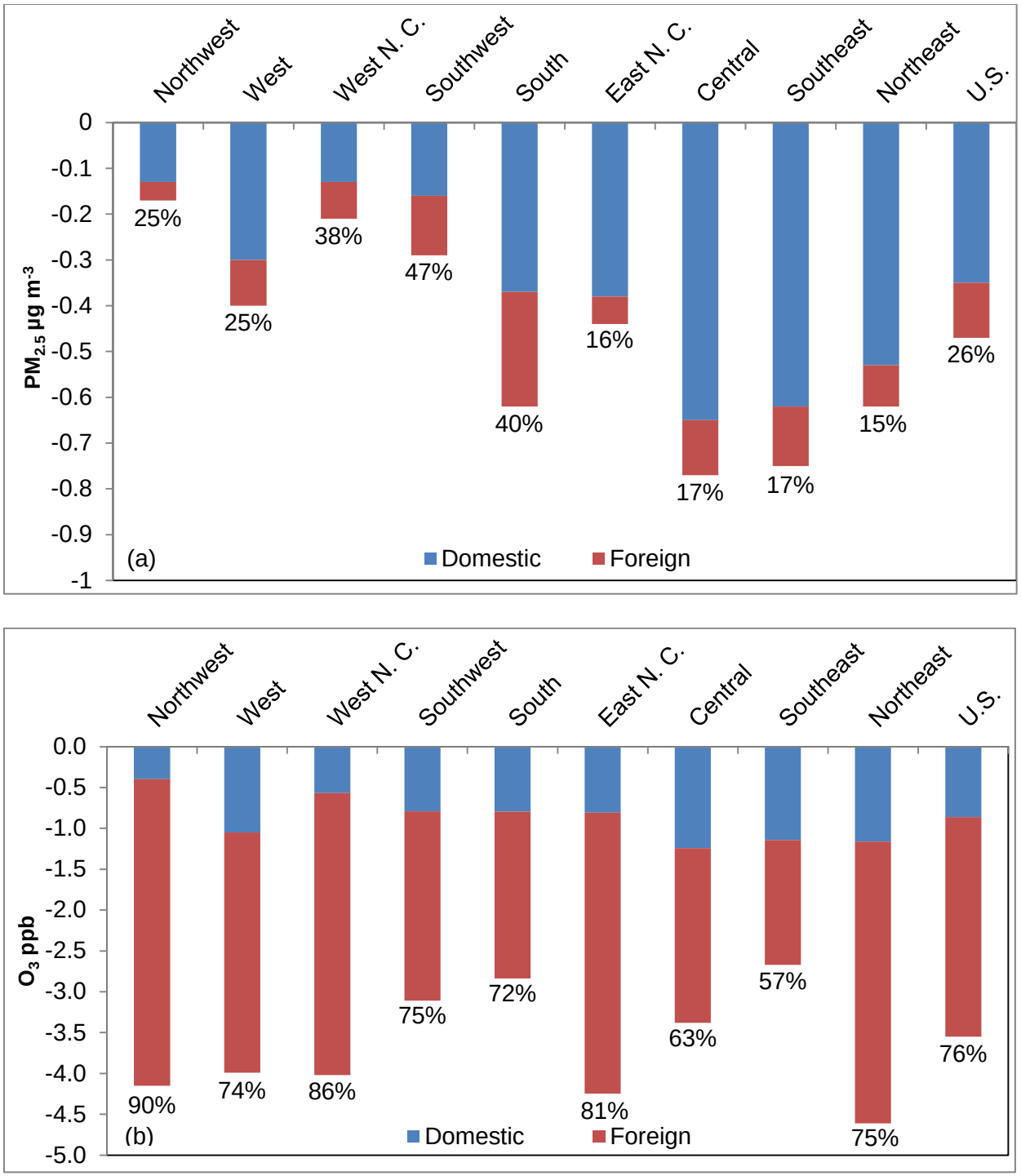

Fig. 2. 8. Mean values of domestic (blue) and foreign co-benefits (red) for U.S. average (a) annual $PM_{2.5}$, and (b) ozone season MDA8 O_3. The numbers below each bar are the percentage (%) of the foreign co-benefit.

CHAPTER 3. CO-BENEFITS OF GLOBAL, DOMESTIC, AND SECTORAL GREENHOUSE GAS MITIGATION ON US AIR POLLUTION AND HUMAN HEALTH IN 2050

(Yuqiang Zhang, Steven J. Smith, J. Jason West. In preparation for submission to ***Environmental Research Letter***)

3.1 Introduction

Exposure to fine particulate matter ($PM_{2.5}$) and ozone (O_3) are associated with both morbidity (e.g. hospitalizations, emergency department visits, school loss days and asthma-related health effects) and premature mortality (e.g. deaths from cardiovascular and respiratory diseases, lung cancer and so on), as revealed in epidemiological studies (US EPA, 2009, 2013). Several cohort studies have shown evidence of the $PM_{2.5}$ chronic effects on mortality (Laden et al., 2006; Krewski et al., 2009; Lepeule et al., 2012). One report from Jerrett et al. (2009) demonstrated the chronic effect of O_3 on human mortality.

Previous research has quantified future air quality changes and their effects on human health under projected emission scenarios, at both global (West et al., 2007; Selin et al., 2009) and regional scales (Fann et al., 2013; Kim et al., 2014; Jiang et al., 2015; Sun et al., 2015). Climate change can also affect air quality through several mechanisms, including photochemical reactions, natural emissions, deposition rates, and air stagnation events (Weaver et al., 2009; Jacob and Winner, 2009; Fiore et al., 2012, 2015). Related studies have quantified the effect of global and regional climate change on air quality and human health (Bell et al., 2007; Tagaris et al., 2009; Post et al., 2012; Fang et al., 2013; Fann et al., 2015; Silva et al., 2016a). Post et al.

(2012) used an ensemble of atmospheric models to study the future climate change in 2050 on the influence of air quality and human health effect in the US and found significant variability from the different models.

Many studies have also investigated the co-benefits of greenhouse gas (GHG) mitigation on air quality and avoided premature mortality, as actions to reduce GHG emissions also tend to reduce co-emitted air pollutants (Bell et al., 2008; Cifuentes et al., 2001; Nemet et al., 2010). When monetized, the health co-benefits of GHG mitigation were found to range across the literature from \$2 to 196/tCO_2 (Nemet et al., 2010), comparable to the costs of GHG reductions. A few studies also analyzed the regional (Driscoll et al., 2015; Thompson et al., 2014; Trail et al., 2015) or local (Plachinski et al., 2014) GHG mitigation on projected co-benefits of future air quality and human health using systemic methods. Thompson et al. (2014) studied the co-benefits from different climate policies in the U.S. on future domestic air quality by 2030. When monetized, the human health benefits due to improved air quality can offset 26-1050% of the cost of the carbon polices.

Previous co-benefits studies have been limited by only considering co-benefits from regional or local climate policies on regional air quality and human health, neglecting (i.) the co-benefits of those actions for other nations or regions, and (ii.) the co-benefits gained domestically from global actions where one country's actions are coordinated with reductions internationally. Both $PM_{2.5}$ and O_3 have long enough lifetimes in the atmosphere to transport intercontinentally, suggesting that emissions from one source region can affect air quality and human health on multiple receptor regions (Anenberg et al., 2009, 2014; Liu et al., 2009; TF HTAP 2010). Previous studies found that the health benefits from O_3 precursor reductions may even be greater outside of the source region than within, due the large population over several receptor regions

(Duncan et al., 2008; Anenberg et al., 2009; West et al., 2009). $PM_{2.5}$ has a much shorter lifetime than O_3, but the intercontinental transport of $PM_{2.5}$ mortality impacts is very large or comparable than ozone due the strong health impacts related with $PM_{2.5}$ (Anenberg et al., 2014). To address these limitations, West et al. (2013, referred to as WEST2013 hereafter) were the first to use a global chemical transport model (CTM) to address the co-benefits of global GHG mitigation on air quality and human health. WEST2013 were also the first to estimate co-benefits via two mechanisms: the reduced co-emitted air pollutants, and slowing climate change and its effects on air quality. They found that global GHG mitigation could avoid 2.2±0.8 million premature deaths in 2100 due to the improved air quality, accounting for both $PM_{2.5}$ and O_3. The co-benefits from the first mechanism of the reduced co-emitted air pollutants are much higher than those from the second mechanism of slowing climate change and its effect on air quality. The monetized co-benefits from health were estimated at \$50–380/tCO_2, higher than previous estimates (Nemet et al., 2010).

WEST2013 was limited by using a coarse resolution global model (horizontally 2˚×2.5˚). We then used several models to downscale the global co-benefits results in WEST2013 to the regional scale, analyzing co-benefits for US air quality in 2050 at much finer resolution (Zhang et al., 2016a). Here we use the same simulations performed in Zhang et al., (2016a) and focus on quantifying the co-benefits of global GHG reductions for avoided air pollution-related mortality in the continental US in 2050. We study the total co-benefits through the two mechanisms, following WEST2013 (WEST2013 and Zhang et al., 2016a), and separate the co-benefits of GHG mitigation in the US versus the contributions from foreign countries. By embedding this study within the previous global study of WEST2013, we are the first to investigate the co-benefits of foreign GHG mitigation for US air quality and human health. Previous studies have

also investigated the sectoral-related premature deaths both globally (Lelieveld et al., 2015; Morita et al., 2014; Silva et al., 2016b) and regionally (Caiazzo et al., 2013; Fann et al., 2012, 2013; Yim et al., 2015). Here, we conduct three new sensitivity simulations to quantify the air quality and health co-benefits of GHG reductions in three US domestic emission sectors: industry (IND), residential (RES) and energy (ENE).

3.2 Methods

3.2.1 Air quality changes in US in 2050 at fine scale

Air quality changes in the US under different GHG mitigation polices in 2050 were downscaled from WEST2013 by Zhang et al., (2016A). First, the global climate in 2000 and 2050 from the Representative Concentration Pathway 8.5 (RCP8.5) and RCP4.5 scenarios used by WEST2013 were dynamically downscaled to the regional scale for the Continental US (CONUS) domain at 36km×36km, using the Weather Research Forecast model (WRF, v3.4.1, Skamarock and Klemp, 2008). Physical configurations of WRF were adopted from Bowden et al. (2012, 2013), and to avoid large persistent bias inside WRF when downscaling, the spectral nudging technique was used (Bowden et al., 2013). Global anthropogenic emissions from RCP4.5 and its reference (REF) scenario were directly processed through Sparse Matrix Operator Kernel Emissions (SMOKE, v3.5). Dynamical chemical boundary conditions were acquired from the global CTM outputs of WEST2013. The Community Multiscale Air Quality model (CMAQ, v5.0.1, Byun and Schere, 2006), with the CB05 chemical mechanism with updated toluene reactions and the latest aerosol module (AE6), was used to simulate air pollutant concentrations (i.e., $PM_{2.5}$ and O_3) in 2000 and 2050. Most of the simulations used in this study (Table B.1) were completed by Zhang et al. (2016a), except for three new sensitivity simulations performed here to quantify the co-benefits of GHG mitigation from domestic emission sectors in

US. All simulations are run for 40 consecutive months, with four months as spin-up, and the results are presented as three-year averages.

As discussed by WEST2013 and Zhang et al., (2016a), RCP4.5 was developed based upon REF, with the only difference between these two scenarios being the application of an aggressive global carbon policy spanning all world regions and emission sectors (Thomson et al., 2011). By comparing these two, we use self-consistent scenarios. The total co-benefits from global GHG mitigation are obtained by comparing scenarios S_RCP45 and S_REF (Table B.1). To separate the total co-benefits from the two mechanisms, we use S_Emis minus S_REF to give the co-benefits from co-emitted air pollutants reduction only, and S_RCP45 minus S_Emis for the co-benefits from slowing climate change only. Domestic co-benefits are estimated as S_Dom minus S_REF, and foreign co-benefits are S_RCP45 minus S_Dom. In addition we simulate three more scenarios to identify the co-benefits from actions to reduce GHG emissions in individual sectors domestically. We choose to simulate reductions in the industry, residential, and energy sectors (S_indUS, S_resUS and S_eneUS) because emission reductions in RCP4.5 are greatest from these sectors in the US. Although ground transportation is the largest contributor for most air pollutants in the US in 2000 and 2050, we did not select transportation as little GHG reductions are seen from this sector in 2050. The air pollutants emission reductions from these three sectors account for more than 98% of the total SO_2 and NO_x reductions between RCP4.5 and REF in US in 2050, 80% of the CO reductions, and more than 50% of the EC and OC reductions (Table B.3).

3.2.2 Human health analysis

We use the environmental Benefits Mapping and Analysis Program–Community Edition (BenMAP-CE, v1.08) (US EPA**,** 2014) to calculate the avoided human mortality associated with future surface air quality changes for both $PM_{2.5}$ and O_3. BenMAP-CE calculates the relationship

between air pollution and certain health effects, using a health impact function (HIF) from epidemiological studies. The HIF for both $PM_{2.5}$ and O_3 used in this study are based on a log-linear relationship between relative risk (RR) and air pollutant concentrations defined by epidemiology studies (Jerrett et al., 2009, Krewski et al., 2009), which are also used by WEST2013. RR then is used to calculate attributable fraction (AF), the fraction of the disease burden attributable to the risk factor, which is defined as:

$$AF = \frac{RR-1}{RR} = 1 - \exp^{-\beta\Delta x} \quad (1)$$

Where β is the concentration–response factor (CRF; i.e., the estimated slope of the log-linear relation between concentration and mortality) and ΔX is the change in concentration of an air pollutant. AF is multiplied by the baseline mortality rate (y_0), and the exposed population (Pop) to yield an estimate of excess deaths attributable to changes in air pollution ($\Delta Mort$):

$$\Delta Mort = y_0 \times (1 - \exp^{-\beta\Delta x}) \times Pop \quad (2)$$

We present results for all-cause mortality from the $PM_{2.5}$ changes, rather than CPD and LC, as all-cause mortality is the most comprehensive estimate of PM-related mortality appropriate for the US. However, we also estimate the PM-related mortality from CPD and LC to compare with the results of WEST2013. We also quantify the premature mortality from respiratory disease associated with O_3 changes. The 90% confidence intervals (CI) presented in this study are calculated using a full Monte-Carlo analysis inside BenMAP-CE considering only uncertainty in the concentration-response function.

BenMAP-CE has incorporated county-level baseline mortality rates projected from 2010 to 2050 at five-year intervals, including respiratory disease (RESP) for O_3, and all-cause, cardiopulmonary disease (CPD), and lung cancer (LC) for $PM_{2.5}$ (RTI International, 2015).

Overall, the projected baseline mortality rates inside BenMAP-CE decrease from 2005 to 2050. However, the baseline mortality rates used by WEST2013 are projected to increase in 2050 in US, which are derived from the International Futures (IFs, version 6.54) under the UNEPGEO Base Case scenario. For population, BenMAP-CE included the future population projection at a county level in the US until 2040 only (totalling 403 million, Woods and Poole, 2012), but our study is focused on 2050 (the RCP4.5 projected total population is 384 million in 2050, Clark et al., 2007). To be consistent with WEST2013, we run BenMAP-CE with baseline mortality rates in 2005 and the population projection in 2040 (aged 30 and above), and then post-process the BenMAP-CE outputs by multiplying by adjustment ratios to match the national population and baseline rates of WEST2013 (Table B.2). By doing this, we assume that future baseline mortality rates are increasing at uniformly national ratio without age, gender or ethnic variations, and also that the spatial distribution of population in 2050 of RCP4.5 is the same as that in 2040 projected by Woods and Poole (2012).

3.3. Results and discussion

The total co-benefits for annual $PM_{2.5}$ (0.47 μg m^{-3} for three-year US averages) are greatest in the East and in the west coast of California (CA), and less in the West (Fig. 3.1). For O_3, we calculate the three-year averages of 6-month ozone-season average of 1-hr daily maximum of O_3, to be consistent with the epidemiology study of Jerrett et al. (2009), and the total co-benefits for O_3 (2.96 ppbv for US average) are fairly uniform over the US domain (Fig. 3.1), slightly higher over Western U.S. and lower over the East. The population-weighted average (Pop-Weighted Avg, for the future exposed population age 30 and older) for $PM_{2.5}$ (0.84 μg m^{-3} for US average) is almost twice the simple average (Simple Avg), as the shorter lifetime of $PM_{2.5}$ has lead it to be a regional problem (Punger and West, 2013). but these two indexes are nearly identical for O_3

(Table 3.1), consistent with the fact that the total co-benefits for O_3 are less significant in East populated areas and more significant in the West, controversy with $PM_{2.5}$.

When calculating human health benefits, our results show that 24500 (90% CI: 17800-31100) premature deaths yr^{-1} will be avoided in the US due to $PM_{2.5}$ decreases in 2050 from the global GHG mitigation. The highest states are CA (3800 deaths yr^{-1}, CI:2800-4900), New York (NY, 2100 deaths yr^{-1}, CI:1500-2600) and Texas (TX, 1800 deaths yr^{-1}, CI:1300-2300), which all have large $PM_{2.5}$ decreases (Fig. 3.1, Table B.4) and population. For O_3, the total avoided deaths are 12200 deaths yr^{-1} in the US (CI:5400-18900), roughly half that from $PM_{2.5}$, and also highest in CA (2200 deaths yr^{-1}, CI:1000-3300), NY(800 deaths yr^{-1}, CI:400-1200) and TX (700 deaths yr^{-1}, CI:300-1100). We then quantify the human health co-benefits by calculating the avoided mortality per capita (MPC, the avoided deaths per million people age 30 and older) for both $PM_{2.5}$ and O_3 (Fig. B.1, Table B.4). The MPC for $PM_{2.5}$ has larger spatial variations than for O_3, consistent with the finding that the total concentration co-benefits for $PM_{2.5}$ are more urban-centred, and more spatially uniform for O_3 (Fig. 3.1).

We compare the avoided deaths from 2000 to 2050 under the REF (S_REF-S_2000) and RCP4.5 (S_RCP45-S_2000) scenarios in this study with WEST2013, and also the total co-benefits (S_RCP45-S_REF). Zhang et al., (2016a) concluded that the total co-benefits for $PM_{2.5}$ at finer resolution (36km×36km) in CMAQ were lower than those of WEST2013 at coarse resolution (2˚×2.5˚) by a factor of 2, while the downscaled future O_3 changes in 2050 were comparable with WEST2013. However, when quantifying human health impact, Fig. 3.3 shows that the avoided premature mortality for both the REF and RCP4.5 scenarios as well as the total co-benefits in this study are much higher than for WEST2013 for both $PM_{2.5}$ and O_3. The avoided premature mortality from WEST 2013 is within the 90% CI of the estimation in this

study, except for CPD in both REF and RCP4.5 scenarios, and RESP in REF. These discrepancies could be caused by the fact that the finer-resolution CMAQ model can better capture the hotspots of future air quality changes near areas of dense population (Fig. 3.1), whereas the coarse resolution of WEST2013 can dilute peak air quality concentrations that usually occur in populated regions (Punger and West, 2013; Li et al., 2015). Our study shares the same CRF as WEST2013, and the underestimation in WEST2013 is largely attributed to the county-level baseline mortality rates used in this study, less extent to the county-level population data embedded in BenMAP-CE as the total co-benefits of the Pop-Weighted Avg for both $PM_{2.5}$ (1.25 μg m^{-3}) and O_3 (4.61 ppbv) in WEST2013 are higher than those in this study.

We then separate the total co-benefits into the two mechanisms. The emission benefit accounts for 98% of the total co-benefits (three-year Pop-Weighted Avg of 0.84 μg m^{-3}, Table 3.1) for $PM_{2.5}$, and 96% of the total (three-year Pop-Weighted Avg of 3.02 ppb) for O_3, consistent with WEST2013 and Zhang et al. (2016a). When calculating the co-benefits on human health, the co-benefits from reduction in co-emitted air pollutants also dominate the total co-benefits, with 24100 deaths yr^{-1} (CI, 17500-30600) avoided deaths for $PM_{2.5}$ (accounting for 98% of the total), and 11500 deaths yr^{-1} (CI, 5100-17800) for O_3 (94% of the total) (Fig. 3.4). Notice that some locations have negative climate co-benefits (Fig. 3.4c,d), e.g. in the Northern states for $PM_{2.5}$, and Southeast for O_3, as $PM_{2.5}$ and O_3 increase due to slowing climate change causing more deaths over these regions. However, as pointed out in previous studies (Post et al., 2012; Silva et al., 2013), single model to predict past and future climate change is unreliable and can have significant uncertainties.

GHG reductions from foreign countries account for 3700 avoided deaths yr^{-1} (CI, 2700-4700) for $PM_{2.5}$-related all-cause mortality, and 7600 deaths yr^{-1} (CI, 2700-4700) deaths for O_3-

related RESP, which are 15% and 62% of the total deaths for $PM_{2.5}$ and O_3. Foreign GHG mitigation contributes 15% (0.13 μg m^{-3} for three-year Pop-Weighted Avg) of the total co-benefits for the $PM_{2.5}$ national annual average, and accounts for 65% (1.95 ppbv) of the total co-benefits for O_3 (6-month ozone season of 1-hr daily maximum), emphasizing that the $PM_{2.5}$ is more influenced by the regional emission reductions in US, while O_3 is more influenced by the global methane reductions as well as the intercontinental transport of air pollutants (Zhang et al., 2016a). The foreign co-benefits for both $PM_{2.5}$- and O_3-related mortality are centred in urban areas even though foreign countries' GHG mitigation reduce surface O_3 pretty uniformly in US (Fig. B.2). The contributions from domestic GHG mitigation on Pop-Weighted Avg of $PM_{2.5}$ (85% of the total) and O_3 (35%) are higher than those for Simple Avg (74% for $PM_{2.5}$ and 27% for O_3 in Table 3.1), due to the fact that the air quality improvement from domestic GHG mitigation happen in the dense population areas. CA has the highest human health benefits from foreign countries GHG mitigation, with 700 deaths yr^{-1} (CI, 500-800) avoided from $PM_{2.5}$-related all-cause mortality, and 1300 deaths yr^{-1} (CI, 600-2000) avoided from O_3 (for the domestic and foreign co-benefits in each state, see Tables B.5, B.6).

For the co-benefits from domestic sectoral GHG reductions, the residential sector has the largest co-benefits on $PM_{2.5}$-related human health, avoiding 4300 deaths yr^{-1} (3200-5500), accounting for 21% of the total domestic co-benefits for $PM_{2.5}$, followed by industry (3300 deaths yr^{-1}, CI:2400-4100) and energy (2700 deaths yr^{-1}, CI:900-3400). Residential also has the largest decrease of Pop-Weighted Avg of annual $PM_{2.5}$, with 0.15 μg m^{-3} for the US average, even though the simple annual average is comparable to the effect from the industry sector, demonstrating that dense populations around the residential sector. GHG mitigation from industry has the largest effect on O_3-related human health, which avoids 800 deaths yr^{-1} (300-

1200), accounting for 17% of the total domestic co-benefits for O_3, followed by energy (500 deaths yr^{-1}, CI:200-800), and residential (200 deaths yr^{-1}, CI:100-400). The total co-benefits for air quality are also highest in industry, with 0.20 ppb for the Pop-Weighted Avg and 0.22 ppv for Simple Avg. The emission reductions from these three sectors account for 50% of the $PM_{2.5}$-related deaths from domestic co-benefits (20800 deaths yr^{-1}), and 33% of the O_3-related deaths in domestic co-benefits (4600 deaths yr^{-1}).

3.4 Conclusions

We quantify the co-benefits of global GHG mitigation under the RCP4.5 scenario on US air quality and human health in 2050 at fine resolution by using dynamical downscaling techniques, and find that more than 24500 deaths yr^{-1} will be avoided for $PM_{2.5}$-related all-cause mortality and 12200 deaths yr^{-1} will be avoided for O_3-related respiratory mortality. When separating the total co-benefits into two mechanisms, the emission co-benefits are more significant than the climate co-benefits for both $PM_{2.5}$ and O_3, accounting for 98% and 94% of the total avoided deaths. Foreign GHG mitigation contributes to 15% of total $PM_{2.5}$-related deaths and 62% of the total O_3-related deaths. Among the three domestic emission sectors which have higher reductions for the co-emitted air pollutants under the RCP4.5 scenario, RES has the highest co-benefits for $PM_{2.5}$-related mortality, leading to 4300 avoided deaths, and IND has the highest co-benefits for O_3, avoiding 800 premature deaths in US.

Previous studies have estimated co-benefits of GHG mitigation mainly on local, national, or continental scales (Cifuentes et al., 2001; Nemet et al., 2010). These studies have presumed that most co-benefits are realized on those scales, and that the contributions of foreign GHG mitigations to total co-benefits would be small. Here we show that the US can gain significantly greater co-benefits for air quality and human health, especially for ozone, by collaborating with

other countries to combat global climate change. Similar results would also be expected for foreign countries, which will likely also benefit from GHG mitigation in other countries. Previous studies which only estimate co-benefits from regional or local GHG mitigation may significantly underestimate the full co-benefits of coordinated global actions to mitigate climate.

Significant uncertainties exist in our results. The uncertainty in CRFs can exert a large influence on the magnitudes of the human health co-benefits. When quantifying the avoided deaths from improved air quality, we only account for adults above 30s. Large uncertainty also arises from the global emission inventory, especially when we downscaled the inventory from coarse resolution to fine resolution, and add new inorganic species for the primary $PM_{2.5}$. Different components of $PM_{2.5}$ may have different risk on human health, like BC particles (Li et al., 2015; Zanobetti and Schwartz, 2009). However, we consider all of the components of $PM_{2.5}$ to have equal toxicity. Only a single model (e.g., WRF, CMAQ) is used for each downscaling step, and ensemble model means could reduce the errors raised from one single model (Post et al., 2012). Our conclusions are specific to the REF and GHG mitigation (RCP4.5) scenarios we choose, and would differ for other scenarios. We only account for the co-benefits from air quality changes due to the GHG mitigation, neglecting other impacts of climate change on health, like heat-waves and infectious disease, for which we may also underestimate the health benefits of the global climate policy.

3.5 Figures and Tables

Table 3. 1. Co-benefits for air quality changes in the US in 2050 from global, domestic and sectoral GHG mitigation. For $PM_{2.5}$ (μg m^{-3}) we use three-year averages, and for O_3 (ppbv), we calculate the 6-month ozone season of 1-hr daily maximum, and then average over three years.

		$PM_{2.5}$		O_3	
		Simple Avg	Pop-Weighted Avg	Simple Avg	Pop-Weighted Avg
Total	Emission	-0.45	-0.82	-2.75	-2.89
	Climate	-0.02	-0.02	-0.21	-0.13
		-0.47	**-0.84**	**-2.96**	**-3.02**
	Domestic	-0.35	-0.71	-0.80	-1.07
	Foreign	-0.12	-0.13	-2.16	-1.95
Domestic	Industry	-0.057	-0.11	-0.22	-0.20
	Residential	-0.058	-0.15	-0.11	-0.058
	Energy	-0.046	-0.089	-0.13	-0.14

Table 3. 2. Estimated total co-benefits for avoided premature mortality in 2050 from $PM_{2.5}$-related all-cause mortality and O_3-related respiratory mortality. The values in the brackets are 90% confidence intervals (CI).

		$PM_{2.5}$ (90% CI)	O_3 (90% CI)
Total	Emission	24100 (17500-30600)	11500 (5100-17800)
	Climate	400 (300-500)	700 (300-1100)
		24500 (17800-31100)	**12200 (5400-18900)**
	Domestic	20800 (15100-26400)	4600 (2000-7100)
	Foreign	3700 (2700-4700)	7600 (3400-11900)
Domestic	Industry	3300 (2400-4100)	800 (300-1200)
	Residential	4300 (3200-5500)	200 (100-400)
	Energy	2700 (1900-3400)	500 (200-800)

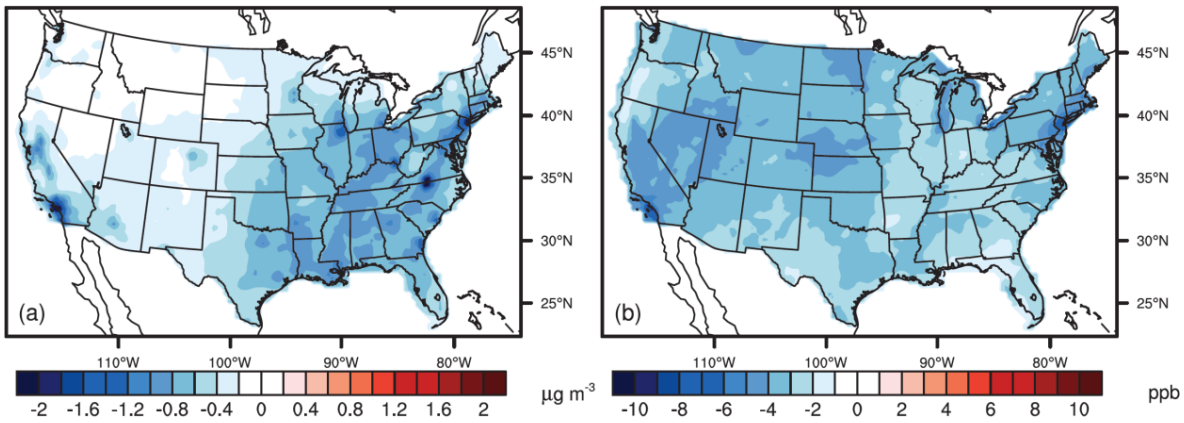

Fig. 3. 1. Total air quality co-benefits in 2050 for (a) annual average $PM_{2.5}$, and (b) 6-month ozone-season average of 1-hr daily maximum of O_3. Results are presented as three-year averages.

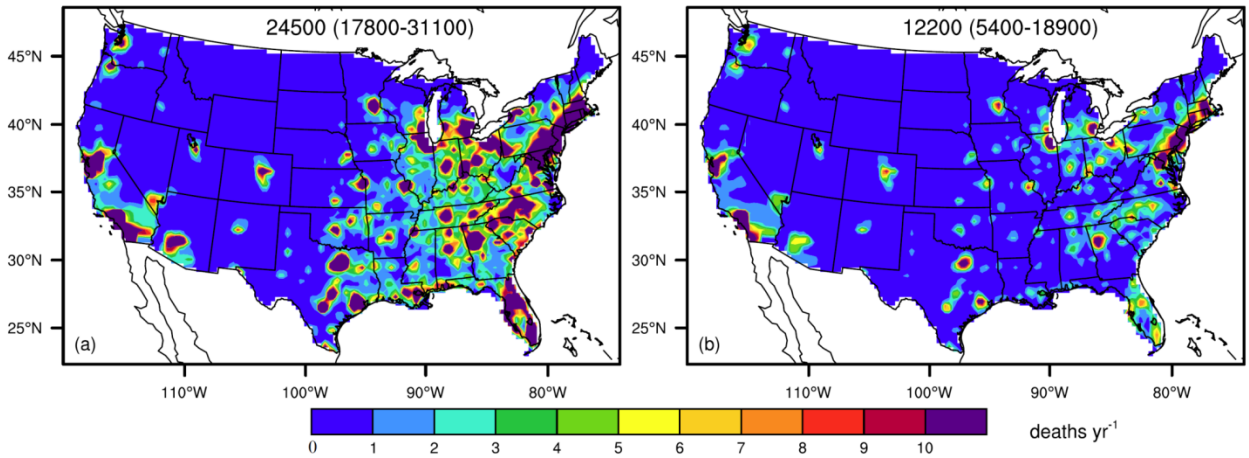

Fig. 3. 2. Total co-benefits (S_RCP45-S_REF) for avoided premature mortality (deaths yr^{-1}) for (a) $PM_{2.5}$ (all-cause mortality), and (b) O_3 (respiratory mortality) in US in 2050. Total avoided deaths and 90% confidence intervals are shown at the top of each panel.

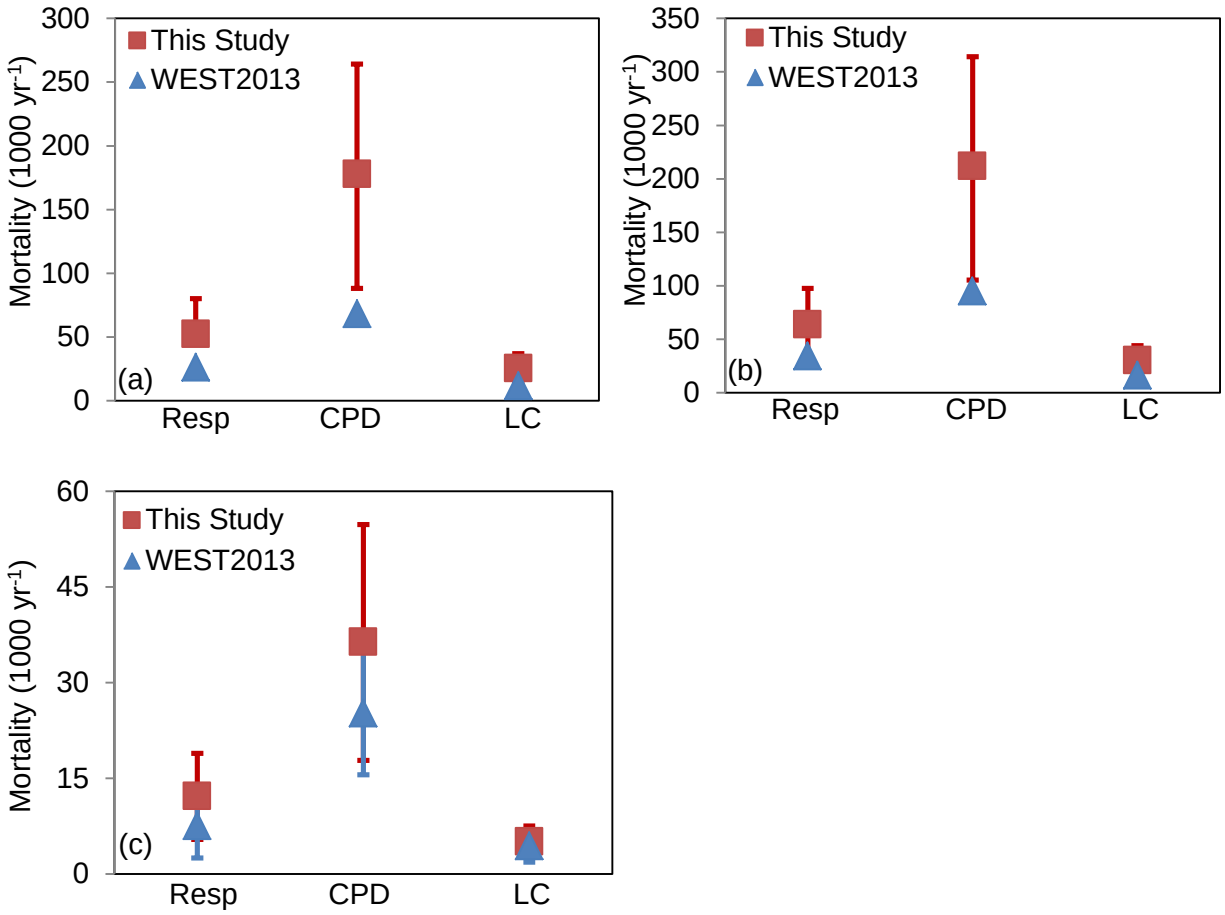

Fig. 3. 3. Comparisons between this study (red) and WEST2013 (blue) of the avoided human mortality (1000 deaths yr^{-1}) from air quality changes in 2050 compared with 2000, for (a) REF scenario, (b) RCP4.5 scenario, and (c) the total co-benefits in 2050. The red lines represent the 90% confidence intervals (CI) for this study, and blue lines are 95% CI for WEST2013. RESP indicates for the mortality from O_3-related respiratory deaths, CPD for $PM_{2.5}$-related cardiopulmonary deaths, and LC for $PM_{2.5}$-related lung cancer.

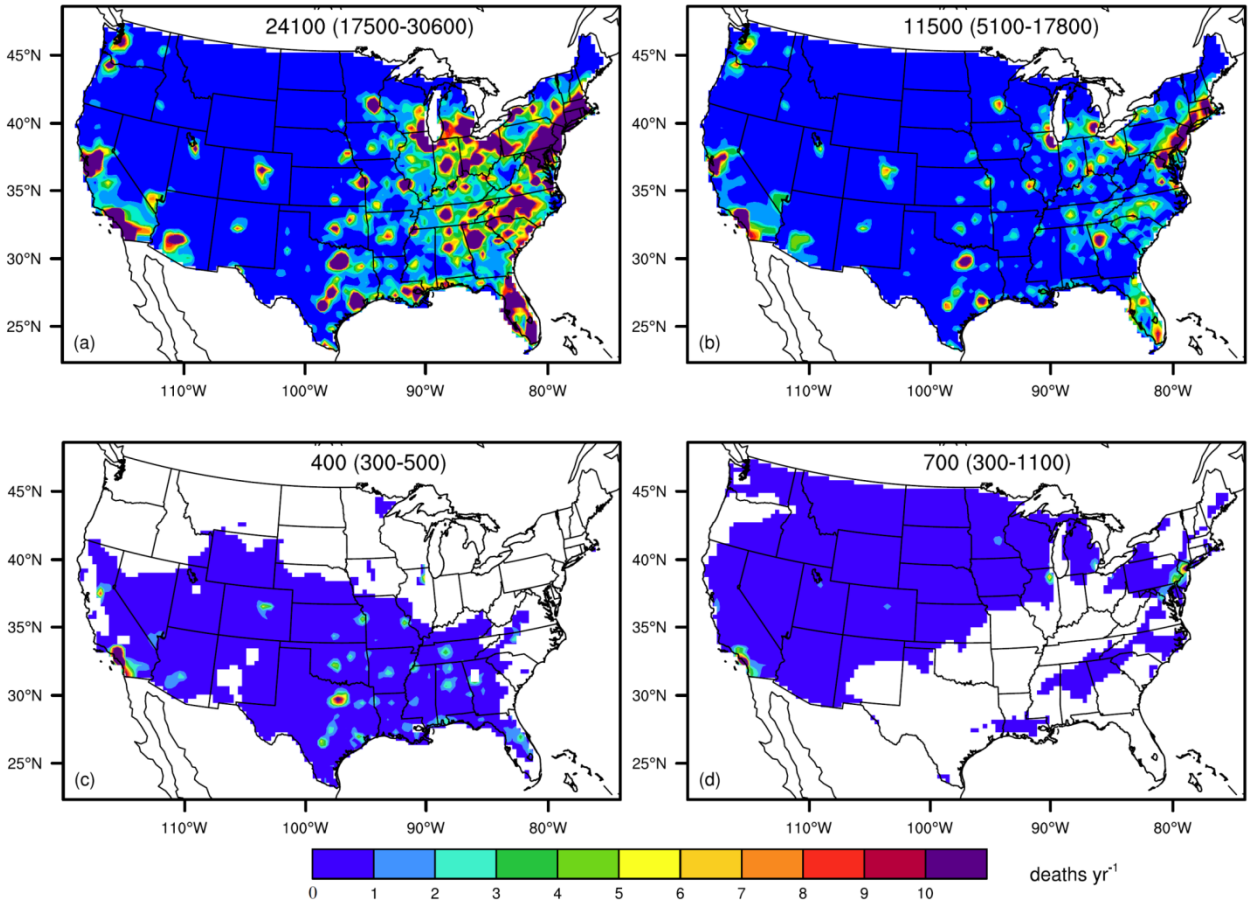

Fig. 3. 4. The emission co-benefits (a, b) and climate co-benefits (c, d) for avoided human mortality (deaths yr^{-1}) from $PM_{2.5}$ (a, c) and O_3 (b, d). White in panels c and d indicates increased mortality attributed to slowing climate change, from increases in air pollutant concentrations. Total avoided deaths and 90% confidence intervals are shown at the top of each panel.

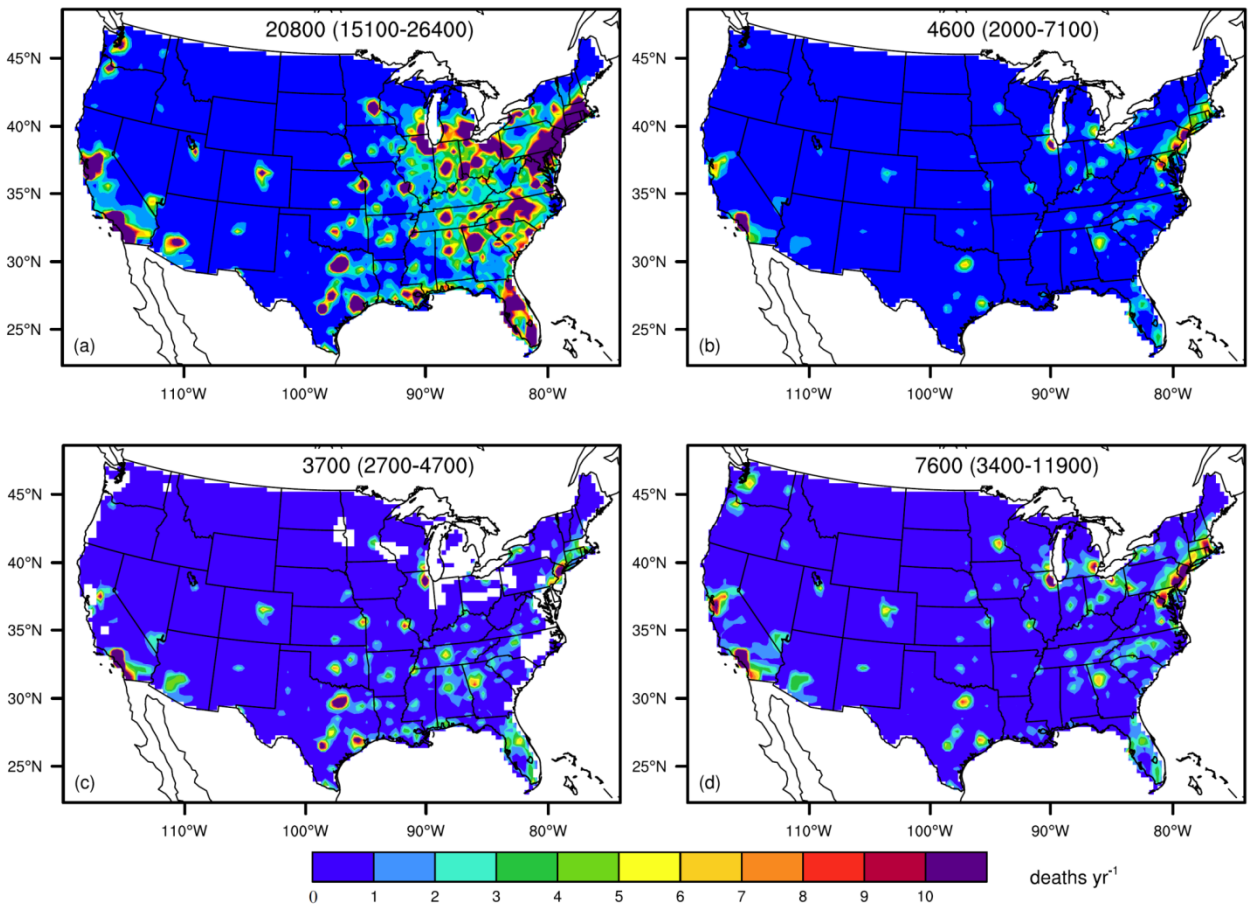

Fig. 3. 5. The domestic co-benefits (a, b) and foreign co-benefits (c, d) for avoided all-cause mortality from $PM_{2.5}$ (a, c) and respiratory mortality from O_3 (b, d) in US in 2050. Total avoided deaths and 90% confidence intervals are shown at the top of each panel.

CHAPTER 4. SOUTHWARD REDISTRIBUTION OF EMISSIONS DOMINATES THE 1980 TO 2010 TROPOSPHERIC OZONE CHANGE

(Yuqiang Zhang, Owen R. Cooper, J. Jason West. In preparation for submission to ***Nature Geoscience***)

4.1 Introduction

Ozone (O_3) at the surface is an important air pollutant, detrimental to human health and crop yield (Royal society, 2008). O_3 in the troposphere is also the third largest anthropogenic greenhouse gas, with an estimated radiative forcing (RF) of 0.40 (0.20–0.60) W m^{-2} since the preindustrial (Myhre et al., 2013). O_3 is produced in the troposphere by the chemical oxidation of carbon monoxide (CO), non-methane volatile organic compounds (NMVOCs), and methane (CH_4) in the presence of nitrogen oxides (NO_x) and sunlight, and this production exceeds the stratosphere-to-troposphere exchange by a factor of 5–7 (Young et al., 2013). Tropospheric O_3 is an important urban and regional air pollutant, but it is also sufficiently long lived (approximately 22 days globally averaged, Young et al., 2013) that its baseline concentrations are elevated over the entire Northern Hemisphere (HTAP, 2010) (NH). Observations have shown that emission increases in Asia are associated with increasing O_3 in the free troposphere above western North America (Cooper et al., 2012), and model simulations indicate that the rising Asian emissions are consistent with increasing O_3 at some high elevation sites in the western US (Cooper et al., 2015; Lin et al., 2012; Verstraeten et al., 2015). The tropospheric O_3 burden is important for RF as O_3 in the middle to upper troposphere is more effective as a greenhouse gas (Forster et al., 1997),

but also important for surface air quality because it influences the baseline ozone that affects surface sites in urban and rural settings.

In the decades prior to 1980, global anthropogenic emissions of O_3 precursors (including biomass burning) increased, but the spatial distribution pattern remained fairly unchanged, with the greatest emissions from middle and high latitudes of the NH. Starting in 1980, emissions began to shift southward as China and other nations became more industrialized. From 1980 to 2010, global anthropogenic emissions of CO, NO_x, and NMVOCs increased by 6.4% (62.1 Tg), 21.2% (14.4 Tg NO) and 6.0% (10.3 Tg) (Lamarque et al., 2010; Moss et al., 2010; Riahi et al., 2011) and the global CH_4 mixing ratio increased by 14.7% (231 ppbv, Prather et al., 2013). During the same period, emissions of CO and NMVOCs increased south of 30°N but decreased north of this latitude, while for NO_x, emissions increased south of 40°N but decreased to the north. Consequently, the latitude band with greatest emissions shifted from 30–40°N in 1980 to 20–30°N in 2010 for CO and NMVOCs, and from 40–50°N to 30–40°N for NO_x (Figs C.1 and C.2).

Modeling studies have shown that the tropospheric ozone burden and resulting radiative forcing are much more sensitive to emission changes in the tropics and Southern Hemisphere than other regions (Naik et al., 2005; Derwent et al., 2008; West et al., 2009a; Fry et al., 2012, 2014). However, the effect of the spatial redistribution of emissions has not been isolated. The emissions spatial redistribution may also be responsible for the shift in the seasonal ozone peak from summer to spring at rural Northern Hemisphere sites (Parrish et al., 2013; Cooper et al., 2014).

Here we investigate the influences of global emission changes from 1980 to 2010 on the tropospheric O_3 burden (B_{O_3}) and surface O_3, separating the influences of changes in: (i.) the

spatial distribution of ozone precursor emissions; (ii.) the global magnitude of emissions; and (iii.) the global CH_4 mixing ratio. Simulations are conducted with the CAM-chem global chemical transport model (Lamarque et al., 2012) for 1980 and 2010, and sensitivity simulations alter these three parameters individually to 1980 conditions, relative to the 2010 simulation (Table 4. 1**)**.

4.2 Methods

4.2.1 Global emissions spatial pattern change

Here we use anthropogenic emissions including biomass burning in 1980 from the Atmospheric Chemistry and Climate Model Intercomparison Project (ACCMIP, Lamarque et al., 2010), and in 2010 from the Representative Concentration Pathways 8.5 (RCP8.5) scenario (Moss et al., 2010; Riahi et al., 2011), which are downloaded from the RCP database (http://tntcat.iiasa.ac.at:8787/RcpDb/dsd?Action=htmlpage&page=download, accessed 10/31/2014) to analyze emission trends and drive the global model (Figs. C.1 and C.2). RCP8.5 2010 emissions are self-consistent with the ACCMIP 1980 emissions, and are considered to be the most reasonable scenario to extend the ACCMIP emission beyond 2000 (Granier et al., 2011). These emission trends are supported by observations from satellites that show that NO_2 in developed regions, such as Europe and North America, have greatly diminished emissions since 1980, but the emissions are increasing in developing countries, especially in China and India, shifting global emissions southward (Richter et al., 2005; van der A et al., 2008; Hilboll et al., 2013; Parrish et al., 2013). The global total anthropogenic emissions of CO, NO_x and NMVOCs are 1030 Tg, 82 Tg NO, and 180 Tg in 2010, respectively.

4.2.2 CAM-chem model configuration

We use the global chemistry-climate model CAM-chem, which is based on the global Community Atmosphere Model (CAM) version 4, the atmospheric component of the Community Earth System Model (CESM, v1.2.2) (Lamarque et al., 2012; Tilmes et al., 2015). The model has a horizontal resolution of 1.9° (latitude) × 2.5° (longitude), and 56 vertical levels between the surface and 4 hPa (≈40 km) with a time step of 1800 s. We use the NASA Global Modeling and Assimilation Office GEOS-5 meteorology to drive the model as a chemical transport model. Monthly-mean distributions of the chemically-active stratosphere species (such as O_3, NO, NO_2 and N_2O_5) are prescribed using the climatology from the WACCM simulations (Garcia et al., 2007), following Lamarque et al. (2012).

The non-methane volatile organic compound (NMVOCs) species from the ACCMIP (1980) and RCP8.5 (2010) are both re-speciated to match the CAM-chem VOC categories following previous studies (Fry et al., 2013, 2014; West et al., 2013). Monthly temporal variations for all anthropogenic emissions sectors are also added by scaling to monthly emissions from the RETRO project (Schultz et al., 2007; Fry et al., 2013, 2014; West et al., 2013), except for aircraft, shipping and biomass burning which all have their own seasonal variations. The Model of Emissions of Gases and Aerosols from Nature (MEGAN-v2.1, Guenther et al., 2012) simulates biogenic emissions for 150 compounds online within CAM-chem, yielding global biogenic emissions of isoprene, monoterpene, methanol and acetone of 420.69 Tg yr^{-1}, 133.23 Tg yr^{-1}, 91.99 Tg yr^{-1} and 42.67 Tg yr^{-1} for four years average. Lightning NO_x emissions are calculated online at 3.21 TgN yr^{-1} for four-year averages. Other natural emissions (ocean, volcano and soil) are from the standard CAM-chem emissions files (in 2000), and remain the same for all the simulations, with soil NO_x at 8.0 TgN yr^{-1} (Emmons et al., 2010; Lamarque et al., 2012). The

CH_4 volume mixing ratio (ppb) is fixed at uniform global values of 1567 and 1798 ppbv for 1980 and 2010 (Prather Annex II).

In addition to simulating 1980 and 2010, we conduct three sensitivity simulations in which the spatial pattern of global emissions (S_Distribution), the magnitude of the global emissions (S_Magnitude), and the global CH_4 mixing ratio (S_CH_4) are individually set to 1980 levels and all other parameters stay the same as the 2010 simulation (Table 4.1). The differences between S_2010 and S_1980 reflect the total emission changes from 1980 to 2010. Each of the other three simulations is subtracted from S_2010 to isolate individual influences. For all simulations, we run CAM-chem for five consecutive years, with the first-year as spin-up and results are shown as a four-year average. We use meteorology from 2009-2012 with 2008 as a spin-up for all simulations, isolating the effects of changes in emissions and neglecting possible effects of climate change from 1980 to 2010.

Tropospheric O_3 burden is defined as the total below the chemical tropopause of 150 ppbv ozone in the S_2010 simulation. The four-year averages B_{O3} in S_2010 is 342.7 Tg, within the range of ACCMIP models (337±23 Tg for 1995-2005, Young et al., 2013). The three-month ozone season average MDA8 is the consecutive three-month period with the highest O_3 in each grid cell. NO_y (total reactive nitrogen), is calculated as NO + NO_2 + NO_3 + HNO_3 + HO_2NO_2 + 2×N_2O_5 + $CH_3CO_3NO_2$ (PAN) + $CH_2CCH_3CO_3NO_2$ (MPAN, methacryloyl peroxynitrate) + $CH_2CHCCH_3OOCH_2ONO_2$ ($ISOPNO_3$, peroxy radical from NO_3+ isoprene) from CAM-chem outputs.

4.2.3 CAM-chem evaluation

A comprehensive evaluation of the CAM-chem 2010 simulation is performed, using present-day climatology of O_3 data from multi-year ozonesonde, satellite data, aircraft

campaigns, and ground-based observations, compared with the four-year averages of CAM-chem output. Our model captures the vertical distribution of O_3 in ozonesondes very well, slightly higher in the Sancristobal station (Fig. C.9). The seasonal trends of O_3 at specific pressure levels from the ozonesonde data are also captured well in the model simulation (Fig. C.10), with a correlation coefficient between the observed and simulated seasonal regional O_3 average that is usually greater than 0.8 (Fig. C.11**)**. When evaluating the model performance with aircraft campaign observations, we focus on the regional average over the campaign areas, and analyze the data at different altitudes. Generally, the model performs better in the NH than the SH (Table C.1 and Fig. C.12**)**. When evaluated with multi-year satellite data, the model usually overestimates O_3 between 30°S and 0°S, as well as in North America and Asia, and the global mean of the tropospheric column O_3 is 2.62 Dobson Unit (DU) higher for the model than for OMI (Fig. C.13**)**. Compared with surface O_3 observations, CAM-chem overestimates O_3 by 5.75 ppbv over the whole U.S. (Fig. C.14), and 0.65 ppbv over Europe (Fig. C.15). However, the seasonal trends from the O_3 observation are well captured by CAM-chem. We also compare the simulated O_3 changes from 1980 to 2010 with six long-term remote observation sites (Table 4.2), as few ozone observations are available for 1980. Generally, the model captures well the trend of O_3 changes from 1980 to 2010 for the four observation sites in the NH and the South Pole, although it overestimates O_3 in the NH and underestimates them in the SH (Fig. C.16).

4.2.4 Data sources

The hourly O_3 observation data for the remote sites of Barrow, Mauna Loa, Samoa and South Pole are maintained by the NOAA Global Monitoring Division (GMD) and the data can be found here:

ftp://aftp.cmdl.noaa.gov/data/ozwv/SurfaceOzone/

The Hohenpeissenberg site is run by the Global Atmosphere Watch World Data Centre for Greenhouse Gases and data can be downloaded from here:

http://ds.data.jma.go.jp/gmd/wdcgg/cgi-bin/wdcgg/download.cgi?index=HPB647N00-DWD&param=200612120588&select=inventory#monthly

The Whiteface Mountain summit site in upstate NY is used with the permission from its operator Dr. Jim Schwab from University at Albany-SUNY.

4.2.5 Code availability

The CAM-chem model code used to perform all the simulations is available here:

https://www2.cesm.ucar.edu/models.

The diagnostic package used to perform the model evaluation is developed and maintained by the NCAR AMWG, and code can be found here:

https://www2.cesm.ucar.edu/working-groups/amwg/amwg-diagnostics-package/find-code.

4.3 Discussions and Results

The global B_{O3} is modeled to have increased by 28.12 Tg (8.9% of the total B_{O3} in 1980 for four-year average simulation) from 1980 to 2010, with greater increases in the NH (accounting for 57% of the total increase) than the Southern Hemisphere (SH) (Fig. 4.1). The largest increases of B_{O3} are over 30°S–30°N (17.93 Tg, Figs. 4.1 and 4.2). The influence of the change in the spatial distribution of global anthropogenic emissions contributes 16.39 Tg of the total tropospheric O_3 burden change (ΔB_{O_3}), also higher in the NH than in the SH, slightly greater than the combined influences of the change in emission magnitude (8.59 Tg) and the global CH_4 change (7.48 Tg) (Fig. 4.2). The effect of changing CH_4 on the tropospheric O_3 burden in this study (0.123 Tg B_{O3} per Tg CH_4 a^{-1}) is within the range of sensitivities found

previously (0.11–0.16 Tg B_{O3} per Tg CH_4 a^{-1}, Fiore et al., 2008). Notice that the total ΔB_{O_3} from the sum of the three sensitivity simulations (32.46 Tg) is larger than that from direct comparison between S_2010 and S_1980 (28.12 Tg), as only one variable is changed to 1980 condition in all sensitivity simulations. In particular latitude bands the ΔB_{O_3} from the emission spatial pattern change is much higher over 30°S–30°N than the other influences. In extratropical regions, the ΔB_{O_3} from the emission spatial pattern change is only slightly greater or comparable to ΔB_{O_3} from the other two. North of 60°N, the ΔB_{O_3} due to the emission spatial pattern change is lowest, as less O_3 and its precursors are transported to the high latitudes from North America and Europe.

Between 1980 and 2010, the greatest increases in O_3 (5–9 ppb) are over 0°–35°N in the middle and upper troposphere (750 to 150 hPa), greater than O_3 increases near the surface (Fig. 4.3). Notable O_3 increases are also seen over 30°S–0° (4–7 ppb) in the higher altitudes. Between 35°–60°N, O_3 near the surface shows only small changes, but O_3 increases above the middle troposphere, even though the anthropogenic emissions over these regions (North America and Europe) decreased between 1980 and 2010 (Figs. C.1 and C.2). The influences of the global emission magnitude change and the global CH_4 change both increases the O_3 concentration over the 30°S–35°N, but the largest increases are due to the influence of the global emission spatial pattern change. The spatial distribution change best explains the overall change, particularly the regions with greatest ozone increases. The O_3 precursors increases South of 35ºN are transported efficiently to the middle and upper troposphere, due to strong tropical convection (Hadley cell), and emission decreases North of 35ºN stay at higher latitudes and lower elevation, due to Ferrell cell circulation (Fig. 4.4). When the global emissions shifts southwards, strong convective mixing over the tropical regions lifts O_3 and NO_y to higher altitudes (Fig. 4.3b, Fig. 4.4b), where

the O3 lifetime is longer, favorable for O_3 accumulation. When the global emission increases sit on mid-latitudes in the NH, the weak convection mixing hardly loft the NO_y to high altitudes, but instead to polar region (Fig. 4.4c). We conclude that the global increases are affected by the strong convective mixing over the tropical region. The O_3 increases at high altitudes over the middle and high latitudes are affected by the intercontinental transport of air pollutants from tropical regions due to the strong convection (Lawrence et al., 2003), and this influence is larger and more widespread over the middle and high troposphere than that over the surface, consistent with previous finding (Verstraeten et al., 2015).

We then discuss the other three factors which could contribute to the significant O_3 increases from the emissions shifting southward: chemical reaction rates, O_3-NO_x-VOC sensitivity, and O_3 lifetime. The tropical regions have faster chemical reaction rates than other regions (Fig. C.3**)**, due to the strong sunlight and positively temperature-dependent for the O_3 production (Pusede et al., 2015). Therefore B_{O_3} as well as O_3 chemical production rate (P_{O3}) and loss rate (L_{O3}) are higher in the scenarios with greater emissions in the lower latitudes of the NH (e.g., S_2010 and S_Magnitude) (Fig. C.4). Shifting emission southwards (S_2010-S_Distribution) increases the global ozone production efficiency (define as gross P_{O3} per NO_x emitted, Liu et al., 1997) (Fig. C.4). Strong NO_x-sensitivity is prevalent over tropical regions, especially in the middle and upper troposphere (Figs. C.5 and C.6), and emission trends show greater increases of NO_x that of VOCs (Fig. C.1). Notice that we use the monthly-averaged values to calculate the ozone sensitivity here, instead of using the instantaneous sensitivity indicted by Sillman et al. (1997), as an approximation for large areas. Sillman et al. (1997) used surface observation data when calculating the ozone sensitivity calculations and it is unlikely for us to calculate the instantaneous values from the model outputs. So the actual values in Figs. C.5

and C.6 could be different in reality when using the instantaneous values. O_3 lifetime is lower over the tropical areas, due to the destruction caused by greater water vapor concentration and dry deposition over the vegetated surface (Lawrence et al., 2003). However, this effect is clearly not dominant as we see larger O_3 increases over the tropical regions.

The global surface O_3 changes from 1980 to 2010 using the three month O_3-season Maximum Daily 8-hr Average O_3 (MDA8, see Methods) are also examined in this study (Fig. C.7). The surface O_3 changes are dominated by their regional emissions trends from 1980 to 2010: decreases within Europe and North America, and increases over East Asia and Southeast Asia, consistent with observations (Royal society, 2008; Cooper et al., 2012). Similar regional variations of the MDA8 O_3 are also seen from the influence of the global emission spatial pattern change. We conclude that the MDA8 change between 1980 and 2010 is also controlled by the global emission spatial pattern change, rather than the global emission magnitude change and the global CH_4 change. Seasonal ozone peak has found to shift from summer to spring at rural Northern Hemisphere sites since 1970s, but these seasonal differences are not obvious in our model results (Fig. C.8). The uncertainty in the historical emission inventory as well as missing of important chemical or physical processes inside the model could attribute to this discrepancy (Parrish et al., 2014)

For this study, we only use one global chemical transport model, and ensemble model means could be adopted to reduce single model bias. In the model setup, we use the base case simulation in 2010 to subtract the other scenarios with conditions in 1980, and the O_3 burden changes from the different aspects of the global emissions change will be smaller when we do the opposite. However, we expect the conclusions to stay the same as the emission spatial pattern change dominates the total O_3 changes from 1980 to 2010, but with lower values. O_3 is also a

very important greenhouse gas, especially in the upper troposphere (Forster et al., 1997). So the increases in tropospheric O_3 burdens, especially over the middle to upper troposphere will have positive forcing to the future climate change**,** leading to climate warming. However, increasing NO_x can cause negative RF (Naik et al., 2005; Fry et al., 2012, 2014), and the RF changes response different to the emission changes over different regions and sectors (Shindell et al., 2009; Unger et al., 2008). For further study, radiative transfer model can be used to quantify the RF changes from 1980 to 2010 and from the three aspects of emission changes.

Our research reveals that the change in the spatial pattern of the global anthropogenic emissions from 1980 to 2010 dominates the tropospheric O_3 burden change, even larger than the combined effects of changes in the global emission magnitude and global CH_4. Tropical regions are favorable for O_3 production due to the strong photochemical reaction rates, convection, and NO_x-sensitivity. Increases in O_3 precursor emissions within the Tropics (e.g., China, India and Southeast Asia) exert a significant influence on the global tropospheric O_3 burden. Further work could be conducted to identify the largest influential source regions. The global tropospheric O_3 burden might be expected to continue to increase due to a continued southward shift of emissions, even if the global anthropogenic emissions remains unchanged or even decreases.

4.4 Conclusions

Since 1980, anthropogenic emissions of ozone precursors have decreased in developed regions such as North America and Europe, but increased in developing regions, particularly East and South Asia, redistributing the emissions southwards (Lamarque et al., 2010; Granier et al., 2011; Ohara et al., 2007; Richter et al., 2005; van der A et al., 2008;). Modeling studies have shown that the tropospheric ozone burden and resulting radiative forcing are much more sensitive to emission changes in the tropics and Southern Hemisphere than other regions (Fry et

al., 2012, 2014; Naik et al., 2005; West et al., 2009a). However, the effect of the spatial redistribution of emissions has not been isolated. The emissions spatial redistribution may also be responsible for the shift in the seasonal ozone peak from summer to spring at rural Northern Hemisphere sites (Parrish et al., 2013). Here we use a global chemical transport model to separate the influence of changes in the spatial pattern of emissions from that in the magnitude of emissions, from 1980 to 2010, on the tropospheric ozone burden and surface ozone. We estimate that the spatial pattern change increases the tropospheric ozone burden by 16.39 Tg from 1980 to 2010, accounting for more than half of the total tropospheric ozone burden changes (28.12 Tg), slightly greater than the combined influences of changes in the global emission magnitude itself and in global methane. We attribute the southward emissions dominating the tropospheric O_3 burden to the strong convective mixing, fast chemical reactions rates and more NO_x sensitive in the tropical regions. The spatial distribution of emissions has a dominant effect on global tropospheric ozone, suggesting that the future ozone burden will be determined mainly by emissions from the tropics.

4.5 Figures and Tables

Table 4.1. Model simulations for this study. The last three are the sensitivity simulations described in the main paper.

	Emission total in year	Spatial pattern in year	CH_4 concentration
S_2010	2010	2010	1798 ppb
S_1980	1980	1980	1567 ppb
S_Distribution	2010	1980	1798 ppb
S_Magnitude	1980	2010	1798 ppb
S_CH_4	2010	2010	1567 ppb

Table 4. 2. long-term ozone observation sites used in this study.

Monitor sites	Latitude/Longitude	Elevation (m)	Data available
Barrow, US	71.1ºN /156.6 ºW	11	1975-2015
Hohenpeissenberg, Germany	47.8ºN/11.2ºE	975	1971-2008
Whiteface Mountain, US	44.4ºN/73.9ºW	1484	1973-2014
Manua Loa, US	19.5ºN/155.6ºW	3397	1973-2015
Matatula Pt, Samoa	14.3ºS/170.6ºW	82	1976-2015
South Pole, Antarctica	90.0ºS/24.8ºW	2840	1975-2015

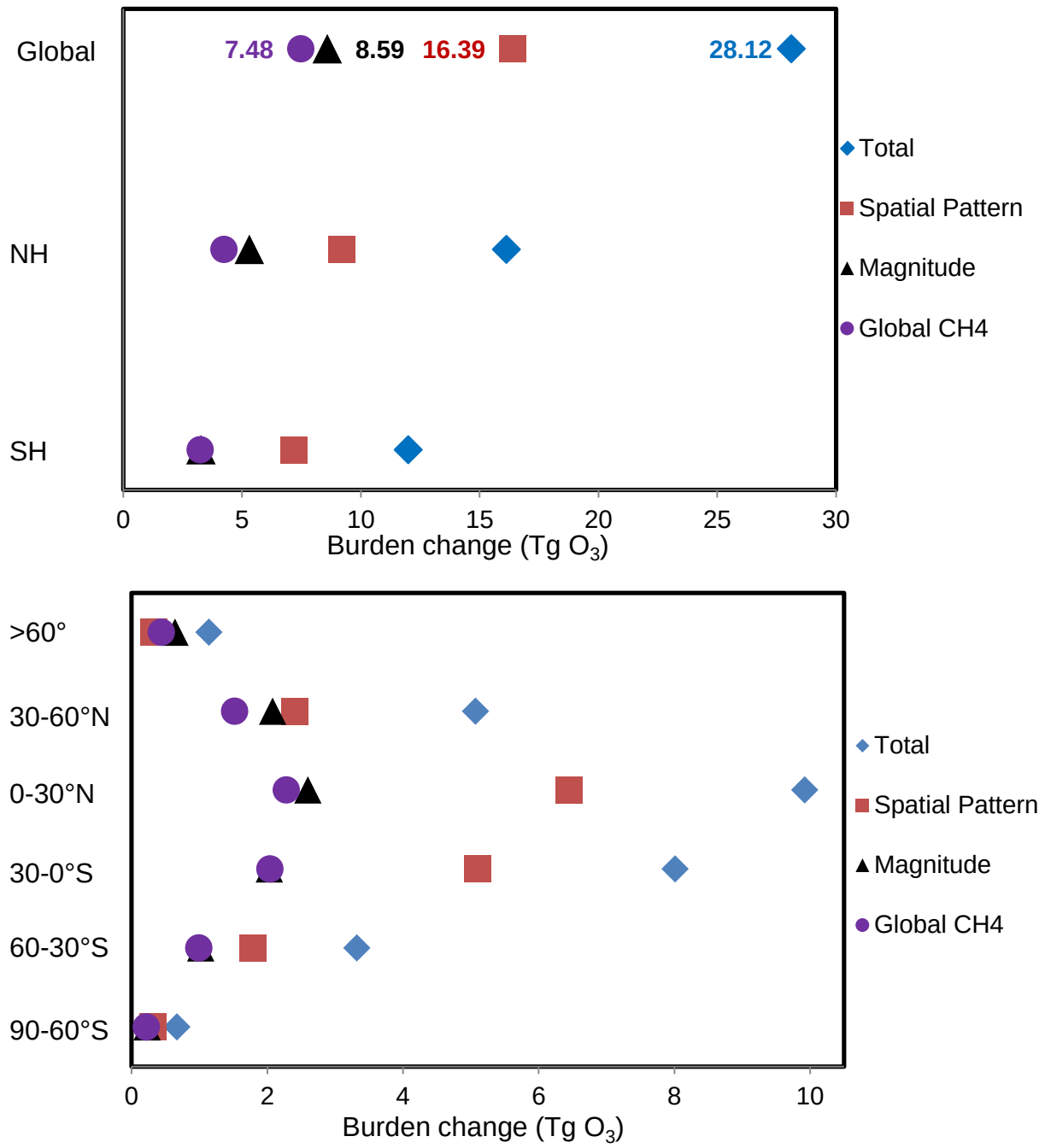

Fig. 4. 1. Tropospheric O_3 burden change (ΔB_{O_3}) from 1980 to 2010. a, For global, NH and SH. b, For different latitudinal bands. The estimated components for ΔB_{O_3} due to the spatial pattern change (red rectangle), magnitude change (black triangle) and global CH_4 change (purple circle) are also seen in each plot.

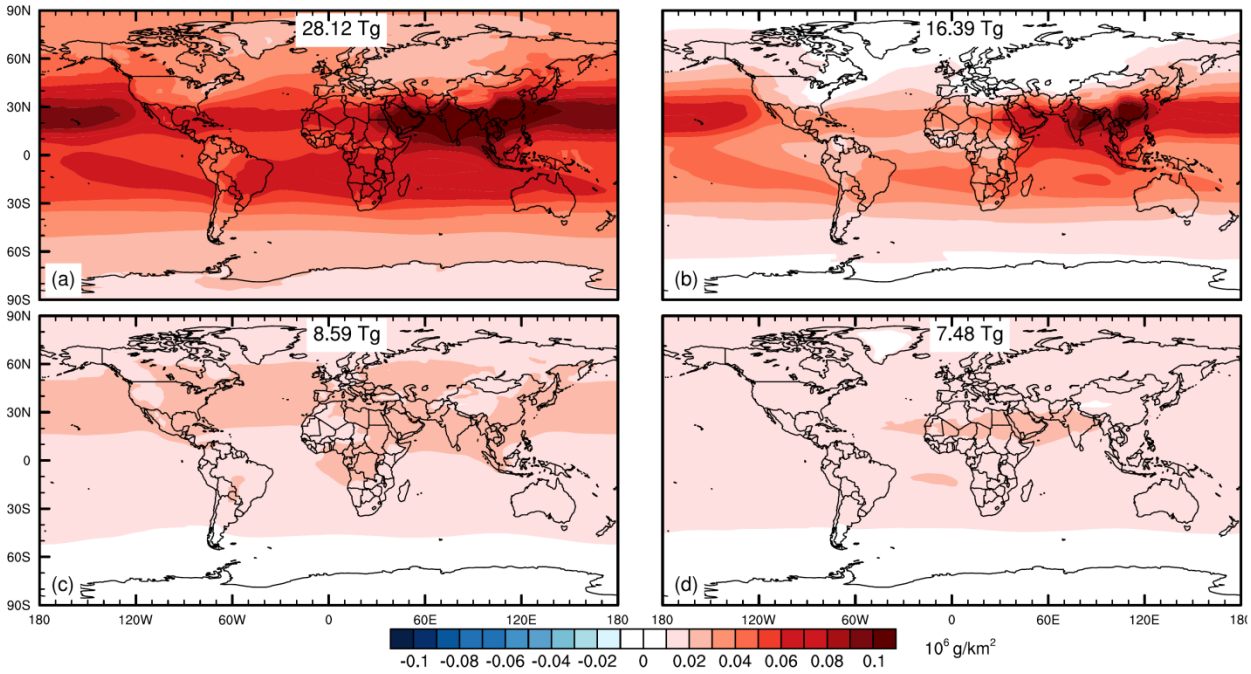

Fig. 4. 2. Spatial distributions for ΔB_{O_3} (unit 10^6 g/km^2) from 1980 to 2010. a, Total changes from 1980 to 2010. b-d, Influences of changes in the global emissions spatial pattern, the global emissions magnitude, and global CH_4 mixing ratio.

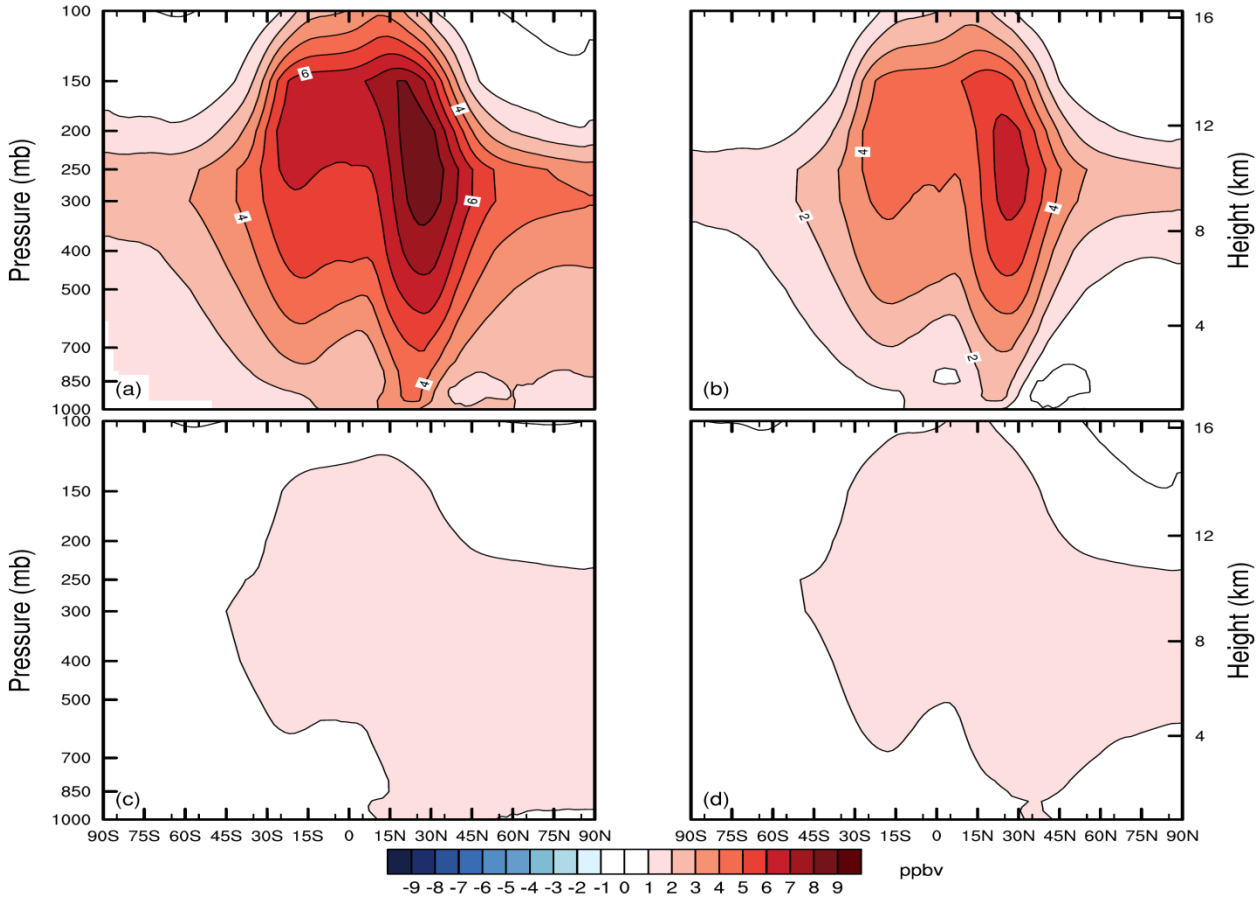

Fig. 4. 3. Zonal annual average O_3 change. a, Total change from 1980 to 2010. b-d, Influences of changes in the global emissions spatial pattern, the global emissions magnitude, and global CH_4 mixing ratio.

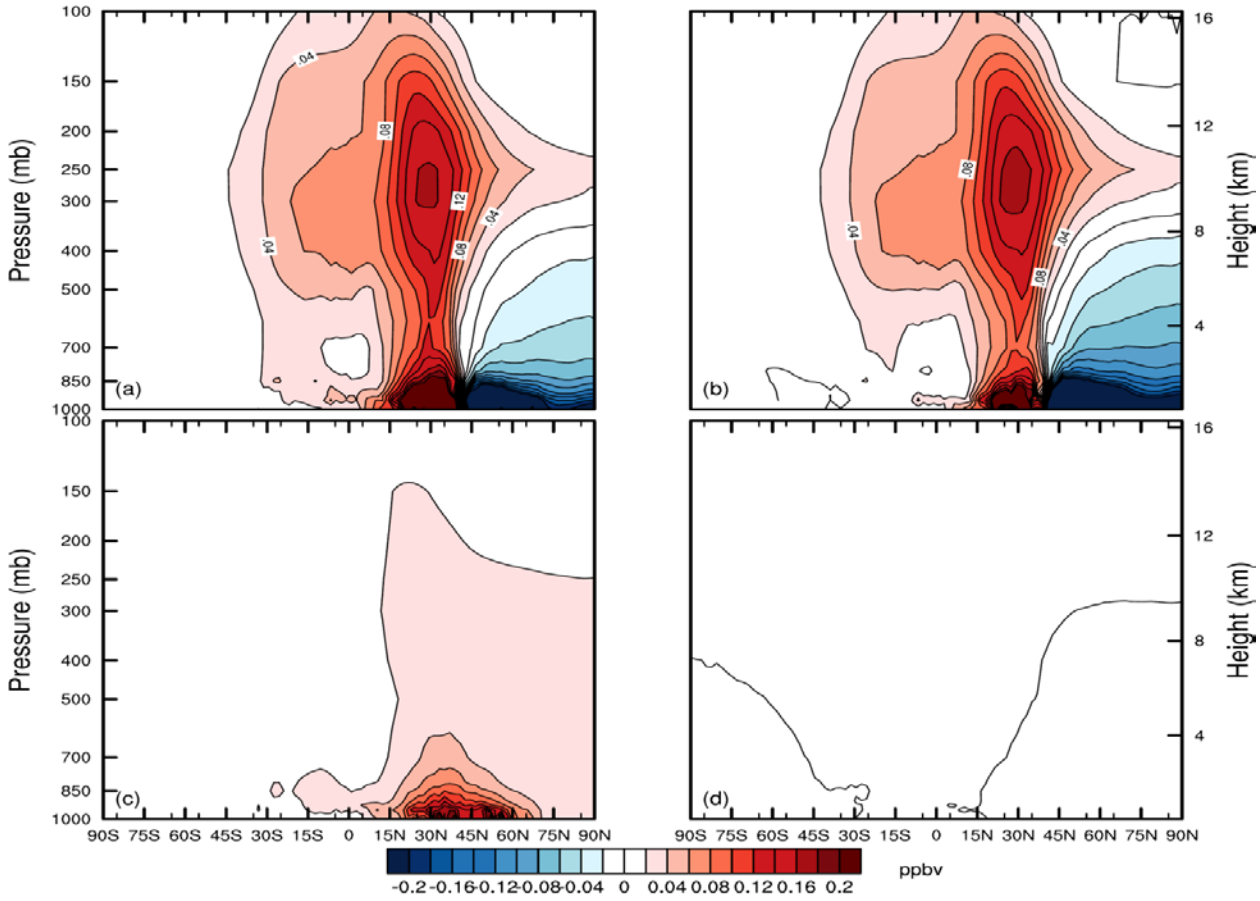

Fig. 4. 4. Zonal annual average NO_y change. a, Total changes from 1980 to 2010. b-d, Influences of changes in the global emissions spatial pattern, the global emissions magnitude, and global CH_4 mixing ratio. See methods for the NO_y definition and calculation from CAM-chem.

CHAPTER 5. CONCLUDINGS REMARKS

Here the major work for my Ph.D. research is to quantify the co-benefits of global GHG mitigation on US air quality and human health in 2050 at fine resolution, embedding upon a global co-benefits study (West et al., 2013; referred as WEST2013 thereafter). We also separate the co-benefits into two mechanisms: the co-benefits through reduced co-emitted air pollutants, and the co-benefits through the slowing climate change and its effect on air quality. Based on the global co-benefits study, we can also separate the influence of domestic GHG mitigations from that of foreign countries' reductions. Chapters 2 and 3 quantify the co-benefits from global and domestic GHG mitigation on US air quality and human health. We also look into the co-benefits from top three domestic emission sectors which have the largest air pollutants decrease in US under the RCP4.5 scenario. Chapter 4 investigates the influence of global emission spatial pattern redistribution on global O_3 burden change from 1980 to 2010. This chapter focuses on the main scientific findings and policy implications from these three studies. Uncertainty analysis and future research directions are also discussed in the end of this chapter.

5.1 Key scientific findings

5.1.1 Co-benefits from GHG mitigation

Actions to reduce GHG emissions often reduce co-emitted air pollutants, bringing co-benefits for air quality and human health. Previous studies typically evaluated the short-term benefits from the reduced co-emitted air pollutants, neglecting the long-range transport of air pollutants, and the influence of climate change on air quality (Bell et al., 2004; Nemet et al.,

2010; Thompson et al., 2014). Under this circumstance, WEST2013 was the first study to discuss the co-benefits from global GHG mitigations on air quality and human health by using a global CTM. They found that 2.2±0.8 million deaths will be avoided globally by 2100 due to the air quality improvement from global GHG mitigation, considering both $PM_{2.5}$ and O_3. When monetized, the global average marginal co-benefits of avoided mortality were \$50–380/tCO_2, higher than the previous estimates (Nemet et al., 2010). However, WEST2013 was limited by using a coarse resolution in the model (horizontally 2º×2.5º). This dissertation is to downscale the global co-benefits results into regional scale (US domain) at finer resolution, using dynamically downscaling methods.

By using the WRF model, SMOKE program to downscale global results into regional scale, and running the air quality simulations with the CMAQ model, we find that the total co-benefits of global GHG mitigation from RCP4.5 scenario compared with its reference are estimated to be higher in the eastern U.S. (ranging from 0.6-1.0 μg m^{-3}) than the west (0-0.4 μg m^{-3}) for annual average $PM_{2.5}$, with an average of 0.47 μg m^{-3} over U.S.; for ozone-season maximum daily 8-hour average O_3, the total co-benefits are more uniform at 2-5 ppb with U.S. average of 3.55 ppb (Chapter 2). The total co-benefits for O_3 are comparable to WEST2013, but much lower for $PM_{2.5}$, which could be explained by the different chemical mechanisms and deposition processes adopted for organic aerosols in MZ4 and CMAQ. Also the differences of the meteorology (e.g., the precipitation and temperature) between the downscaled WRF and the GFDL could also contribute to this difference. When quantifying the total co-benefits on human health in US using the BenMAP-CE tool, We find that more than 24500 deaths (90% confidence interval, 17800 to 31100) will be avoided for the $PM_{2.5}$-related all-cause mortality, and 12200 (5400 to 18900) deaths for the O_3-related respiratory mortality in US in 2050 from global GHG mitigation

(Chapter 3). For both $PM_{2.5}$ and O_3, the mortality estimates in fine resolution in this study are biased higher than the results in coarse resolution in WEST2013 (ranging from 17%-161% for PM2.5, and 62%-99% for O_3). These discrepancies could be caused by the fact that the finer-resolution CMAQ model can better capture the hotspots of future air quality changes near areas of dense population, and the coarse-resolution in WEST2013 could dilute the peak air quality concentrations which usually occur in populated regions (Punger and West, 2013. Li et al., 2015). Our study shares the same CRF as WEST2013, and the positive bias are largely caused by the county-level baseline mortality rates used in this study, less extent to the county-level population data embedded in BenMAP-CE as the total co-benefits of the Pop-Weighted Avg for both $PM_{2.5}$ (1.25 $\mu g\ m^{-3}$) and O_3 (4.61 ppbv) in WEST2013 are higher than those in this study.

We also separate the total co-benefits through the two mechanisms. The reductions of co-emitted air pollutants have a much greater influence on both $PM_{2.5}$ (96% of the total co-benefits) and O_3 (89% of the total) than the second co-benefits mechanism via slowing climate change, consistent with West et al. (2013) (Chapter 2). The improved air quality leads to 24100 (CI, 17500-30600) avoided deaths for $PM_{2.5}$-related all-cause mortality (accounting for 98% of the total avoided deaths from $PM_{2.5}$), and 11500 (CI, 5100-17800) deaths for O_3-related respiratory (94% of the total) (Chapter 3). The co-benefits from the second mechanism is less significant than those from the first mechanism, but it still accounts for 2%-11% for the total co-benefits on US air quality and human health. The slowing climate change may also degrade the air quality and increase the premature mortality in US as seen in the dissertation, as the model runs are only for three years and we may see the influence of the climate variability.

By building this dissertation onto WEST2013, we can also separate the total co-benefits from contributions of domestic GHG mitigation versus foreign countries climate policies. This is

the first study to quantify the influences of foreign countries climate policies on US air quality and human health. We conclude that foreign countries GHG mitigation accounts for 26% (0.12 $\mu g\ m^{-3}$) of the total annual $PM_{2.5}$ decrease over the whole US, but 76% (2.69 ppb) of the total O_3 decrease as a result of intercontinental air pollutants transport and global CH_4 influence. When accounting for the human health, the foreign co-benefits could avoid 3700 deaths (2700-4700) for $PM_{2.5}$-related mortality (accounting for 15% of the total deaths), and 7600 deaths (3400-11900) for O_3-related mortality (62% of the total). The influence is huge, especially for O_3. The contribution fractions are specific to the climate policies we choose (RCP4.5 versus its REF), but we believe the conclusion holds true that foreign countries reductions could have significant influence on US domestic air pollutants, especially for O_3. So previous studies which only estimated the co-benefits from domestic or single state's climate policy, may greatly underestimate the real co-benefits which could be achieved by the internationally collaboration.

We also consider the co-benefits from three domestic emission sectors in US: Industry, Residential, and Energy, because they are among the top three cost-effective sectors to be considered to carry on the GHG mitigation in US under the RCP4.5 scenario. We find that GHG mitigation in the residential sector in US will bring the largest co-benefits for the $PM_{2.5}$-related premature mortality, accounting for 21% of the total domestic co-benefits. For O_3, industry has the largest effect by avoiding 800 deaths/yr (300-1200), and accounting for 17% of the total. Caiazzo et al. (2013) concluded that largest contributors for both $PM_{2.5}$-and O_3-related mortalities in 2005 in US are road transportation. However, we didn't consider co-benefits from road transportation in our study, as we didn't see large air pollutants reductions in this sector resulted from its GHG mitigation policy under the RCP4.5 scenario.

5.1.2 Emission pattern redistribution on global ozone burden

The last project for my dissertation is not directly related with the first two, but they share a common notion that intercontinental transport of ozone and its precursors are very important to global and regional air quality. We study the influence of global emission change from 1980 to 2010 on the global ozone burden change in Chapter 4, as the emissions have shifting southwards. Previous research have shown that global ozone burden are more sensitive to the ozone precursors changes in tropical regions and Southern Hemisphere (SH) (Naik et al., 2005; West et al., 2009a; Fry et al., 2012, 2014). However no studies have separated the different aspects of emissions changes on the burden change. Our study in Chapter 4 has demonstrated that the influence of global emission spatial change accounts for more than half of the global ozone burden changes, even larger than the combined effect of global emission magnitude change and global CH_4 change. The fast chemical reactions rates, more NO_x sensitive as well as the strong convective mixing in the tropical regions which can lift up ozone and its precursors high into the middle and high troposphere and then transport to other regions are the main cause of the southward emissions dominating the tropospheric O_3 burden.

From Chapter 4, we conclude that the spatial distribution of emissions has a dominant effect on global tropospheric ozone, suggesting that the future ozone burden will be determined mainly by emissions from the tropics. So the global tropospheric O_3 burden might be expected to continue to increase due to a continued southward shift of emissions, even if global anthropogenic emissions remain unchanged or even decreases. This provides motivations for international collaborations on controlling global ozone issues. Ozone is not only a regional problem anymore, but also an international issue. The ozone burden changes happen mostly from the middle to upper troposphere, which exerts much larger influence on radiative forcing changes

than that from the surface. So the emission spatial pattern shifting may also have influences on future climate change (Wang et al., 2015).

5.2 Policy implications

In the first two co-benefits studies (Chapters 2 and 3), we conclude that previous studies that estimate co-benefits for one nation or region (e.g., Driscoll et al., 2015; Thomson et al., 2014), may significantly underestimate the full co-benefits when many countries reduce GHGs together, particularly for O_3. By being the first study to quantify the influence of foreign countries GHG mitigation on US future air quality and human health, we find that U.S. can gain significantly greater domestic air quality co-benefits by engaging with other nations for GHG control to combat climate change, especially for O_3. This also applies to other nations which can be expected to have ancillary air quality benefits from foreign countries' GHG mitigation.

Co-benefits from GHG mitigation are appealing to countries as they will gain near-term and immediate benefits of air quality improvement and then the reduced premature mortality. This is a "Win-Win" strategy for both air quality regulations and climate change control. Now our studies find that foreign countries GHG reduction strategies can also bring significant co-benefits on domestic air quality and human health, which means global actions to reduce GHG could bring greater co-benefits. This provides an incentive for worldwide collaborations on combating global climate change and regulating air quality together. Air quality regulations can also have effects on global climate change, but more model simulations should be carried out to identify the benefits or disbenefits as different air pollutants have either positive or negative effect on climate forcing.

The emission spatial distribution study (Chapter 4) has shown that global ozone burden changes are more sensitive to the ozone precursors' change in tropical regions, especially over

South and Southeast Asia. The O_3 burden can still increase even we keep the global emissions constant or decreasing in the near future, as the O_3 burden change is more sensitive to the emission spatial pattern change, other than the global emission magnitude change. O_3 can also transport long-distance from one source region to another receptor region. So to reach their own air quality standard, developed countries, such as US and Europe, should establish long-term collaborations with countries in tropical regions to control their air pollutants emissions; otherwise, attaining a lower ozone concentration may be in particularly challenging or even failed (Cooper et al., 2015).

5.3 Uncertainties and future research

The co-benefits we present here (Chapters 2 and 3) are specific to the reference (REF) and mitigation (RCP4.5) scenarios we choose, and results would differ for other baseline and mitigation scenarios. Further research could carry out studying the co-benefits based on different climate policy scenarios to find the most cost-effective way to both control the climate change and air quality in a coordinated way. The real total co-benefits are also depending on participation of many nations in the mitigation policies, and delaying participation will likely change the co-benefits.

By comparing the co-benefits study from this study with WEST2013, the work in my dissertation do capture some local features better than the global model, such as the effects of topography and urban areas, especially for $PM_{2.5}$. The resolution in my dissertation (36km by 36 km in Chapters 2 and 3) is fine enough to characterize the co-benefits at a state level, but not fine enough on city level. So finer resolutions simulations (e.g., 12km by 12 km) can be carried out to better quantify the co-benefits over urban areas. The results from the global co-benefits have demonstrated that China and India will have the largest co-benefits on human health from the

global GHG mitigation under the RCP4.5 scenario. So the similar downscaling methods could be adopted to study the real co-benefits in those countries at fine resolution, and then compare with the global study.

For each step in our three studies (Chapters 2-4), only one model is used, and ensemble model means could reduce the bias from each single model. Post et al. (2012) has shown that the choice of the climate change and the air quality model reflected the greatest source of uncertainty for accounting for future climate change related mortality, with the other modeling choices having lesser but still substantial effects. Studies also showed that multi-model mean for the climate change predictions and boundary conditions were better than single model (Tebaldi and Knutti, 2007).

Emissions inventories are another large source of uncertainty in current modeling applications. So future work should also work on to improve the accuracy of emission inventories by further comparing the bottom-top method with top-down (or inverse) methods, such as satellite retrieval, and remote sensing (Donkelaar et al., 2010, 2015; Ma et al., 2014). Also we develop a new method to process the global emission inventory at coarse resolution into regional scale in US at fine resolution, which also introduce errors due to resolution transformation, especially along the boundary regions.

From the results (Fig. 2.4, Fig. A.16), we see that the co-benefits of $PM_{2.5}$ have large contributions from OC and SOA over the Central and East U.S. region. However, our model evaluations show that CMAQ simulations greatly underestimate the OC concentration compared with surface observations in IMPROVE network. SOA evaluation for CMAQ is not included in my dissertation due to the limitation of the observation datasets, even though recent studies found that the CMAQ also greatly underestimated the SOA species (Baek et al., 2015; Hayes et

al., 2015; Woody et al., 2015). New gas-phase and aqueous-phase oxidation pathways for SOA formation are found to play significant roles in producing organic aerosols (Lin et al., 2014; Pye and Pouliot, 2012; Pye et al., 2013), which are also missing in the CMAQ version used in this study, making the CMAQ simulation less reliable. Recently, laboratory work has revealed new chemical pathways of isoprene-derived SOA under different conditions. They have shown that under the high NO_x conditions, the isoprene peroxy radicals primarily react with NO, leading to formation of methacryloylperoxynitrate (MPAN), which then decomposes into methacrylic acid epoxide (MAE) and hydroxymethylmethyl-α-lactone (HMML) by reacting with hydroxyl radical, and then generate SOA (Surratt et al., 2010; Lin et al., 2013). These chemical pathways should be updated into both the global and regional CTMs to better simulate both $PM_{2.5}$ and O_3 (Fiore et al., 2012). The underestimation of the both OC and SOA in the current CMAQ model would greatly reduce the total co-benefits on both air quality and avoided premature mortality estimated from this study.

In quantifying the co-benefits from slowing climate change in the first two Chapters (2 and 3), the predictions for future climate change and air quality change are run less than five years which may reflect meteorological variabilities, due to the limitations of availability of super computer resources and disk storages. For each scenario in Table 2.1 in Chapter 2, it takes more than 1 month to run all the consecutive 40 months simulation, and the outputs of all the simulations take up more than 21 TB, occupying more than a quarter of the total computer storages hold by UNC ITS services. Complaints are received almost every week from ITS staffs to ask me to remove the data. Future simulations should run more years to reduce the influence of the climate variability.

When we quantify the health impacts from air quality changes, another larger uncertainty may arise from the concentration-response function (CRF), which is derived from epidemiology studies that relate $PM_{2.5}$ and O_3 concentrations with mortality. Silva et al. (2013) has demonstrated that the CRF contributes more to overall uncertainty than the spread of model results. When we project the future avoided premature mortality, we assume that the CRF derived from present epidemiology studies may hold true into the future. Also different resources in projecting the future baseline mortality rates in US may also bring larger uncertainties for the results. For example, the IFs projected the baseline mortality rates in 2050 in US will increase, but the projection from RTI international (RTI International 2015) is decreasing.

Both $PM_{2.5}$ and O_3 are also found to have influences on forest damage, crop yields and economical values. Following up studies can also be established to quantify the co-benefits from global and regional climate polices on food security and economy (Shindell et al., 2012; Tai et al., 2014). The benefit-cost assessments on both global and regional scale can be extremely useful for policy makers to make decisions on domestic or international air pollution controls and climate mitigation.

For the emission spatial redistribution on the influence of global ozone burden change, I only use one single global CTM. Ensemble models means could be used to reduce single model's variability. I expect that the results will be different by using ensemble model outputs compared with single model which is used in my dissertation. However, I will not expect the major conclusion will be different, which is that the global emission shifting southwards has a much larger influence on global ozone burden change for the past three decades, larger than the global emission magnitude change and global CH_4 change. Though the emissions inventory in 1980 from RCP8.5 is considered as the best approximation of the historical emissions, there are

still large uncertainties in the inventory. Improving the accuracy of the emissions, especially in larger emitted countries, such as China and India, will shed light on the conclusions of study. O_3 in the troposphere is considered as very important GHG, so future research could be carried out to study the radiative forcing changes from the emission pattern redistribution.

APPENDIX A. CO-BENEFITS OF GLOBAL AND REGIONAL GREENHOUSE GAS MITIGATION ON U.S. AIR QUALITY IN 2050: SUPPORTING MATERIALS

Median Bias: $MdnB = median(C_m - C_o)_N$

Normalized Median Bias: $NMdnB = \frac{median(C_m - C_o)_N}{median(C_o)_N} \times 100\%$

Median Error: $MdnE = median\left|C_m - C_o\right|_N$

Normalized Median Error: $NMdnE = \frac{median\left|C_m - C_o\right|_N}{median(C_o)_N} \times 100\%$

Table A.1. Sectors grouped in RCPs, SCC in the GSREF file, and the speciation profile codes in GSPRO used in SMOKE v3.5. X in the table represents any number.

Sectors	IPCC Code	SCC	Speciation profile codes
Energy	1A1_1B	10100XXXX	92036
Industries	1A2_2A_B_C_D_E	10200XXXX	92084
Transportation	1A3b_c_e	220100XXXX	92050
Residential	1A4	21040080XX	92068
Solvents	2F_3	24XXXXXXX	92052
Agriculture	4A_B_C_D_G	27301000XX	92001
Agriculture waste burning	4F	2610000XXX	92000
Waste	6A_B_C_D	101012XX	92082
Savanna burning	4E	28100010XX	92090
Forest fires	5A	28100010XX	92090

Table A.2. Evaluation of the S_2000 simulation (average of three years modeled) with surface observations in 2000 for $PM_{2.5}$ components (SO_4^{2-}, NO_3^-, NH_4^+, OC and EC) with different networks ($\mu g\ m^{-3}$).

	Pollutant	MdnB	NMdnB (%)	MdnE	NMdnE(%)
IMPROVE	SO_4^{2-}	0.16	20.75	0.45	56.96
IMPROVE	NO_3^-	-0.040	-18.14	0.23	83.91
IMPROVE	OC	-0.55	-63.55	0.60	69.13
IMPROVE	EC	-0.069	-37.00	0.11	57.04
CSN	SO_4^{2-}	-0.10	-4.88	0.91	44.32
CSN	NO_3^-	-0.31	-50.06	0.44	71.39
CSN	NH_3^+	0.029	4.27	0.43	64.67
CASTNET	SO_4^{2-}	-0.40	-15.2	0.73	27.87
CASTNET	NO_3^-	-0.051	-10.50	0.37	74.97
CASTNET	NH_4^+	-0.076	-7.63	0.31	31.30

Table A.3. The regional annual means of total, domestic, and foreign co-benefits for $PM_{2.5}$ and O_3 in the nine U.S. regions. The values (mean ± coefficient of variation (CV, %)) is calculated over three years.

	Annual $PM_{2.5}$ (μg m^{-3})			**Ozone season (May-Oct) average of MDA8 O_3 (ppbv)**		
	Total	Domestic	Foreign	Total	Domestic	Foreign
U.S.	-0.47±7	-0.35±1	-0.12±26	-3.55±37	-0.86±1	-2.69±49
Northwest	-0.16 ±15	-0.13±2	-0.04±66	-4.15±21	-0.40±5	-3.75±28
West	-0.40 ±9	-0.30±3	-0.10±45	-3.99±46	-1.05±3	-2.94±61
West N. Central	-0.21±14	-0.13±3	-0.08±38	-4.02±41	-0.57±3	-3.45±48
Southwest	-0.30±12	-0.16±1	-0.13±24	-3.11±70	-0.79±3	-2.32±93
South	-0.62±11	-0.37±4	-0.25±22	-2.84±69	-0.79±3	-2.04±95
East N. Central	-0.45±3	-0.38±3	-0.06±29	-4.25±30	-0.81±4	-3.44±37
Central	-0.78±9	-0.65±2	-0.12±63	-3.38±55	-1.24±1	-2.14±87
Southeast	-0.75±29	-0.62±3	-0.13±84	-2.67±40	-1.14±3	-1.53±71
Northeast	-0.62±3	-0.53±1	-0.09±22	-4.61±17	-1.16±5	-3.45±21

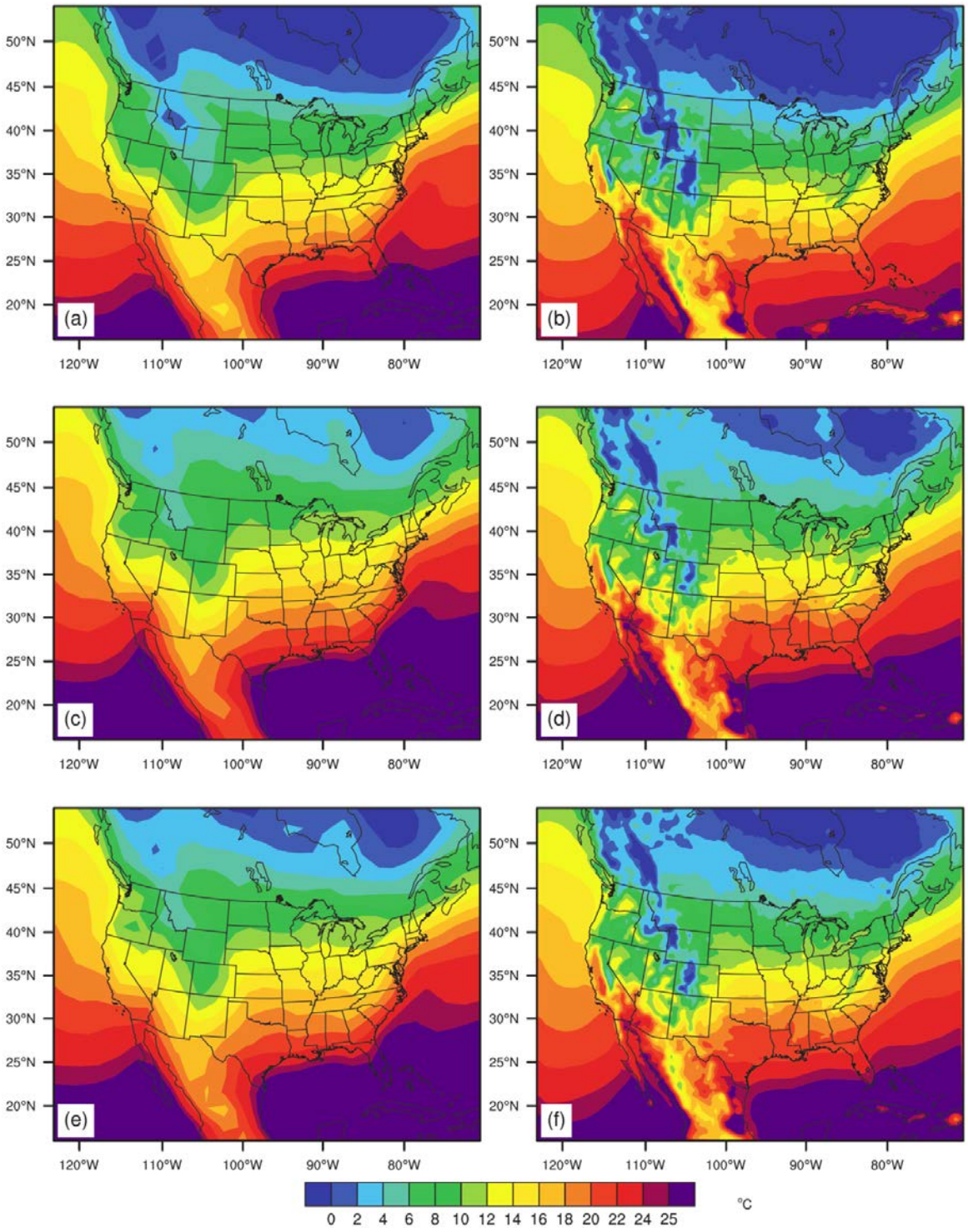

Figure A.1. Comparisons of the 2-m temperature in 2000 (a, b), 2050 from RCP8.5 (c, d) and from RCP4.5 (e, f) for three-year averages of GFDL AM3 simulations on the left (a, c, e) and the WRF downscaling results on the right (b, d, f).

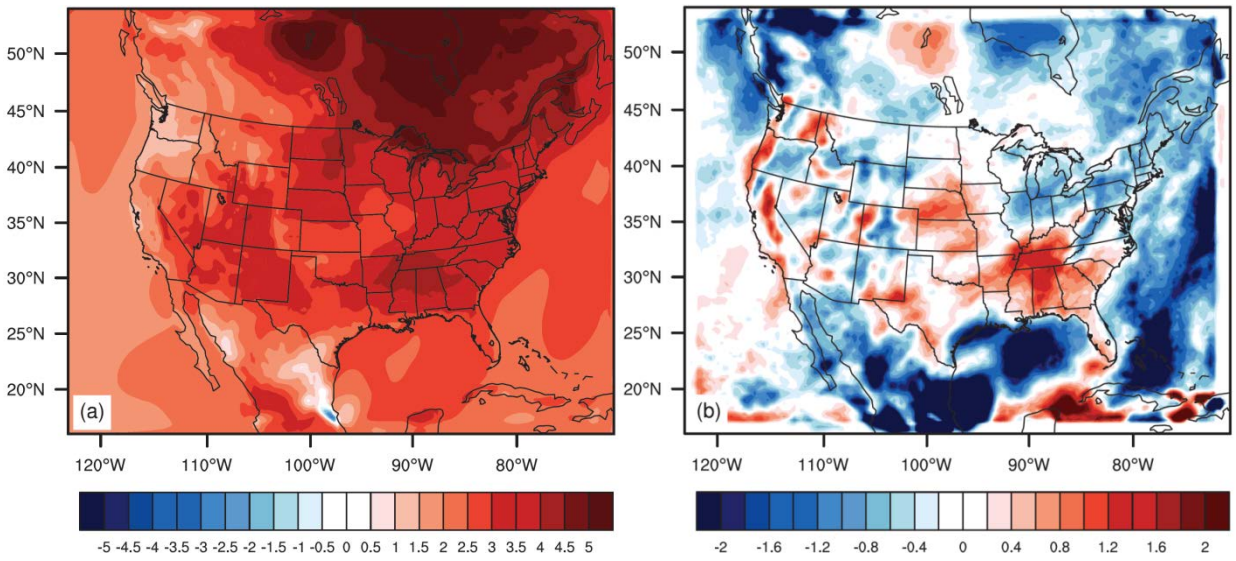

Figure A.2. Changes in (a) 2-m temperature (°C) and (b) precipitation (mm day^{-}`) centered on 2050 from RCP8.5 and 2000 (2050—2000).

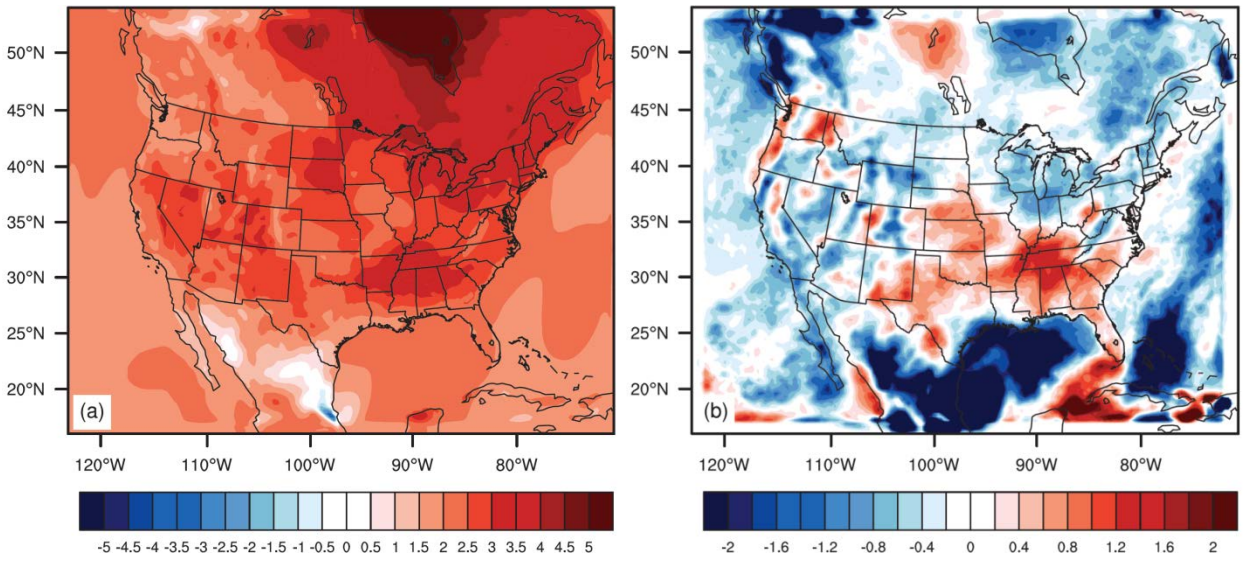

Figure A.3. Changes in (a) 2-m temperature (°C) and (b) precipitation (mm day^{-1}) centered on 2050 from RCP4.5 and 2000 (2050—2000).

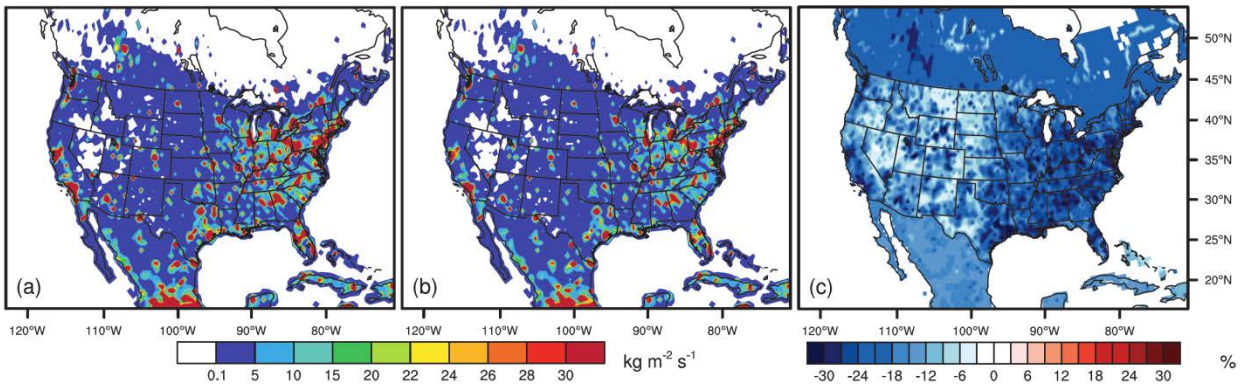

Figure A.4. The spatial distribution of anthropogenic emissions of SO_2 (10^{-12} kg m^{-2} s^{-1}) from (a) REF scenario, (b) RCP45 scenario in 2050, and (c) relative differences between these two scenarios (RCP45-REF)/REF×100%).

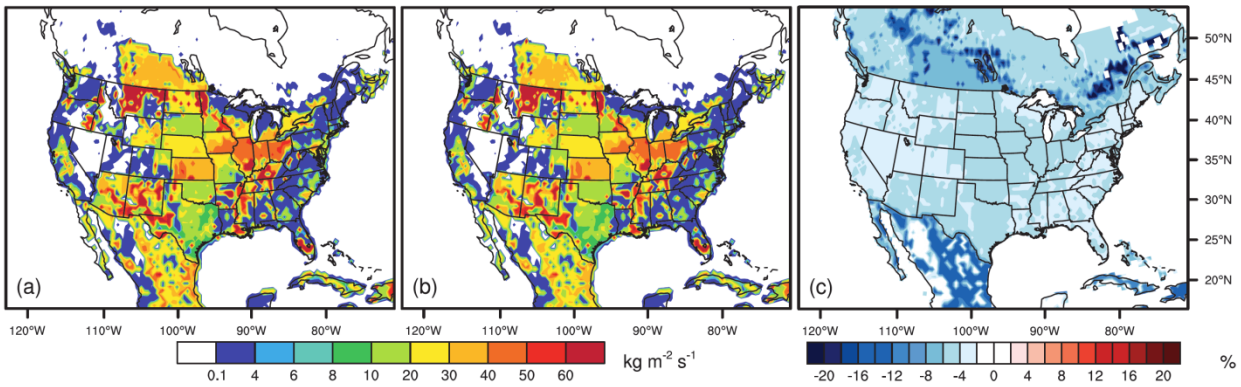

Figure A.5. Same as Fig. A.4 but for NH_3.

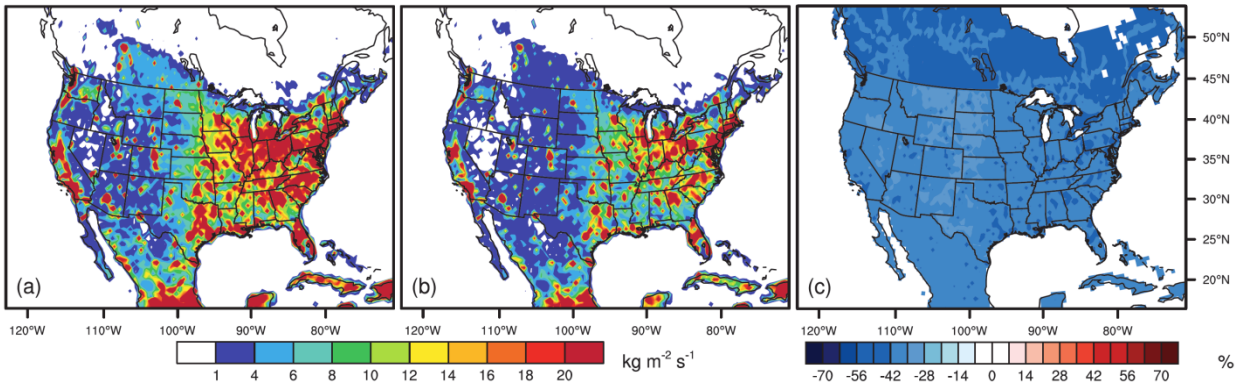

Figure A.6. Same as Fig. A.4 but for NO.

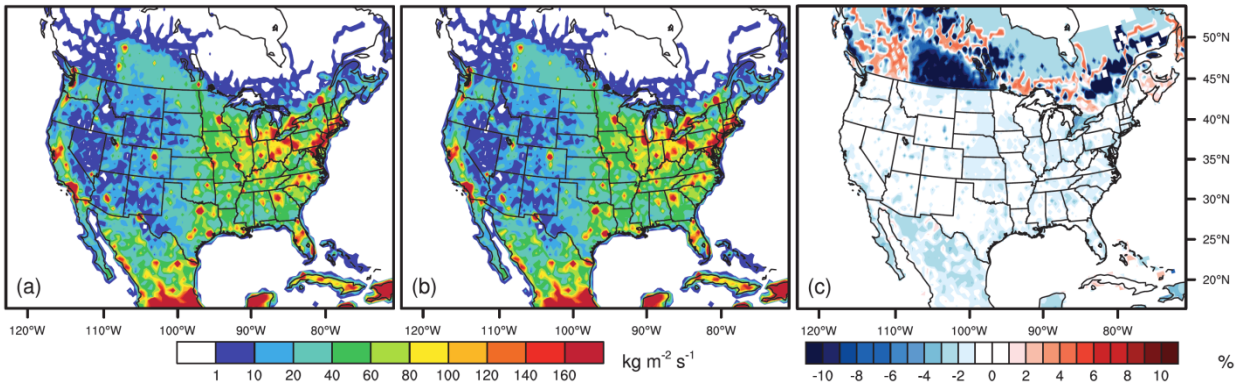

Figure A.7. Same as Fig. A.4 but for CO.

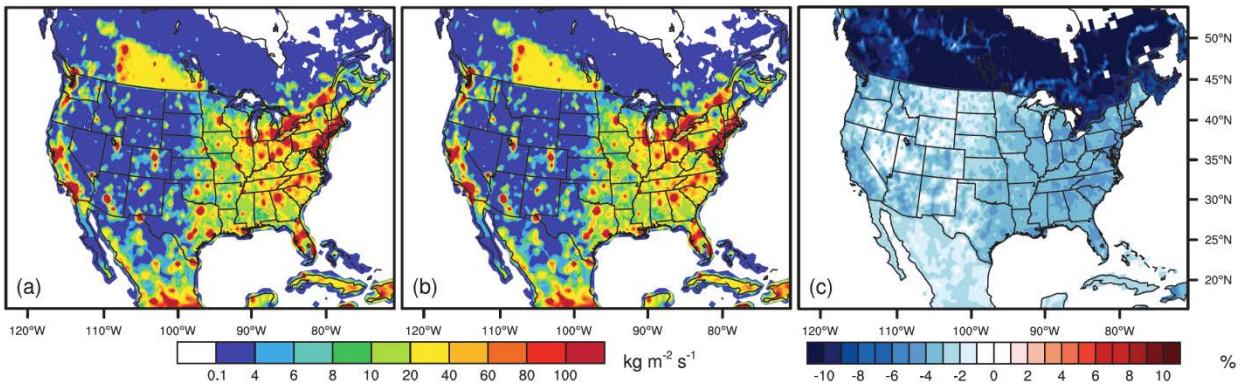

Figure A.8. Same as Fig. A.4 but for NMVOCs.

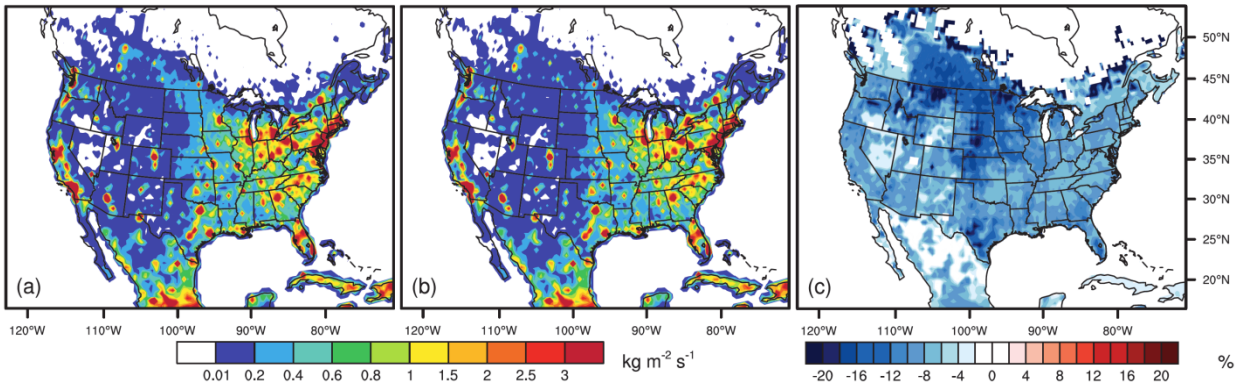

Figure A.9. Same as Fig. A.4 but for EC.

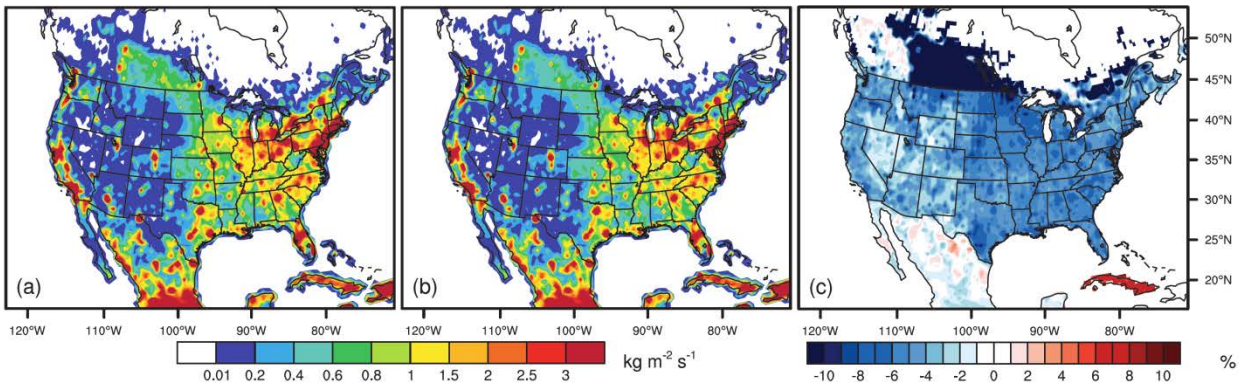

Figure A.10. Same as Fig. A.4 but for OC.

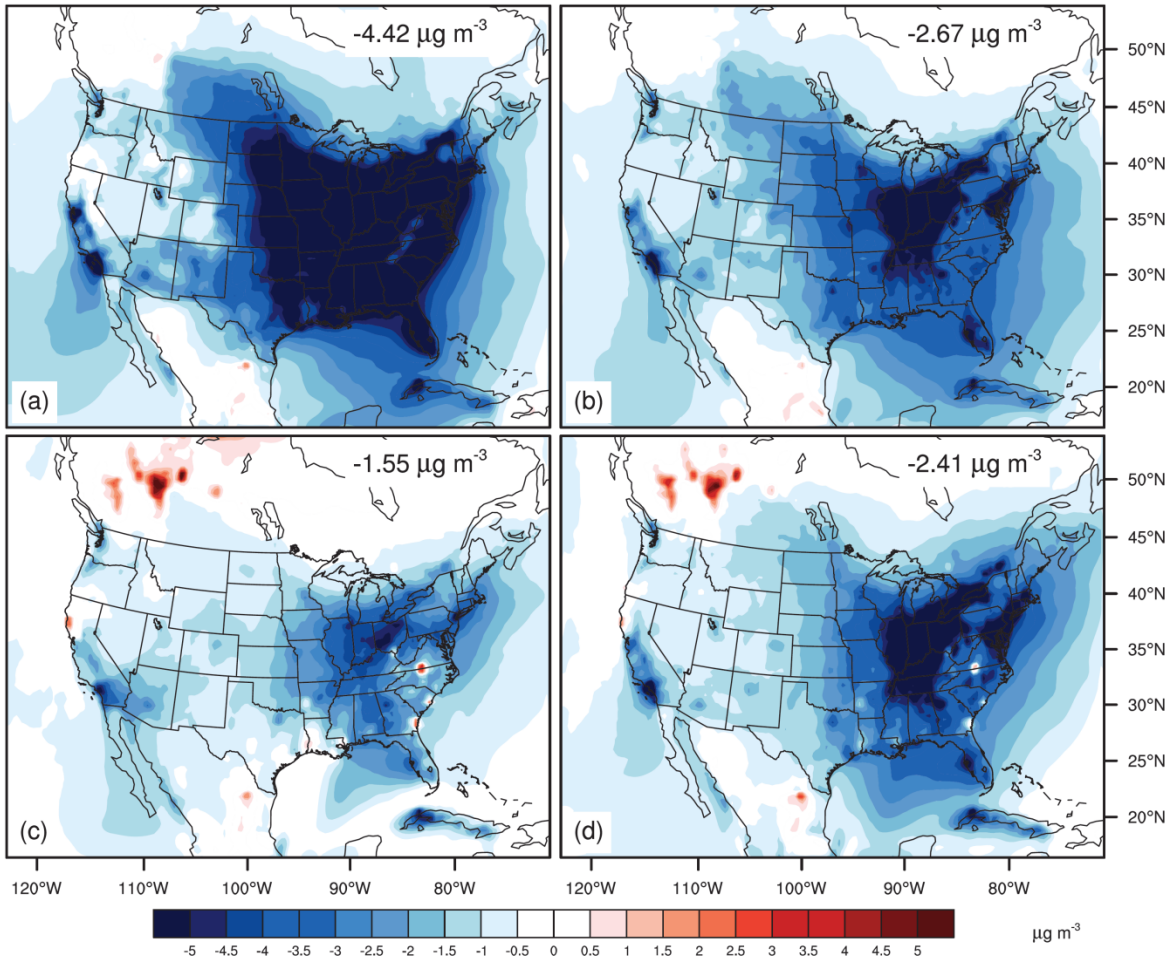

Figure A.11. Seasonal distributions of $PM_{2.5}$ changes (µg m^{-3}) between S_REF in 2050 and S_2000 for (a) winter, (b) spring, (c) summer and (d) fall. The three-year annual averages over the U.S. is -2.76 µg m^{-3}.

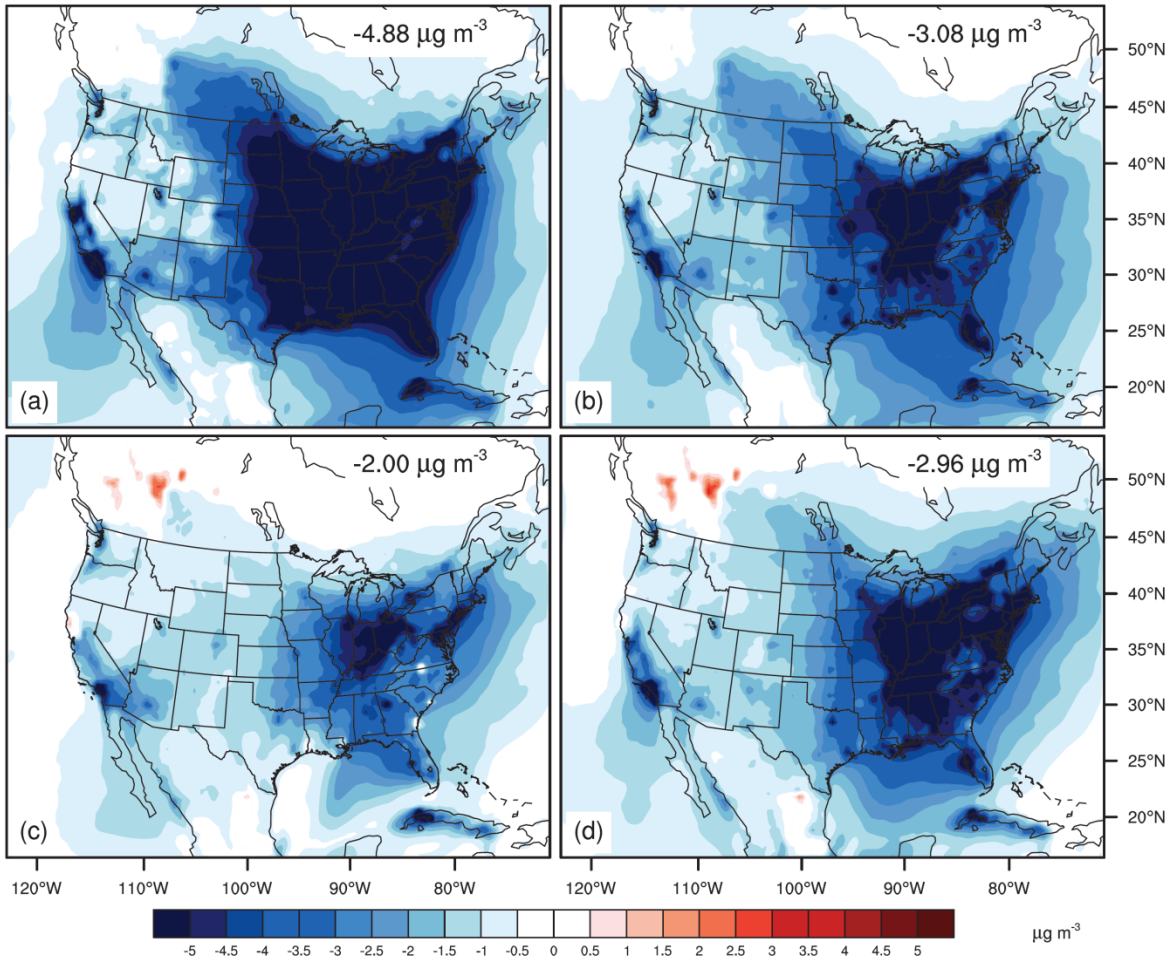

Figure A.12. As Fig. A.11 but for the changes between S_RCP45 in 2050 and S_2000. The U.S. average is -3.23 µg m^{-3}.

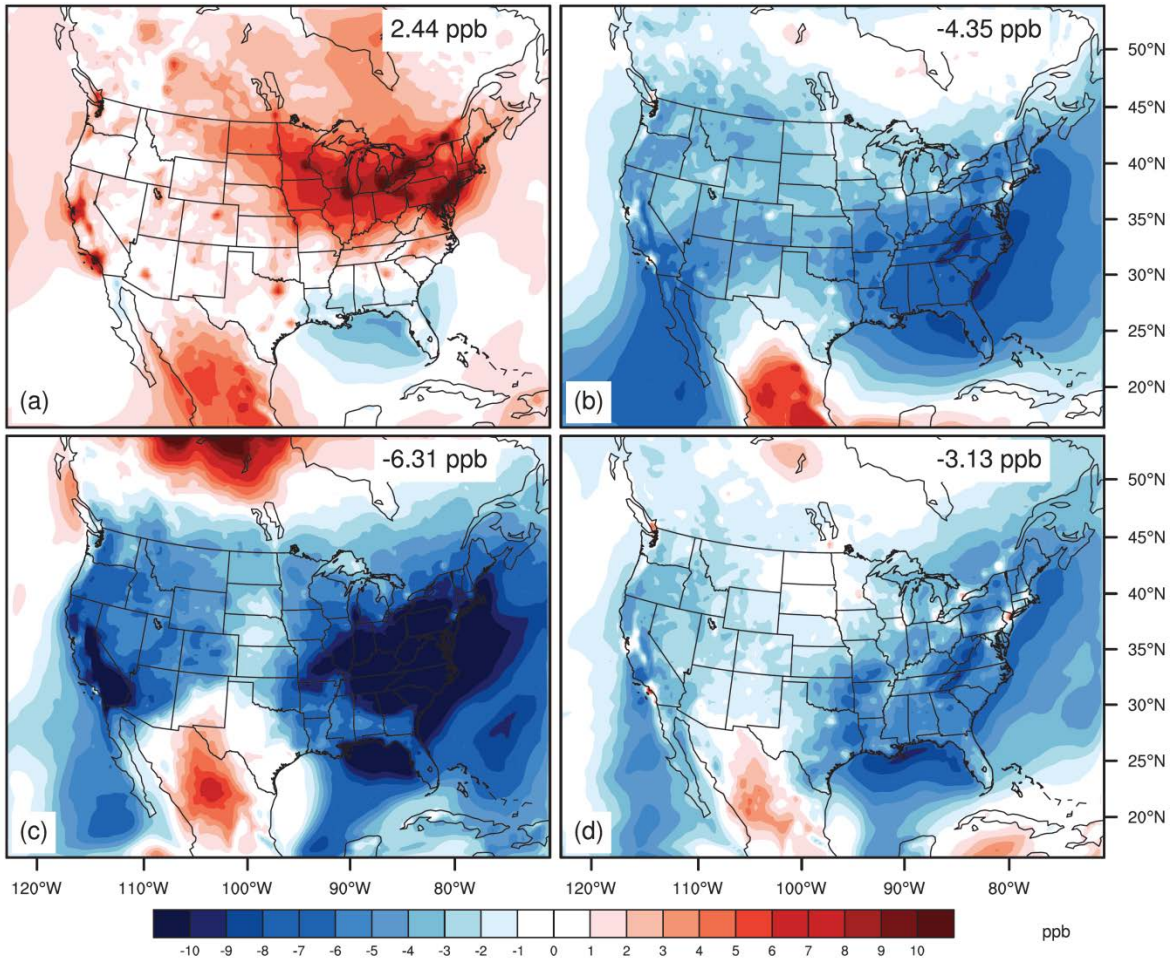

Figure A.13. Seasonal distributions of O_3 changes (ppb) between S_REF in 2050 and S_2000 for (a) winter, (b) spring, (c) summer and (d) fall. The three-year annual averages over U.S. is -2.84 ppb.

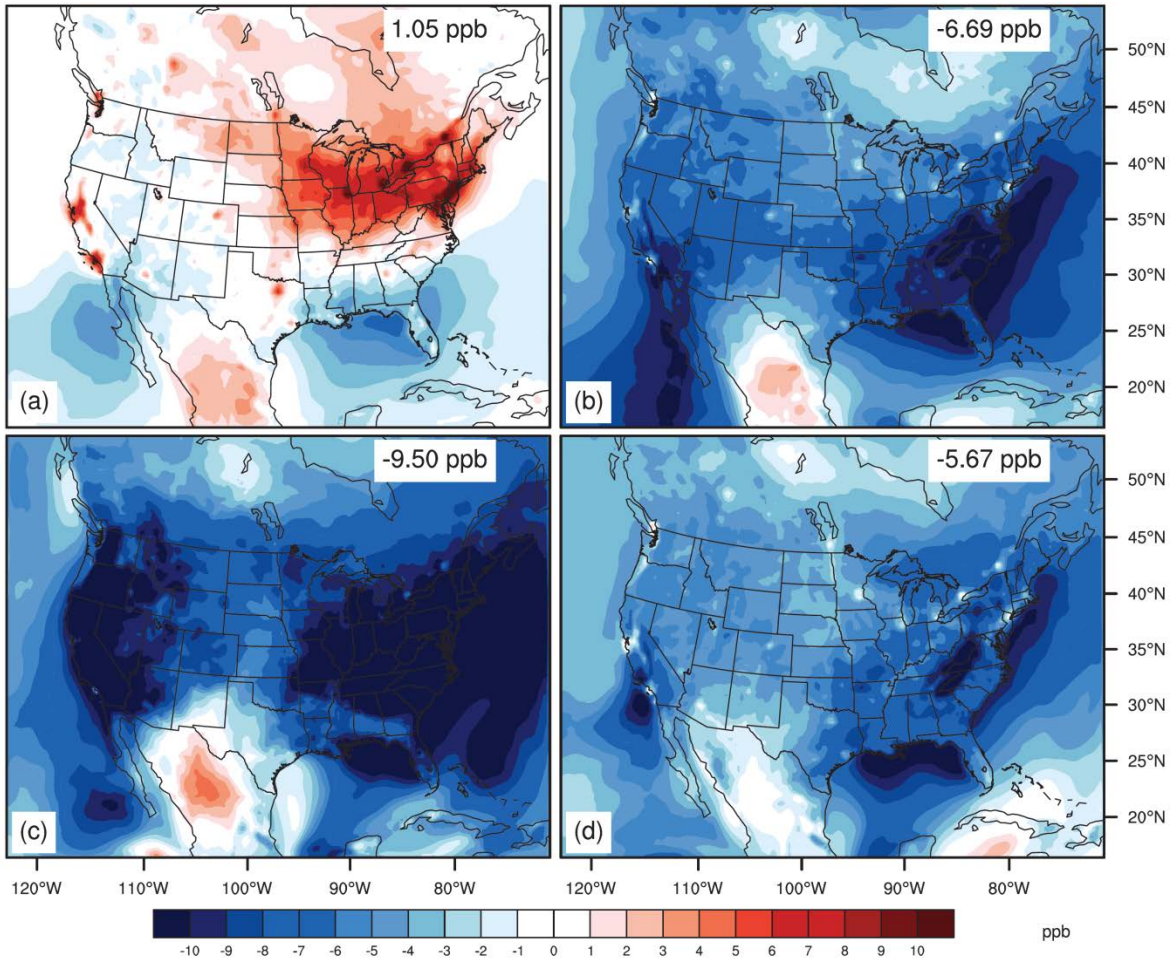

Figure A.14. As for Fig. A.13, but for the changes between S_RCP45 in 2050 and S_2000. The U.S. average is -5.20 ppb.

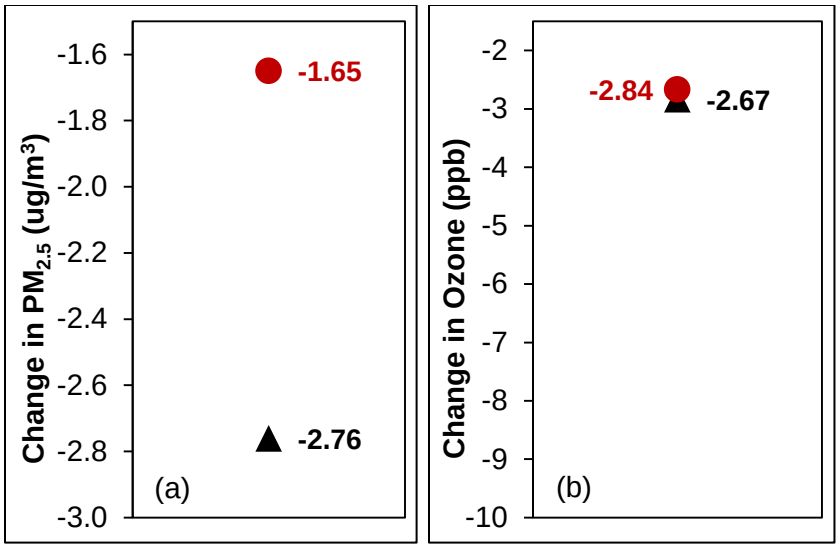

Figure A.15. Comparison of air quality changes over U.S. for REF in 2050 relative to 2000, for this study (black triangle), and MZ4 from WEST2013 (red circle), for (a) the annual average $PM_{2.5}$, and (b) annual average O_3 surface concentration. Values shown are the average of three years for both CMAQ and MZ4.

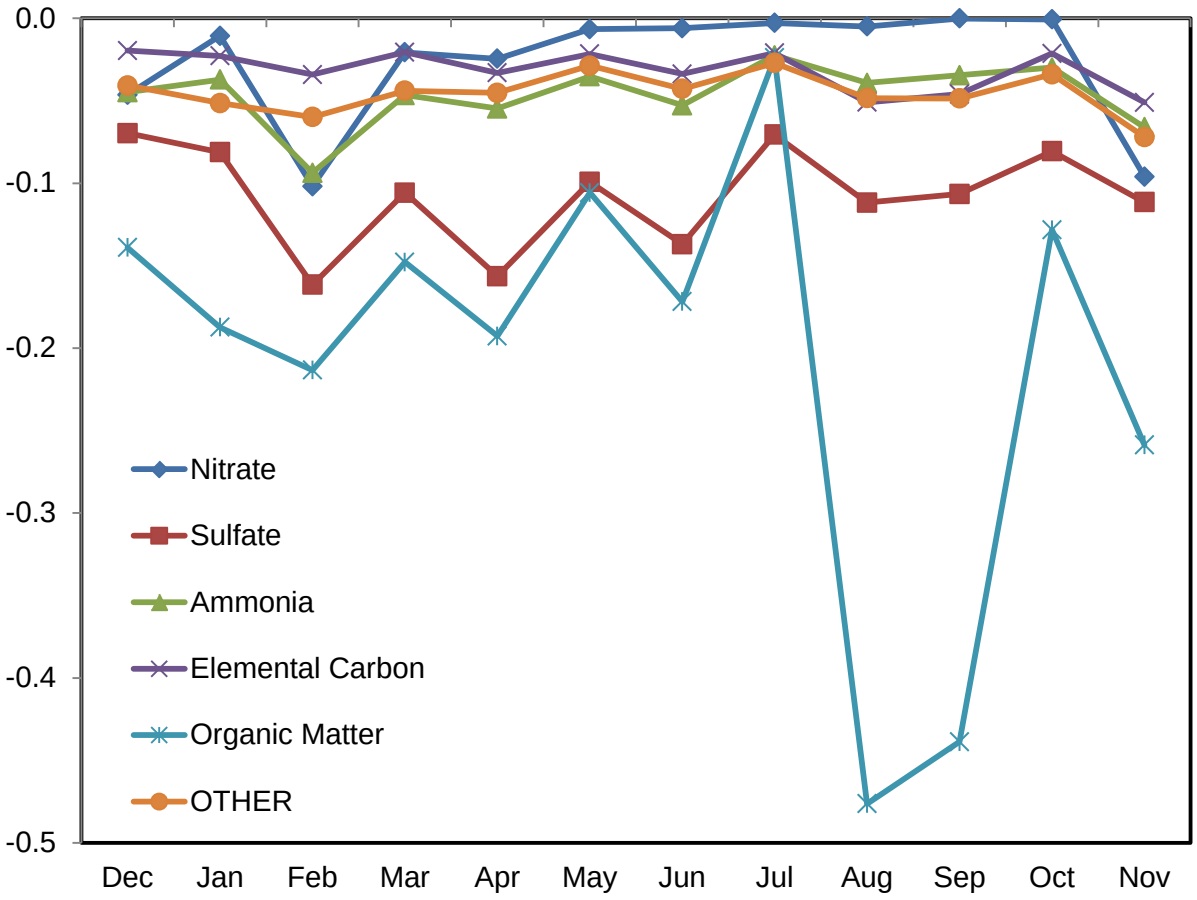

Figure A.16. Seasonal distributions of total co-benefits for major $PM_{2.5}$ components (μg m^{-3}).

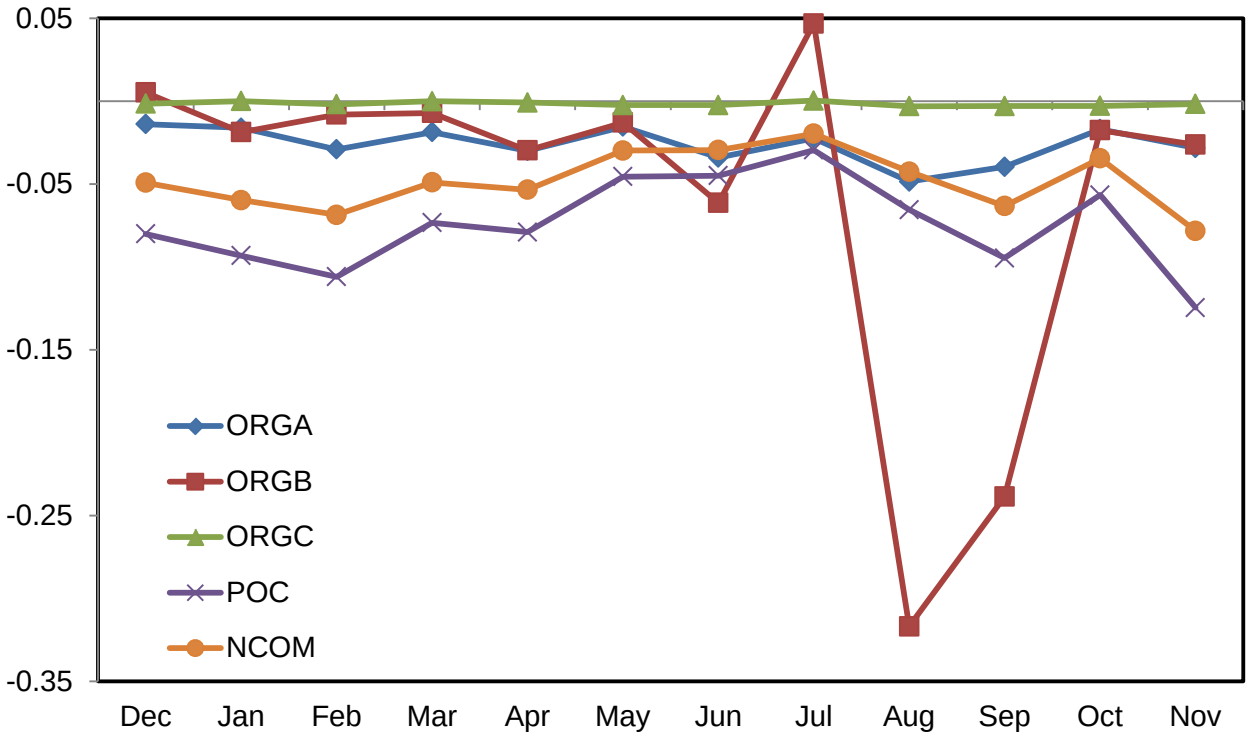

Figure A.17. Seasonal distributions of total co-benefits for organic matter (OM, μg m^{-3}), including SOA from anthropogenic source (ORGA), SOA from biogenic source (ORGB), SOA from aqueous-phase oxidation (ORGC), Primary organic carbon (POC) and non-carbon organic matter (NCOM).

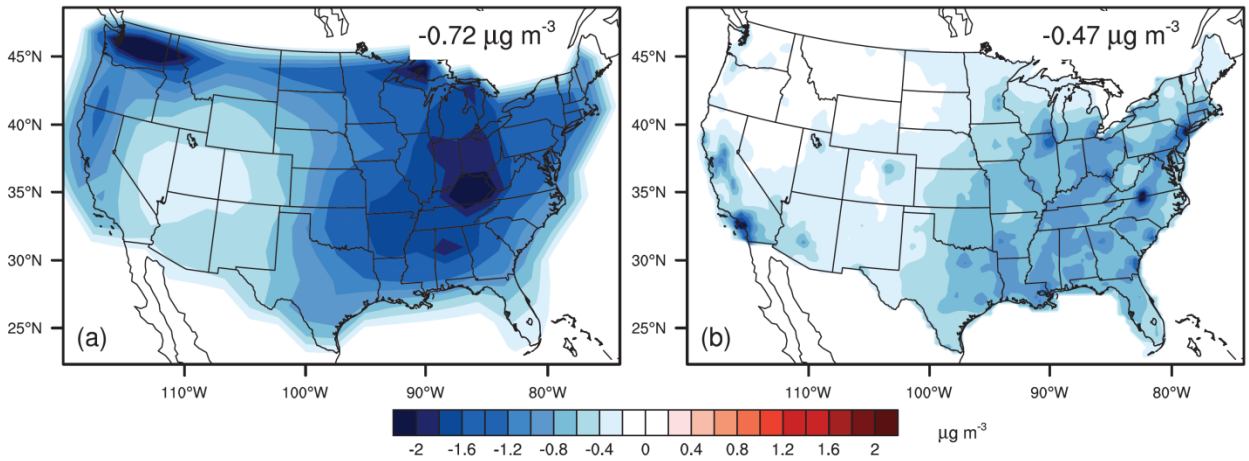

Figure A.18. The total co-benefits for $PM_{2.5}$ (µg m^{-3}) in (a) WEST2013 and (b) this study. Both the results from WEST2013 and this study are using three-year averages.

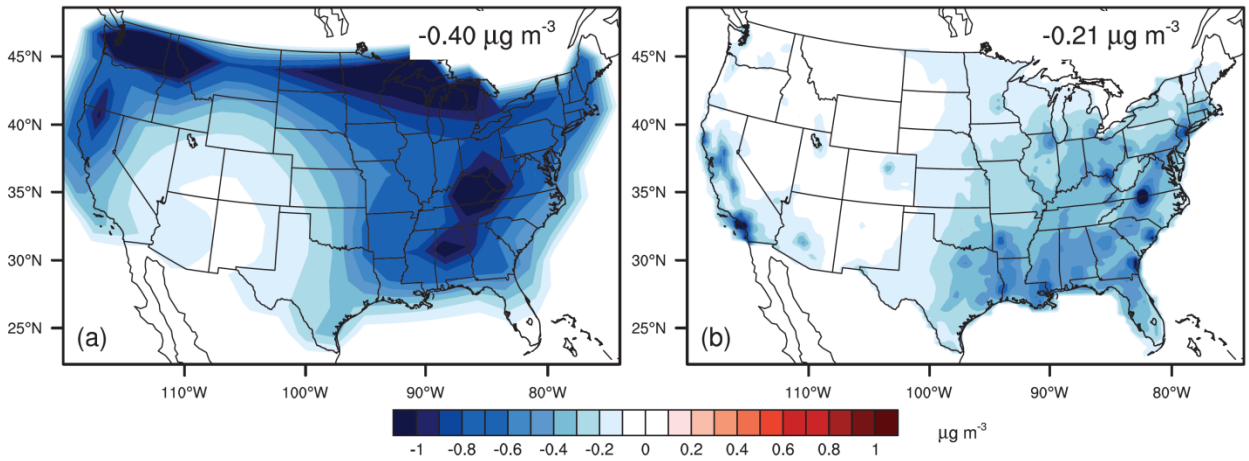

Figure A.19. As for Fig. A.18 but for OM (µg m^{-3}, including primary OC, SOA and NCOM).

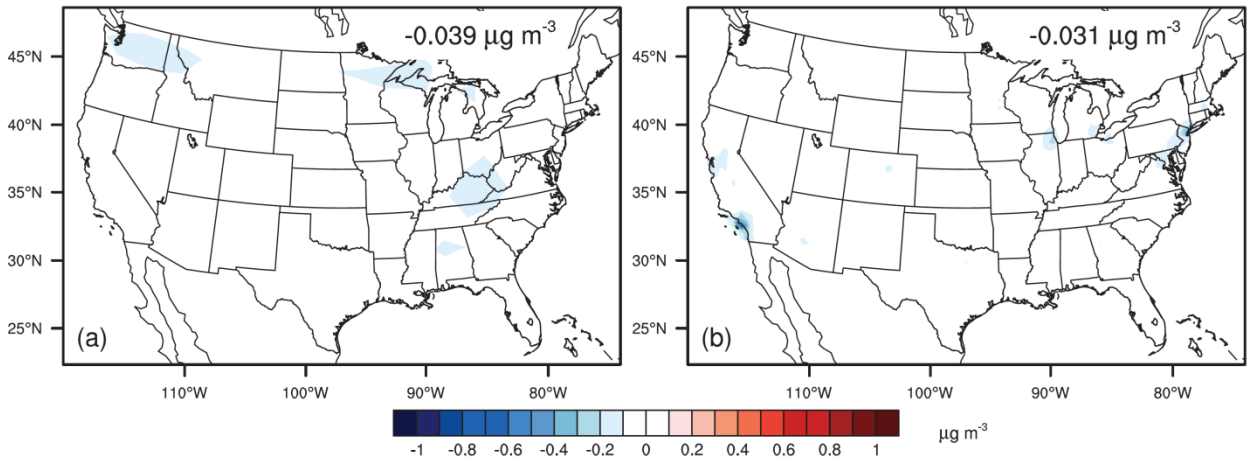

Figure A.20. As for Fig. A.18 but for EC (µg m^{-3}).

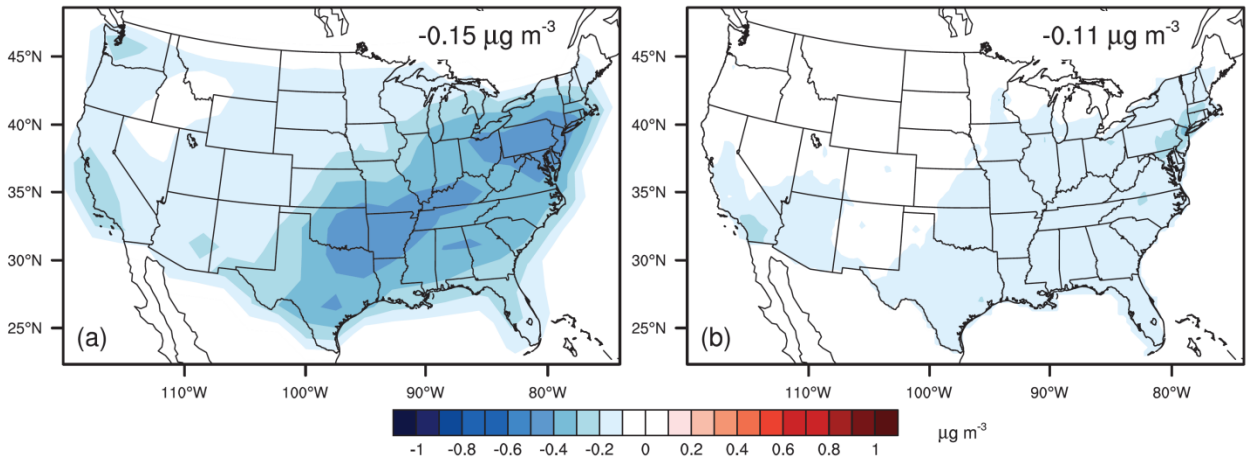

Figure A.21. As for Figure A.18 but for SO_4^{2-} (µg m^{-3}).

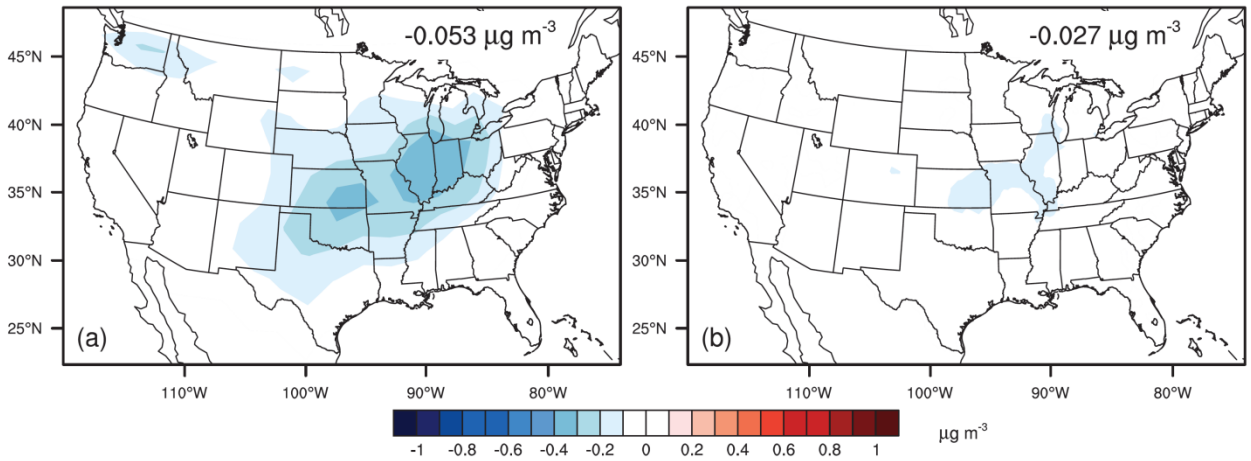

Figure A.22. As for Fig. A.18 but for NO_3^- (µg m^{-3}).

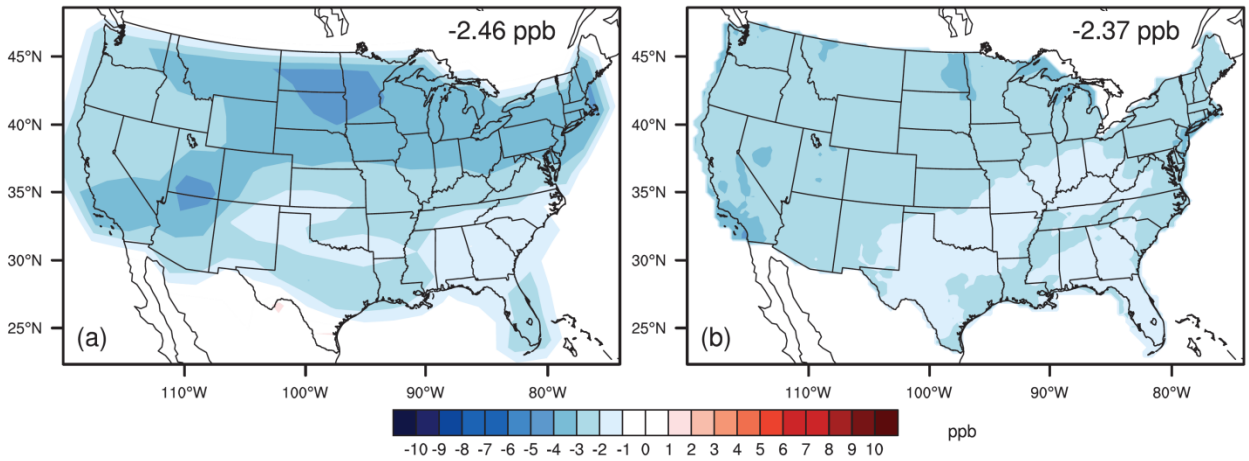

Figure A.23. The total co-benefits for annual area-weighted O_3 (ppb) in (a) WEST2013 and (b) this study. Both WEST2013 and this study are using three-year averages.

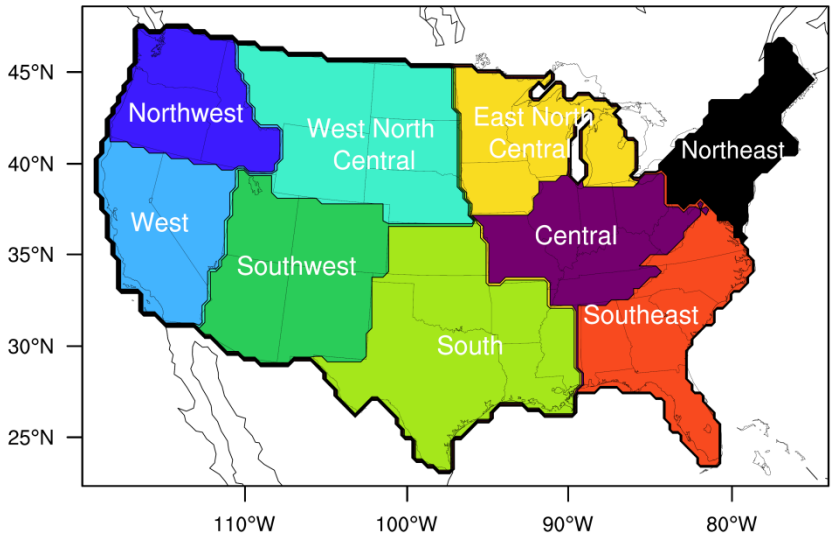

Figure A.24. The nine U.S. climate regions defined by the National Oceanic and Atmospheric Administration (http://www.ncdc.noaa.gov/monitoring-references/maps/us-climate-regions.php, accessed 5 December 2014).

APPENDIX B. CO-BENEFITS OF GLOBAL, DOMESTIC, AND SECTORAL GREENHOUSE GAS MITIGATION ON US AIR QUALITY AND HUMAN HEALTH IN 2050: SUPPORTING MATERIALS

Table B.1. Simulations used for health impact assessment in this study, conducted by Zhang *et al* (2016) and the last three sector simulations for this study. Boundary conditions are from the MOZART-4 (MZ4) simulations of WEST2013. Global methane (CH_4) background concentrations are fixed in CMAQ, consistent with the RCPs and WEST2013. All the simulations are run for three consecutive years, with four months spin-up.

Years	**Scenario**	**Emissions**	**Meteorology**	**BCs**	**CH_4**
2000	S_2000	2000	2000	MZ4 2000	1766 ppbv
2050	S_REF	REF	RCP8.5	MZ4 REF	2267 ppbv
	S_RCP45	RCP4.5	RCP4.5	MZ4 RCP4.5	1833 ppbv
	S_Emis	RCP4.5	RCP8.5	MZ4 e45m85	1833 ppbv
	S_Dom	[a]RCP4.5 for US	RCP8.5	MZ4 REF	2267 ppbv
	S_indUS	[b]RCP4.5 for US Industry	RCP8.5	MZ4 REF	2267 ppbv
	S_resUS	[b]RCP4.5 for US Residential	RCP8.5	MZ4 REF	2267 ppbv
	S_eneUS	[b]RCP4.5 for US Energy	RCP8.5	MZ4 REF	2267 ppbv

[a]apply emissions from RCP4.5 in US and from REF in the parts of Canada and Mexico within the domain

[b]only one sector of emissions from RCP4.5 (e.g., Industry, Residential and Energy) are used, and emissions in other sectors over the U.S., and emissions over Canada and Mexico in the domain are from REF.

Table B.2. The US average baseline mortality rates (y_0 , deaths per 1000 adult population) used by WEST2013 (in 2050 projected in IFs, version 6.54 under the UNEPGEO Base Case scenario) and BenMAP-CE (in 2005), and the adjustment ratio used in this study.

	WEST2013	**BenMAP-CE v1.0.8**	**[a]Adjustment ratio**
Respiratory	1.56	0.82	1.90
Cardiopulmonary	5.90	3.75	1.57
Lung Cancer	0.93	0.57	1.63
All-Cause	8.91	8.34	1.07

[a]Adjustment ratios are calculated by dividing the number in WEST2013 by BenMAP-CE.

Table B.3. Total anthropogenic emission reductions (Tg yr^{-1}) in the US in 2050 in RCP4.5 and REF, and the reductions (Abs Diff, Tg yr^{-1}) in different sectors in RCP4.5 compared with REF in the US. Relative diff (Ref Diff, %) is calculated as

$$(Emissions_{sector} - Emissions_{REF}) / (Emissions_{RCP4.5} - Emissions_{REF}) * 100.$$

	RCP4.5-REF	**Industry**		**Residential**		**Energy**	
		Abs Diff	Rel Diff	Abs Diff	Rel Diff	Abs Diff	Rel Diff
SO_2	-0.71	-0.38	53.52	-0.057	8.03	-0.26	36.62
NH_3	-0.26	-0.0013	0.50	0.00005	-0.02	-0.0004	0.15
NO_x	-0.48	-0.20	41.67	-0.022	4.58	-0.25	52.08
CO	-0.17	-0.071	41.76	0.014	-8.24	-0.078	45.88
EC	-0.01	-0.0012	12.00	-0.0016	16.00	-0.0036	36.00
OC	-0.02	-0.0067	33.50	-0.0040	20.00	-0.0009	4.50

Table B.4. The total co-benefits for avoided premature mortality in the US in 2050 and the mortality per capita (the avoided deaths per million people, for the future exposed population aged 30 and over) for both $PM_{2.5}$- and O_3-related mortality.

	$PM_{2.5}$-related all-cause mortality			**O_3-related Resp mortality**		
	Mortality	90% CI	Mortality per million	Mortality	90% CI	Mortality per million
AL	415	(302, 527)	116	160	(71, 247)	45
AR	227	(166, 289)	99	84	(37, 129)	36
AZ	368	(268, 467)	61	314	(139, 485)	52
CA	3827	(2787, 4857)	133	2155	(959, 3321)	75
CO	173	(126, 220)	41	199	(88, 307)	48
CT	358	(261, 455)	134	179	(80, 276)	67
DC	17	(12, 21)	106	7	(3, 10)	42
DE	64	(47, 82)	119	35	(15, 53)	64
FL	1529	(1113, 1941)	88	603	(268, 931)	35
GA	831	(605, 1056)	104	339	(151, 524)	42
IA	138	(100, 175)	69	109	(49, 169)	55
ID	26	(19, 33)	22	60	(27, 92)	51
IL	1164	(848, 1478)	134	453	(201, 699)	52
IN	458	(333, 581)	102	204	(91, 315)	45
KS	152	(110, 193)	79	85	(38, 132)	44
KY	342	(249, 435)	109	139	(62, 214)	44
LA	395	(287, 501)	124	124	(55, 191)	39
MA	473	(344, 601)	104	286	(127, 442)	63
MD	630	(459, 800)	123	282	(125, 435)	55
ME	62	(45, 79)	58	75	(33, 116)	70
MI	714	(520, 907)	108	384	(171, 592)	58
MN	258	(187, 327)	65	168	(75, 260)	42
MO	362	(264, 460)	91	166	(74, 257)	42
MS	256	(186, 325)	118	89	(40, 138)	41
MT	16	(12, 20)	20	48	(21, 74)	62
NC	824	(600, 1047)	103	387	(172, 597)	48
ND	12	(9, 15)	28	22	(10, 34)	51
NE	59	(43, 75)	55	54	(24, 83)	50
NH	104	(76, 133)	84	74	(33, 114)	59

NJ	1158	(844, 1470)	163	451	(201, 696)	64
NM	80	(58, 102)	43	93	(41, 143)	50
NV	126	(92, 160)	53	159	(71, 246)	67
NY	2057	(1498, 2610)	165	783	(349, 1208)	63
OH	994	(724, 1263)	130	431	(192, 666)	56
OK	231	(168, 293)	87	101	(45, 156)	38
OR	102	(75, 130)	33	139	(62, 214)	45
PA	1111	(809, 1411)	136	561	(249, 865)	68
RI	69	(50, 87)	108	41	(18, 64)	65
SC	452	(329, 575)	117	186	(83, 288)	48
SD	17	(13, 22)	33	28	(12, 43)	53
TN	520	(378, 660)	105	232	(103, 358)	47
TX	1776	(1292, 2255)	82	717	(318, 1107)	33
UT	73	(53, 93)	36	83	(37, 127)	40
VA	710	(517, 901)	108	319	(142, 493)	49
VT	34	(25, 43)	65	29	(13, 45)	57
WA	182	(133, 231)	32	267	(119, 412)	47
WI	369	(268, 468)	87	206	(92, 318)	49
WV	135	(98, 172)	107	73	(33, 113)	58
WY	11	(8, 14)	24	29	(13 45)	62

Table B.5. The domestic co-benefits on avoided premature mortality in the US in 2050 and the mortality per capita (the avoided deaths per million people, for the future exposed population aged 30 and over) both $PM_{2.5}$- and O_3-related mortality.

	$PM_{2.5}$-related all-cause mortality			**O_3-related Resp mortality**		
	Mortality	90% CI	Mortality per million	Mortality	90% CI	Mortality per million
AL	293	(213, 372)	82	60	(27, 93)	17
AR	149	(108, 189)	65	37	(17, 58)	16
AZ	228	(166, 290)	38	89	(39, 138)	15
CA	3179	(2315, 4035)	111	882	(392, 1367)	31
CO	110	(80, 140)	26	56	(25, 86)	13
CT	322	(235, 409)	121	79	(35, 122)	29
DC	17	(12, 22)	109	3	(1, 4)	18
DE	65	(47, 82)	120	15	(7, 23)	27
FL	1291	(939, 1639)	74	257	(114, 398)	15
GA	697	(508, 885)	87	148	(66, 230)	19
IA	115	(84, 146)	57	32	(14, 50)	16
ID	19	(14, 25)	16	9	(4, 13)	7
IL	1029	(749, 1307)	118	180	(80, 280)	21
IN	443	(323, 563)	99	96	(42, 148)	21
KS	99	(72, 126)	52	30	(13, 46)	16
KY	282	(205, 358)	90	70	(31, 108)	22
LA	292	(212, 370)	92	44	(20, 68)	14
MA	424	(308, 538)	93	109	(48, 169)	24
MD	640	(466, 812)	125	122	(54, 190)	24
ME	45	(33, 58)	42	19	(8, 30)	18
MI	711	(517, 902)	108	133	(59, 207)	20
MN	222	(162, 282)	56	40	(18, 62)	10
MO	264	(192, 335)	66	68	(30, 106)	17
MS	176	(128, 224)	82	33	(15, 51)	15
MT	9	(7, 11)	12	5	(2, 8)	7
NC	776	(565, 985)	97	164	(73, 254)	20
ND	9	(7, 12)	21	3	(1, 4)	6
NE	42	(31, 54)	39	14	(6, 22)	13
NH	90	(65, 114)	72	24	(11, 37)	19

NJ	1080	(787, 1372)	152	184	(82, 285)	26
NM	47	(35, 60)	25	23	(10, 35)	12
NV	81	(59, 103)	34	41	(18, 64)	17
NY	1868	(1361, 2371)	150	310	(138, 481)	25
OH	953	(694, 1211)	125	183	(81, 284)	24
OK	138	(101, 176)	52	43	(19, 67)	16
OR	86	(63, 110)	28	18	(8, 28)	6
PA	1057	(769, 1342)	129	221	(98, 343)	27
RI	61	(44, 77)	96	17	(8, 27)	27
SC	406	(295, 515)	105	78	(35, 121)	20
SD	14	(10, 18)	27	6	(2, 9)	11
TN	403	(294, 512)	81	99	(44, 154)	20
TX	1204	(876, 1530)	56	253	(112, 392)	12
UT	54	(39, 68)	26	20	(9, 31)	10
VA	664	(483, 843)	101	140	(62, 217)	21
VT	25	(18, 31)	48	8	(4, 12)	15
WA	169	(123, 215)	30	32	(14, 50)	6
WI	320	(233, 406)	76	66	(29, 103)	16
WV	123	(90, 156)	97	32	(14, 49)	25
WY	6	(4, 8)	13	6	(2, 9)	12

Table B.6. The foreign co-benefits on avoided premature mortality in the US in 2050 and the mortality per capita (the avoided deaths per million people, for the future exposed population aged 30 and over) both $PM_{2.5}$- and O_3-related mortality.

	$PM_{2.5}$-related all-cause mortality			**O_3-related Resp mortality**		
	Mortality	90% CI	Mortality per million	Mortality	90% CI	Mortality per million
AL	123	(89, 156)	34	100	(45, 156)	28
AR	79	(58, 100)	34	46	(21, 72)	20
AZ	140	(102, 178)	23	226	(100, 350)	38
CA	653	(475, 829)	23	1282	(570, 1986)	45
CO	63	(46, 80)	15	144	(64, 223)	34
CT	36	(26, 46)	14	101	(45, 156)	38
DC	-1	(0, -1)	-3	4	(2, 6)	24
DE	-1	(0, -1)	-1	20	(9, 31)	37
FL	239	(174, 303)	14	347	(154, 539)	20
GA	135	(98, 171)	17	192	(85, 298)	24
IA	23	(17, 29)	12	78	(34, 120)	39
ID	6	(5, 8)	5	51	(23, 79)	44
IL	136	(99, 173)	16	274	(121, 424)	31
IN	15	(11, 19)	3	109	(48, 169)	24
KS	52	(38, 67)	27	56	(25, 86)	29
KY	60	(44, 77)	19	69	(31, 107)	22
LA	104	(75, 132)	33	80	(36, 124)	25
MA	50	(36, 63)	11	178	(79, 276)	39
MD	-10	(-7, -13)	-2	161	(71, 249)	31
ME	17	(12, 21)	16	56	(25, 87)	52
MI	4	(3, 5)	1	252	(112, 390)	38
MN	35	(26, 45)	9	128	(57, 199)	32
MO	99	(72, 125)	25	99	(44, 153)	25
MS	79	(58, 101)	37	56	(25, 88)	26
MT	7	(5, 9)	9	43	(19, 67)	55
NC	49	(36, 62)	6	224	(99, 348)	28
ND	3	(2, 4)	7	19	(8, 30)	44
NE	17	(12, 22)	16	40	(18, 62)	37
NH	15	(11, 19)	12	50	(22, 78)	40

NJ	78	(57, 100)	11	270	(120, 418)	38
NM	33	(24, 41)	17	70	(31, 109)	38
NV	45	(33, 57)	19	119	(53, 184)	50
NY	190	(139, 242)	15	477	(212, 738)	38
OH	41	(30, 52)	5	249	(111, 387)	33
OK	93	(68, 118)	35	58	(26, 91)	22
OR	16	(12, 20)	5	121	(54, 187)	39
PA	55	(40, 70)	7	341	(152, 529)	42
RI	8	(6, 10)	12	24	(11, 37)	38
SC	47	(34, 60)	12	109	(48, 168)	28
SD	3	(2, 4)	6	22	(10, 34)	42
TN	117	(85, 149)	24	133	(59, 206)	27
TX	573	(417, 728)	26	466	(207, 722)	22
UT	20	(14, 25)	10	63	(28, 97)	31
VA	46	(33, 58)	7	180	(80, 279)	27
VT	9	(7, 12)	18	22	(10, 33)	42
WA	13	(10, 17)	2	235	(104, 364)	41
WI	49	(36, 63)	12	140	(62, 217	33
WV	12	(9, 15)	10	42	(19, 65)	33
WY	5	(4, 7)	11	24	(10, 36)	51

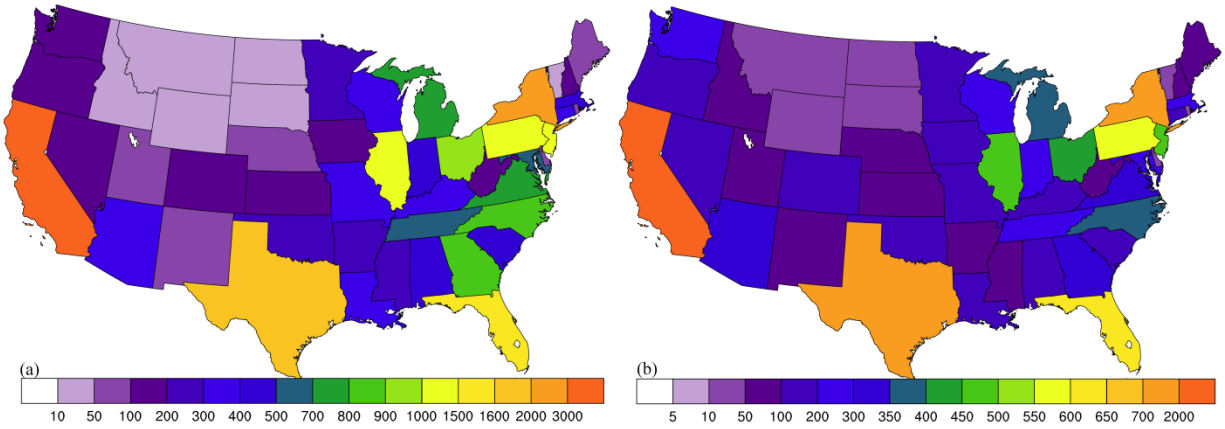

Figure B.1. Spatial distributions of the avoided mortality (deaths $^{-1}$) from the total co-benefits in US in 2050 for (a) $PM_{2.5}$ and (b) O_3. Note that the scales in the two panels differ.

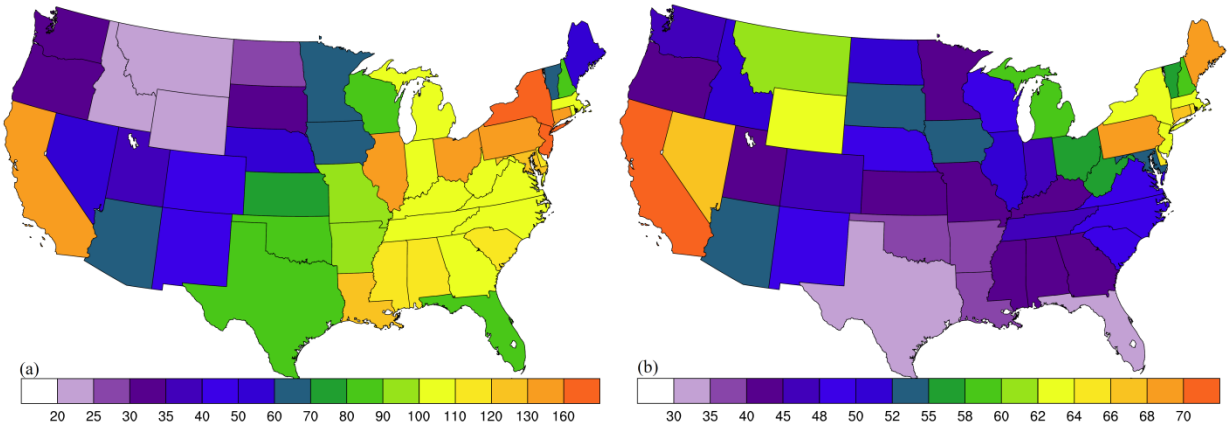

Figure B.2. Spatial distributions of the mortality per capita (MPC, total avoided deaths per million people) from the total co-benefits in US in 2050 for (a) $PM_{2.5}$ and (b) O_3. Note that the scales in the two panels differ.

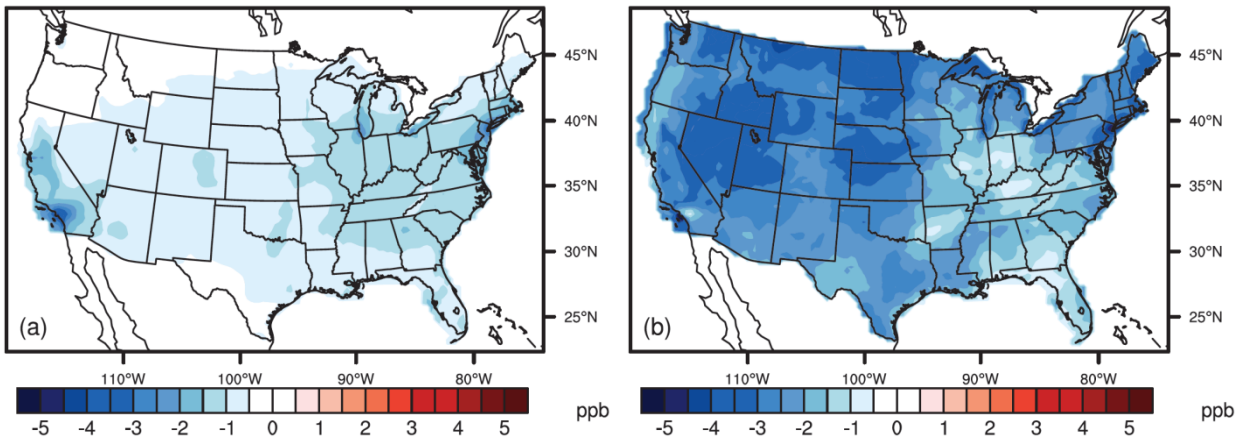

Figure B.3. (a) Domestic (0.80 ppbv for three-year Simple Average in US in 2050) and (b) foreign co-benefits (2.16 ppbv for three-year Simple Average in US in 2050) for 6-month ozone-season average of 1-hr daily maximum of O_3.

APPENDIX C. SOUTHWARD REDISTRIBUTION OF EMISSIONS DOMINATES THE 1980 TO 2010 TROPOSPHERIC OZONE CHANGE: SUPPORTING MATERIALS

Table C.1. Aircraft campaigns used in this study for the model evaluation purpose.

Campaign	Year	Month	Platform
TOTE	1995	December	DC-8
VOTE	1996	January	DC-8
STRAT	1995/96	Jan-Dec	ER-2
PEM-Trop-A	1996	Aug-Oct	P3/DC-8
SONEX	1997	Oct-Nov	DC-8
POLARIS	1997	Apr-Jun, Sep	ER-2
POLINAT-2	1997	Sep-Oct	Falkon
PEM-Trop-B	1999	Mar-Apr	P3/DC-8
ACCENT	1999	Apr, Sep-Oct	WB57
SOS	1999	Jun, Jul	NOAA WP-3D
SOLVE	99/00	Dec-Mar	DC-8
SOLVE	99/00	Dec-Mar	ER-2
TOPSE	2000	Feb-May	C130
TRACE-P	2000	Feb-Apr	P3/DC8
TexAQS	2000	Aug, Sep	NOAA WP-3D
ITCT	2002	Apr, May	NOAA WP-3D
Crystal Face	2002	Jun-Jul	WB57
INTEX-A	2004	Mar-Aug	DC8
NEAQS-ITCT	2004	Jul, Aug	NOAA WP-3D
Ave Fall	2004	Oct, Nov	WB57
Ave Houston	2005	June	WB57
Polar Ave	2005	Jan, Feb	WB57
Cr-Ave	2006	Jan, Feb	WB57
INTEX-B	2006	Mar-Aug	DC8
TexAQS	2006	Sep, Oct	NOAA WP-3D
TC4	2007	July	WB57
APCPAC	2008	Mar, Apr	NOAA WP-3D
APCTAS	2008	Apr-Jun	DC-8
START08	2008	Apr-Jun	G5
CalNex	2010	May, Jun	NOAA WP-3D

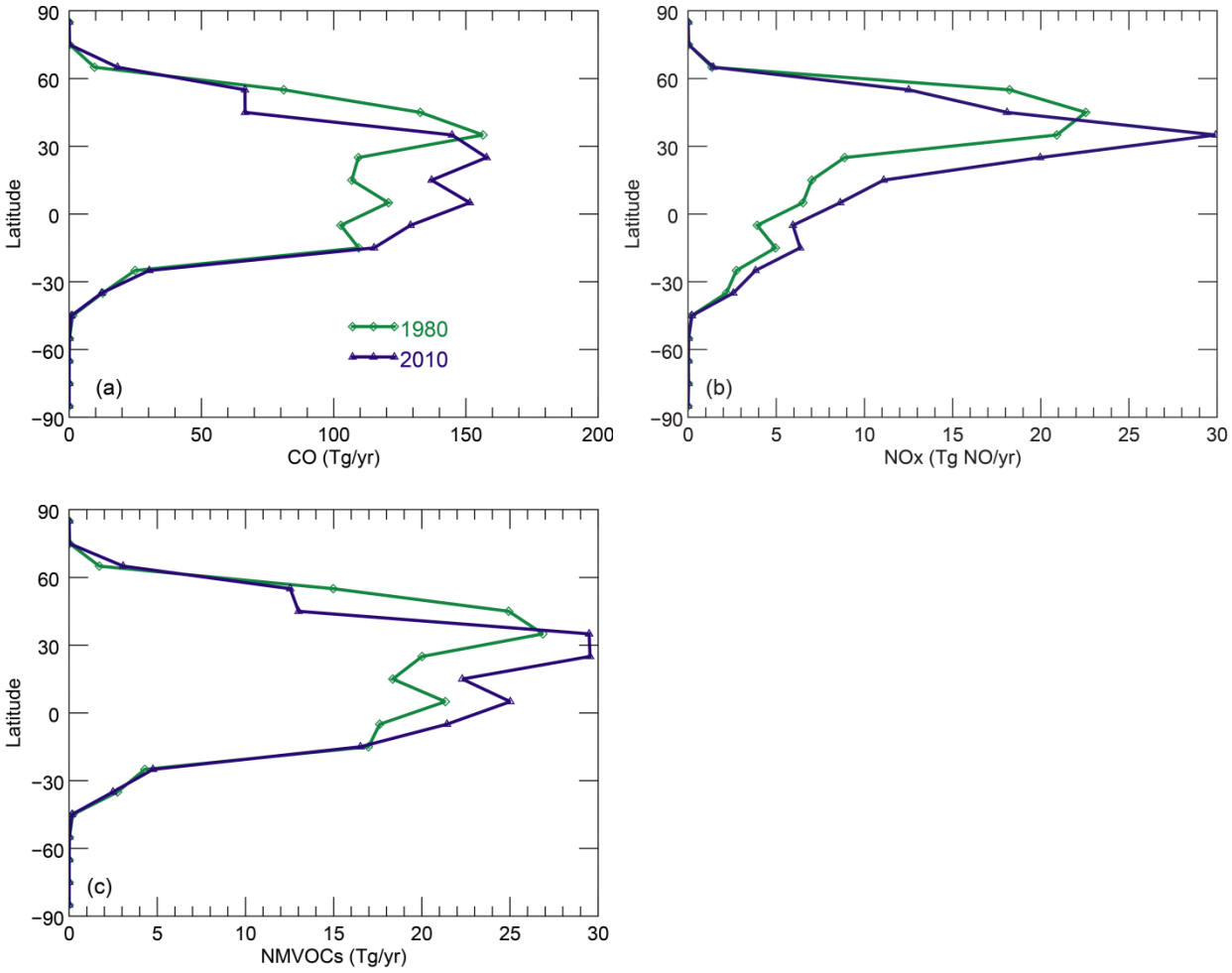

Figure C.1. Latitudinal distributions of global anthropogenic emissions in 1980 and 2010, including fire emissions defined as anthropogenic, shown in 10° increments.

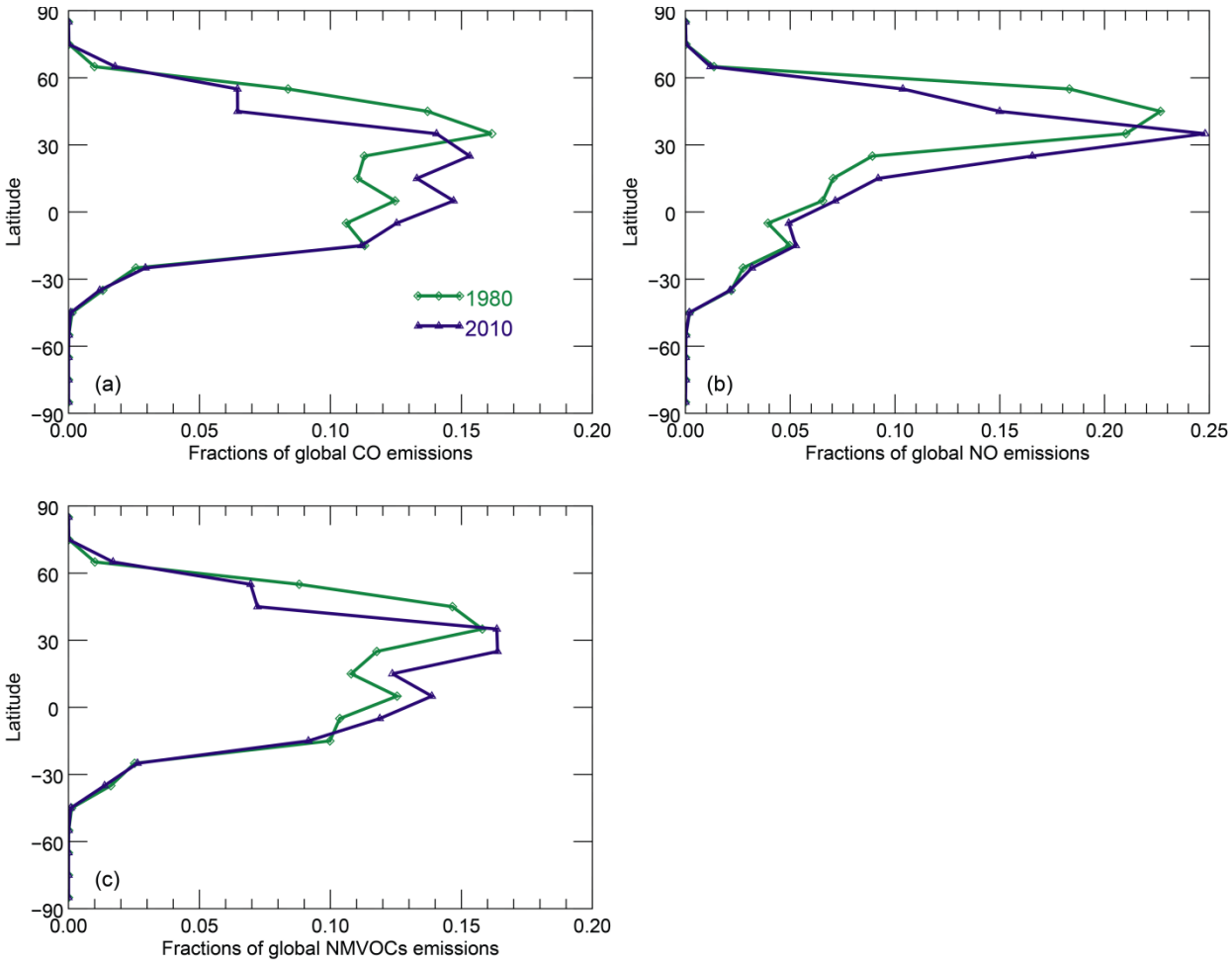

Figure C.2. As for Figure C.1, but for the emission fractions of global total emissions for each latitudinal band.

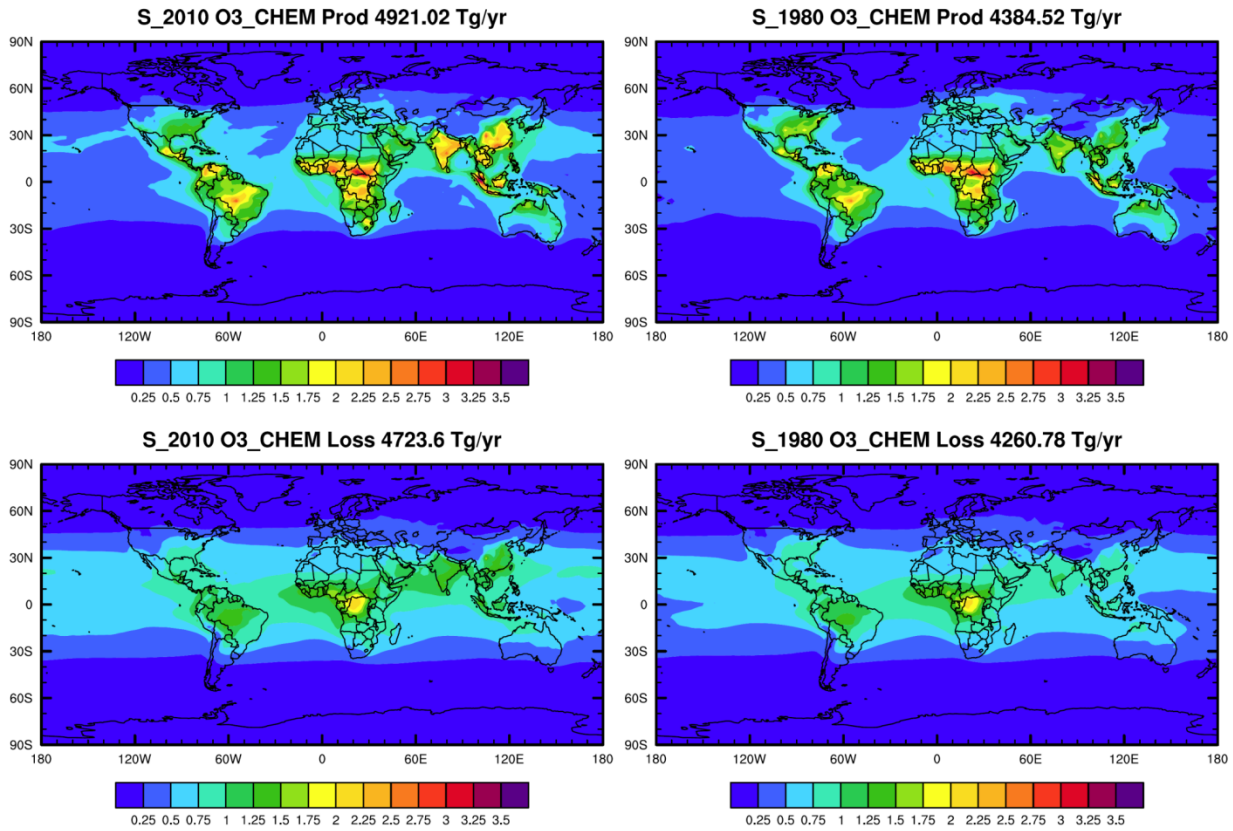

Figure C.3. Global O_3 chemical production and loss in 2010 (a, c) and 1980 (b,d), including the O_3 chemical production rate (P_{O3}, a, b) and O_3 chemical loss rate (L_{03}, c, d).

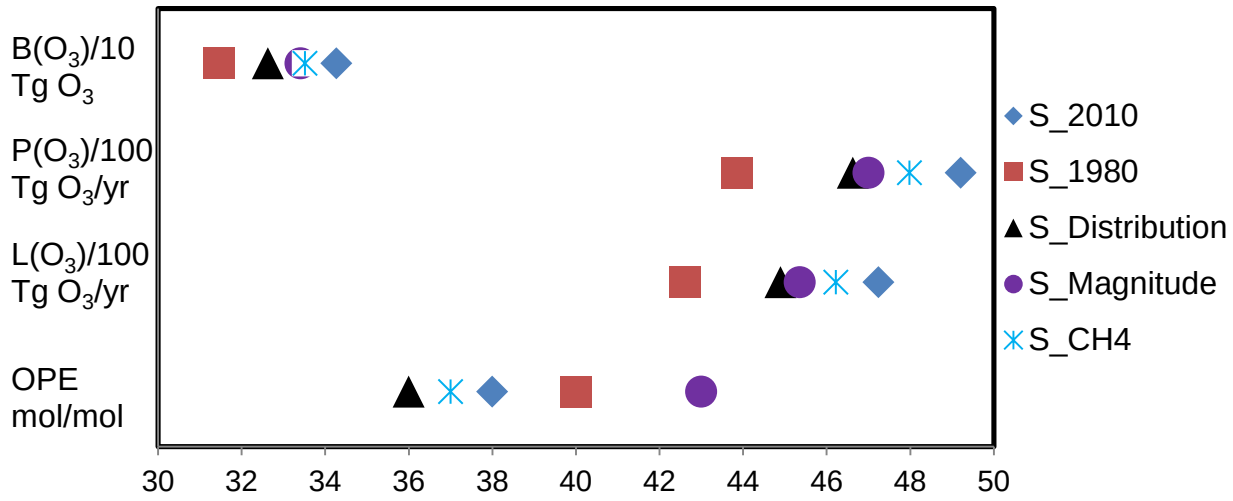

Figure C.4. Tropospheric O_3 budget from the different simulations, for global annual mean tropospheric O_3 burden ($B_{O3}/10$), global annual O_3 chemical production ($P_{O3}/100$), global annual O_3 chemical loss ($L_{O3}/100$), and the global O_3 production efficiency (OPE, mol/mol, defined as the gross O_3 chemical production (P_{O3}) per NO_x emitted, Liu et al., 1997).

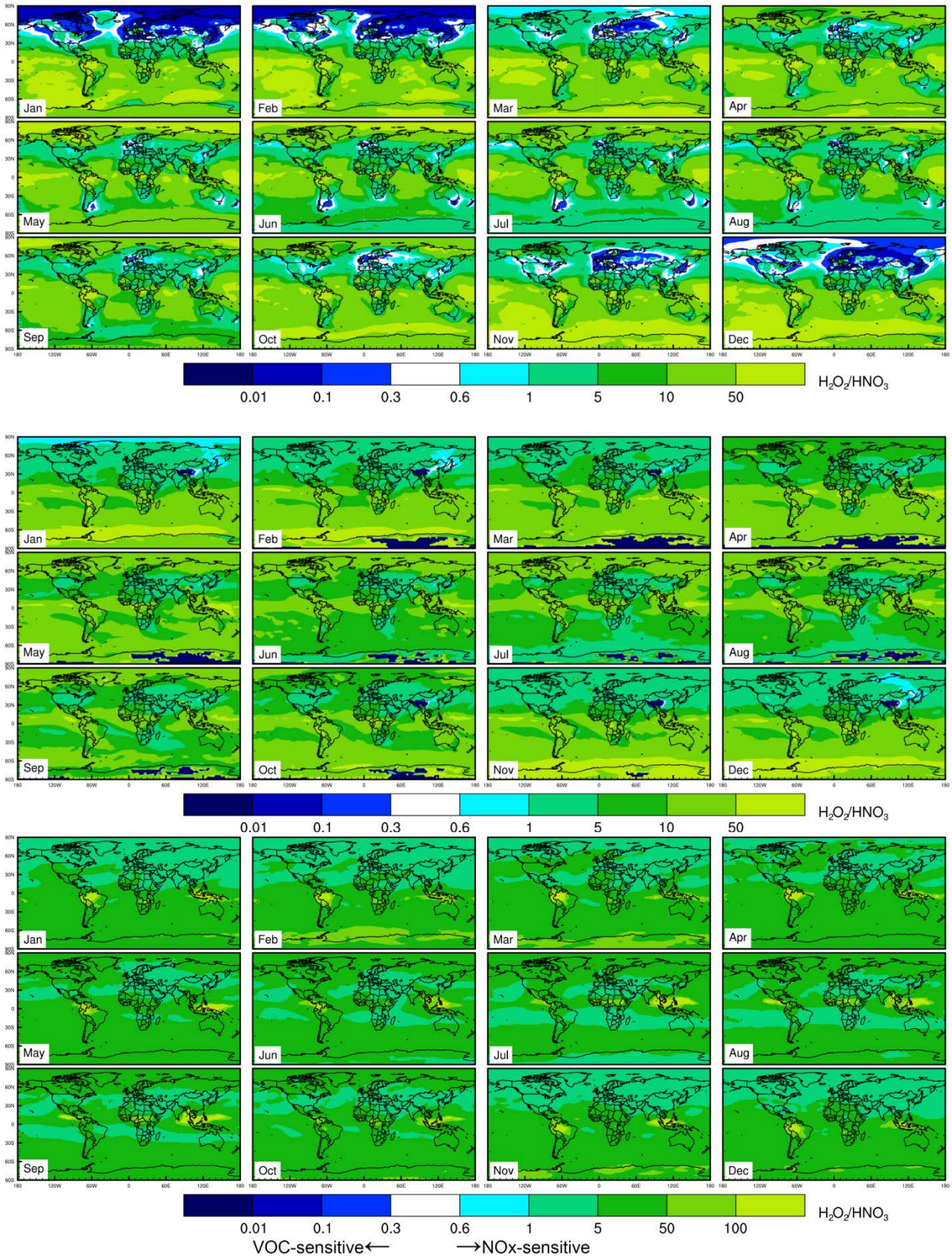
Jan
Feb
Mar
Apr
May
Jun
Jul
Aug
Sep
Oct
Nov
Dec
0.01
0.1
0.3
0.6
1
5
10
50
100
H_2O_2/HNO_3
VOC-sensitive←
→NOx-sensitive

Figure C.5. Global distributions of the monthly average surface (top), mid-troposphere (750hpa, middle) and upper-troposphere (500hpa, bottom) H_2O_2/HNO_3, with the transition between VOCs-sensitive and NO_x-sensitive conditions at roughly 0.3-0.6 (Sillman et al., 1997).

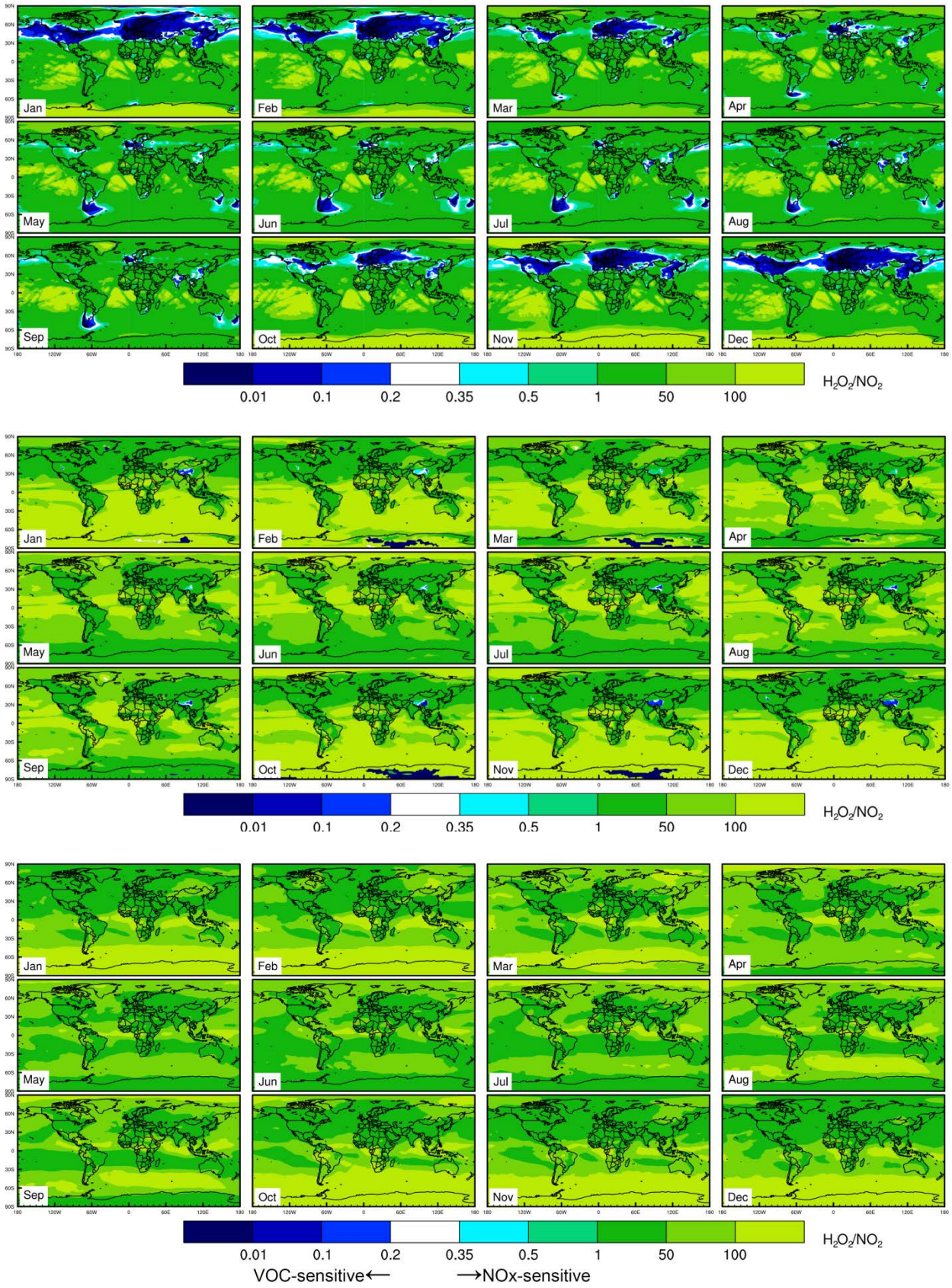
Jan
Feb
Mar
Apr
May
Jun
Jul
Aug
Sep
Oct
Nov
Dec
0.01
0.1
0.2
0.35
0.5
1
50
100
H2O2/NO2
VOC-sensitive←
→NOx-sensitive

Figure C.6. Global distributions of the monthly average surface (top), mid-troposphere (750hpa, middle) and upper-troposphere (500hpa, bottom) H_2O_2/NO_2, with the transitions between VOCs-sensitive and NOx-sensitive conditions at roughly 0.2-0.35 (Sillman et al., 1997).

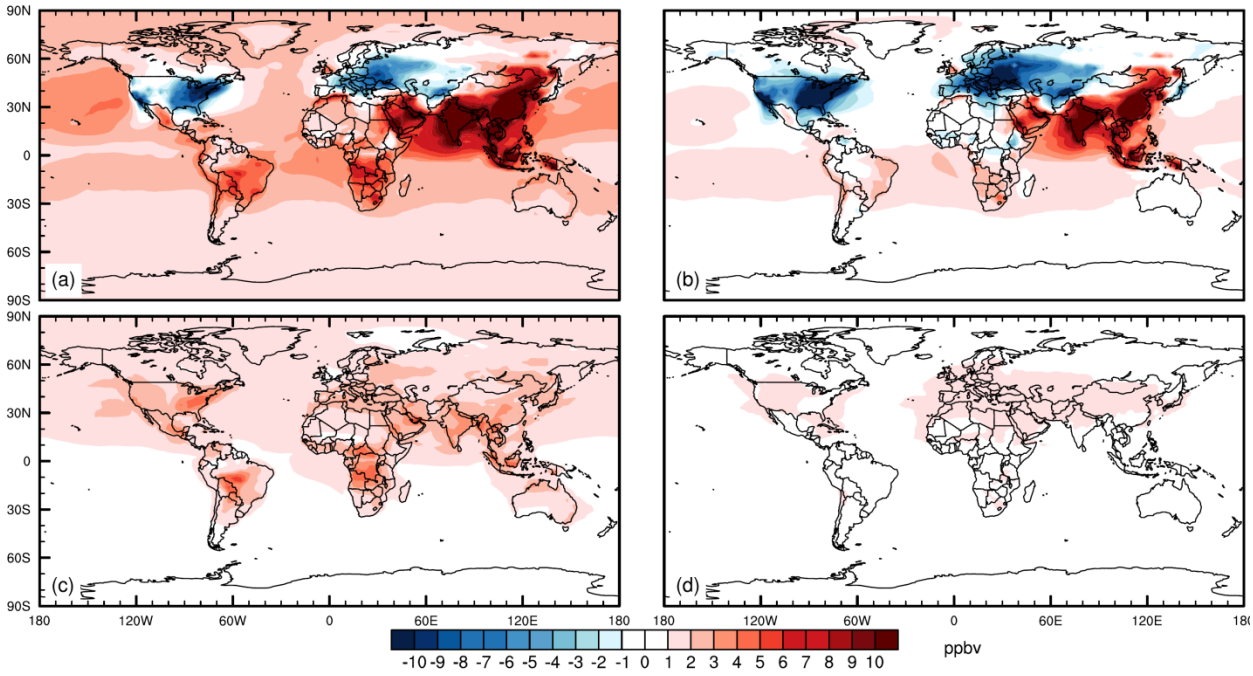

Figure C.7. (a) Global surface three-month O_3 season MDA8 change from 1980 to 2010, and influences of changes in (b) the global emissions spatial pattern, (c) the global emissions magnitude, and (d) global CH_4 mixing ratio.

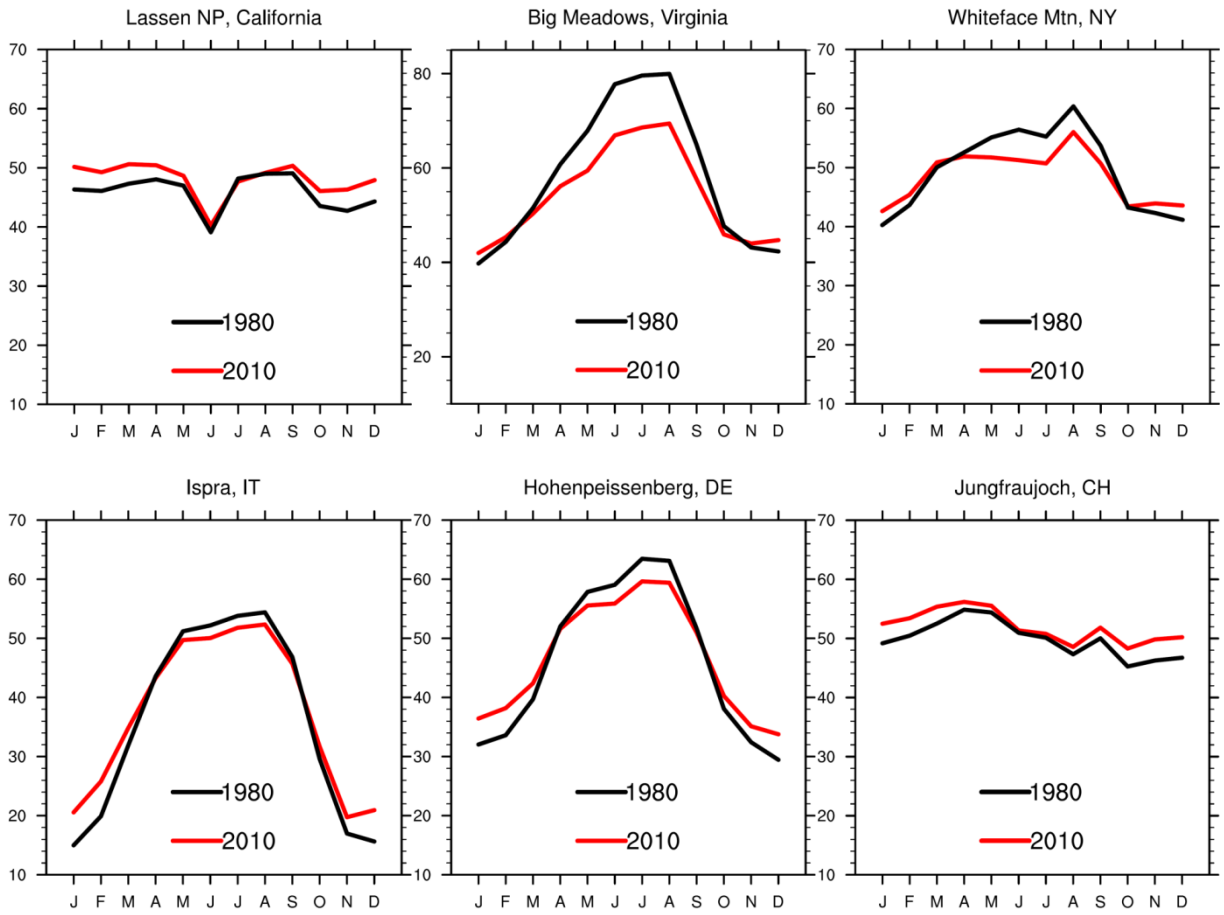

Figure C.8. Seasonal peak O_3 in 1980 and 2010 for rural observation sites which are shown to experience changes in the seasonal cycle (Parrish, 2013; Cooper, 2014).

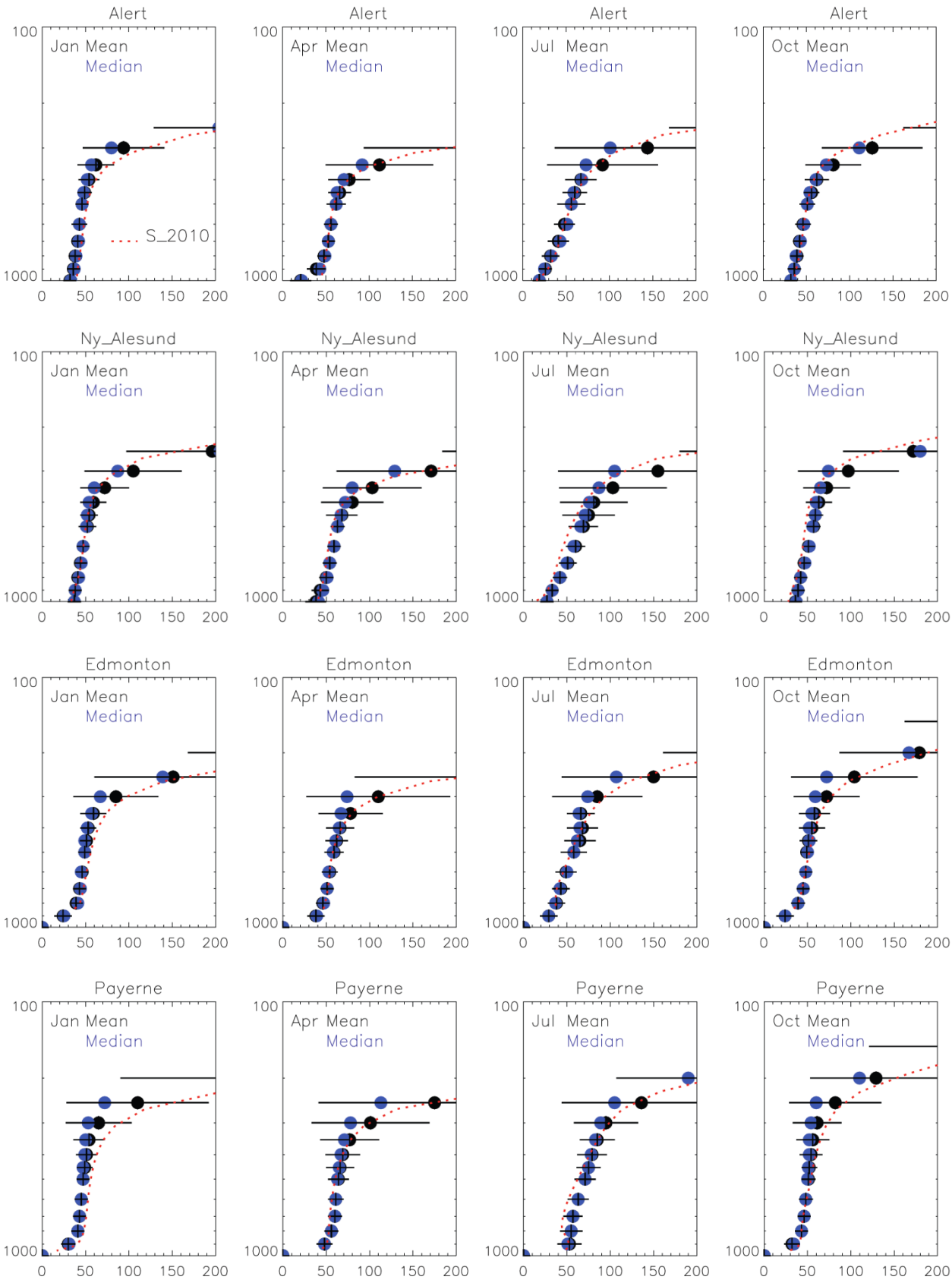
Alert
Jan Mean
Median
S_2010
Alert
Apr Mean
Median
Alert
Jul Mean
Median
Alert
Oct Mean
Median
Ny_Alesund
Jan Mean
Median
Ny_Alesund
Apr Mean
Median
Ny_Alesund
Jul Mean
Median
Ny_Alesund
Oct Mean
Median
Edmonton
Jan Mean
Median
Edmonton
Apr Mean
Median
Edmonton
Jul Mean
Median
Edmonton
Oct Mean
Median
Payerne
Jan Mean
Median
Payerne
Apr Mean
Median
Payerne
Jul Mean
Median
Payerne
Oct Mean
Median
100
1000
0
50
100
150
200

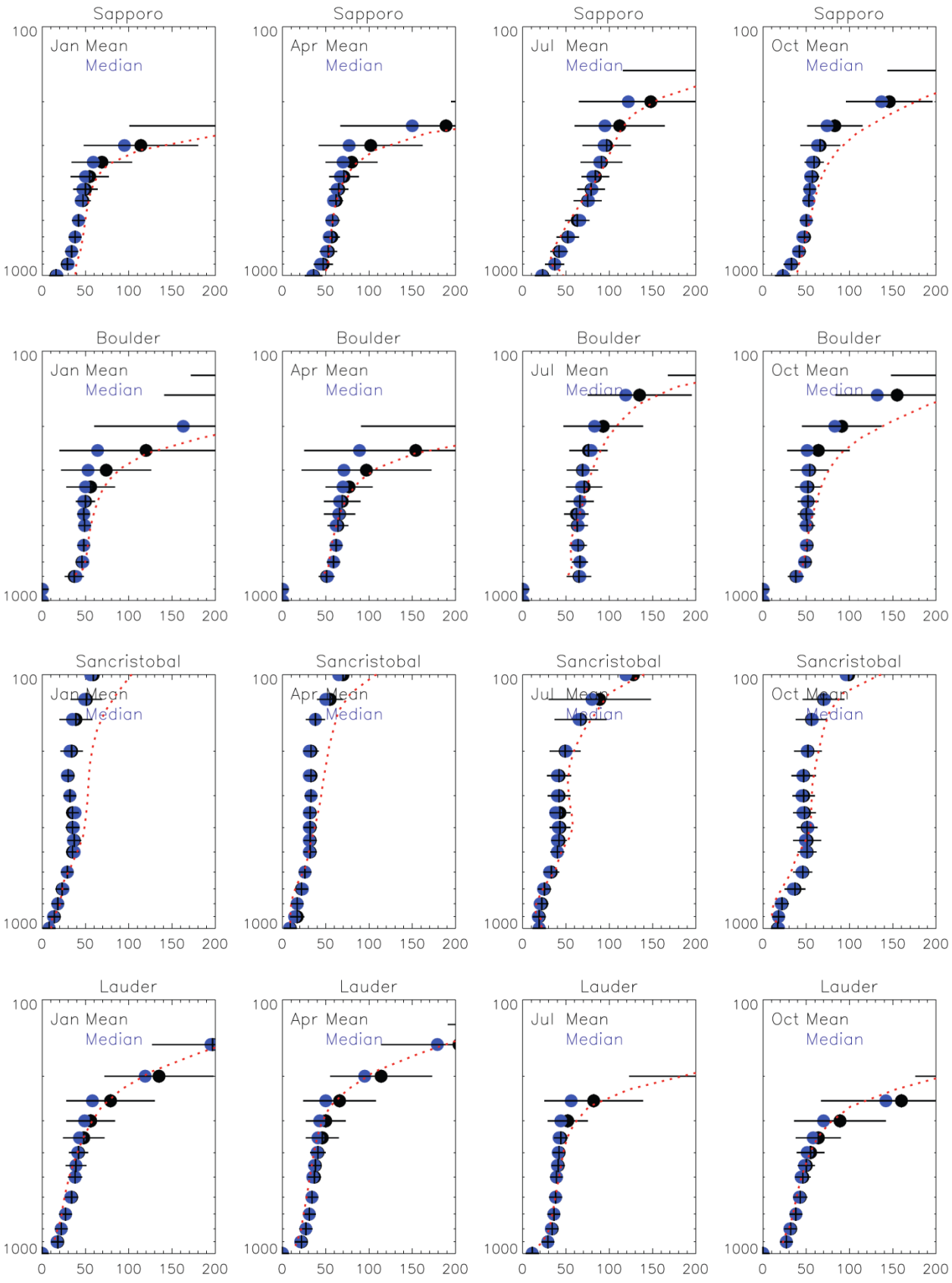
Sapporo
Jan Mean
Median
Sapporo
Apr Mean
Median
Sapporo
Jul Mean
Median
Sapporo
Oct Mean
Median
Boulder
Jan Mean
Median
Boulder
Apr Mean
Median
Boulder
Jul Mean
Median
Boulder
Oct Mean
Median
Sancristobal
Jan Mean
Median
Sancristobal
Apr Mean
Median
Sancristobal
Jul Mean
Median
Sancristobal
Oct Mean
Median
Lauder
Jan Mean
Median
Lauder
Apr Mean
Median
Lauder
Jul Mean
Median
Lauder
Oct Mean
Median
100
1000
0
50
100
150
200

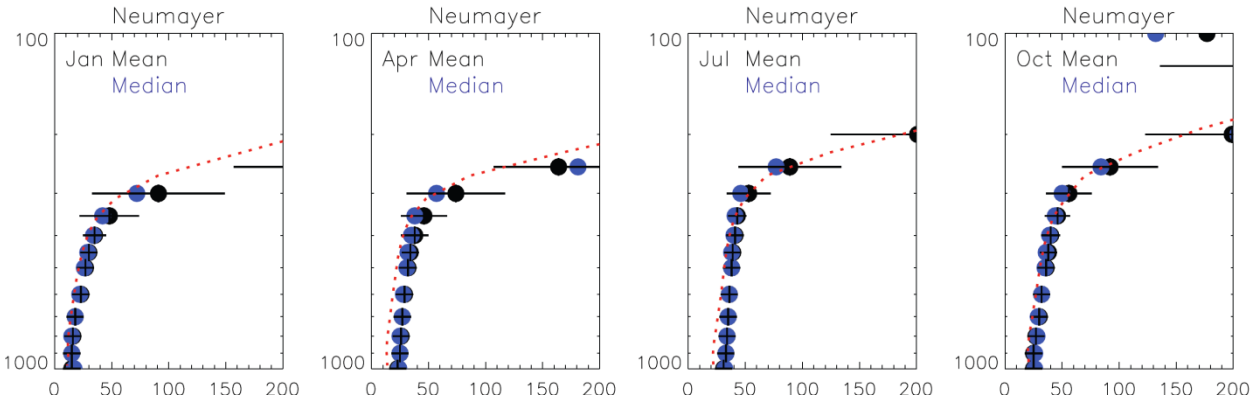

Figure C.9. Vertical profile (hPa in the y axis) comparisons of tropospheric O_3 concentrations (ppbv in the x axis) from the model outputs (red dot) for four-year averages from the S_2010 simulation with the monthly mean (black dot) and median (blue dot) ozonesonde climatology (average of 1995 through 2011, Tilmes et al., 2012) for nine selected ozonesonde stations that are latitudinally representative across the NH and SH in four months (Larmarque et al., 2012).

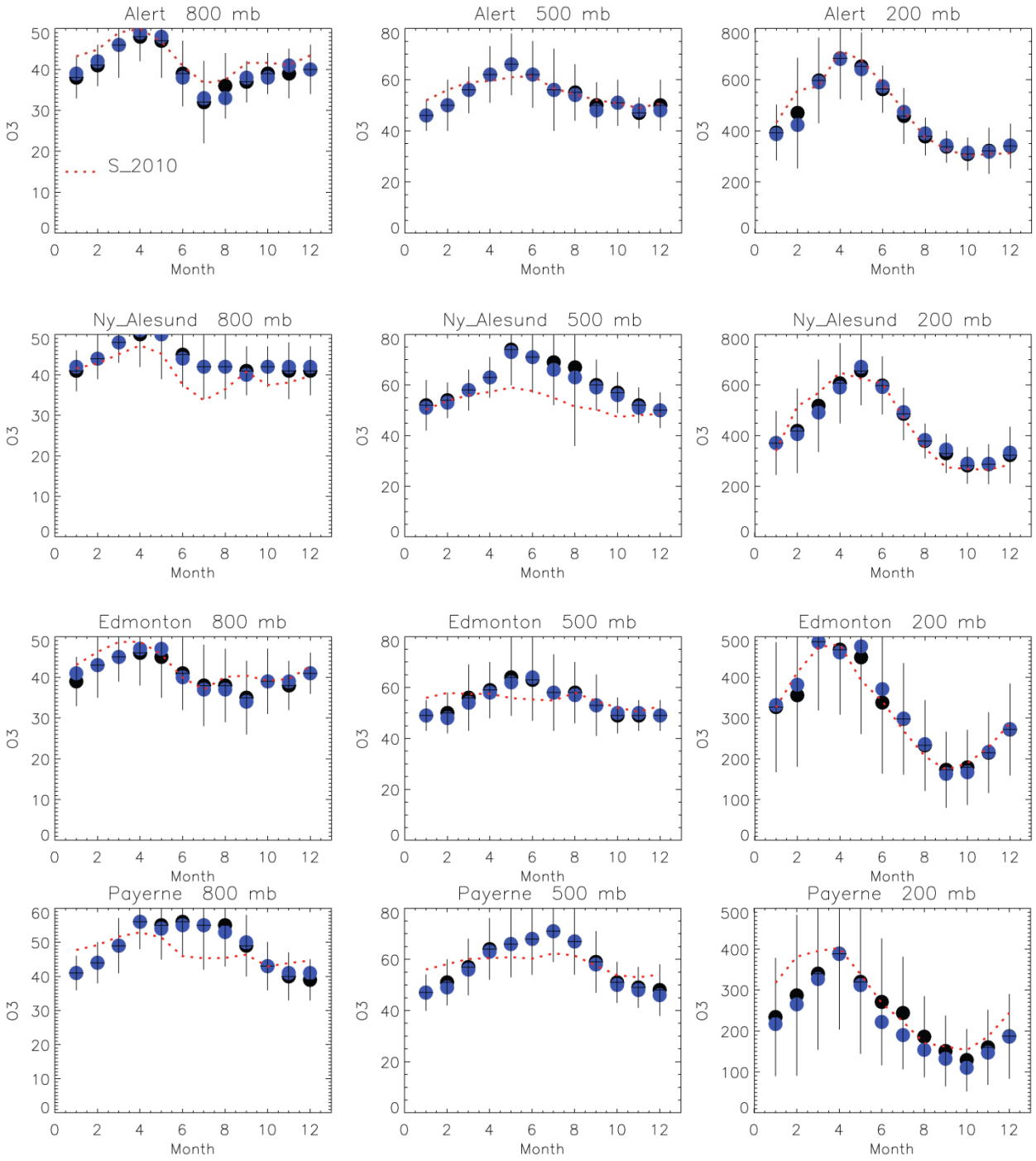
Alert 800 mb
Alert 500 mb
Alert 200 mb
Ny_Alesund 800 mb
Ny_Alesund 500 mb
Ny_Alesund 200 mb
Edmonton 800 mb
Edmonton 500 mb
Edmonton 200 mb
Payerne 800 mb
Payerne 500 mb
Payerne 200 mb
S_2010
O3
Month

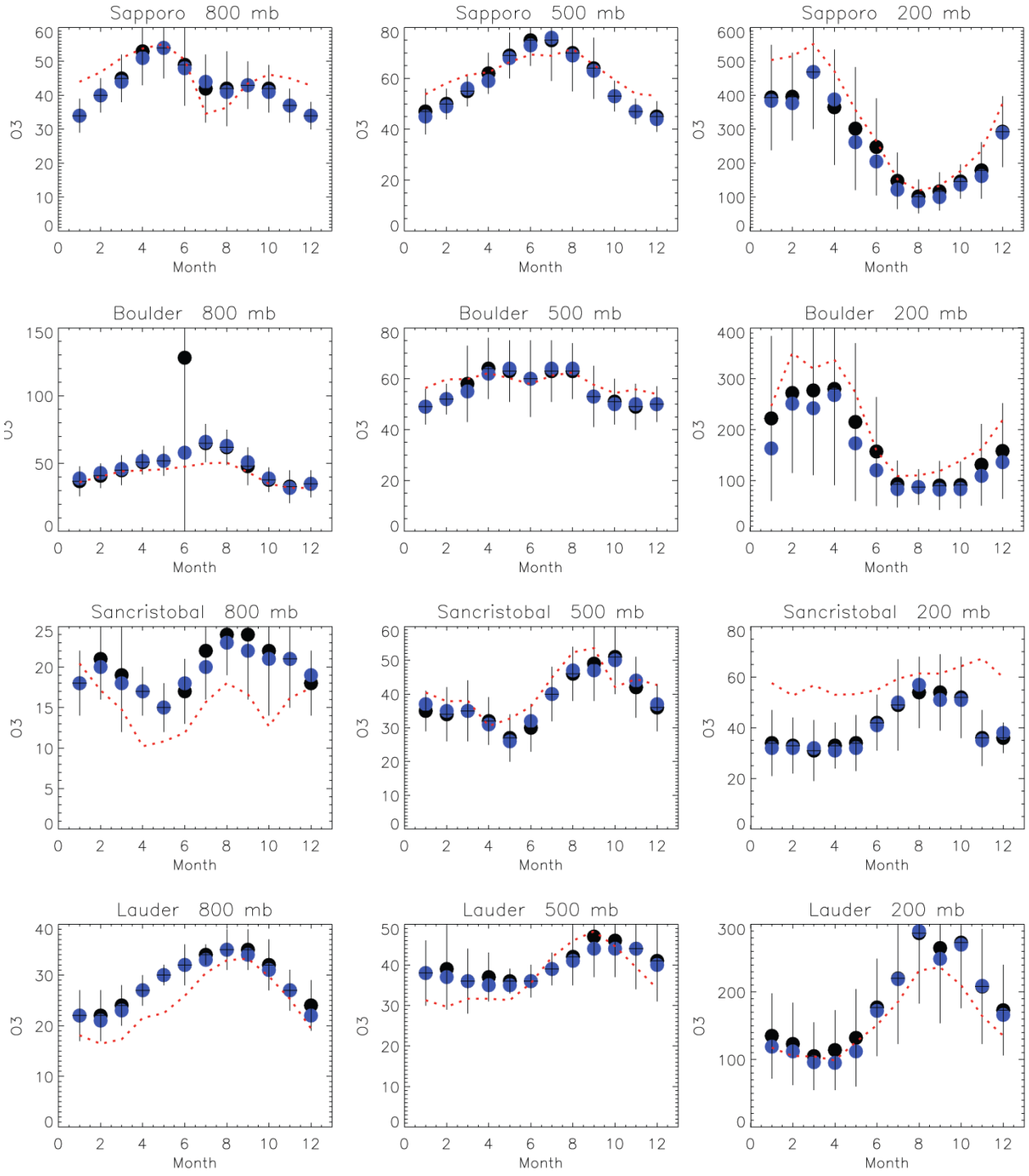
Sapporo 800 mb
Sapporo 500 mb
Sapporo 200 mb
Boulder 800 mb
Boulder 500 mb
Boulder 200 mb
Sancristobal 800 mb
Sancristobal 500 mb
Sancristobal 200 mb
Lauder 800 mb
Lauder 500 mb
Lauder 200 mb
O3
Month

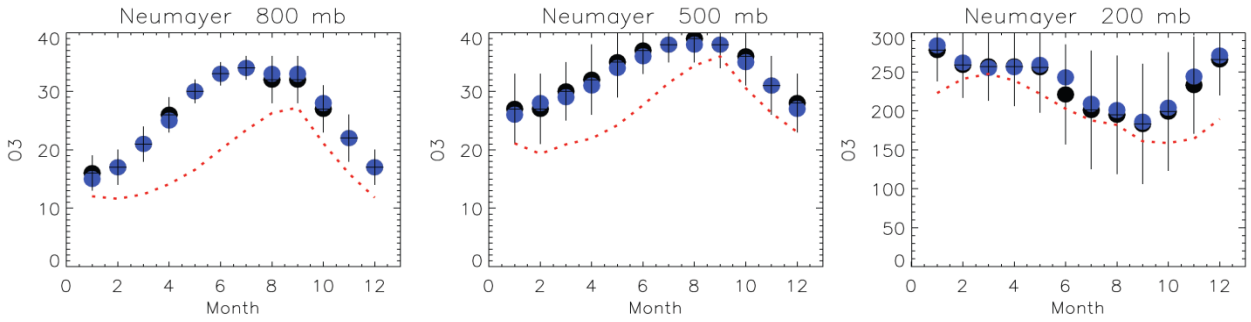

Figure C.10. Time series (months in the x axis) comparisons of the base simulated monthly mean tropospheric O_3 concentrations from the S_2010 simulation (ppbv in the y axis) for the years 2009-2012 (red dot) with the monthly mean (black dot) and median (blue dot) ozonesonde climatology (averaged over 1995 through 2011, Tilmes et al., 2012) for nine selected ozonesonde stations that are latitudinally representative across the northern and southern hemispheres at altitudes of 800, 500, and 200 millibars (mb).

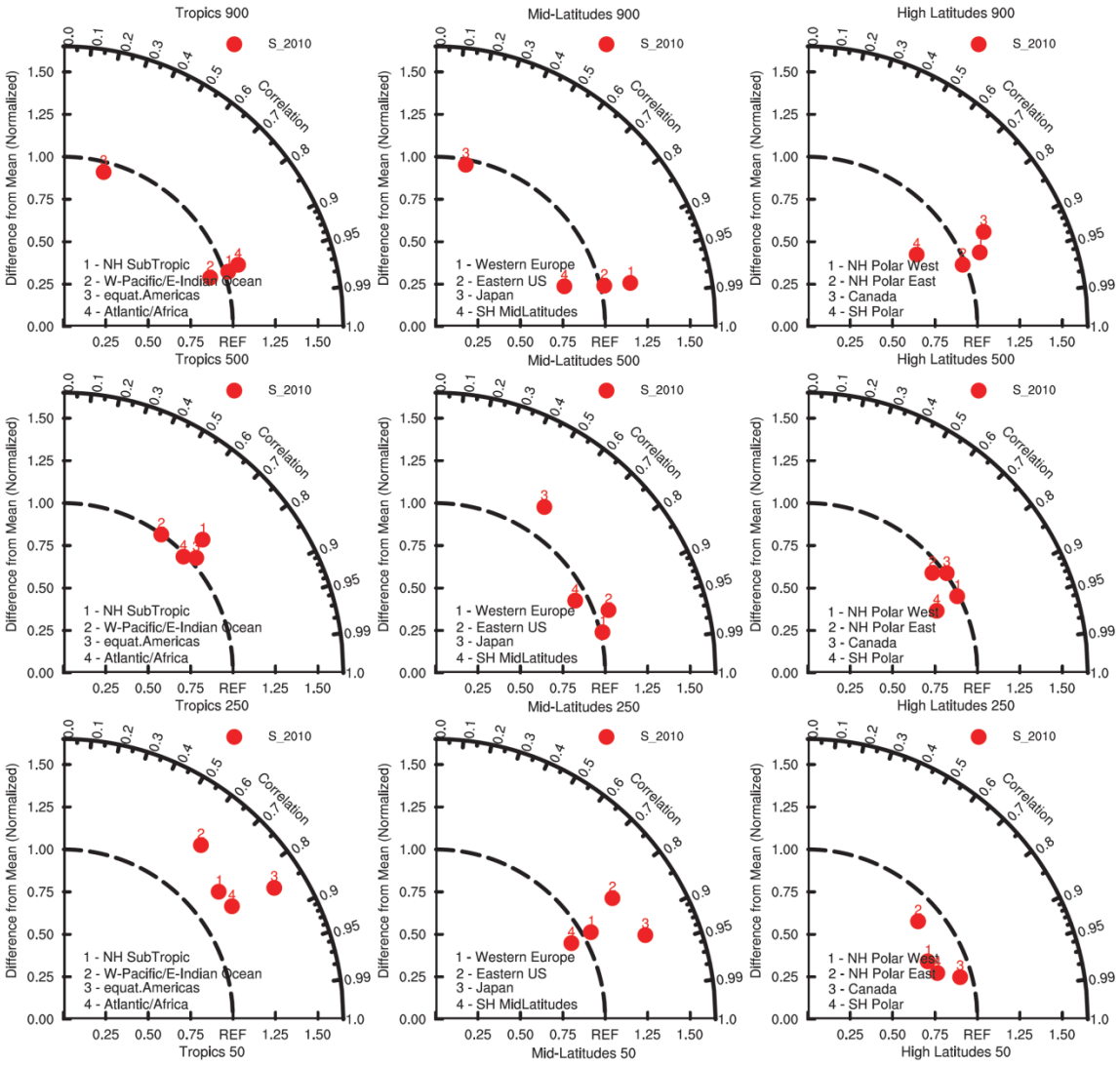

Figure C.11. Taylor diagram of comparisons between modeled ozone from the S_2010 simulation and the ozonedes data in high Tropics (left), mid-latitudes (middle), and the high-latitudes (right) for three different altitude levels (900hpa, 500hpa and 250hpa) in the troposphere. The x-axis shows the relative ozone normalized bias of the simulations compared to the observations, whereas the radiant describes the correlation coefficient of seasonal averaged ozone values between simulated and observed values. Numbers symbolize different regions.

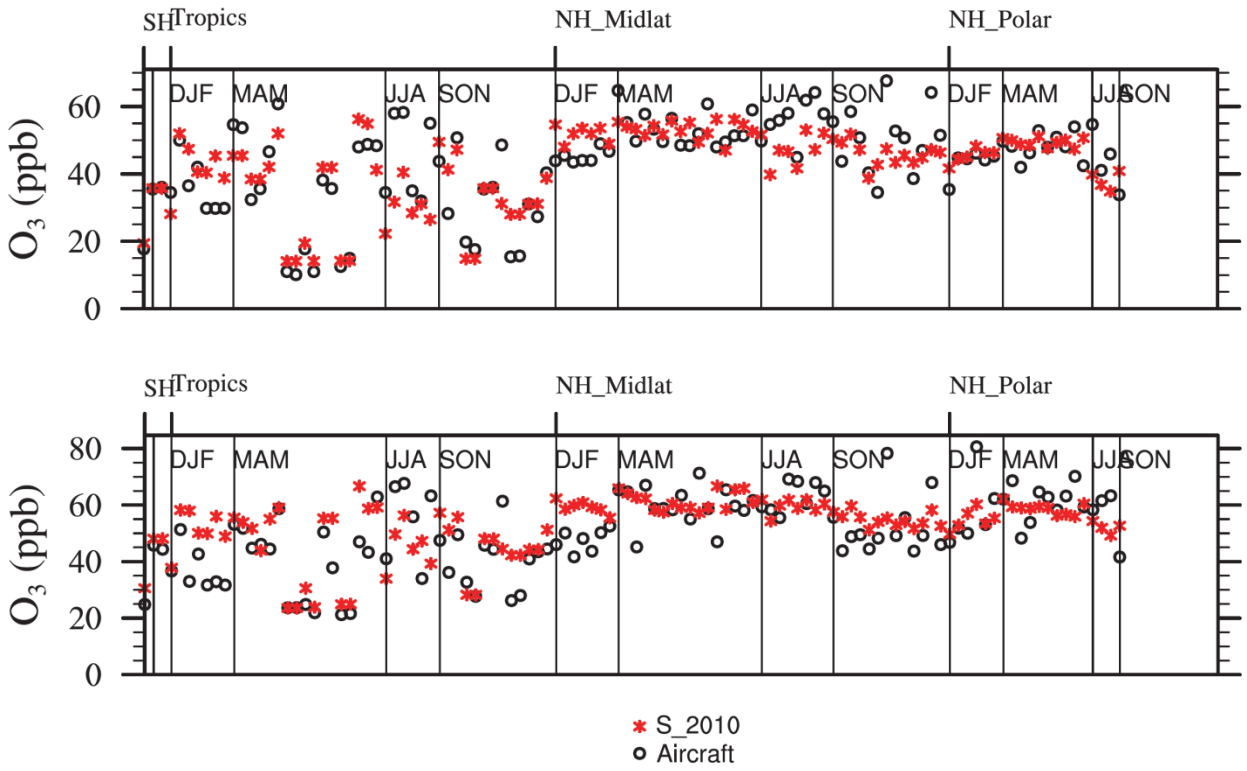

Figure C.12. Comparisons O_3 from modelled output (red) at specific time period and location with aircraft profiles (black, Tilmes et al., 2015; Table S3) for four-year average from S_2010 simulation with averaged over 0-3 km (top) and 2-7 km (bottom).

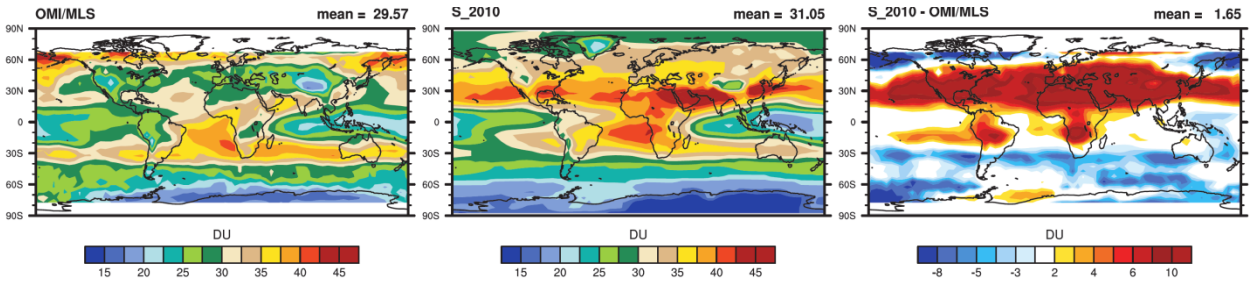

Figure C.13. Comparisons of tropospheric column O_3 climatology data (Dobson Unit, DU) profile from modelled outputs for four-year averages from S_2010 with OMI satellite data from 2004 to 2010, for (a) OMI, (b) CAM-chem simulation, and (c) the differences between CAM-chem and OMI.

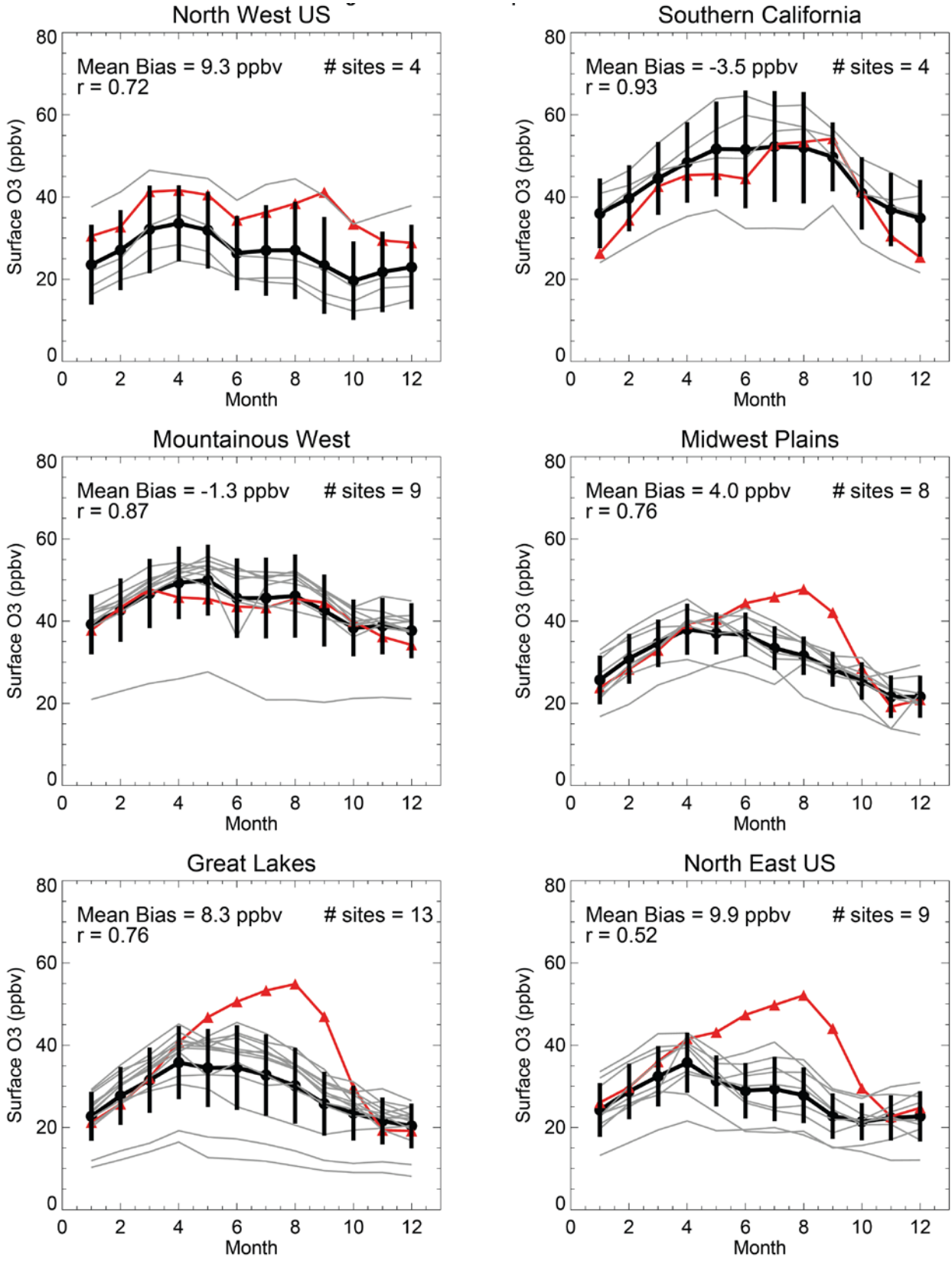
North West US
Mean Bias = 9.3 ppbv
r = 0.72
# sites = 4
Southern California
Mean Bias = -3.5 ppbv
r = 0.93
# sites = 4
Mountainous West
Mean Bias = -1.3 ppbv
r = 0.87
# sites = 9
Midwest Plains
Mean Bias = 4.0 ppbv
r = 0.76
# sites = 8
Great Lakes
Mean Bias = 8.3 ppbv
r = 0.76
# sites = 13
North East US
Mean Bias = 9.9 ppbv
r = 0.52
# sites = 9
Surface O3 (ppbv)
Month

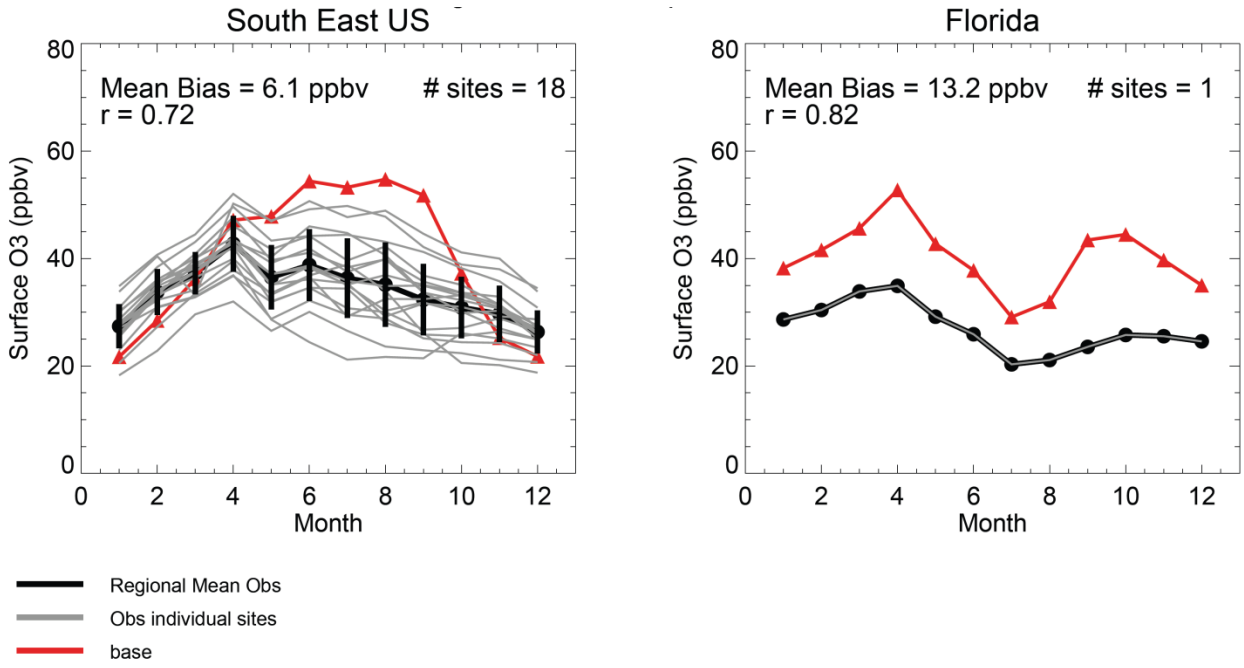

Figure C.14. Comparison of four-year averages surface O_3 concentrations from the S_2010 simulation (red) with observations from the CASTNET monitoring network in the U.S. from 2009 to 2012, showing CASTNET regional mean (black) and individual monitoring locations (grey). The overall mean bias is 5.75 ppbv.

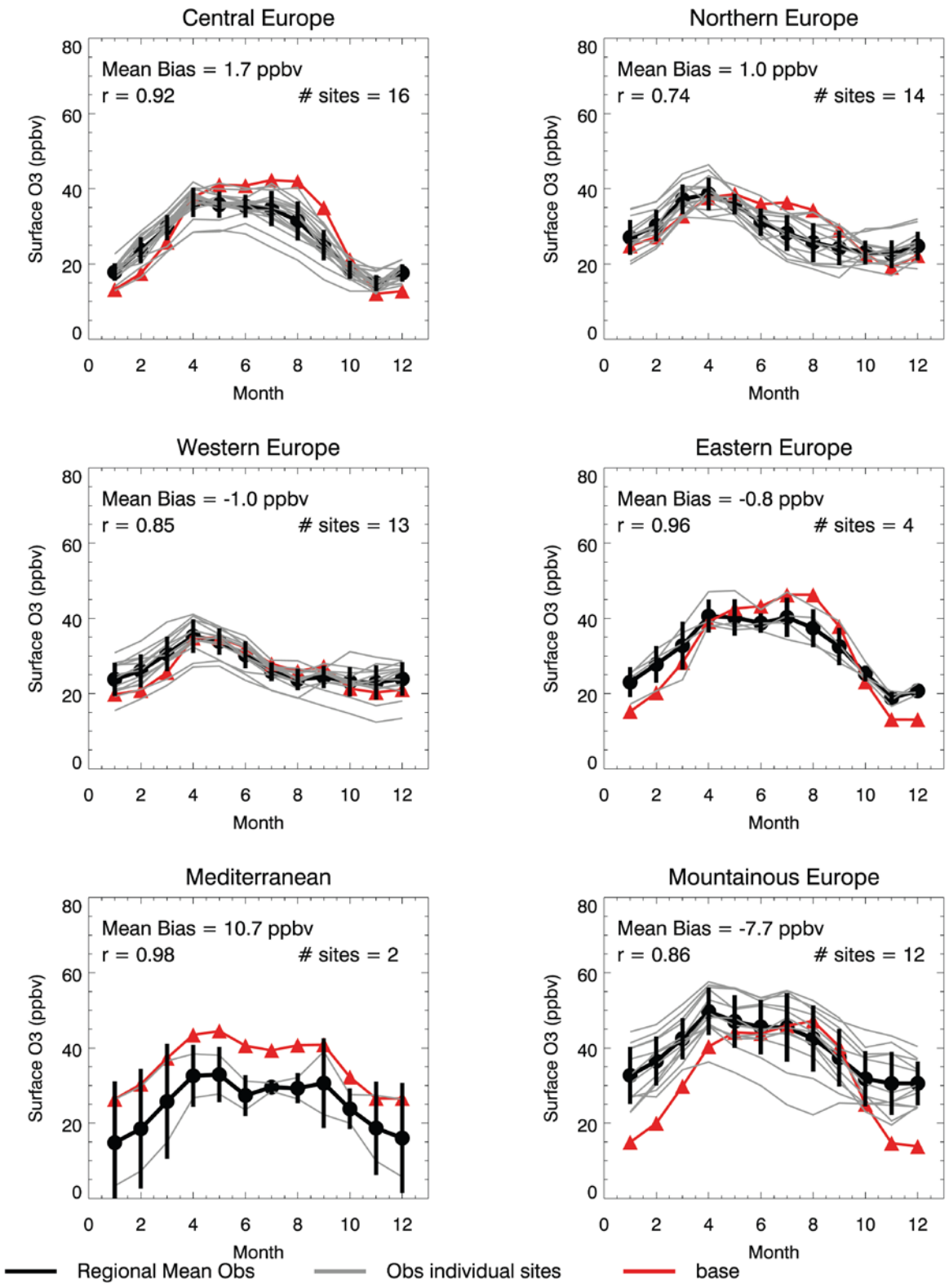

Figure C.15. Comparison of four-year averages surface O_3 concentrations from the S_2010 simulation (red) with observations from the EMEP monitoring network in Europe from 2009-

2011, showing EMEP regional mean (black) and individual monitoring locations (grey). The overall mean bias is 0.65 ppbv.

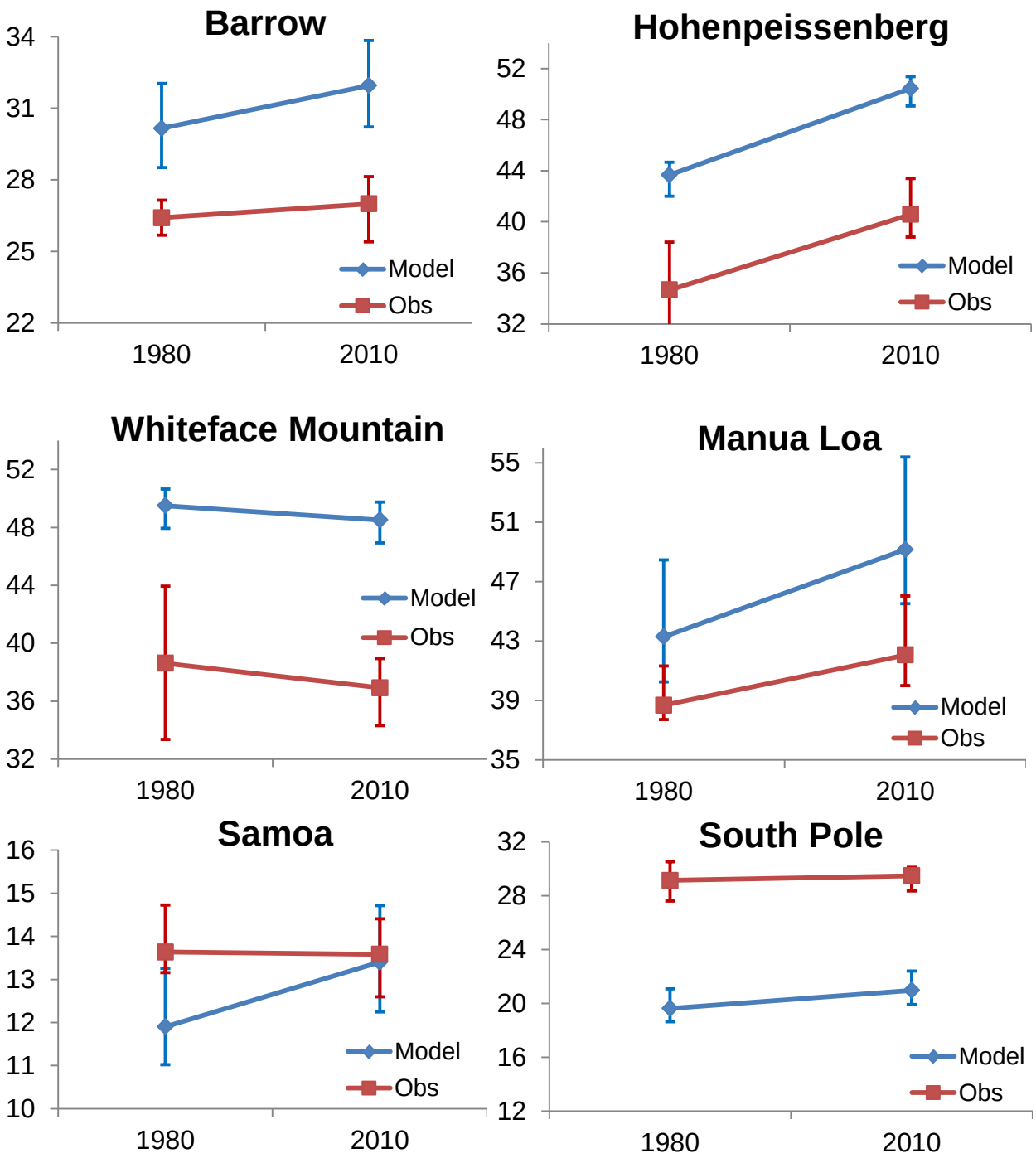

Figure C.16. Comparison for the trends of daily maximum O_3 changes from 1980 to 2010 between model and six long-term remotes sites. The bars are the full range across four annual averages. All the values for both model and obsservation are for four-year average. The observation site means are from 1979 to 1982 for the value in 1980, and from 2009 to 2012 for

the value in 2010, except for the Hohenpeissenberg site which is four-year average from 2005 to 2008, as no observation data past 2008 is reported yet.

APPENDIX D. GUIDE TO RUNNING CAM-CHEM MODEL ON UNC'S KILLDEVIL CLUSTER

This document is created to run CAM-Chem (active model for ATMOSPHERE and LAND in CESM 1.2.2) on UNC Killdevil. For instructions to import a new version of CESM on UNC Killdevil, please contact me by yuqiangzhang.thu@gmail.com, or refer to the official website: http://www2.cesm.ucar.edu/models/current. CESM is coupled climate models for simulating Earth's climate system, including different components, such as atmosphere, land model, rive run-off, ocean model, land-ice, and sea-ice. For the majority of scientific or research purposes at CHAQ lab, we only need to run the CESM with coupled ATMOSPHERE and LAND model, with the other models turned off and using prescribed data.

To begin with, you first need to create an account on UNC Killdevil cluster. Please refer to the UNC ITS help website on how to do it:

http://help.unc.edu/help/getting-started-on-killdevil/#P41_2630

Also on this website, you will be acquainted with how to use the supercomputer clusters on the UNC Killdevil. Read careful as it will help you to get the setting right for running CAM-chem.

Steps to run the CAM-chem are as following:

1) First load the required modules on your account:

   module add perl

   module add cmake/2.8.12.2

   module add netcdf/4.2

   module rm mvapich_intel/11.1 (when you load netcdf/4.2, it will automatically load mvapich_intel/11.1)

   module add mvapich2_intel/13.1-2

2) Copy the CESM 1.2.2 source code

You will be able to copy the precompiled source code of CESM 1.2.2 to your own directory:

“cp –r /nas02/depts/ese/chaq/yuqiangz/cesm1_2_2_compiled /nas02/home/O/N/ONYEN/cesm1_2_2”

PS: the O, N means the first and second letter of your ONYEN.

3) Define the path of the root directory of CESM:

For this step, it depends on which shell you are using. Type “echo $SHELL”, and you will find out:

A) If you are using tcsh/csh”, type:

“setenv $CCSMROOT /nas02/home/O/N/ONYEN/cesm1_2_2”

You can also include this setting in your home directory. Add this line in the file:

“/nas02/home/O/N/ONYEN/.cshrc”

B) If using “bach”, please type:

“export CCSMROOT=/nas02/home/O/N/ONYEN/cesm1_2_2”

To include this setting in your home directory, add this line in this file:

“/nas02/home/O/N/ONYEN/.bashrc”

4) Create a case:

Go to $CCSMROOT/scripts, and use “create_newcase” command to create a new case:

“./create_newcase -case $CCSMROOT/test_ FGEOS_C4MOZ_L40CN -res f19_f19 -compset FGEOS_C4MOZ_L40CN -mach killdevil”

A) The CESM use the “component set”, AKA “compset” to define a particular mix of components, along with component-specific configuration and/or namelist setting,

also including the choices of chemical mechanisms and prescribe dynamics. For our group, we will use the "F" component for most of the cases. For more information, please refer to the guide, "CESM Components" and "CESM Component Sets", and also here: http://www.cesm.ucar.edu/models/cesm1.2/cesm/doc/modelnl/compsets.html

B) For the meanings of variable "-case", "-res", "-compset", and "-mach", please read the UG1.2.2.

C) Here, "test_ FGEOS_C4MOZ_L40CN" is the variable of $CASE.

D) There variables are important to define the domain, resolution, configuration of the simulation.

5) Go to the run directory (for this case, $CCSMROOT/test_ FGEOS_C4MOZ_L40CN), and call "cesm_setup" to create Macros files (see pg. 21-22—UG 1.2.2).

It's always a good idea to save the log file on a local disk in case there are something when you compile the model:

"./cesm_setup >& log_cesm_setup &"

A) This step is to create the Macros files

B) You will also see the namelists for different models, **"user_nl_xxxx"** (**xxxx** here means the atmospheric model—CAM, land model—clm).

C) Also create the **"$CASEROOT/$CASE.run"** file which is used to run the CESM model.

D) Customize the PE layout in **"env_mach_pes.xml"** file before running **"cesm_setup"**. If **"cesm_setup"** has been run before **"env_mach_pes.xml"** has been made changes, a cleanup step should be done first: **"./cesm_setup -clean"**

6) Build the model in the same directory:

   Call ./$CASE.build to build the model. In my test run, it's

   "./test_FGEOS_C4MOZ_L40CN.build"

   To save the build time, submit the command to Killdevil queues:

   "bsub -q debug -n 8 -o log_test_MOZMAM.build ./test_

   FGEOS_C4MOZ_L40CN.buil"

   A) Be default, the compile require 8 CPUs in parallel, because I already changed the setting in **"config_compilers.xml"**

   B) When you see "CESM BUILDEXE SCRIPT HAS FINISHED SUCCESSFULLY", it means you successfully build the model. Also The build log files have names of the form **"$model.bldlog.$datestamp"** and are located in $RUNDIR. If they are compressed (indicated by a .gz file extension), then the build ran successfully.

7) Run the CESM model

   A) Modify the **"env_run.xml"** file to control the start date, duration, end date, etc. Also talk a look at "Customizing runtime settings" in the user guide on how to carry out an initial runs, and how to resubmit the job.

   B) Change the options of how we submit the job:

   ./xmlchnge BATCHQUERYa="bjobs -w"

   ./xmlchange BATCHSUBMIT="bsub <"

   C) Most of times, we need to read our own datasets, such as anthropogenic emissions, and save some variables at specific intervals for the data analysis, instead of the default set by the **"compset"**, we need to make changes to the **"user_nl_cam"**. You can refer to the one I created for my study:

"/nas02/depts/ese/chaq/yuqiangz/CAM_v5.3/cesm1_2_2/zyq_FGEOS_C4MOZ_L40CN2_2010/user_nl_cam"

The references for CAM namelist is listed here:

http://www.cesm.ucar.edu/cgi-bin/eaton/namelist/nldef2html-cam5_1

D) Run CESM by submitting the script of "./$CASE.submit"

8) To add the online option for MEGANv2.1, please refer to the manual:

"MEGAN_Running_CESM1_MEGAN-v0408.pdf" by Simone Tilmes.

http://www.cesm.ucar.edu/working_groups/Chemistry/roadmap_cesm120.pdf

A) In **"env_build.xml"**:

<entry id="CLM_CONFIG_OPTS" value="-bgc none" />

B) In **"env_run.xml",**

<entry id="CLM_BLDNML_OPTS" value="-megan" />

C) To see the namelist defined in the "**user_nl_cam"**, please refer to the files in my directory:

"/nas02/depts/ese/chaq/yuqiangz/CAM_v5.3/cesm1_2_2/zyq_FGEOS_C4MOZ_L40CN2_2010/ user_nl_cam"

9) The global meteorology for the GEOS-5 from 2005 to 2013 are put here:

"/ms/depts/ese/yuqiangz/inputdata/atm/cam/met/GEOS5"

The global emission inventories from the ACCMIP for 1980 and RCP8.5 for 2010 are put here:

/nas02/depts/ese/chaq/yuqiangz/CAM_v5.3/cesm1_2_2/RCP_process/1980

/nas02/depts/ese/chaq/yuqiangz/CAM_v5.3/cesm1_2_2/RCP_process/2010_RCP85

Sample “**user_nl_cam**” in my runs:

! Users should add all user specific namelist changes below in the form of

! namelist_var = new_namelist_value

! http://www.cesm.ucar.edu/cgi-bin/eaton/namelist/nldef2html-cesm1_2_2-cam ;1/14/15, zyq

&cam_inparm

avgflag_pertape = 'A', 'A', 'A'

mfilt = 1, 5, 24

nhtfrq = 0, -24, -1

empty_htapes = .true.

fincl1 = 'Q', 'U', 'V', 'OMEGA', 'T', 'PS', 'TROP_P', 'PBLH', 'PRECC', 'PRECL', 'PHIS', 'Z3', 'ORO', 'QFLX', 'SHFLX', 'TAUX', 'TAUY', 'O3', 'O', 'O1D', 'N2O', 'NO', 'NO2', 'NO_Lightning', 'LNO_COL_PROD', 'NO3', 'HNO3', 'HO2NO2', 'N2O5', 'H2', 'OH', 'HO2', 'H2O2', 'LCH4', 'CO', 'CH3O2', 'CH3OOH', 'CH2O', 'CH3OH', 'C2H5OH', 'C2H4', 'EO', 'EO2', 'CH3COOH', 'GLYALD', 'C2H6', 'C2H5O2', 'C2H5OOH', 'CH3CHO', 'CH3CO3', 'CH3COOOH', 'C3H6', 'C3H8', 'C3H7O2', 'C3H7OOH', 'PO2', 'POOH', 'CH3COCH3', 'RO2', 'ROOH', 'BIGENE', 'ENEO2', 'MEK', 'MEKO2', 'MEKOOH', 'BIGALK', 'ALKO2', 'ALKOOH', 'ISOP', 'ISOPO2', 'ISOPOOH', 'MVK', 'MACR', 'MACRO2', 'MACROOH', 'MCO3', 'HYDRALD', 'HYAC', 'CH3COCHO', 'XO2', 'XOOH', 'C10H16', 'TERPO2', 'TERPOOH', 'TOLUENE', 'CRESOL', 'TOLO2', 'TOLOOH', 'XOH', 'BIGALD', 'GLYOXAL', 'PAN', 'ONIT', 'MPAN', 'ISOPNO3', 'ONITR', 'CB1', 'CB2', 'OC1', 'OC2', 'SOA', 'SO2', 'SO4', 'DMS', 'NH3', 'NH4', 'NH4NO3', 'SSLT01', 'SSLT02', 'SSLT03', 'SSLT04', 'DST01', 'DST02', 'DST03', 'DST04', 'Rn', 'Pb', 'HCN',

'CH3CN', 'SFNO', 'SFNO2', 'SFCO', 'SFBIGALK', 'SFBIGENE', 'SFC10H16', 'SFC2H4', 'SFC2H5OH', 'SFC2H6', 'SFC3H6', 'SFC3H8', 'SFCH2O', 'SFCH3CHO', 'SFCH3COCH3', 'SFCH3OH', 'SFDMS', 'SFISOP', 'SFMEK', 'SFNH3', 'SFCB1', 'SFCB2', 'SFOC1', 'SFOC2', 'SFSO2', 'SFTOLUENE', 'SFHCN', 'SFCH3CN', 'MEG_CH3COCH3', 'MEG_CH3CHO', 'MEG_CH2O', 'MEG_CO','MEG_C2H6', 'MEG_C3H8', 'MEG_C2H4', 'MEG_C3H6', 'MEG_C2H5OH', 'MEG_C10H16', 'MEG_ISOP', 'MEG_CH3OH', 'DV_HCN', 'DV_CH3CN', 'WDR_HCN', 'WDR_CH3CN', 'WD_HCN', 'WD_CH3CN', 'WDR_SO2', 'WDR_HNO3', 'WDR_H2O2', 'WDR_CH2O', 'WD_SO2', 'O3_CHMP', 'O3_CHML', 'CO_CHMP', 'CO_CHML', 'SO4_CHMP', 'SO4_CHML', 'NO_CHML', 'NO2_CHML', 'NO3_CHML', 'HNO3_CHML'

fincl2 = 'PS', 'Z3', 'T', 'U', 'V', 'Q', 'CLOUD', 'LCH4', 'O1D', 'O3', 'OH', 'HO2', 'NO', 'NO2', 'NO3', 'N2O5', 'HO2NO2', 'HNO3', 'NOX', 'NOY', 'CO', 'CH2O', 'CH3OOH', 'C2H2', 'HCOOH', 'C2H4', 'C2H6', 'CH3COOH', 'CH3CHO', 'CH3OH', 'C2H5OH', 'GLYOXAL', 'PAN', 'C3H6', 'C3H8', 'CH3COCH3', 'BIGENE', 'BIGALK', 'MEK', 'MVK', 'MACR', 'ONIT', 'ONITR', 'ISOP', 'CH3CN', 'TOLUENE', 'C10H16', 'HCN', 'SO2', 'SO4', 'NH3', 'NH4', 'NH4NO3', 'DMS', 'CB1', 'CB2', 'OC1', 'OC2', 'SSLT01', 'SSLT02', 'SSLT03', 'SSLT04', 'DST01', 'DST02', 'DST03', 'DST04'

fincl3 = 'O3'

/

&solar_inparm

solar_data_file = '/netscr/yuqiangz/inputdata/atm/cam/solar/spectral_irradiance_Lean_1610-2140_ann_c100408.nc'

/

&metdata_nl

met_data_file = '2008/GEOS5.1_19x2_2008-JAN_c110728.nc'

met_data_path = '/netscr/yuqiangz/inputdata/atm/cam/met/GEOS5'

met_filenames_list =

'/netscr/yuqiangz/inputdata/atm/cam/met/GEOS5_filenames_list_c120516.txt'

/

&satellite_options_nl

sathist_fincl = ''

/

srf_emis_cycle_yr = 2010

srf_emis_specifier = 'BIGALK ->

/nas02/depts/ese/chaq/yuqiangz/CAM_v5.3/cesm1_2_2/RCP_process/2010_RCP85/emissions.B

IGALK.surface.1.9x2.5_c110426.nc',

'BIGENE ->

/nas02/depts/ese/chaq/yuqiangz/CAM_v5.3/cesm1_2_2/RCP_process/2010_RCP85/emissions.B

IGENE.surface.1.9x2.5_c110426.nc',

'C2H2 ->

/nas02/depts/ese/chaq/yuqiangz/CAM_v5.3/cesm1_2_2/RCP_process/2010_RCP85/emissions.C

2H2.surface.1.9x2.5_c110426.nc',

'C2H4 ->

/nas02/depts/ese/chaq/yuqiangz/CAM_v5.3/cesm1_2_2/RCP_process/2010_RCP85/emissions.C

2H4.surface.1.9x2.5_c110426.nc',

'C2H5OH -> /nas02/depts/ese/chaq/yuqiangz/CAM_v5.3/cesm1_2_2/RCP_process/2010_RCP85/emissions.C2H5OH.surface.1.9x2.5_c110426.nc',

'C2H6 -> /nas02/depts/ese/chaq/yuqiangz/CAM_v5.3/cesm1_2_2/RCP_process/2010_RCP85/emissions.C2H6.surface.1.9x2.5_c110426.nc',

'C3H6 -> /nas02/depts/ese/chaq/yuqiangz/CAM_v5.3/cesm1_2_2/RCP_process/2010_RCP85/emissions.C3H6.surface.1.9x2.5_c110426.nc',

'C3H8 -> /nas02/depts/ese/chaq/yuqiangz/CAM_v5.3/cesm1_2_2/RCP_process/2010_RCP85/emissions.C3H8.surface.1.9x2.5_c110426.nc',

'CB1 -> /nas02/depts/ese/chaq/yuqiangz/CAM_v5.3/cesm1_2_2/RCP_process/2010_RCP85/emissions.CB1.surface.1.9x2.5_c110426.nc',

'CB2 -> /nas02/depts/ese/chaq/yuqiangz/CAM_v5.3/cesm1_2_2/RCP_process/2010_RCP85/emissions.CB2.surface.1.9x2.5_c110426.nc',

'CH2O -> /nas02/depts/ese/chaq/yuqiangz/CAM_v5.3/cesm1_2_2/RCP_process/2010_RCP85/emissions.CH2O.surface.1.9x2.5_c110426.nc',

'CH3CHO -> /nas02/depts/ese/chaq/yuqiangz/CAM_v5.3/cesm1_2_2/RCP_process/2010_RCP85/emissions.CH3CHO.surface.1.9x2.5_c110426.nc',

'CH3CN -> /nas02/depts/ese/chaq/yuqiangz/CAM_v5.3/cesm1_2_2/RCP_process/2010_RCP85/emissions.CH3CN.surface.1.9x2.5_c110426.nc',

'CH3COCH3 -> /nas02/depts/ese/chaq/yuqiangz/CAM_v5.3/cesm1_2_2/RCP_process/2010_RCP85/emissions.CH3COCH3.surface.1.9x2.5_c110426.nc',

'CH3COOH -> /nas02/depts/ese/chaq/yuqiangz/CAM_v5.3/cesm1_2_2/RCP_process/2010_RCP85/emissions.CH3COOH.surface.1.9x2.5_c110426.nc',

'CH3OH -> /nas02/depts/ese/chaq/yuqiangz/CAM_v5.3/cesm1_2_2/RCP_process/2010_RCP85/emissions.CH3OH.surface.1.9x2.5_c110426.nc',

'CO -> /nas02/depts/ese/chaq/yuqiangz/CAM_v5.3/cesm1_2_2/RCP_process/2010_RCP85/emissions.CO.surface.1.9x2.5_c110426.nc',

'DMS -> /nas02/depts/ese/chaq/yuqiangz/CAM_v5.3/cesm1_2_2/RCP_process/2010_RCP85/emissions.DMS.surface.1.9x2.5_c110426.nc',

'HCN -> /nas02/depts/ese/chaq/yuqiangz/CAM_v5.3/cesm1_2_2/RCP_process/2010_RCP85/emissions.HCN.surface.1.9x2.5_c110426.nc',

'HCOOH -> /nas02/depts/ese/chaq/yuqiangz/CAM_v5.3/cesm1_2_2/RCP_process/2010_RCP85/emissions.HCOOH.surface.1.9x2.5_c110426.nc',

'MEK -> /nas02/depts/ese/chaq/yuqiangz/CAM_v5.3/cesm1_2_2/RCP_process/2010_RCP85/emissions.MEK.surface.1.9x2.5_c110426.nc',

'NH3 -> /nas02/depts/ese/chaq/yuqiangz/CAM_v5.3/cesm1_2_2/RCP_process/2010_RCP85/emissions.NH3.surface.1.9x2.5_c110426.nc',

'NO -> /nas02/depts/ese/chaq/yuqiangz/CAM_v5.3/cesm1_2_2/RCP_process/2010_RCP85/emissions.NO.surface.1.9x2.5_c110426.nc',

'OC1 -> /nas02/depts/ese/chaq/yuqiangz/CAM_v5.3/cesm1_2_2/RCP_process/2010_RCP85/emissions.OC1.surface.1.9x2.5_c110426.nc',

'OC2 -> /nas02/depts/ese/chaq/yuqiangz/CAM_v5.3/cesm1_2_2/RCP_process/2010_RCP85/emissions.OC1.surface.1.9x2.5_c110426.nc',

```
      'SO2     ->
/nas02/depts/ese/chaq/yuqiangz/CAM_v5.3/cesm1_2_2/RCP_process/2010_RCP85/emissions.S
O2.surface.1.9x2.5_c110426.nc',
      'TOLUENE  ->
/nas02/depts/ese/chaq/yuqiangz/CAM_v5.3/cesm1_2_2/RCP_process/2010_RCP85/emissions.T
OLUENE.surface.1.9x2.5_c110426.nc'
 srf_emis_type         = 'CYCLICAL'
/
&megan_emis_nl
 megan_factors_file =
'/netscr/yuqiangz/inputdata/atm/cam/chem/trop_mozart/emis/megan21_emis_factors_c20130304
.nc'
 megan_specifier = 'ISOP = isoprene',
      'C10H16 = myrcene + sabinene + limonene + carene_3 + ocimene_t_b + pinene_b +
pinene_a + 2met_styrene + cymene_p + cymene_o + phellandrene_a + thujene_a + terpinene_a
+ terpinene_g + terpinolene + phellandrene_b + camphene + bornene + fenchene_a +
ocimene_al + ocimene_c_b',
      'CH3OH = methanol',
      'C2H5OH = ethanol',
      'CH2O = formaldehyde',
      'CH3CHO = acetaldehyde',
      'CH3COOH = acetic_acid',
      'CH3COCH3 = acetone',
```

```
      'HCOOH = formic_acid',
      'HCN = hydrogen_cyanide',
      'CO = carbon_monoxide',
      'C2H6 = ethane',
      'C2H4 = ethene',
      'C3H8 = propane',
      'C3H6 = propene',
      'BIGALK = pentane + hexane + heptane + tricyclene',
      'BIGENE = butene',
      'MEK = butanone_2',
      'TOLUENE = toluene'
 megan_mapped_emisfctrs = .false.
/
&chem_surfvals_nl
 co2vmr        = 0.000001e-6
 ch4vmr        = 1798.e-9
 flbc_file             = '/netscr/yuqiangz/inputdata/atm/waccm/lb/LBC_1765-
2500_1.9x2.5_CMIP5_RCP85_za_c091214.nc'
 flbc_list             = 'H2','N2O'
 flbc_type             = 'SERIAL'/
```

REFERENCES

Adar, S. D., Gold, D. R., Coull, B. A., Schwartz, J., Stone, P. H., & Suh, H. (2007). Focused exposures to airborne traffic particles and heart rate variability in the elderly. Epidemiology (Cambridge, Mass.), 18(1), 95-103.

Akimoto, H. (2003). Global air quality and pollution. Science (New York, N.Y.), 302(5651), 1716-1719.

Andreae, M. O., Jones, C. D., & Cox, P. M. (2005). Strong present-day aerosol cooling implies a hot future. Nature, 435(7046), 1187-90.

Anenberg, S. C., West, J. J., Fiore, A. M., Jaffe, D. A., Prather, M., Bergmann, D., Cuvelier, K., et al. (2009). Intercontinental Impacts of Ozone Pollution on Human Mortality. Environmental Science and Technology, 43(17), 6482 - 6487.

Anenberg, S. C., Horowitz, L. W., Tong, D. Q., & West, J. J. (2010). An estimate of the global burden of anthropogenic ozone and fine particulate matter on premature human mortality using atmospheric modeling. Environmental Health Perspectives, 118(10), 1189-1195.

Anenberg, S. C., Schwartz, J., Shindell, D., Amann, M., Faluvegi, G., Klimont, Z., Janssens-Maenhout, G., et al. (2012). Global air quality and health co-benefits of mitigating near-term climate change through methane and black carbon emission controls. Environmental Health Perspectives, 120(6), 831-839.

Anenberg, S. C., West, J. J., Yu, H., Chin, M., Schulz, M., Bergmann, D., Bey, I., et al. (2014). Impacts of intercontinental transport of anthropogenic fine particulate matter on human mortality. AIR QUALITY ATMOSPHERE AND HEALTH, 7(3), 369-379.

Appel, K. W., Roselle, S. J., Gilliam, R. C., & Pleim, J. E. (2010). Sensitivity of the Community Multiscale Air Quality (CMAQ) Model v4.7 results for the eastern United States to MM5 and WRF meteorological drivers. Geoscientific Model Development, 3, 169–188.

Appel, K. W., Foley, K. M., Bash, J. O., Pinder, R. W., Dennis, R. L., Allen, D. J., & Pickering, K. (2011). A multi-resolution assessment of the Community Multiscale Air Quality (CMAQ) model v4.7 wet deposition estimates for 2002-2006. Geoscientific Model Development, 4, 357-371.

Appel, K. W., Pouliot, G. A, Simon, H., Sarwar, G., Pye, H. O. T., Napelenok, S. L., Akhtar, F., et al. (2013). Evaluation of dust and trace metal estimates from the Community Multiscale Air Quality (CMAQ) model version 5.0. Geoscientific Model Development, 6, 883-899.

Arneth, A., Unger, N., Kulmala, M., & Andreae, M. O. (2009). Clean the air, heat the planet? Science (New York, N.Y.), 326(5953), 672-673.

Auvray, M., & Bey, I. (2005). Long-range transport to Europe: Seasonal variations and implications for the European ozone budget. Journal of Geophysical Research D: Atmospheres, 110(11), 1-22.

Avise, J., Chen, J., Lamb, B., Wiedinmyer, C., Guenther, A., Salath, E., & Mass, C. (2009). Attribution of projected changes in summertime US ozone and $PM_{2.5}$ concentrations to global changes. Atmospheric Chemistry and Physics, 9, 1111-1124.

Baek, J., Hu, Y., Odman, M. T., & Russell, A. G. (2011). Modeling secondary organic aerosol in CMAQ using multigenerational oxidation of semi-volatile organic compounds. Journal of Geophysical Research Atmospheres, 116(22).

Bell, M. L. M. L., McDermott, A., Zeger, S. L. S. L., Samet, J. M., & Dominici, F. (2004). Ozone and short-term mortality in 95 US urban communities, 1987-2000. JAMA, 292(19), 2372-2378.

Bell, M. L., Dominici, F., & Samet, J. M. (2005). A meta-analysis of time-series studies of ozone and mortality with comparison to the national morbidity, mortality, and air pollution study. Epidemiology (Cambridge, Mass.), 16(4), 436-445.

Bell, M. L., Goldberg, R., Hogrefe, C., Kinney, P. L., Knowlton, K., Lynn, B., Rosenthal, J., et al. (2007). Climate change, ambient ozone, and health in 50 US cities. Climatic Change, 82(1-2), 61-76.

Bell, M. L., Davis, D. L., Cifuentes, L. A, Krupnick, A. J., Morgenstern, R. D., & Thurston, G. D. (2008). Ancillary human health benefits of improved air quality resulting from climate change mitigation. Environmental health, 7, 41.

Bell, M. L., Ebisu, K., Peng, R. D., Samet, J. M., & Dominici, F. (2009). Hospital admissions and chemical composition of fine particle air pollution. American Journal of Respiratory and Critical Care Medicine, 179(12), 1115-1120.

Berntsen, T. K., Fuglestvedt, J. S., Joshi, M. M., Shine, K. P., Stuber, N., Ponater, M., Sausen, R., et al. (2005). Response of climate to regional emissions of ozone precursors: Sensitivities and warming potentials. Tellus, Series B: Chemical and Physical Meteorology, 57(4), 283-304.

Bowden, J. H., Otte, T. L., Nolte, C. G., & Otte, M. J. (2012). Examining interior grid nudging techniques using two-way nesting in the WRF model for regional climate modeling. Journal of Climate, 25(8), 2805-2823.

Bowden, J. H., Nolte, C. G. & Otte, T. L. (2013). Simulating the impact of the large-scale circulation on the 2-m temperature and precipitation climatology, Clim. Dyn., 40(7-8), 1903–1920.

Byun, D. W., Moon, N. K., Jacob, D., and Park, R.: Regional transport study of air pollutants with linked global tropospheric chemistry and regional air quality models, 2nd ICAP Workshop, Research Triangle Park, NC, USA, 2004.

Byun, D., & Schere, K. L. (2006). Review of the Governing Equations, Computational Algorithms, and Other Components of the Models-3 Community Multiscale Air Quality (CMAQ) Modeling System. Applied Mechanics Reviews.

Caiazzo, F., Ashok, A., Waitz, I. a, Yim, S. H. L., & Barrett, S. R. H. (2013). Air pollution and early deaths in the United States. Part I: Quantifying the impact of major sectors in 2005. Atmospheric Environment, 79, 198-208.

Chen, F., & Dudhia, J. (2001). Coupling an Advanced Land Surface–Hydrology Model with the Penn State–NCAR MM5 Modeling System. Part II: Preliminary Model Validation. Monthly Weather Review, 129(4), 587-604.

Chen, J., Avise, J., Lamb, B., Salath, E., Mass, C., Guenther, A., C.Wiedinmyer, Lamarque, J.-F., O'Neill, S., McKenzie, D. & Larkin, N. (2009). The effects of global changes upon regional ozone pollution in the United States, Atmos. Chem. Phys., 9, 1125–1141.

Cifuentes, L., Borja-Aburto, V. H., Gouveia, N., Thruston, G., & Davis, D. L. (2001). Hidden health benefits of greenhouse gas mitigation. Science, 293, 1257-1259.

Clarke, L. E., Edmonds, J. A, Jacoby, H. D., Pitcher, H. M., Reilly, J. M., & Richels, R. G. (2007). Scenarios of Greenhouse Gas Emissions and Atmospheric Concentrations. Program, 2011(July), 164.

Cooper, O. R., Parrish, D. D., Stohl, a, Trainer, M., Nédélec, P., Thouret, V., Cammas, J. P., et al. (2010). Increasing springtime ozone mixing ratios in the free troposphere over western North America. Nature, 463(7279), 344-348.

Cooper, O. R., Gao, R. S., Tarasick, D., Leblanc, T., & Sweeney, C. (2012). Long-term ozone trends at rural ozone monitoring sites across the United States, 1990-2010. Journal of Geophysical Research: Atmospheres, 117(22), 1990-2010.

Cooper, O. R., Parrish, D. D., Ziemke, J., Balashov, N. V., Cupeiro, M., Galbally, I. E., Gilge, S., et al. (2014). Global distribution and trends of tropospheric ozone: An observation-based review. Elementa: Science of the Anthropocene, 2, 000029.

Cooper, O. R., Langford, A. O., Parrish, D. D., & Fahey, D. W. (2015). Challenges of a lowered U.S. ozone standard. Science, 348(6239), 1096-1097.

Dawson, J. P., Racherla, P. N., Lynn, B. H., Adams, P. J., & Pandis, S. N. (2008). Simulating present-day and future air quality as climate changes: Model evaluation. Atmospheric Environment, 42(19), 4551-4566.

Dawson, J. P., Racherla, P. N., Lynn, B. H., Adams, P. J., & Pandis, S. N. (2009). Impacts of climate change on regional and urban air quality in the eastern United States: Role of meteorology. Journal of Geophysical Research, 114(D5), 1-11.

Derwent, R. G., Stevenson, D. S., Collins, W. J., & Johnson, C. E. (2004). Intercontinental transport and the origins of the ozone observed at surface sites in Europe. Atmospheric Environment, 38(13), 1891-1901.

Derwent, R. G., Stevenson, D. S., Doherty, R. M., Collins, W. J., Sanderson, M. G., & Johnson, C. E. (2008). Radiative forcing from surface NOx emissions: Spatial and seasonal variations. Climatic Change, 88(3-4), 385-401.

Driscoll, C. T., Buonocore, J. J., Levy, J. I., Lambert, K. F., Burtraw, D., Reid, S. B., Fakhraei, H., et al. (2015). US power plant carbon standards and clean air and health co-benefits. Nature Climate Change, 1-8.

Dockery, D. W., Pope, C. A. I. I. I., Xu, X., Spengler, J. D., Ware, J. H., Fay, M. E., Ferris, B. G., & Speizer, F. E. (1993). An Association between Air Pollution and Mortality in Six U.S. Cities. The New England Journal of Medicine, 329, 1753-1759.

Doherty, R. M., Stevenson, D. S., Collins, W. J. & Sanderson, M. G. (2005). Influence of convective transport on tropospheric ozone and its precursors in a chemistry-climate model. Atmospheric Chemistry and Physic, 5, 3205–3218.

Doherty, R. M., Wild, O., Shindell, D. T., Zeng, G., MacKenzie, I. a, Collins, W. J., Fiore, a M., et al. (2013). Impacts of climate change on surface ozone and intercontinental ozone pollution: A multi-model study. Journal of Geophysical Research: Atmospheres, 118(9), 3744-3763.

Donkelaar, A. van, Martin, R. V., Brauer, M., Kahn, R., Levy, R., Verduzco, C., & Villeneuve, P. J. (2010). Global estimates of ambient fine particulate matter concentrations from satellite-based aerosol optical depth: Development and application. Environmental Health Perspectives, 118(6), 847-855.

Donkelaar, A. van, Martin, R. V., Brauer, M., & Boys, B. L. (2015). Use of satellite observations for long-term exposure assessment of global concentrations of fine particulate matter. Environmental health perspectives, 123(2), 135-43.

Donner, L. J., Wyman, B. L., Hemler, R. S., Horowitz, L. W., Ming, Y., Zhao, M., Golaz, J. C., et al. (2011). The dynamical core, physical parameterizations, and basic simulation characteristics of the atmospheric component AM3 of the GFDL global coupled model CM3. Journal of Climate, 24(13), 3484-3519.

Driscoll, C. T., Buonocore, J. J., Levy, J. I., Lambert, K. F., Burtraw, D., Reid, S. B., Fakhraei, H., Schwartz, J. (2015). US power plant carbon standards and clean air and health co-benefits (SI). Nature Climate Change, 1-8.

Duncan, B. N., West, J. J., Yoshida, Y., Fiore, A. M., & Ziemke, J. R. (2008). The influence of European pollution on ozone in the Near East and northern Africa. Atmospheric Chemistry and Physics, 8(1), 1913-1950.

Emmons, L. K., Walters, S., Hess, P. G., Lamarque, J.-F., Pfister, G. G., Fillmore, D., Granier, C. et al. (2010). Description and evaluation of the Model for Ozone and Related chemical Tracers, version 4 (MOZART-4), Geoscientific Model Development., 3, 43–67.

Ewing, S. A., Christensen, J. N., Brown, S. T., Vancuren, R. A., Cliff, S. S., & Depaolo, D. J. (2010). Pb isotopes as an indicator of the Asian contribution to particulate air pollution in urban California. Environmental Science and Technology, 44(23), 8911-8916.

Fang, Y., Mauzerall, D. L., Liu, J., Fiore, A. M., & Horowitz, L. W. (2013). Impacts of 21st century climate change on global air pollution-related premature mortality. Climatic Change, 121(2), 239-253.

Fann, N., Fulcher, C. M., & Hubbell, B. J. (2009). The influence of location, source, and emission type in estimates of the human health benefits of reducing a ton of air pollution. Air Quality, Atmosphere and Health, 2(3), 169-176.

Fann, N., Fulcher, C. M., & Baker, K. (2013). The recent and future health burden of air pollution apportioned across U.S. sectors. Environmental Science and Technology, 47(8), 3580-3589.

Fann, N., Nolte, C, G., Dolwick, P., Spero, T, L., Brown, A, C., Phillips, S., & Anenberg, S. (2015). The geographic distribution and economic value of climate change-related ozone health impacts in the United States in 2030. Journal of the Air & Waste Management Association, 65(6), 570-580.

Fiore, A. M., Jacob, D. J., Liu, H., Yantosca, R. M., Fairlie, T. D., & Li, Q. (2003). Variability in surface ozone background over the United States: Implications for air quality policy. Journal of Geophysical Research.

Fiore, A. M., West, J. J., Horowitz, L. W., Naik, V., & Schwarzkopf, M. D. (2008). Characterizing the tropospheric ozone response to methane emission controls and the benefits to climate and air quality. Journal of Geophysical Research: Atmospheres, 113(8), 1-16.

Fiore, A. M., Dentener, F. J., Wild, O., Cuvelier, C., Schultz, M. G., Hess, P., Textor, C., et al. (2009). Multimodel estimates of intercontinental source-receptor relationships for ozone pollution. Journal of Geophysical Research: Atmospheres, 114(4), 1-21.

Fiore, A. M., Levy, H., & Jaffe, D. A. (2011). North American isoprene influence on intercontinental ozone pollution. Atmospheric Chemistry and Physics, 11(4), 1697-1710.

Fiore, A. M., Naik, V., Spracklen, D. V., Steiner, A., Unger, N., Prather, M., Bergmann, D., et al. (2012). Global air quality and climate. Chemical Society Reviews, 41(19), 6663-6683.

Fiore, A. M., Naik, V., & Leibensperger, E. M. (2015). Air Quality and Climate Connections. Journal of the Air & Waste Management Association, 65(6), 645-685.

Forster, P. M. de, & Shine, K. P. (1997). Radiative forcing and temperature trends from stratospheric ozone changes. Journal of Geophysical Research.

Fountoukis, C., & Nenes, A. (2007). ISORROPIA II: a computationally efficient thermodynamic equilibrium model for K^+–Ca^{2+}–Mg^{2+}–NH^{4+}–Na^+–$SO4^{2-}$–NO^{3-}–Cl^-–H_2O aerosols. Atmospheric Chemistry and Physics, 7(17), 4639-4659.

Fry, M. M., Naik, V., West, J., Schwarzkopf, M. D., Fiore, A. M., Collins, W. J., Dentener, F. J., et al. (2012). The influence of ozone precursor emissions from four world regions on tropospheric composition and radiative climate forcing. Journal of Geophysical Research: Atmospheres, 117(7), 1-16.

Fry, M. M., Schwarzkopf, M. D., Adelman, Z., Naik, V., Collins, W. J., & West, J. J. (2013). Net radiative forcing and air quality responses to regional CO emission reductions. Atmospheric Chemistry and Physics, 13(10), 5381-5399.

Fry, M. M., Schwarzkopf, M. D., Adelman, Z., & West, J. J. (2014). Air quality and radiative forcing impacts of anthropogenic volatile organic compound emissions from ten world regions. Atmospheric Chemistry and Physics, 14, 523-535.

Fu, J., Jang, C., Streets, D., Li, Z., Kwok, R., Park, R., & Han, Z. (2008). MICS-Asia II: Modeling gaseous pollutants and evaluating an advanced modeling system over East Asia. Atmospheric Environment, 42(15), 3571-3583.

Fuglestvedt, J. S., Berntsen, T. K., Isaksen, I. S. A, Mao, H., Liang, X. Z., & Wang, W. C. (1999). Climatic forcing of nitrogen oxides through changes in tropospheric ozone and methane; global 3D model studies. Atmospheric Environment, 33(6), 961-977.

Fuglestvedt, J. S., Shine, K. P., Berntsen, T., Cook, J., Lee, D. S., Stenke, A, Skeie, R. B., et al. (2010). Transport impacts on atmosphere and climate: Metrics. Atmospheric Environment, 44(37), 4648-4677.

Gao, Y., Fu, J. S., Drake, J. B., Lamarque, J.-F. & Liu, Y. (2013). The impact of emission and climate change on ozone in the United States under representative concentration pathways (RCPs), Atmos. Chem. Phys., 13, 9607–9621.

Garcia, R. R., Marsh, D. R., Kinnison, D. E., Boville, B. A, & Sassi, F. (2007). Simulation of secular trends in the middle atmosphere, 1950-2003. Journal of Geophysical Research: Atmospheres, 112(9), 1-23.

Garcia-Menendez, F., Saari, R. K., Monier, E., & Selin, N. E. (2015). U.S. Air Quality and Health Benefits from Avoided Climate Change under Greenhouse Gas Mitigation. Environmental Science & Technology, 49(13), 7580-7588.

Granier, C., Bessagnet, B., Bond, T., D'Angiola, A., Gon, H. D. van der, Frost, G. J., Heil, A., et al. (2011). Evolution of anthropogenic and biomass burning emissions of air pollutants at global and regional scales during the 1980-2010 period. Climatic Change, 109(1), 163-190.

Grell, G. A., & Devenyi, D. (2002). A generalized approach to parameterizing convection combining ensemble and data assimilation techniques, Geophys. Res. Lett., 29(14), 10–13.

Guenther, A. B., Jiang, X., Heald, C. L., Sakulyanontvittaya, T., Duhl, T., Emmons, L. K., & Wang, X. (2012). The model of emissions of gases and aerosols from nature version 2.1 (MEGAN2.1): An extended and updated framework for modeling biogenic emissions. Geoscientific Model Development, 5(6), 1471-1492.

Hadley, O. L., Ramanathan, V., Carmichael, G. R., Tang, Y., Corrigan, C. E., Roberts, G. C., & Mauger, G. S. (2007). Trans-Pacific transport of black carbon and fine aerosols (D < 2.5 μm) into North America. Journal of Geophysical Research, 112(D5), D05309.

Haines, A., McMichael, A. J., Smith, K. R., Roberts, I., Woodcock, J., Markandya, A., Armstrong, B. G., et al. (2009). Public health benefits of strategies to reduce greenhouse-gas emissions: overview and implications for policy makers. The Lancet, 374(9707), 2104-2114.

Han, Y., Fang, X., Zhao, T., & Kang, S. (2008). Long range trans-Pacific transport and deposition of Asian dust aerosols. Journal of environmental sciences (China), 20(4), 424-8.

Hayes, P. L., Carlton, A. G., Baker, K. R., Ahmadov, R., Washenfelder, R. A., Alvarez, S., Rappenglück, B., Gilman, J. B., Kuster, W. C., de Gouw, J. A., Zotter, P., Prévôt, A. S. H., Szidat, S., Kleindienst, T. E., Offenberg, J. H., Ma, P. K., & Jimenez, J. L. (2015). Modeling the formation and aging of secondary organic aerosols in Los Angeles during CalNex 2010, Atmos. Chem. Phys., 15, 5773-5801, doi:10.5194/acp-15-5773-2015.

Heald, C. L., Jacob, D. J., Park, R. J., Alexander, B., Fairlie, T. D., Yantosca, R. M., & Chu, D. A. (2006). Transpacific transport of Asian anthropogenic aerosols and its impact on surface air quality in the United States. Journal of Geophysical Research: Atmospheres, 111, 1-13.

Heald, C. L., & Spracklen, D. V. (2015). Land Use Change Impacts on Air Quality and Climate, Chem. Rev., (x), 150403095328008.

Hilboll, A., Richter, A., & Burrows, J. P. (2013). Long-term changes of tropospheric NO_2 over megacities derived from multiple satellite instruments. Atmospheric Chemistry and Physics, 13(8), 4145-4169.

Holloway, T., Fiore, A., & Hastings, M. G. (2003). Intercontinental transport of air pollution: Will emerging science lead to a new hemispheric treaty? Environmental Science and Technology, 37(20), 4535-4542.

Hogrefe, C. Lynn, B., Civerolo, K., Ku, J.-Y., Rosenthal, J., Rosenzweig, C., Goldberg, R., Gaffin, S., Knowlton, K. & Kinney, P. L. (2004). Simulating changes in regional air pollution

over the eastern United States due to changes in global and regional climate and emissions. Journal of Geophysical Research, 109(D22), D22301.

Hogrefe, C., Isukapalli, S. S., Tang, X., Georgopoulos, P. G., He, S., Zalewsky, E. E., Hao, W., et al. (2011). Impact of Biogenic Emission Uncertainties on the Simulated Response of Ozone and Fine Particulate Matter to Anthropogenic Emission Reductions. Journal of the Air and Waste Management Association, 61, 92-108.

Hong, S, & Lim, J. (2006). The WRF single-moment 6-class microphysics scheme (WSM6), J. Korean Meteorol. Soc., 42(2), 129–151.

Hong, S.-Y., Noh, Y., & Dudhia, J. (2006). A New Vertical Diffusion Package with an Explicit Treatment of Entrainment Processes, Mon. Weather Rev., 134(9), 2318–2341.

Horton, D. E., Skinner, C. B., Singh, D., & Diffenbaugh, N. S. (2014). Occurrence and persistence of future atmospheric stagnation events. Nature Climate Change, 1-13.

Iacono, M. J., Delamere, J. S., Mlawer, E. J., Shephard, M. W., Clough, S. a, & Collins, W. D. (2008). Radiative forcing by long-lived greenhouse gases: Calculations with the AER radiative transfer models. Journal of Geophysical Research: Atmospheres, 113(13), 2-9.

Ito, K., De Leon, S. F., & Lippmann, M. (2005). Associations between ozone and daily mortality: analysis and meta-analysis. Epidemiology (Cambridge, Mass.), 16(4), 446-457.

Jacob, D. J., Logan, J. A, & Murti, P. P. (1999). Effect of rising Asian emissions on surface ozone in the United States. Geophysical Research Letters.

Jacob, D. J., & Winner, D. A. (2009). Effect of climate change on air quality. Atmospheric Environment, 43(1), 51-63.

Jacobson, M. Z. (2008). On the causal link between carbon dioxide and air pollution mortality. Geophysical Research Letters, 35(3), 1-5.

Janssen, N. A. H., Hoek, G., Simic-Lawson, M., Fischer, P., Bree, L. van, Brink, H. ten, Keuken, M., Atkinson, R. W., Anderson, H. R., Brunekreef, B., et al. (2011). Black Carbon as an Additional Indicator of the Adverse Health Effects of Airborne Particles Compared with PM_{10} and $PM_{2.5}$. Environmental Health Perspectives.

Janssen, N. A., Gerlofs-Nijland, M. E., Lanki, T., Salonen, R. O., Cassee, F., Hoek, G., Fischer, P., Brunekreef, B., et al. (2012). Health effects of black carbon. World Health Organization.

Jerrett, M., Burnett, R. T., Pope, C. A., Ito, K., Thurston, G., Krewski, D., Shi, Y., et al. (2009). Long-term ozone exposure and mortality. The New England Journal of Medicine, 360(11), 1085-95.

Keating, T. J., West, J. J., & Farrell, A. E. (2004). Prospects for international management of intercontinental air pollution transport. In Intercontinental Transport of Air Pollution A. Stohl, ed. (Berlin: Springer), p. 295–320.

Kelly, J. T., Bhave, P. V., Nolte, C. G., Shankar, U., & Foley, K. M. (2010). Simulating emission and chemical evolution of coarse sea-salt particles in the Community Multiscale Air Quality (CMAQ) model. Geoscientific Model Development, 3, 257-273.

Kim, Y.-M., Zhou, Y., Gao, Y., Fu, J. S., Johnson, B. A, Huang, C., & Liu, Y. (2015). Spatially resolved estimation of ozone-related mortality in the United States under two Representative Concentration Pathways (RCPs) and their uncertainty. Climatic change, 128(1-2), 71-84.

Kloster, S., Dentener, F., Feichter, J., Raes, F., Lohmann, U., Roeckner, E., & Fischer-Bruns, I. (2010). A GCM study of future climate response to aerosol pollution reductions. Climate Dynamics, 34, 1177-1194.

Kondo, Y., Matsui, H., Moteki, N., Sahu, L., Takegawa, N., Kajino, M., Zhao, Y., et al. (2011). Emissions of black carbon, organic, and inorganic aerosols from biomass burning in North America and Asia in 2008. Journal of Geophysical Research: Atmospheres, 116, 1-25.

Koo, B., Chien, C.-J., Tonnesen, G., Morris, R., Johnson, J., Sakulyanontvittaya, T., Piyachaturawat, P., et al. (2010). Natural emissions for regional modeling of background ozone and particulate matter and impacts on emissions control strategies. Atmospheric Environment, 44(19), 2372-2382.

Krewski, D., Jerrett, M., Burnett, R. T., Ma, R., Hughes, E., Shi, Y., Turner, M. C., et al. (2009). Extended follow-up and spatial analysis of the American Cancer Society study linking particulate air pollution and mortality. Research report (Health Effects Institute), (140), 5-114; discussion 115-136.

Laden, F., Schwartz, J., Speizer, F. E., & Dockery, D. W. (2006). Reduction in fine particulate air pollution and mortality: Extended follow-up of the Harvard Six Cities Study. American Journal of Respiratory and Critical Care Medicine, 173(6), 667-672.

Lam, Y. F., Fu, J. S., Wu, S., & Mickley, L. J. (2011). Impacts of future climate change and effects of biogenic emissions on surface ozone and particulate matter concentrations in the United States. Atmospheric Chemistry and Physics, 11(10), 4789-4806.

Lamarque, J.-F., Bond, T. C., Eyring, V., Granier, C., Heil, a, Klimont, Z., Lee, D., et al. (2010). Historical (1850-2000) gridded anthropogenic and biomass burning emissions of reactive gases and aerosols: Methodology and application. Atmospheric Chemistry and Physics, 10(15), 7017-7039.

Lamarque, J.-F., Emmons, L. K., Hess, P. G., Kinnison, D. E., Tilmes, S., Vitt, F., Heald, C. L., et al. (2012). CAM-chem: Description and evaluation of interactive atmospheric chemistry in the Community Earth System Model. Geoscientific Model Development, 5(2), 369-411.

Lamarque, J.-F., Shindell, D. T., Josse, B., Young, P. J., Cionni, I., Eyring, V., Bergmann, D., et al. (2013). The atmospheric chemistry and climate model intercomparison Project (ACCMIP): Overview and description of models, simulations and climate diagnostics. Geoscientific Model Development, 6(1), 179-206.

Lawrence, M. G., Rof, von K., Salzmann, M., & Rasch, P. J. (2003). The balance of effects of deep convective mixing on tropospheric ozone. Geophysical Research Letters, 30(18), 3-6.

Lelieveld, J., Evans, J. S., Fnais, M., Giannadaki, D., & Pozzer, A. (2015). The contribution of outdoor air pollution sources to premature mortality on a global scale. Nature, 525,367–71.

Lepeule, J., Laden, F., Dockery, D., & Schwartz. J. (2012). Chronic exposure to fine particles and mortality: An extended follow-up of the Harvard six cities study from 1974 to 2009 Environ. Health Perspect, 120, 965–70.

Leung, L. R. & Gustafson, W. I. (2005). Potential regional climate change and implications to U.S. air quality. Geophysical Research Letters, 32(August), 1-4.

Levy, J. I., Chemerynski, S. M., & Sarnat, J. A. (2005). Ozone exposure and mortality: an empiric bayes metaregression analysis. Epidemiology (Cambridge, Mass.), 16(4), 458-468.

Levy, H., Schwarzkopf, M. D., Horowitz, L., Ramaswamy, V., & Findell, K. L. (2008). Strong sensitivity of late 21st century climate to projected changes in short-lived air pollutants. Journal of Geophysical Research: Atmospheres, 113(6), 1-13.

Li, Y., Henze, D. K., Jack, D., and Kinney, P. L. (2015). The influence of air quality model resolution on health impact assessment for fine particulate matter and its components Air Qual. Atmos. Heal. Online: http://link.springer.com/10.1007/s11869-015-0321-z.

Li, Y., Henze, D. K., Jack, D., Henderson, B. H., and Kinney, P. L. (2015). Assessing public health burden associated with exposure to ambient black carbon in the United States Sci. Total Environ. 539, 515–25.

Liang, Q., Jaeglé, L., Jaffe, D. a, Weiss-Penzias, P., Heckman, A., & Snow, J. A. (2004). Long-range transport of Asian pollution to the northeast Pacific: Seasonal variations and transport pathways of carbon monoxide. Journal of Geophysical Research D: Atmospheres, 109, 1-16.

Liang, Q., Jaeglé, L., Hudman, R. C., Turquety, S., Jacob, D. J., Avery, M. A., Browell, E. V., et al. (2007). Summertime influence of Asian pollution in the free troposphere over North America. Journal of Geophysical Research, 112(D12), D12S11.

Lim S. S. et al. (2013). A comparative risk assessment of burden of disease and injury attributable to 67 risk factors and risk factor clusters in 21 regions, 1990-2010: a systematic analysis for the Global Burden of Disease Study 2010. Lancet 380:2224–60.

Lin, J.-Tai, Wuebbles, D. J., & Liang, X.-Zhong. (2008). Effects of intercontinental transport on surface ozone over the United States: Present and future assessment with a global model. Geophysical Research Letters, 35(2), 1-6.

Lin, M., Fiore, A. M., Horowitz, L. W., Cooper, O. R., Naik, V., Holloway, J., Johnson, B. J., et al. (2012). Transport of Asian ozone pollution into surface air over the western United States in spring. Journal of Geophysical Research: Atmospheres, 117(4), 1-20.

Lin, Y.-H. Y., Zhang, H., Pye, H. H. O. T., Zhang, Z., Marth, W. J., Park, S., Arashiro, M., et al. (2013). Epoxide as a precursor to secondary organic aerosol formation from isoprene photooxidation in the presence of nitrogen oxides. Proceedings of the National Academy of Sciences of the United States of America, 110(17), 6718-23.

Liu, H.-Y., Jacob, D. J., Bey, I., Yantosca, R. M., Duncan, B. N., & Sachse, G. W. (2003). Transport Pathways for Asian Pollution Outflow Over the Pacific: Interannual and Seasonal Variations. Journal of Geophysical Research, 108(D20), 8786.

Liu, J., Mauzerall, D. L., Horowitz, L. W., Ginoux, P., & Fiore, A. M. (2009a). Evaluating inter-continental transport of fine aerosols: (1) Methodology, global aerosol distribution and optical depth. Atmospheric Environment, 43(28), 4327-4338.

Liu, J., Mauzerall, D. L., & Horowitz, L. W. (2009b). Evaluating inter-continental transport of fine aerosols: (2) Global health impact. Atmospheric Environment, 43(28), 4339-4347.

Liu, P., Tsimpidi, A. P., Hu, Y., Stone, B., Russell, A., & Nenes, A. (2012). Differences between downscaling with spectral and grid nudging using WRF. Atmospheric Chemistry and Physics, 12(8), 3601-3610.

Liu, S. C., Trainer, M., Fehsenfeld, F. C., Parrish, D. D., Williams, E. J., Fahey, D. W., Hübler, G., et al. (1987). Ozone production in the rural troposphere and the implications for regional and global ozone distributions. Journal of Geophysical Research.

IMF (2000). World Economic Outlook; Asset Prices and the Business Cycle. International Monetary Fund: Washington.

Ma, Z., Hu, X., Huang, L., Bi, J., & Liu, Y. (2014). Estimating ground-level $PM_{2.5}$ in China using satellite remote sensing. Environmental Science & Technology, 48, 7436-7444.

Markandya, A., Armstrong, B. G., Hales, S., Chiabai, A., Criqui, P., Mima, S., Tonne, C., Wilkinson, T. (2009). Public health benefits of strategies to reduce greenhouse-gas emissions: low-carbon electricity generation. The Lancet, 374(9706), 2006-2015.

Mickley, L. J., Jacob, D. J. & Field, B. D. (2004). Effects of future climate change on regional air pollution episodes in the United States. Geophysical Research Letters, 31(24), L24103.

Morita, H., Yang, S., Unger, N., & Kinney, P. L. (2014). Global health impacts of future aviation emissions under alternative control scenarios. Environmental science & technology, 48(24), 14659-67.

Moss, R. H., Edmonds, J. A, Hibbard, K. a, Manning, M. R., Rose, S. K., Vuuren, D. P. van, Carter, T. R., et al. (2010). The next generation of scenarios for climate change research and assessment. Nature, 463(7282), 747-756.

Myhre, G., D. Shindell, F.-M. Bréon, W. Collins, J. Fuglestvedt, J. Huang, D. Koch, J.-F. Lamarque, D. Lee, B. Mendoza, T. Nakajima, A. Robock, G. Stephens, T. Takemura and H. Zhang, 2013: Anthropogenic and Natural Radiative Forcing. In: Climate Change 2013: The Physical Science Basis. Contribution of Working Group I to the Fifth Assessment Report of the Intergovernmental Panel on Climate Change [Stocker, T.F., D. Qin, G.-K. Plattner, M. Tignor, S.K. Allen, J. Boschung, A. Nauels, Y. Xia, V. Bex and P.M. Midgley (eds.)]. Cambridge University Press, Cambridge, United Kingdom and New York, NY, USA, pp. 659–740.

Nam, J., Wang, Y., Luo, C., & Chu, D. A. (2010). Trans-Pacific transport of Asian dust and CO: accumulation of biomass burning CO in the subtropics and dipole structure of transport. Atmospheric Chemistry and Physics, 10(1), 3297-3308.

Naik, V., Mauzerall, D., Horowitz, L., Schwarzkopf, M. D., Ramaswamy, V., & Oppenheimer, M. (2005). Net radiative forcing due to changes in regional emissions of tropospheric ozone precursors. Journal of Geophysical Research: Atmospheres, 110, D24306.

Naik, V., Horowitz, L. W., Fiore, A. M., Ginoux, P., Mao, J., Aghedo, A. M., & Levy, H. (2013). Impact of preindustrial to present-day changes in short-lived pollutant emissions on atmospheric composition and climate forcing. Journal of Geophysical Research: Atmospheres, 118, 8086-8110.

Nakicenovic, N., & Swart, R. (2000). IPCC Special Report on Emissions Scenarios: A special report of Working Group III of the Intergovernmental Panel on Climate Change. (N. Nebojsa & R. Swart, Eds.) emissions scenarios (p. 608). Cambridge University Press.

Nemet, G. F., Holloway, T., & Meier, P. (2010). Implications of incorporating air-quality co-benefits into climate change policymaking. Environmental Research Letters.

Nolte, C. G., Gilliland, A. B., Hogrefe, C., & Mickley, L. J. (2008). Linking global to regional models to assess future climate impacts on surface ozone levels in the United States. Journal of Geophysical Research: Atmospheres, 113(14), 1-14.

Nolte, C. G., Sperno, T, O., Pinder, R., Bowden, H. J., Herwehe, J., Faluvegi, G., & Shindell, D. (2014). Influences of Regional Climate Change on Air Quality Across the Continental US Projected from Downscaling IPCC AR5 Simulations (Chapter 2, Air Pollution Modeling and its Application XXII).

Nolte, C. G., Appel, K. W., Kelly, J. T., Bhave, P. V., Fahey, K. M., Collett Jr., J. L., Zhang, L., and Young, J. O. (2015). Evaluation of the Community Multiscale Air Quality (CMAQ) model v5.0 against size-resolved measurements of inorganic particle composition across sites in North America, Geosci. Model Dev., 8, 2877-2892.

Ohara, T., Akimoto, H., Kurokawa, J., Horii, N., Yamaji, K., Yan, X., & Hayasaka, T. (2007). An Asian emission inventory of anthropogenic emission sources for the period 1980–2020. Atmospheric Chemistry and Physics, 7, 4419-4444.

Ostro, B., Feng, W. Y., Broadwin, R., Green, S., & Lipsett, M. (2007). The effects of components of fine particulate air pollution on mortality in California: Results from CALFINE. Environmental Health Perspectives, 115(1), 13-19.

Otte, T. L. & Pleim, J. E. (2010). The Meteorology-Chemistry Interface Processor (MCIP) for the CMAQ modeling system, Geosci. Model Dev., 3, 243–256.

Otte, T. L., Nolte, C. G., Otte, M. J., & Bowden, J. H. (2012). Does nudging squelch the extremes in regional climate modeling? Journal of Climate, 25(20), 7046-7066.

Parrish, D. D., & Zhu, T. (2009). Clean Air for Megacities. Science, 326(30 October 2009), 674-675.

Parrish, D. D., Law, K. S., Staehelin, J., Derwent, R., Cooper, O. R., Tanimoto, H., Volz-Thomas, A, et al. (2013). Lower tropospheric ozone at northern midlatitudes: Changing seasonal cycle. Geophysical Research Letters, 40(8), 1631-1636.

Plachinski, S. D., Holloway, T., Meier, P. J., Nemet, G. F., Rrushaj, A., Oberman, J. T., Duran, P. L., et al. (2014). Quantifying the emissions and air quality co-benefits of lower-carbon electricity production. Atmospheric Environment, 94(March 2013), 180-191.

Pouliot, G.: A Tale of Two Models: A Comparison of the Biogenic Emission Inventory System (BEIS3.14) and Model of Emissions of Gases and Aerosols from Nature (MEGAN 2.04), 7th Annual CMAS Conference, Chapel Hill, NC, USA, 7 October 2008.

Pouliot, G. & Pierce, T. E. (2009). Integration of the Model of Emissions of Gases and Aerosols from Nature (MEGAN) into the CMAQ Modeling System, 18th International Emission Inventory Conference, Baltimore, Maryland, 14–17 April 2009.

Peng, R. D., Bell, M. L., Geyh, A. S., McDermott, A., Zeger, S. L., Samet, J. M., & Dominici, F. (2009). Emergency admissions for cardiovascular and respiratory diseases and the chemical composition of fine particle air pollution. Environmental Health Perspectives, 117(6), 957-963.

Post, E. S., Grambsch, A., Weaver, C., Morefield, P., Huang, J., Leung, L. Y., Nolte, C. G., et al. (2012). Variation in estimated ozone-related health impacts of climate change due to modeling choices and assumptions. Environmental Health Perspectives, 120(11), 1559-1564.

Power, M. C., Weisskopf, M. G., Alexeeff, S. E., Coull, B. a, Avron, S., & Schwartz, J. (2011). Traffic-related air pollution and cognitive function in a cohort of older men. Environmental Health Perspectives, 119(5), 682-687.

Pusede, S. E., Steiner, A. L. & Cohen, R. C. (2015). Temperature and Recent Trends in the Chemistry of Continental Surface Ozone. Chemical. Review. 115, 3898–3918.

Pun, B. K., Wu, S. Y., & Seigneur, C. (2002). Contribution of biogenic emissions to the formation of ozone and particulate matter in the Eastern United States. Environmental Science and Technology, 36(16), 3586-3596.

Punger, E. M., & West, J. J. (2013). The effect of grid resolution on estimates of the burden of ozone and fine particulate matter on premature mortality in the USA. Air Quality, Atmosphere and Health, 6(3), 563-573.

Pye, H. O. T. & Pouliot, G. A. (2012). Modeling the Role of Alkanes, Polycyclic Aromatic Hydrocarbons, and Their Oligomers in Secondary Organic Aerosol Formation, Environ. Sci. Technol., 46(11), 6041–6047.

Pye, H. O. T., Pinder, R. W., Piletic, I. R., Xie, Y., Capps, S. L., Lin, Y.-H., Surratt, J. D., et al. (2013). Epoxide pathways improve model predictions of isoprene markers and reveal key role of acidity in aerosol formation. Environmental science & technology, 47(19), 11056-64.

Qiao, L. P., Cai, J., Wang, H. L., Wang, W. B., Zhou, M., Lou, S. R., Chen, R. J., et al. (2014). $PM_{2.5}$ Constituents and Hospital Emergency-Room Visits in Shanghai, China. Environmental Science & Technology, 48(17), 10406-10414.

Ramanathan, V., & Feng, Y. (2009). Air pollution, greenhouse gases and climate change: Global and regional perspectives. Atmospheric Environment, 43(1), 37-50.

Reff, A., Bhave, P. V., Simon, H., Pace, T. G., Pouliot, G. a, Mobley, J. D., Houyoux, M., et al. (2009). Emissions inventory of $PM_{2.5}$ trace elements across the United States. Environmental science & technology, 43(15), 5790-6.

Reynolds, C. C. O., & Kandlikar, M. (2008). Climate impacts of air quality policy: Switching to a natural gas-fueled public transportation system in New Delhi. Environmental Science and Technology, 42(16), 5860-5865.

Riahi, K., Rao, S., Krey, V., Cho, C., Chirkov, V., Fischer, G., Kindermann, G., et al. (2011). RCP 8.5-A scenario of comparatively high greenhouse gas emissions. Climatic Change, 109(1), 33-57.

Richter, A., Burrows, J. P., Nüss, H., Granier, C., & Niemeier, U. (2005). Increase in tropospheric nitrogen dioxide over China observed from space. Nature, 437(7055), 129-32.

Roman, H. A, Walker, K. D., Walsh, T. L., Conner, L., Richmond, H. M., Hubbell, B. J., & Kinney, P. L. (2008). Expert judgment assessment of the mortality impact of changes in ambient fine particulate matter in the U.S. Environmental Science and Technology, 42(7), 2268-2274.

Royal Society (2008). Ground-level ozone in the 21st century: future trends, impacts and policy implications. The Royal Society Science Policy, London.

RTI International (2015). BenMAP-CE: Environmental Benefits Mapping and Analysis Program-Community Edition, User's Manual Appendices. Available from RTI International, http://www2.epa.gov/benmap/manual-and-appendices-benmap-ce, [1 December 2015]

Selin, N. E., Wu, S., Nam, K. M., Reilly, J. M., Paltsev, S., Prinn, R. G., & Webster, M. D. (2009). Global health and economic impacts of future ozone pollution. Environmental Research Letters, 4(4), 044014.

Sillman, S., He, D., Cardelino, C., & Imhoff, R. E. (1997). The use of photochemical indicators to evaluate ozone-NO_x-hydrocarbon sensitivity: Case studies from Atlanta, New York, and Los Angeles. Journal of the Air & Waste Management Association, 47(10), 1030-1040.

Simon, H., & Bhave, P. V. (2012). Simulating the degree of oxidation in atmospheric organic particles. Environmental Science and Technology, 46, 331-339.

Schultz, M. G., L. Backman, Y. Balkanski, S. Bjoerndalsaeter, R. Brand, J. P. Burrows, S. Dalsoeren, M. de Vasconcelos, et al., (2007), REanalysis of the TROpospheric chemical composition over the past 40 years (RETRO) — A long-term global modeling study of tropospheric chemistry, Final Report, Jülich/Hamburg, Germany.

Schucht, S., Colette, A., Rao, S., Holland, M., Schöpp, W., Kolp, P., Klimont, Z., et al. (2015). Moving towards ambitious climate policies: Monetised health benefits from improved air quality could offset mitigation costs in Europe. Environmental Science & Policy, 50, 252-269..

Shindell, D., Lamarque, J. F., Unger, N., Koch, D., Faluvegi, G., Bauer, S., Ammann, M., Cofala, J., & Teich., He. (2008). Climate forcing and air quality change due to regional emissions reductions by economic sector. Atmospheric Chemistry and Physics, 8(23), 7101-7113.

Shindell, D. T., Faluvegi, G., Koch, D. M., Schmidt, G. A, Unger, N., & Bauer, S. E. (2009). Improved attribution of climate forcing to emissions. Science (New York, N.Y.), 326(5953), 716-718.

Shindell, D., Kuylenstierna, J. C. I., Vignati, E., Dingenen, R. van, Amann, M., Klimont, Z., Anenberg, S. C., et al. (2012). Simultaneously mitigating near-term climate change and improving human health and food security. Science (New York, N.Y.), 335(6065), 183-9.

Silva, R. A, West, J. J., Zhang, Y., Anenberg, S. C., Lamarque, J.-F., Shindell, D. T., Collins, W. J., et al. (2013). Global premature mortality due to anthropogenic outdoor air pollution and the contribution of past climate change. Environmental Research Letters, 8(3), 034005..

Skamarock, W. C., & Klemp, J. B. (2008). A time-split nonhydrostatic atmospheric model for weather research and forecasting applications. Journal of Computational Physics, 227(7), 3465-3485.

Smil, V. (2003). Energy at the Crossroads: Global perspectives and uncertainties; Chapter 1. MIT Press: Cambridge, MA.

Smith, K. R., Woodward, A., Campbell-Lendrum, D., Chadee, D. D., Honda, Y., Liu, Q., Olwoch, J. M., Revich, B. and Sauerborn, R., (2014). Human health: impacts, adaptation, and co-benefits. In: Climate Change 2014: Impacts, Adaptation, and Vulnerability. Part A: Global and Sectoral Aspects. Contribution of Working Group II to the Fifth Assessment Report of the Intergovernmental Panel on Climate Change. Cambridge UniversityPress, Cambridge, United Kingdom and New York, NY, USA, pp. 709-754.

Song, C.-K., Byun, D. W., Pierce, R. B., Alsaadi, J. A., Schaack, T. K., & Vukovich, F. (2008). Downscale linkage of global model output for regional chemical transport modeling: Method and general performance. Journal of Geophysical Research: Atmosphere, 113(D8).

Suh, H. H., & Zanobetti, A. (2010). Exposure error masks the relationship between traffic-related air pollution and heart rate variability. Journal of Occupational and Environmental Medicine, 52(7), 685-692.

Sun, J., Fu, J. S., Huang, K., & Gao, Y. (2015). Estimation of future $PM_{2.5}$- and ozone-related mortality over the continental United States in a changing climate: An application of high-resolution dynamical downscaling technique. Journal of the Air and Waste Management Association, 65, 611-623.

Surratt, J. D., Chan, A. W. H., Eddingsaas, N. C., Chan, M., Loza, C. L., Kwan, A. J., Hersey, S. P., et al. (2010). Reactive intermediates revealed in secondary organic aerosol formation from isoprene. Proceedings of the National Academy of Sciences of the United States of America, 107(15), 6640-6645.

Tagaris, E., Manomaiphiboon, K., Liao, K.-J., Leung, L. R., Woo, J.-H., He, S., Amar, P., et al. (2007). Impacts of global climate change and emissions on regional ozone and fine particulate matter concentrations over the United States. Journal of Geophysical Research, 112(D14), D14312.

Tagaris, E., Liao, K.-J., Delucia, A. J., Deck, L., Amar, P., & Russell, A. G. (2009). Potential impact of climate change on air pollution-related human health effects. Environmental science & technology, 43(13), 4979-4988.

Tai, A. P. K., Mickley, L. J., & Jacob, D. J. (2010). Correlations between fine particulate matter ($PM_{2.5}$) and meteorological variables in the United States: Implications for the sensitivity of $PM_{2.5}$ to climate change. Atmospheric Environment, 44(32), 3976-3984. Elsevier Ltd. Retrieved from http://dx.doi.org/10.1016/j.atmosenv.2010.06.060.

Tai, A. P. K., Martin, M. V., & Heald, C. L. (2014). Threat to future global food security from climate change and ozone air pollution. Nature Climate Change, 4, 817–821.

Tang, Y., Carmichael, G. R., Thongboonchoo, N., Chai, T., Horowitz, L. W., Pierce, R. B., Al-Saadi, J. A, et al. (2007). Influence of lateral and top boundary conditions on regional air quality prediction: A multiscale study coupling regional and global chemical transport models. Journal of Geophysical Research: Atmospheres, 112(10), 1-21.

Task Force on Hemispheric Transport of Air Pollution (TF HTAP, 2010). Hemispheric Transport of Air Pollution 2010. United Nations Economic Commission for Europe: Geneva.

Tebaldi, C., & Knutti, R. (2007). The use of the multi-model ensemble in probabilistic climate projections. Philosophical transactions. Series A, Mathematical, physical, and engineering sciences, 365(1857), 2053-2075.

Thomson, A. M., Calvin, K. V., Smith, S. J., Kyle, G. P., Volke, A., Patel, P., Delgado-Arias, S., et al. (2011). RCP4.5: A pathway for stabilization of radiative forcing by 2100. Climatic Change, 109(1), 77-94.

Thompson, T. M., Saari, R. K., & Selin, N. E. (2013). Air quality resolution for health impacts assessment: influence of regional characteristics. Atmospheric Chemistry and Physics, 14141-14161.

Thompson, T. M., Rausch, S., Saari, R. K., & Selin, N. E. (2014). A systems approach to evaluating the air quality co-benefits of US carbon policies. Nature Climate Change, (August), 1-11.

Tilmes, S., Lamarque, J. F., Emmons, L. K., Conley, A, Schultz, M. G., Saunois, M., Thouret, V., et al. (2012). Technical Note: Ozonesonde climatology between 1995 and 2011: Description, evaluation and applications. Atmospheric Chemistry and Physics, 12, 7475-7497.

Tilmes, S., Lamarque, J.-F., Emmons, L. K., Kinnison, D. E., Ma, P.-L., Liu, X., Ghan, S., et al. (2015). Description and evaluation of tropospheric chemistry and aerosols in the Community Earth System Model (CESM1.2). Geoscientific Model Development, 8(5), 1395-1426.

Trail, M. A, Tsimpidi, A, P., Liu, P., Tsigaridis, K., Hu, Y., Nenes, A. & Russell, A. G. (2013). Downscaling a global climate model to simulate climate change over the US and the implication on regional and urban air quality. Geoscientific Model Development, 6, 1429-1445.

Trail, M. A, Tsimpidi, A. P., Liu, P., Tsigaridis, K., Hu, Y., Rudokas, J. R., Miller, P. J., et al. (2015). Impacts of Potential CO_2-Reduction Policies on Air Quality in the United States. Environmental Science & Technology, 49(8), 5133–5141.

Trickl, T. (2003). Intercontinental transport and its influence on the ozone concentrations over central Europe: Three case studies. Journal of Geophysical Research, 108(D12), 1-23.

Unger, N., Shindell, D. T., Koch, D. M., & Streets, D. G. (2006). Cross influences of ozone and sulfate precursor emissions changes on air quality and climate. Proceedings of the National Academy of Sciences of the United States of America, 103(12), 4377-80.

Unger, N., Shindell, D. T., Koch, D. M., & Streets, D. G. (2008). Air pollution radiative forcing from specific emissions sectors at 2030. Journal of Geophysical Research: Atmospheres, 113(2), 2048-2058.

Unger, N. (2014). Human land-use-driven reduction of forest volatiles cools global climate. NATURE CLIMATE CHANGE, 4(10), 907-910.

United States Environmental Protection Agency. (2007). Guidance on the Use of Models and Other Analyses for Demonstrating Attainment of Air Quality Goals for Ozone, $PM_{2.5}$ and Regional Haze, EPA-454/B-07e002.

United States Environmental Protection Agency. (2009). Final Report: Integrated Science Assessment for Particulate Matter. U.S. Environmental Protection Agency, Washington, DC, EPA/600/R-08/139F, 2009.

United States Environmental Protection Agency. (2010). Quantitative Health Risk Assessment for Particulate Matter.

United States Environmental Protection Agency. (2013). Final Report: Integrated Science Assessment of Ozone and Related Photochemical Oxidants. U.S. Environmental Protection Agency, Washington, DC, EPA/600/R-10/076F, 2013.

United States Environmental Protection Agency 2014 Environmental Benefits Mapping and Analysis Program—Community Edition (BenMAP-CE) (Research Triangle Park, NC. http://www2.epa.gov/benmap).

United States Environmental Protection Agency. (2015). Final Report: Integrated Science Assessment of Ozone and Related Photochemical Oxidants. U.S. Environmental Protection Agency, Washington, DC, EPA

van der A, R. J., Eskes, H. J., Boersma, K. F., Noije, T. P. C. van, Van Roozendael, M., De Smedt, I., Peters, D. H. M. U., et al. (2008). Trends, seasonal variability and dominant NO_x source derived from a ten year record of NO_2 measured from space. Journal of Geophysical Research: Atmospheres, 113(4), D04302.

Vuuren, D. P. van, Edmonds, J., Kainuma, M., Riahi, K., Thomson, A., Hibbard, K., Hurtt, G. C., et al. (2011). The representative concentration pathways: An overview. Climatic Change, 109(1), 5-31.

Wang, S., & Hao, J. (2012). Air quality management in China: Issues, challenges, and options. Journal of Environmental Sciences, 24(1), 2-13.

Wang, S. X., Zhao, B., Cai, S. Y., Klimont, Z., Nielsen, C. P., Morikawa, T., Woo, J. H., et al. (2014). Emission trends and mitigation options for air pollutants in East Asia. Atmospheric Chemistry and Physics, 14(13), 6571-6603.

Wang, Y., Jiang, J. H., & Su, H. (2015). Atmospheric responses to the redistribution of anthropogenic aerosols. Journal of Geophysical Research: Atmosphere, 120(18), 9625-9641.

Weaver, C. P., Liang, X. Z., Zhu, J., Adams, P. J., Amar, P., Avise, J., Caughey, M., et al. (2009). A preliminary synthesis of modeled climate change impacts on U.S. regional ozone concentrations. Bulletin of the American Meteorological Society, 90(12), 1843-1863.

West, J. J., Osnaya, P., Laguna, I., Martínez, J., & Fernández, A. (2004). Co-control of urban air pollutants and greenhouse gases in Mexico City. Environmental science & technology, 38(13), 3474-3481.

West, J. J., Szopa, S., & Hauglustaine, D. A. (2007). Human mortality effects of future concentrations of tropospheric ozone. Comptes Rendus - Geoscience, 339, 775-783.

West, J. J., Naik, V., Horowitz, L. W., & Fiore, A. M. (2009a). Effect of regional precursor emission controls on long-range ozone transport – Part 1: Short-term changes in. Atmospheric Chemistry and Physics, 9, 6077-6093.

West, J. J., Naik, V., Horowitz, L. W., & Fiore, A. M. (2009b), Effect of regional precursor emission controls on long-range ozone transport – Part 2: Steady-state changes in ozone air quality and impacts on human mortality, Atmos. Chem. Phys., 9, 6095-6107.

West, J. J., Smith, S. J., Silva, R. A., Naik, V., Zhang, Y., Adelman, Z., Fry, M. M., et al. (2013). Co-benefits of mitigating global greenhouse gas emissions for future air quality and human health. Nature Climate Change, 3, 885-889.

Wiedinmyer, C., Tie, X., Guenther, A., Neilson, R., & Granier, C. (2006). Future Changes in Biogenic Isoprene Emissions: How Might They Affect Regional and Global Atmospheric Chemistry? Earth Interactions, 10(3), 1-19.

Wild, O., & Akimoto, H. (2001). Intercontinental transport of ozone and its precursors in a three-dimensional global CTM. Journal of Geophysical Research-Atmospheres, 106(D21), 27729-27744.

Wilker, E. H., Mittleman, M. a, Coull, B. a, Gryparis, A., Bots, M. L., Schwartz, J., & Sparrow, D. (2013). Long-term exposure to black carbon and carotid intima-media thickness: the normative aging study. Environmental health perspectives.

Woods and Poole Economics Inc. (2012). Complete Demographic Database. Washington, DC:W&P Economics Inc.

Woody, M. C., Baker, K. R., Hayes, P. L., Jimenez, J. L., Koo, B., & Pye, H. O. T. (2015). Understanding sources of organic aerosol during CalNex-2010 using the CMAQ-VBS, Atmos. Chem. Phys. Discuss., 15, 26745-26793, doi:10.5194/acpd-15-26745-2015.

World Health Organization (WHO, 2012). Health Effects of Black Carbon Technical Report World Health Organization, European Centre for Environment and Health, Bonn Office, (www.euro.who.int/_data/assets/pdf_file/0004/162535/e96541.pdf)

Wuebbles, D. J., Lei, H., & Lin, J. (2007). Intercontinental transport of aerosols and photochemical oxidants from Asia and its consequences. Environmental Pollution, 150, 65-84.

Wu, S., Mickley, L. J., Leibensperger, E. M., Jacob, D. J., Rind, D., & Streets, D. G. (2008a). Effects of 2000-2050 global change on ozone air quality in the United States. Journal of Geophysical Research: Atmospheres, 113, 1-12.

Wu, S., Mickley, L. J., Jacob, D. J., Rind, D., & Streets, D. G. (2008b). Effects of 2000–2050 changes in climate and emissions on global tropospheric ozone and the policy-relevant background surface ozone in the United States. Journal of Geophysical Research, 113(D18), D18312.

United Nations (2001). World Population Monitoring 2001. Population, environment and development. Department of Economic and Society Affairs Population Division. United Nations: New York.

Verstraeten, W. W., Neu, J, L., Williams, J. E., Bowman, K. W., Worden, J. R., & Boersma, K. F. (2015). Rapid increases in tropospheric ozone production and export from China. Nature Geoscience, DOI: 10.1038/NGEO2493.

Xing, J., Pleim, J., Mathur, R., Pouliot, G., Hogrefe, C., Gan, C.-M. & Wei, C. (2013). Historical gaseous and primary aerosol emissions in the United States from 1990 to 2010, Atmos. Chem. Phys., 13, 7531–7549.

Yim, S. H. L., Lee, G. L., Lee, I. H., Allroggen, F., Ashok, A., Caiazzo, F., Eastham, S. D., et al. (2015). Global, regional and local health impacts of civil aviation emissions. Environmental Research Letters, 10(3), 034001.

Young, P. J., Archibald, a T., Bowman, K. W., Lamarque, J.-F., Naik, V., Stevenson, D. S., Tilmes, S., et al. (2013). Pre-industrial to end 21st century projections of tropospheric ozone from the Atmospheric Chemistry and Climate Model Intercomparison Project (ACCMIP). Atmospheric Chemistry and Physics, 13(8), 2063–2090.

Yu, H., Remer, L. A, Chin, M., Bian, H., Tan, Q., Yuan, T., & Zhang, Y. (2012). Aerosols from Overseas Rival Domestic Emissions over North America. Science, 337(6094), 566-569.

Yumimoto, K., Eguchi, K., Uno, I., Takemura, T., Liu, Z., Shimizu, A, Sugimoto, N., et al. (2010). Summertime trans-Pacific transport of Asian dust. Geophysical Research Letters, 37(18), 1-7.

Yoshitomi, M., Wild, O., & Akimoto, H. (2011). Contributions of regional and intercontinental transport to surface ozone in the Tokyo area. Atmospheric Chemistry and Physics, 11(15), 7583-7599.

Zanobetti, A., & Schwartz, J. (2009). The effect of fine and coarse particulate air pollution on mortality: A national analysis. Environmental Health Perspectives, 117(6), 898-903.

Zhang L. (2010). Intercontinental transport of air pollution. Frontiers of Environmental Science & Engineering in China, 4, 20-29.

Zhang, L., Jacob, D. J., Boersma, K. F., Jaffe, D. A., Olson, J. R., Bowman, K. W., Worden, J. R., et al. (2011). Transpacific transport of ozone pollution and the effect of recent Asian emission increases on air quality in North America: an integrated analysis using satellite, aircraft, ozonesonde, and surface observations. Atmospheric Chemistry and Physics, 8 (20), 6117-6136.

Zhang, Y., Bowden, J. H., Adelman, Z., Naik, V., Horowitz, L. W., Smith, S. J., & West, J. J. (2016a). Co-benefits of global and regional greenhouse gas mitigation on U.S. air quality in 2050. Atmos. Chem. Phys. Discuss., doi:10.5194/acp-2015-1054, 2016.

Zhang, Y., Smith, S. J., & West, J. J. (2016b). Co-benefits of global, domestic, and sectoral greenhouse gas mitigation for US air quality and human health in 2050. Prepare to submit.

Zhang, Y., Cooper, O. W., & West, J. J. (2016c). Southward redistribution of emissions dominates the 1980 to 2010 tropospheric ozone change. Submitted to Nature Geoscience.